

**Design Guidance and Development of Construction Stormwater Technologies**

by

Lan Liu

A dissertation submitted to the Graduate Faculty of  
Auburn University  
in partial fulfillment of the  
requirements for the Degree of  
Doctor of Philosophy

Auburn, Alabama  
December 12, 2020

Keywords: stormwater, silt fence,  
Lamella settler, electrocoagulation, sediment removal

Copyright 2020 by Lan Liu

Approved by

Dr. Michael A. Perez, Chair, Assistant Professor of Civil Engineering  
Dr. Xing Fang, Professor of Civil Engineering  
Dr. Jose G. Vasconcelos, Associate Professor of Civil Engineering  
Dr. Wesley Donald, Research Fellow IV of Civil Engineering  
Dr. Joey Shaw, Professor of Crop, Soil and Environmental Sciences

## ABSTRACT

As one of the largest sources of nonpoint source pollution, soil erosion has become an increasingly important topic in the U.S. Construction sites. Erosion and sediment control (ESC) practices are commonly used on construction sites to reduce soil erosion and sediment discharge. To avoid eroded sediment discharging into receiving surface water bodies, the environmental protection regulations and technologies are developed by federal, state, and local agencies to capture the eroded sediments from the construction stormwater. The regulations contain the design, installation, inspection, and maintenance of ESC practices and the technologies include their innovation and application in the industry.

This dissertation explores the improvements of design guidance of ESC and construction stormwater technologies through the development of SILTspread: a silt fence design tool, bench scale tests of different lamella settlers and electrocoagulation technology, the innovation of ESC technology corresponding to the application of flocculants in the lamella settlers.

Erosion and sediment controls, typically passive “best management practices” (BMPs), are the most popular methods used to eliminate soil erosion and reduce the environmental impacts. As a type of BMPs, silt fence retains soil particles from disturbed areas by forming the impoundments. A tool was developed to assist silt fence design. The tool simplifies the application of the silt fence design approach by incorporating the automation of hydrologic design calculations, silt fence segment volumetric sizing, and estimation of maintenance needs. This developed tool is applicable for various types of projects and locations, due to the ability to manually enter the basic site-specific data under a 2-yr, 24-hr rainfall event.

In addition to improved design guidance, traditional erosion and sediment control practices can benefit from advanced treatment mechanisms used in other water treatment operations. For

example, lamella settler and electrocoagulation technologies. Lamella settlers (LSs) are a type of water treatment system that consist of a set of inclined plates installed for wastewater treatments. This research sought to bridge the gap between theoretical knowledge and practical application of lamella settlers by conducting experiments to determine the settling performance across several design factors. A Full-Factorial Method (FFM) statistical analysis was conducted to estimate influence of different design factors (e.g., sediment concentration, particle settling distance, and residence time) on efficiency of evaluated treatments. The design factors were independent variables used for analysis, and the calculated turbidity reduction rates between influent and effluent water samples were dependent variables. The results of this research indicated that the optimal turbidity removal rates for all five soil samples was achieved through the use 1.5 hr residence time in  $R_c$  (with 0.18 cm settling distance provided by a 1.27 cm of plate spacing). The calculated turbidity removal rates for different types of soils were correlated corresponding to the calculated settling velocities and measured particle sizes  $D_x$ . The higher turbidity removal rates were found when the settling velocity and  $D_x$  reduction were higher in the soil sample. In statistical approach, a model was developed based on turbidity reductions to assist designers by changing the values of design parameters (inflow concentration, settling distance, and residence time) to meet the desired turbidity of outflow at the design stage. Ultimately, results obtained from this research effort provide design guidance for developing field-scale lamella systems to treat polluted stormwater runoff.

Electrocoagulation is a water-treatment technology that uses an electrochemical anode corrosion process to destabilize and remove contaminants. Electrocoagulation has been shown to have higher contaminant removal efficiency than conventional coagulation and has widespread applications for treatment of a variety of wastes. This research determines and evaluates the

optimal design parameters of EC through the observations of turbidity measurements. According to the results of turbidity reduction rates, the optimal condition is using aluminum electrodes for 0.75 min. at 2 cm (0.8 in.) cell spacing and 39 A/m<sup>2</sup> (3.6 A/ft<sup>2</sup>) current density with 90 min. residence time after 10 sec of rapid mixing. Besides the ability of turbidity removal, another factor considered was energy requirements for different metal cells. In this study, the total cost considers material, cell degradation and electric power for different metals. According to the results of turbidity removal, aluminum was the optimal cell material.

Further research is necessary to investigate how to improve the sediment removal performance of lamella settlers and EC. Combining these two treatment mechanisms has the potential to decrease the required size of the lamella settler while simultaneously maximizing the sedimentation process. In this research, bench-scale experiments were conducted using electrocoagulation as pretreatment for a lamella settler reactor. Synthetic silica filler at concentrations of 500 mg/L, 1,000 mg/L, and 5,000 mg/L were used to evaluate treatment efficiency at 0.5-h, 1.0-h, and 1.5-h residence times. The collected data, including turbidity, total suspended solids, and particle size distribution were used to statistically characterize the system's sediment removal performance. It was found that an optimized electrocoagulation lamella settler reactor with 1.27-cm (0.5 in) plate spacing and 1.5-h residence time reduced turbidity by up to 98% and total suspended solids by 99% in the effluent when compared to the base condition (using a LS with 31.8 cm [12.5 in.] plate spacing for 0.5-hr residence time without the pretreatment of the electrocoagulation). In addition, particle size distribution analyses indicated a decrease in the D<sub>90</sub> value by 84%, indicating that the optimized reactor was effective in capturing larger-diameter soil particles. To validate laboratory results with synthetic sediment-laden influent, stormwater samples were collected from a construction site and treated in the developed EC+LS system.

Turbidity and TSS reduction rates of the field-collected stormwater runoff were 50% and 66%, respectively. In addition, the field collected samples had a Na reduction of 51%, indicating a potential application for treating urban stormwater with high levels of deicing materials. Compared to chemical-based flocculation, the EC+LS system demonstrated similar capability in removing sediment.

Through the outcomes of these four research studies, the designs of ESC were analyzed and improved by investigate new tool and technology. These improvements are sought to bridge the gap between theoretical knowledge and industrial application of ESC practices. This dissertation provides several recommendations for the design of ESC practices and introduces new technology to assist industry professionals for the field implementation.

## ACKNOWLEDGEMENTS

I would like to express my sincere acknowledgements to my advisor, Dr. Michael Perez for his guidance, mentorship, and support during my study at Auburn University. I would also like to express my sincere gratitude to my committee members, Dr. Xing Fang, Dr. Wesley Donald, Dr. Jose Vasconcelos and Dr. Joey Shaw, for their valuable comments regarding my dissertation. In addition, I am thankful to Dr. Blake Whitman and Dr. Wesley Zech for guidance and project design.

I would also like to thank my colleagues, Jaime Schussler and Billur Kazaz, for supporting me throughout the study. I value my friendship developed at Auburn. Natalie Palmquist, Yushan Mu, Danyang Wang, Xuanmeng Wei, and Meredith Ayers offered support and encouragement during my time at Auburn. I would also like to thank my friends in Iowa: Loulou Dickey, Andrea McEachran, and for friendship.

Finally, I want to thank my fiancé, Bo Zhang, for his enduring love, support, and encouragement in these six years. I want to express my sincere thanks to my parents, Weihong Xue and Guiqun Liu, who raised me to always expand my horizon with their selfless support. The constant encouragement and selfless love from my family helps, guides, and inspires me in my life continuously.

## TABLE OF CONTENTS

ABSTRACT.....	II
ACKNOWLEDGEMENTS.....	VI
CHAPTER 1. INTRODUCTION.....	1
1.1. Stormwater Quality .....	2
1.2. Erosion and Sediment Control Practices.....	3
1.3. Lamella Settler and Electrocoagulation .....	4
1.4. Research Motivation and Objectives.....	5
1.5. Dissertation Organization.....	6
CHAPTER 2. SILTSPREAD: SILT FENCE DESIGN TOOL.....	7
2.1. Introduction .....	7
2.2. Literature Review.....	8
2.2.1. Silt Fence State-of-the-Practice .....	8
2.2.2. Silt Fence Performance.....	10
2.3. Research Objectives .....	12
2.4. Developed Design Approach .....	13
2.5. Hydrologic Design .....	19
2.6. Installation Recommendations .....	21
2.7. Maintenance Considerations .....	22
2.8. SILTSPREAD Silt Fence Design Tool .....	23
2.9. Case Study.....	26
2.10. Implementation Pathway .....	30
2.11. Conclusions .....	31
CHAPTER 3. BENCH-SCALE LAMELLA SETTLER EXPERIMENTS.....	33
3.1. Introduction .....	33
3.2. Research Objectives .....	36
3.3. Materials and Methods.....	37
3.3.1. Lamella Settler Design.....	37
3.3.2. Sample Preparation and Flow Introduction .....	38
3.3.3. Turbidity Analysis .....	42
3.3.4. Particle Size Distribution (PSD) Analysis .....	43

3.3.5.	Settling Velocity Calculation.....	44
3.4.	Results .....	46
3.4.1.	Turbidity Reduction .....	46
3.4.2.	PSD .....	51
3.4.3.	Settling Velocity .....	55
3.5.	Discussion .....	56
3.6.	Conclusions .....	57
CHAPTER 4.	ELECTROCOAGULATION (EC) .....	60
4.1.	Introduction .....	60
4.2.	Literature Review.....	61
4.2.1.	History.....	61
4.2.2.	Mechanism.....	63
4.2.3.	EC Factors.....	65
4.2.4.	Power Supply .....	67
4.3.	Research Objectives .....	68
4.4.	Bench-Scale Experiments .....	69
4.5.	Electrode's Consumption .....	72
4.6.	Results .....	74
4.6.1.	Optimal Design Parameters .....	74
4.6.2.	Electrode's Consumption.....	82
4.6.3.	pH.....	85
4.7.	Conclusions .....	86
CHAPTER 5.	DEVELOPMENT AND EVALUATION OF LS+EC FOR TREATING SUSPENDED SEDIMENT .....	87
5.1.	Introduction .....	87
5.2.	Research Objectives .....	91
5.3.	System Development.....	91
5.4.	Turbidity, TSS, Particle Size Analysis, and pH .....	96
5.5.	Results .....	98
5.5.1.	Turbidity Reduction Rates, PSD, and TSS Analysis .....	98
5.5.2.	Extension of EC+LS .....	105
5.5.3.	Scaling Guidance .....	107
5.5.4.	pH.....	108



5.6. Conclusions .....	109
CHAPTER 6. CONCLUSIONS .....	111
6.1. Introduction .....	111
6.2. Conclusions .....	111
6.2.1. SILTspread: Silt Fence Design Tool.....	111
6.2.2. Bench-Scale Lamella Settler Experiments.....	112
6.2.3. Development and Evaluation of Lamella Settlers combined with Electrocoagulation for Treating Suspended Sediment.....	113
6.3. Limitations and Future Study.....	114
6.3.1. SILTspread: Silt Fence Design Tool.....	114
6.3.2. Bench-Scale Lamella Settler Experiments.....	115
6.3.3. Development and Evaluation of Lamella Settlers combined with Electrocoagulation for Treating Suspended Sediment.....	115
6.3.4. Summary .....	116
REFERENCES .....	117
APPENDICES .....	129
Appendix A Silt Fence Design .....	130
Appendix B: Procedure of turbidity and TSS Measurements.....	136
Appendix C: Procedure of Particle Size Distribution Analysis .....	140
Appendix D: Fact Sheets of Soils .....	143
Appendix E: Turbidity Observations for Different Lamella Settlers.....	150
Appendix F: Regression Analysis for Turbidity Measurements.....	156
Appendix G: PSD Analysis for All Types of Soils.....	160
Appendix H: PSD Measurements .....	173
Appendix I: Settling Velocity Estimation.....	178
Appendix J: Turbidity Observations Along Time in EC .....	184
Appendix K: Turbidity and TSS Observations in EC +LS System.....	194
Appendix L: Regression Analysis for EC + LS System.....	199

## LIST OF FIGURES

Figure 2.1 Dewatering Board with Weir Installation.....	18
Figure 2.2 Silt Fence Design Flow Chart.....	21
Figure 2.3 Recommended Silt Fence Installation Techniques.....	22
Figure 2.4 SILTspread Tool.....	25
Figure 2.5 Defined Phases in Case Study. ....	28
Figure 2.6 Drainage Areas in the Defined Phases (drawings not to scale).....	29
Figure 3.1 Lamella Mechanism. ....	36
Figure 3.2 Reactor Tank Design Profiles.....	37
Figure 3.3 Sample Scanned Electron Microscope Results. ....	40
Figure 3.4 Lamella Reactors Experimental Setup. ....	41
Figure 3.5 Experimental Procedure. ....	42
Figure 3.6 Average Turbidity Results for Soil A, 1,000 mg/L, 30 min. Residence Time.....	43
Figure 3.7 Mastersizer 3000. ....	44
Figure 3.8 Turbidity Reduction Rates versus Plate Spacings. ....	49
Figure 3.9 Turbidity Reduction Rates versus Inflow Concentrations.....	50
Figure 3.10 Turbidity Reduction Rates versus $D_{90}$ .....	54
Figure 3.11 Average Measurements of Turbidity and $D_{90}$ for All Tested Soils. ....	54
Figure 3.12 The Calculation of Settling Velocity.....	55
Figure 4.1 EC Process (Holt 2002).....	61
Figure 4.2 Original Investigation of EC. ....	62
Figure 4.3 Relationship of the Conventional Technologies (Kuokkanen 2016). ....	64
Figure 4.4 Arrangements of Electrodes Connection.....	64

Figure 4.5 EC Bench-Scale Experiments.....	72
Figure 4.6 Turbidity Reduction Efficiency versus Reaction Time.....	78
Figure 4.7 Turbidity Reduction Efficiency versus Cell Spacing.....	79
Figure 4.8 Turbidity Reduction Efficiency versus Current Density.....	80
Figure 4.9 Degradation of Different Metals in EC.....	84
Figure 5.1 Lamella Settler Crystallizer	90
Figure 5.2 EC Plate Assembly.....	93
Figure 5.3 EC+LS Experimental Setup.....	95
Figure 5.4 Turbidity Removal Rates for Different Mixers.....	96
Figure 5.5 Experimental Protocol.....	97
Figure 5.6 Sediment Removal for A25.....	99
Figure 5.7 Turbidity and TSS Reduction Rates vs. Settling Distance at Evaluated Influent Concentrations.....	101
Figure 5.8 Turbidity and TSS Reduction Rates vs. Inflow Concentration at Evaluated Settling Distance.....	103
Figure 5.9 Mass loss ratios of Aluminum under Different Current Densities.....	107

## LIST OF TABLES

Table 2.1 Silt Fence Configurations .....	15
Table 2.2: Sizing Factors as a Function of Contributing Drainage Area.....	30
Table 3.1 Soil Information.....	39
Table 3.2 Turbidity Reduction.....	47
Table 3.3 Results of ANOVA Test.....	51
Table 3.4 D Values of Size Diffraction .....	53
Table 3.5 Settling Velocity .....	56
Table 4.1 Analysis of EC at Different Concentrations .....	69
Table 4.2 Power Supply from Different Metal Cells.....	70
Table 4.3 EC Parameters.....	71
Table 4.4 Turbidity Reduction Rates with Aluminum Cells .....	76
Table 4.5 Reduction Rates with Stainless Steel Cells.....	76
Table 4.6 Reduction Rates with Low-Carbon Steel Cells .....	76
Table 4.7 Results of MLR Analysis for Different EC cells.....	82
Table 4.8 Mass Loss for Different EC cells.....	83
Table 4.9 pH Impact at Different Current Densities and Reaction Time .....	85
Table 5.1 Reaction Time of EC .....	94
Table 5.2 Turbidity Reduction with Different Mixing .....	96
Table 5.3 Turbidity and TSS removal efficiencies of LS and EC+LS systems.....	99
Table 5.4 Regression Results of LS and EC Systems.....	104
Table 5.5 Field-Scale Design Parameters .....	108
Table 5.6 Observations of pH change along EC reaction.....	109

## CHAPTER 1. INTRODUCTION

Stormwater quality has become an increasingly important topic across agricultural, urban, and construction sectors (Nayebare et al. 2014). Soil loss from erosion during rainfall events has become the greatest source of degradation to stormwater quality (Makepeace, Smith, and Stanley 1995). It is estimated that there are over four billion tons (3.6 billion tonnes) of soil loss due to erosion from agricultural and non-agricultural lands in the U.S. (Brady, Weil, and Brady 2010). Compared to other land uses, construction operations produce a large amount of sediment yield due to the earth disturbing nature of land-grading activities. Construction sites lose average 79.3 metric tons/hectare/year (200 tons/acre/year) of soil, which is 12 times more soil loss than from forested lands and agriculture lands (GSWCC 2002). As pollutants can attach on eroded soil particles, construction sites have the potential to create enormous amounts of sediment pollutants that may impact the environment (Barrett et al. 1995).

Soil loss in construction predominantly occurs when sediment detaches due to rainfall or wind. The detachment of soil from rainfall becomes a serious problem as the eroded sediments discharge into surface water. In addition to sediment, other contaminants (fertilizers, pesticides, fuels, and pollutants spilled from construction sites) can also be carried by soil particles to create adverse water quality impacts to downstream receiving water bodies (Faucette and Risse 2001; Reardon 2005). Over \$44 billion is spent annually to mitigate the downstream implications of erosion during construction. To prevent the downstream effects of sediment and associated pollution, erosion and sediment controls are implemented throughout construction phasing (Faucette et al. 2007).

It has been shown that stormwater quality impacts receiving water bodies which can significantly damage aquatic life (Makepeace et al. 1995). The U.S. Environmental Protection Agency

(USEPA) reported that sediment contamination in surface waters is the greatest threat to water sources across the U.S., and has become very important to quantify and mitigate contaminants in stormwater (Makepeace et al. 1995).

### **1.1.Stormwater Quality**

According to regulation from the National Pollution Discharge Elimination System (NPDES), construction stormwater can be classified as point source pollution or nonpoint source pollution depending on its site size (Eastman 2009). When the construction site is less than one acre, the stormwater is defined as nonpoint source pollution which is classified as point source when the site is larger than one acre. Point source is legally defined as “any discernible, confined and discrete conveyance” provided in Section 502(14) of the Clean Water Act (CWA). Depending on the source, stormwater can also be classified as nonpoint source. Nonpoint source (NPS) pollution is transported by rainfall or snowmelt from the ground (Mandelker 1989). NPS has been identified as the main cause of degraded water quality for surface water in the U.S (Mannina and Viviani 2010).

Decreased stormwater quality influences aquatic life and downstream consumers. Considering public health, water facilities are highly concerned about quality of stormwater discharged into water sources (Makepeace et al. 1995). Turbidity and total suspended solids (TSS) are general parameters measured and used to assess water quality. Turbidity is a measure of the amount of light that can pass through a water sample. The lower the turbidity, the less particulates are associated with the sample. TSS is the measurement of all suspended material in a sample and is determined by removing all water through filtration or evaporation. Turbidity and total solids levels impact the environment in several mechanisms such as photosynthesis and pollutant transport.

In another approach, stormwater quality can be estimated according to different measurements of pollutants. Some chemical pollutants (herbicides, pesticides, and radioactive contaminants) can attach to or get absorbed by sediment and are transported through stormwater discharge. The concentrations of those absorbed contaminants vary proportionally according to fraction of fines. As coarse particles settle more rapidly, it is critical to capture finer particles that carry relatively more pollutants (Foster, Young, and Neibling 1985).

## **1.2.Erosion and Sediment Control Practices**

Construction stormwater is managed through the use of erosion and sediment controls. Erosion controls prevent topsoil from being eroded from disturbed areas, whereas sediment controls capture eroded sediment from site. The erosion and sediment controls installed on construction sites are typically passive “best management practices” (BMPs). There are several types of BMPs to prevent soil loss and capture eroded soil particles (Forrest and Harding 1994a). Examples of BMPs include: sediment barriers, sediment basins, inlet protection practices, ditch checks, erosion control blankets, and slope drains (Pitt, Clark, and Lake 2007).

Among the BMPs, silt fence and sediment basins are common practices used to provide sedimentation process. When used as a barrier, silt fence is identified as sediment control which retains eroded sediment on site by forming impoundment and slowing stormwater runoff. Sediment basins provide extended detention to allow sediment to settle from suspension, which is identified as sediment control. Both practices create extended detention for stormwater runoff through different approach: impoundment and detention time. To maximize performance of these two practices, reliable design guidance is necessary to assist designers, engineers, and practitioners. It is challenging to create a universal design as sites in the U.S. vary significantly which can explain why designs and requirements for erosion and sediment control practices greatly

vary from state to state. As awareness and regulations increase around stormwater, research studies to improve the performance of BMPs are essential for reliable and feasible designs.

### **1.3.Lamella Settler and Electrocoagulation**

In addition to improved design guidance, traditional erosion and sediment control practices can benefit from advanced treatment mechanisms used in other water treatment operations. For example, lamella settler and electrocoagulation technologies. Lamella settlers (LSs) are a type of water treatment system that consist of a set of inclined plates installed for wastewater treatments. Lamella settlers create “counter flow” through the system where suspended solids settle from water as it flows through the plates in different directions (Weiss 2013). Additionally, the narrow spacing between these parallel plates shortens vertical traveling distance and reduces flow velocity, which creates laminar flow and constrains re-suspension in the system. Recent research using large-scale testing techniques indicated that high-rate lamella settlers could be an innovative approach to treat construction site stormwater runoff, providing an improvement of up to 33% in the efficiency of an optimized sediment basin (Perez et al. 2019).

Another advanced technology that is considered to improve sediment removal efficiency from stormwater runoff is electrocoagulation (EC). EC is the process of electrochemical reactions used in water and wastewater treatment, which corrodes anodes to destabilize and remove contaminants (Holt et al. 2005; Sahu et al. 2014). The EC process consists of electrically charged two metal elements (iron, aluminum and stainless steel) as cathode and anode placed in a treatment tank, where the current flows out of cathode (considered as positive) and then flows into anode (considered as negative). EC’s wide applications can be used to remove various unwanted pollutants including: suspended solids, colloidal material, metals, and dissolved solids-including



inorganic contaminants and pathogens (Emamjomeh and Sivakumar 2009; Merzouk et al. 2009; Sahu et al. 2014).

#### **1.4. Research Motivation and Objectives**

Opportunities exist to improve the design of current erosion and sediment control practices and to introduce novel treatment technologies to the construction stormwater field. This dissertation aims at closing this gap through four main projects including tasks for each study.

The first objective for this research was to develop a design approach for silt fence sediment barriers. This objective was met by, (1) conducting a literature review, (2) developing a design-based approach, and (3) creating a spreadsheet-based design tool.

The second objective for this dissertation was to determine the efficiency of lamella settlers in treating suspended sediment. This objective was met by, (1) developing an apparatus and methodology of experiments, (2) constructing the lamella settlers, (3) conducting experiments testing different parameters including: soil types, sample concentrations, residence time, and plates' spacings, and (4) analyzing results of turbidity, TSS, and particle sizes, and make the design recommendations.

The third objective for this dissertation was to evaluate EC reactions treating suspended sediment. This objective was met by, (1) conducting batch testing to develop design parameters (cell's material, cell spacing, pH, power, reaction time, and settling time), (2) analyzing results of turbidity and power supply, and (3) making the design recommendations.

The fourth objective for this dissertation was to develop EC applications with lamella settler for treating suspended sediment in continuous flow. This objective was met by, (1) constructing EC system for continuous flow, (2) conducting experimental testing applying continuous flow, and (3)

collecting measurements of turbidity, TSS, pH, and particle sizes of sample, and (4) analyzing results and make the final design recommendations for the large-scale experiments in future.

### **1.5.Dissertation Organization**

This dissertation is divided into six chapters to achieve the research goals introduced in the previous section. Following the introduction and literature review stated in Chapter 1, Chapter 2. *SILTspread: Silt Fence Design Tool*, presents the design guidance in excel spreadsheet according to literature review summarized from state-based guidance and research recommendations. Chapter 3: *Bench-Scale Lamella Settler Experiments*, analyzes and optimizes different design factors for lamella settler through turbidity, TSS, and particle size analysis. Chapter 4: *Electrocoagulation (EC)*, analyzes and optimizes different design factors for EC in bench scale. Chapter 5: *Development and Evaluation of LS+EC for Treating Suspended Sediment*, investigates a novel system with optimized design parameter obtained from Chapter 4 and Chapter 5. Finally, Chapter 6. *Conclusions*: summarizes the recommendations from study about silt fence, lamella settler, and EC and states limitations and future work.

## CHAPTER 2. SILTSPREAD: SILT FENCE DESIGN TOOL

### 2.1.Introduction

As one of the largest sources of nonpoint source pollution, soil erosion has become an increasingly important topic in the U.S. Construction sites, when compared to agricultural and naturally forested lands, have the potential to create 10 to 20 times and 1,000 to 2,000 times more sediment discharge, respectively (USEPA 2000). Soil loss in construction applications predominantly occurs when sediment detaches from a disturbed soil surface due to rainfall. Eroded sediment has the potential to discharge downstream into receiving surface water bodies resulting in pollution. Contaminants such as fertilizers, pesticides, hydrocarbons, and other construction-related pollutants, can also be carried by soil particles and create adverse water quality impacts (Issaka and Ashraf 2017; Reardon 2005). At the federal level, the National Pollutant Discharge Elimination System (NPDES) and Construction General Permit (CGP) regulates earth-disturbing construction activities to minimize water quality impacts (USEPA 2009). Most state environmental agencies have been delegated authority by the U.S. Environmental Protection Agency (USEPA) to manage NPDES permitting at the state level. Furthermore, many local municipalities have stormwater ordinances to protect jurisdictional water quality. These delegated authorities often create design standards for the use of temporary erosion and sediment control (E&SC) practices on construction sites in their respective jurisdiction. To obtain NPDES coverage, regulated construction activities require the development, implementation, and maintenance of a Stormwater Pollution Prevention Plan (SWPPP). The SWPPP provides stormwater-related management requirements during land development. E&SC practices are commonly used on construction sites to reduce soil erosion and sediment discharge, protecting downstream water quality. E&SC practices include devices to prevent soil loss (i.e. erosion

controls) and capture eroded sediment (i.e., sediment controls). For example, vegetative establishment, erosion control blankets, ditch checks, and slope drains are examples of erosion controls. Sediment barriers, sediment basins, inlet protection practices, are examples of common sediment controls (Pitt et al. 2007).

Silt fence is arguably the most common and recognizable E&SC practice used in the industry. Silt fence consists of a geotextile material anchored into the soil and supported by posts, installed perpendicular to the direction of flow.(Norman et al. 1997). In sediment barrier applications, silt fence is used to intercept sediment-laden sheet flow runoff from disturbed areas and facilitate sediment capture by reducing the velocity of sheet flow runoff and promoting deposition by settling (USEPA 2012). Silt fence can also be used as an erosion control practice when used as a ditch check practice within channels to reduce the velocity and shear stress of concentrated flows (Donald et al. 2013).

## **2.2.Literature Review**

### ***2.2.1.Silt Fence State-of-the-Practice***

Silt fence design and installation standards are two critical factors that ultimately influence performance. Sizing, design, and implementation of E&SC practices is dictated by the USEPA CGP. The permit provides sizing guidance for the design of practices that are intended to create impoundments. Volume-based practices are sized by one of two options: (a) calculating volume of runoff from a 2-yr, 24-hr storm; or (b) using a volume sizing factor (VSF) of 252 m<sup>3</sup>/ha (3,600 ft<sup>3</sup>/ac) drained (US Environmental Protection Agency (USEPA) 2017). A design using the 252 m<sup>3</sup>/ha (3,600 ft<sup>3</sup>/ac) VSF accounts for 2.5 cm (1.0 in.) of runoff volume per unit area. This volume can be correlated to a 0.6 cm (1.56 in.) rainfall depth using a Curve Number (CN) of 94, representative of a hydrologic soil group D on newly graded areas (pervious areas only, no

vegetation), typical of construction sites with highly disturbed and compacted soils. The USEPA recommends drainage areas be considered based on local design storm and hydrologic conditions so that silt fence is not expected to overtop (Cronshey 1986). State environmental agencies, such as the Alabama Department of Environmental Management (ADEM), dictate that sediment control measures must be properly selected based on site-specific conditions and shall be designed and maintained to minimize erosion and maximize sediment removal resulting from a 2-yr, 24-hr storm event (US Environmental Protection Agency (USEPA) 2017).

While the USEPA and state agencies outline performance and design expectations, a design-based approach using local hydrological parameters and site conditions is not currently used for the design and placement of silt fence sediment barriers on construction sites. Construction stormwater design manuals are developed by state environmental agencies as well as by state transportation agencies; however, many temporary E&SC practices are designed using “rules-of-thumb” rather than site-specific design-based approaches (Perez et al. 2016). For example, according to different states’ institutions including Alabama Soil and Water Conservation Committee (AL-SWCC), Georgia Soil and Water Conservation Commission (GSWCC), South Carolina Department of Health and Environmental Control (SCDHEC), and Tennessee Department of Environment and Conservation Activities (TDECA), a design guidance for silt fence sediment barriers was summarized. The design of silt fence is typically given as 0.1 ha (0.25 ac) and 0.2 ha (0.5 ac) of contributing drainage area for every 30.5 linear m (100 ft) of unreinforced or reinforced silt fence, respectively (AL-SWCC 2009; GSWCC 2016; SCDHEC 2005; TDECA 2012).

Limitations in silt fence design approaches have long been recognized by professionals within the E&SC industry. In 2004, a spreadsheet-based silt fence assessment tool, “Silt Fence

Aid”, was created to estimate the performance of silt fence designs. The tool relies on detailed user inputs including: site parameters (i.e., up-slope length, width along slope, slope to fence, etc.), soil information (i.e., particle size characteristics, cover factor, eroded size distribution, etc.), hydrologic information (i.e., design rainfall depth), silt fence geotextile properties (i.e., fabric type or discharge coefficient), and impoundment information (i.e., length of extension, angle of extension between the toe, and performance factor). The spreadsheet-based tool estimates silt fence failures due to scouring of toe and total mass of sediment discharged through silt fence (Stevens et al. 2004). The spreadsheet-based tool estimates silt fence performance based on these input parameters. This model-based tool failed to be widely adopted or used by stormwater professionals and the USEPA has questioned its accuracy due to the use of clean water flow-through rates reported by silt fence manufacturers, rather than sediment-laden flow rates encountered in field applications (USEPA 2009).

In 2007, another silt fence tool was developed for highway construction applications that relied on the rational method to determine appropriate silt fence tieback (i.e. J-hook) spacing using local hydrologic parameters (Zech, Halverson, and Clement 2007). This tool can predict stormwater runoff and impoundment storage per unit length of silt fence, which can assist designers in selecting appropriate tieback dimensions and interval spacing used on highway construction sites. However, this tool has limited application to J-hook configurations and is developed specifically for linear highway construction applications.

### ***2.2.2.Silt Fence Performance***

The USEPA reports a total suspended solids (TSS) capture effectiveness of 70% for silt fence. This effectiveness is further categorized by soil type: 80-90% for sand, 50-80% for silt-loam, and 0-20% for silt-clay-loam soils. Actual trapping efficiencies can vary widely based on

differences in contributing hydrologic regimes and soil types, as well as the design and installation of the silt fence (United States Environmental Protection Agency 1993). In sediment barrier applications, the performance of the silt fence is represented by the efficiency of capturing and containing eroded sediment within the site. Temporary impoundments formed upstream of installed silt fence barriers create conditions favorable for sedimentation to occur. Contrary to manufacturer claims, only a small portion of sediment is trapped by filtration through the silt fence geotextile (Barrett et al. 1995). Research and testing have shown silt fence geotextiles will blind quickly and reduce flow-through capabilities (Bugg et al. 2017; Donald et al. 2016; Perez et al. 2015). Manufacturer reported silt fence geotextile flow rates, evaluated through ASTM D4491, are often misleading as they are reported for clear-water conditions. Research studies have been conducted to correlate reported clear water flow-through rates with sediment-laden flow rates. Through a series of scaled experiments, Whitman et al. reported sediment-laden flow rates through silt fence geotextiles at an average of 126.3 L/min/m<sup>2</sup> (3.1 gal/min/ft<sup>2</sup>) for woven silt fence and 65.2 L/min/m<sup>2</sup> (1.6 gal/min/ft<sup>2</sup>) for nonwoven silt fence. These were 3% and 1% of the manufacturer reported flow through rates of 4,482 L/min/m<sup>2</sup> (110 gal/min/ft<sup>2</sup>) for woven and 6,723 L/min/m<sup>2</sup> (165 gal/min./ft<sup>2</sup>) for nonwoven (J B Whitman, Zech, and Donald 2019). Similar water quality studies have evaluated the differences in performance between woven and nonwoven silt fence geotextiles, reporting turbidity reductions of 14% (23% of sediment concentration removal) for woven silt fence, and 52% (56% of sediment concentration removal) for nonwoven silt fence, respectively (Gogo-Abite and Chopra 2013).

In addition to design approaches, installation and material standards such as: type of geotextile material, post type, post spacing, fasteners, installed height, and trenching mechanism vary state-by-state based on local preferences (Bugg et al. 2017). Whitman et. al conducted large-

scale testing through modified ASTM D7351 protocols on 20 ft (6.1 m) segments of silt fence sediment barriers (Whitman et al. 2018). Treatment modifications were made to the Alabama Department of Transportation (ALDOT) standard silt fence design by increasing steel t-post weight from 1.4 to 1.9 kg/m (0.95 to 1.25 lb/ft), reducing post spacing from 3.0 to 1.5 m (10 to 5 ft), decreasing fence height from 81.3 to 61.0 cm (32 to 24 in.), and implementing a 15.2 cm (6 in.) trench offset from the face of the silt fence. This modified installation was able to capture 97% of total sediment introduced. In subsequent testing, polypropylene-backed woven silt fence installed on hardwood posts were able to capture 91% of total sediment (Bugg et al. 2017).

### **2.3. Research Objectives**

Design guidance for silt fence sediment barriers varies significantly across the U.S. In addition, current standards lack local design-based inputs and fail to conform to the impoundment design requirements of the CGP. The USEPA recognizes this deficiency and calls for silt fence to be placed as a function of the contributing area and resulting runoff volume (Stevens et al. 2004). The lack of site-specific design-based guidance results in designs where silt fence is installed along the perimeter of a construction site, completely enveloping the site. Guidance on silt fence installation technique also varies widely, with recent performance-based research providing enhancement opportunities.

While efforts have been made to provide design models and to conduct testing to better understand the performance of silt fence sediment barriers, a need exists to develop a practical design-based silt fence implementation approach that can be applied uniformly across the U.S., while implementing research-backed installation improvements. The objective of this research was to develop a design-based approach for the implementation of silt fence using local site conditions. Guidance was developed using state-of-the-art approaches along with research-based



findings and implementation recommendations. In addition, SILTspread, a spreadsheet-based design tool, was created to allow designers to seamlessly incorporate the developed guidance in future silt fence designs.

#### **2.4.Developed Design Approach**

For a silt fence sediment barrier design standard to be effective, it must be universally applicable and practical to implement using readily available site information. To create such a design standard, an understanding of how silt fence is implemented and used on a site is required. To meet the intent of the USEPA CGP, the developed silt fence design approach has two general guiding principles: (a) silt fence sediment barrier segments must be able to temporarily detain the runoff volume from the local 2-yr, 24-hr storm, and (b) silt fence segments must be able to pass the runoff volume of larger storm events through a dedicated outlet mechanism. This approach allows silt fence segments to be designed to local hydrologic conditions, accounting for topography, 2-yr, 24-hr rainfall, soil type, land cover, and project duration.

Construction sites are highly dynamic in nature, with constantly changing amounts of soil disturbance and drainage areas. Thus, SWPPPs are typically designed for three phases of construction: (a) pre-development (referred as Phase I), (b) grading and earthmoving (developing condition referred as Phase II), and (c) final stabilization or developed conditions (referred as Phase III). In Phase I, the site condition consists of pre-development contours with clearing and grubbing complete and topsoil stripping underway. Initial E&SC practices present during Phase I include perimeter sediment barrier practices and sediment basins. Phase II includes heavy grading operations and can include permanent storm sewer installation and building pad grading. As slopes, channels, and stormwater infrastructure are established, erosion control blankets, turf reinforcement mats, ditch checks, and inlet protection practices are installed. Phase III refers to

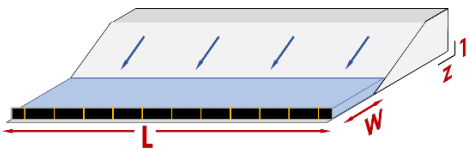
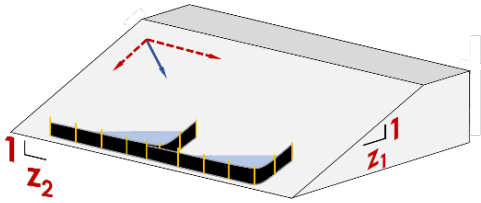
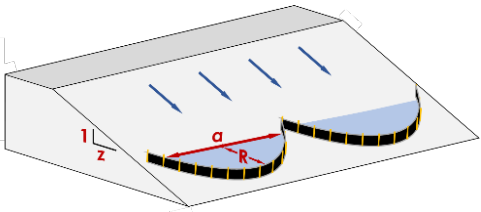
the condition where final grading contours are achieved and all impervious areas (i.e., buildings, roadways, parking lots, etc.) have been constructed. During Phase III, the site is transitioning towards final vegetative stabilization, however, is still susceptible to erosion. Plan sets, including pertinent grading, drainage areas, and site stabilization information are commonly developed for these three phases of construction as part of the SWPPP. Based on the availability of this information, a silt fence design standard was developed that would meet the criteria of these three major phases of construction.

To effectively implement a silt fence sediment barrier, a designer should consider and evaluate the practice across the three major construction phases. It is recommended that the initial layout and placement of silt fence be done using Phase III plan sets to limit potential conflicts with planned construction activities (i.e. clashes with grading, structures, pavement, etc.). By using the final phase, a designer can select placement areas outside limits of major earthmoving and grading activities. Following this methodology, reinstallation of silt fence sediment barriers throughout the project life will be minimized.

Silt fence sediment barriers are often installed in three different configurations: (a) linear, (b) J-hook (tiebacks), and (c) C-shape segments. These three configurations were selected for analysis based on reviewed literature and typical guidance used by state agencies and their ability to meet different site-specific needs to control sediment based on different topographic conditions. Linear segments of silt fence sediment barriers are placed parallel to contour lines along relatively flat areas with uniform elevation. The segments are installed perpendicular to the flow of water, which decreases the flow velocity and captures eroded sediments. For the placement of silt fence along a slope, J-hook configurations can be used in areas where a transverse gradient would otherwise prevent the effective installation of a linear segment. J-hook installation configurations

break impoundment into localized pools that can be temporarily detained. This limits the amount of runoff that travels to the lowest point of a linear silt fence segment and has been shown to trap sediment effectively (Barrett et al. 1995; Robichaud et al. n.d.; Stevens et al. 2004; Zech et al. 2007; Zech, McDonald, and Clement 2009). C-shape configurations are used to effectively impound runoff where linear installations are not feasible or desirable. Similar to J-hook segments, C-shape installations break the contributing area to smaller segments, localizing impoundment. As shown in Table 2.1, mathematical storage volume relationships were developed for each of these three installation configurations. Equations 2.1, 2.2, and 2.3 yield maximum stormwater storage capabilities for each silt fence installation based on geometric parameters associated with the respective configuration.

**Table 2.1 Silt Fence Configurations**

Segment	Configuration	Equation	
Linear		$V = hL(W + \frac{z}{2})$	Eq. 2.1
J-hook		$V = \frac{h^3 z_1 z_2}{2}$	Eq. 2.2
C-shape		$V = \frac{ahR}{3}$	Eq. 2.3

Note:  $V$  is impoundment volume,  $\text{ft}^3$  ( $\text{m}^3$ ),  $h$  is height of silt fence,  $\text{ft}$  ( $\text{m}$ ),  $L$  is silt fence length,  $\text{ft}$  ( $\text{m}$ ),  $W$  is width of level area,  $\text{ft}$  ( $\text{m}$ ),  $z_1$  is horizontal slope,  $\text{ft}/\text{ft}$  ( $\text{m}/\text{m}$ ),  $z_2$  is longitudinal slope,  $\text{ft}/\text{ft}$  ( $\text{m}/\text{m}$ ),  $a$  is width of installation at maximum impoundment,  $\text{ft}$  ( $\text{m}$ ), and  $R$  is the radius of impoundment.



The selection and placement of silt fence segment type and location is an iterative process that requires a designer to determine the 2-yr, 24-hr runoff volume from the upstream contributing drainage area and the volumetric storage area provided by the silt fence segment. A safety factor can be calculated by dividing the silt fence storage volume by the runoff volume. The safety factor should be checked across all design phases (i.e. Phases I, II, and III) to ensure sizing is adequate across the entire duration of earth-disturbing activities. If the safety factor is greater than 1.0 for all phases, then the silt fence design is adequate. If the safety factor is less than 1.0, then the silt fence segment must be reconfigured to provide for additional storage. This iterative process may include the addition of upstream controls (i.e. runoff diversions, sediment basins, etc.) to achieve a suitable design. Note that silt fence geotextile flow-through rates are not considered during the design process due to negligible flow-through capabilities resulting from geotextile blinding (J B Whitman et al. 2019). For design purposes, all geotextile materials are treated as impervious, however, a designer can use professional judgment when selecting specialty geotextiles designed for high flow-through conditions.

Due to the expected blinding of silt fence geotextiles after storm events, an effective means for dewatering must be included to prepare segments for subsequent storms and minimize periods of extended ponding and risk of overtopping. Ideally, dewatering should be implemented to allow the silt fence segment to dewater the design impoundment capacity within 4 to 12 hours, which has been shown to be an effective detention time, restoring volumetric storage without compromising turbidity treatment effectiveness (J Blake Whitman, Zech, and Donald 2019). One outlet option that has been tested is a perforated plywood dewatering board with a weir. The dewatering board is made up of a series of 2.5 cm (1.0 in.) diameter orifices spaced 7.6 cm (3 in.) apart. A V-notch overflow weir is placed at the top of the board, 45.7 cm (18 in.) from the ground.

The dewatering board is installed at the lowest elevation of a silt fence segment, secured behind the geotextile. Downstream of the dewatering board and overflow outlet, proper erosion control should be provided to prevent scour. A geotextile apron or riprap can be used to act as a splash pad. Examples of a dewatering board with weir installation is shown in Figure 2.1 (Perez et al. 2016). Large-scale testing of silt fence sediment barriers with installed dewatering and overflow weirs have reported insignificant effects to effluent turbidity measurements, further emphasizing that water quality improvements are primarily achieved through impoundment rather than filtration through the geotextile (J Blake Whitman et al. 2019).

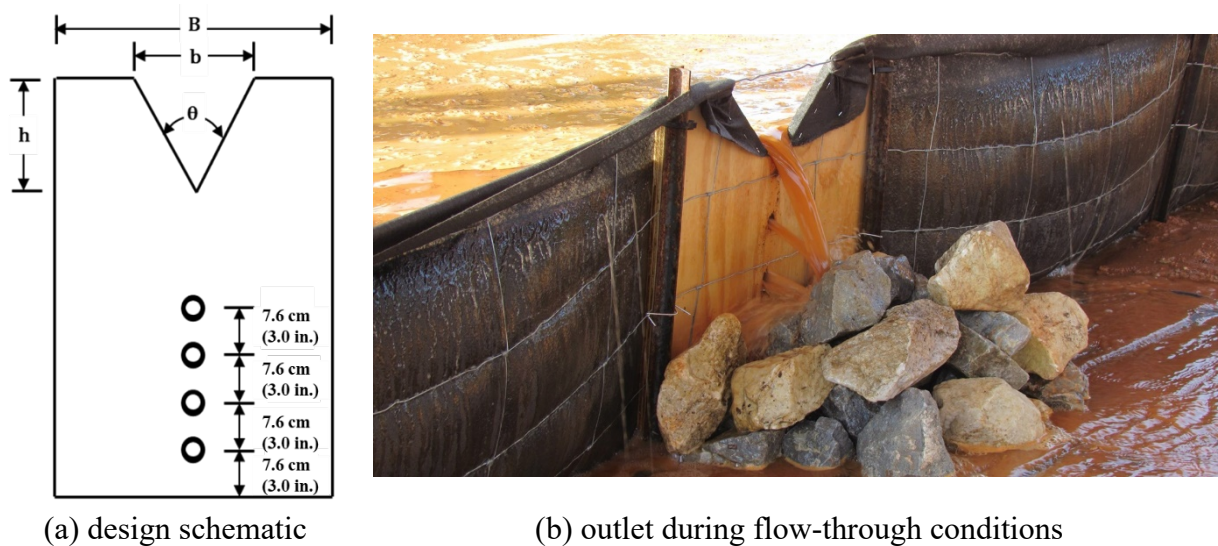


**Figure 2.1 Dewatering Board with Weir Installation.**

The V-notch weir should be sized to pass the peak flow rate from the 2-yr, 24-hr design storm. Sizing of the weir can be calculated by using Eq. 2.4-2.7 (USBR 1953). These equations are restricted to where  $h$  is less than 0.38 m (1.25 ft) or  $b$  is over 0.91 m (3.00 ft), height between silt fence and V-notch is over 0.46 m (1.50 ft),  $b/h$  is greater than or equal to 2.00, or  $h/B$  is less than or equal to 0.2.

$$Q_{weir} = 4.28 C \tan\left(\frac{\theta}{2}\right) (h + k)^{5/2} \quad \text{Eq. 2.4}$$

$$\theta = \arctan\left(\frac{0.5B - b}{h}\right) \quad \text{Eq. 2.5}$$

$$C = 0.607165052 - 0.000874466963 \theta + 6.10393334 \times 10^{-6} \theta^2 \quad \text{Eq. 2.6}$$

$$k = 0.0144902648 - 0.00033955535 \theta + 3.29819003 \times 10^{-6} \theta^2 - 1.06215442 \times 10^{-8} \theta^3 \quad \text{Eq. 2.7}$$

$Q_{weir}$  is flow rate capacity of the weir, m<sup>3</sup>/s (ft<sup>3</sup>/s),  $h$  is height of V-notch, m (ft),  $C$  is discharge coefficient,  $k$  is head correction factor, m (ft),  $\theta$  is notch angle, degrees,  $b$  is width of V-notch, m (ft),  $B$  is width of the dewatering and overflow board, m (ft). In the event that the weir is undersized for the 2-yr, 24-hr peak flow rate, the weir or the silt fence configuration must be modified for additional flow capacity or decrease the expected flow rate.

## 2.5. Hydrologic Design

The Natural Resources Conservation Service (NRCS) TR-55 Urban Hydrology for Small Watersheds is the recommended hydrological model for designing E&SC practices as it allows for determination of volume and peak flow (Cronshey 1986). Hydrologic analysis is conducted for each delineated contributing area to calculate the runoff volume and peak flow rate. This process includes the delineation of the contributing drainage area and the selection of CN for individual silt fence segments. Eq. 2.8 was developed through simplification of TR-55 volume parameters and can be used to calculate the runoff volume for each drainage area (Perez et al. 2016).

$$V = \frac{nA \left[ P - 0.2 \left( \frac{1000}{CN} - 10 \right) \right]^2}{12 \left[ P + 0.8 \left( \frac{1000}{CN} - 10 \right) \right]} \quad \text{Eq. 2.8}$$

$V$  is runoff volume, ft<sup>3</sup> (m<sup>3</sup>),  $n$  is constant, 1.86 for m<sup>3</sup> (1.0 for ft<sup>3</sup>),  $A$  is area, m<sup>2</sup> (ft<sup>2</sup>), and  $P$  is the 2-yr, 24-hr rainfall depth, cm (in.). The drainage volume contributing to each silt fence segment must be determined for each phase of construction, as the CN and drainage area may vary throughout grading and land-disturbing activities.

Eq. 2.9 and 2.10 from TR-55 can also be used to determine the peak flow rate ( $Q_p$ ) from drainage areas contributing to silt fence segments (Cronshey 1986). The 2-yr, 24-hr rainfall precipitation can be determined from Atlas 14 for specific sites a CN or weighted CN ( $CN_w$ ) for each drainage area is applied based on corresponding land cover within the drainage area (National Oceanic and Atmospheric Administration's National Weather Service 2014).

$$Q_p = \frac{q_u A (P - I_a)^2}{n_1^2 (P + 4I_a)} \quad \text{Eq. 2.9}$$

$$I_a = 0.2n_2 \left( \frac{1000}{CN} - 10 \right) \quad \text{Eq. 2.10}$$

$Q_p$  is peak flow rate,  $m^3/s$  ( $ft^3/s$ ),  $q_u$  is unit peak discharge (calculated from rainfall distribution type in Eq. 2.11-2.14),  $A$  is contributing drainage area,  $m^2$  ( $ft^2$ ),  $P$  is 2-yr, 24-hr rainfall depth, cm (in.),  $I_a$  is initial abstraction, cm (in.) (calculated from , and  $n_1$  is constant, 2,566 for  $m^3/s$  (5,280 for  $ft^3/s$ ),  $n_2$  is constant, 2.54 for cm (1.0 for in.), and  $CN$  is Curve Number.

The TR-55 method provides charts to determine the applicable  $q_u$  value as a function of the rainfall distribution type, time of concentration, initial abstraction, and rainfall depth. Due to the relatively small contributing areas expected for silt fence segments, resulting times of concentration are expected to be less than or equal to 5 min., the TR-55 minimum values. Therefore, four relationships (Eq. 2.11-Eq. 2.11-2.14) for each type of rainfall distributions were developed by plotting  $q_u$  against  $I_a/P$  at a  $T_c$  of 5 min. The  $R^2$  values for all developed equations were close to 1.0.

$$q_u = 395775(I_a/P)^5 - 540566(I_a/P)^4 + 279752(I_a/P)^3 - 70389(I_a/P)^2 + 7816.6(I_a/P) + 192.51 \quad \text{Eq. 2.11}$$

$$q_u = 31716(I_a/P)^5 - 31683(I_a/P)^4 - 4158.8(I_a/P)^3 + 7440.5(I_a/P)^2 - 1851.1(I_a/P) + 1117.8 \quad \text{Eq. 2.12}$$

$$q_u = 401501(I_a/P)^5 - 540670(I_a/P)^4 + 263940(I_a/P)^3 - 59490(I_a/P)^2 + 5923.9(I_a/P) + 443.57 \quad \text{Eq. 2.13}$$

$$q_u = 18066(I_a/P)^5 - 49518(I_a/P)^4 + 44315(I_a/P)^3 - 16774(I_a/P)^2 + 2366.7(I_a/P) + 54.138 \quad \text{Eq. 2.14}$$

Figure 2.2 presents a flowchart summarizing the developed silt fence design approach.



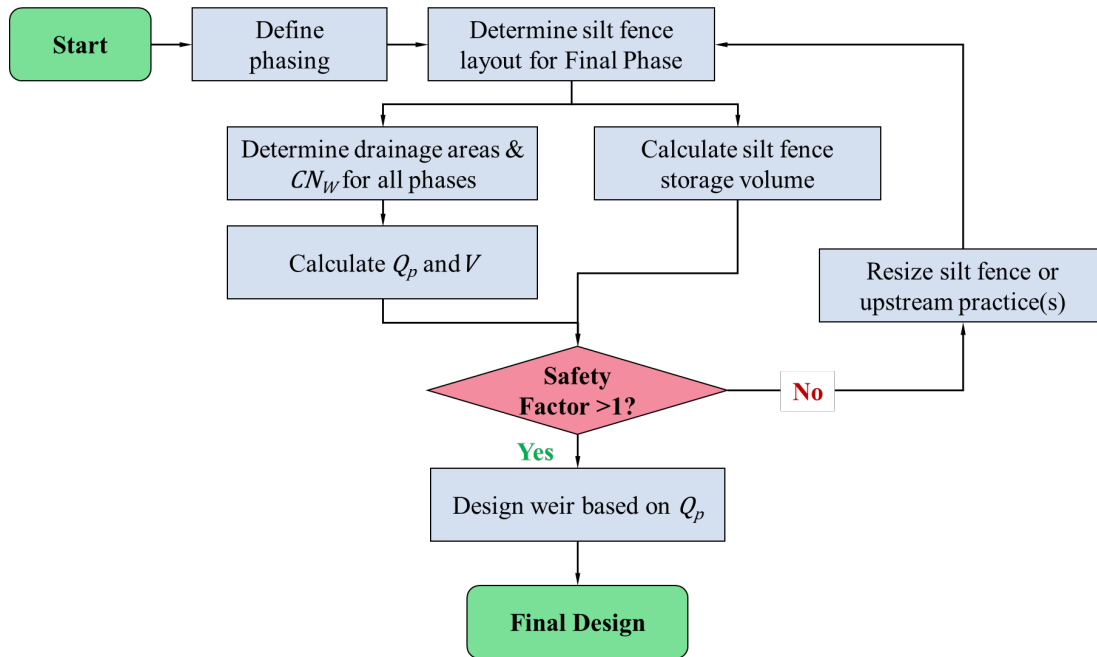


**Figure 2.2 Silt Fence Design Flow Chart.**

## 2.6. Installation Recommendations

The materials, anchoring, and support of the silt fence should provide adequate strength and dimensions to resist hydrostatic and hydrodynamic forces from the impounded runoff of the design storm. It is recommended to use 1.98 kg/m (1.33 lb./ft) steel or 5 by 5 cm (2 by 2 in.) hardwood posts to support the silt fence geotextile material securely (ASWCC 2009). This design method does not differentiate between nonwoven and woven geotextiles as both have resulted in similar performance characteristics in testing; however, support through 14-gauge steel wire fencing with a mesh or equivalent strength material that has a spacing of 15 x 15 cm (6 x 6 in.) is recommended. Silt fence geotextile specifications may thus be a function of longevity and tensile strength.

To provide a stable structure and prevent excessive fence sag, it is recommended to provide 1.2 to 2.4 m (4 to 8 ft) spacing between support posts. The geotextile material must be buried into the trench with compacted soil on top of the geotextile. As shown in Figure 2.3, the minimum

embedment depth of the geotextile is 15 cm (6 in.) to 30 cm (12 in.). To optimize the structural integrity, a 15 cm (6 in.) offset trench installation upstream from the silt fence is highly recommended. The recommended installation method is summarized in Figure 2(a) for trenched silt fence installations and Figure 2(b) for mechanically sliced installations.

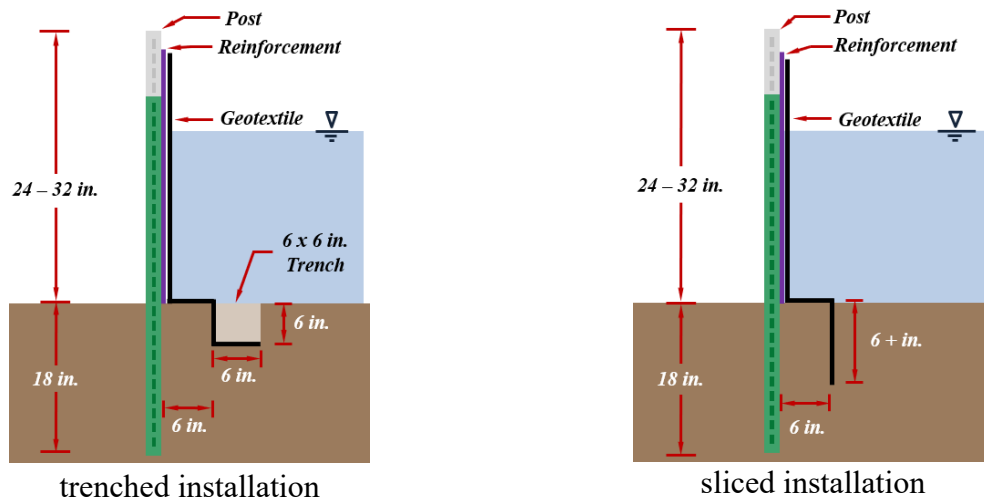


**Figure 2.3 Recommended Silt Fence Installation Techniques**

## 2.7. Maintenance Considerations

As eroded sediment is captured by the silt fence after a runoff event, the inspection of silt fence is necessary and required to identify any signs of damage or deterioration. Several common failures modes can occur: (a) structural failure, (b) undercutting, (c) lack of maintenance; (d) unintended overtopping, and (e) improper installation (Zech et al. 2007). If any silt fence damage or undercutting is identified, immediate repair or replacement is required. In addition, when the accumulated sediment reaches 50% of the storage volume, removal of the accumulated sediment is a commonly accepted maintenance practice.

The Revised Universal Soil Loss Equation (RUSLE) can be used to estimate the annual soil loss from construction areas (Wischmeier and Smith 1978). The principles of RUSLE were used to develop an estimate of when silt fence maintenance may be required. RUSLE considers

five factors: precipitation, soil type, topography, erosion control, and sediment control practices, which generate a linear relationship as stated in Eq. 2.15.

$$A = R \times K \times LS \times C \times P \quad \text{Eq. 2.15}$$

$A$  is annual soil loss due to erosion, t/ha/yr (t/ac/yr),  $R$  is the rainfall erosivity factor,  $K$  is the soil erodibility factor,  $LS$  is the topographic factor derived from slope length and slope gradient,  $C$  is the cover and management factor, and  $P$  is the erosion control practice factor. Using local hydrologic, soil, and topographic inputs, a soil loss rate can be determined from the model. Converting the weight of soil loss to a volume using bulk soil density, the resulting storage volume occupied by eroded soil and the time to occupy the silt fence storage volume can be estimated. This approach can be used by state highway agencies and local municipalities to estimate the number of required silt fence clean-outs during the bid tabulation development process.

## **2.8.SILTSPREAD Silt Fence Design Tool**

To assist and streamline the developed design approach, a Microsoft Excel<sup>®</sup> spreadsheet-based tool (SILTspread) was developed. The tool is made available for download free of charge at: <http://www.eng.auburn.edu/research/centers/auescft/tools/siltspread.html>. This spreadsheet tool can be used by E&SC designers to size silt fence sediment barriers while determining the design volume and design peak flow rates. In addition, the tool allows for estimating the number of maintenance cycles expected for each segment of silt fence. The tool is divided into multiple ‘Drainage Area’ (DA) sheets and a single ‘Summary’ sheet. The tool allows users to develop individual drainage area worksheets for each silt fence segment, accommodating up to 30 drainage areas. For large projects, multiple workbooks may be used.

The ‘DA’ sheets allow designers to input hydrologic characteristics of the contributing drainage area for up to three phases of construction. The sheet calculates runoff volume and peak

flow rates using the NRCS TR-55 methodology (Cronshey 1986). In addition, RUSLE analyses, Figure 2.4(a), is incorporated into the 'DA' sheets to calculate annual soil loss for each drainage area. The *LS-factor* is calculated based on inputs of slope length, slope gradient, and information about mulching or established vegetation. The *C-factor* is selected from a drop-down list corresponding to different erosion control practices. The *K-factor* and *P-factor* are manual entries. The *R-factor* is determined based on geographic area. Results of the hydrologic and RUSLE analyses (i.e., runoff volume, peak flow, and annual soil loss) are automatically transferred to the 'Summary' sheet.

Hydrologic Analysis: DB 1						Units: U.S.
<b>Phase I</b>						
Land Cover Type	Description	HSG	CN	Area	Unit	
Newly_Graded_Areas	Pervious areas only no vegetation	B	86	0.11	ac	
-Select Land Cover Type-					ac	
-Select Land Cover Type-					ac	
<b>Phase II</b>						
Land Cover Type	Description	HSG	CN	Area	Unit	
Newly_Graded_Areas	Pervious areas only no vegetation	B	86	0.11	ac	
-Select Land Cover Type-					ac	
-Select Land Cover Type-					ac	
<b>Phase III</b>						
Land Cover Type	Description	HSG	CN	Area	Unit	
Newly_Graded_Areas	Pervious areas only no vegetation	B	86	0.11	ac	
-Select Land Cover Type-					ac	
-Select Land Cover Type-					ac	
<b>Hydrologic Calculations</b>						
Parameter	Phase I	Phase II	Phase III	Unit		
Total Area	0.11	0.11	0.11	ac		
Weighted CN	86	86	86	-		
Pot. Max. Retention after Runoff, S	1.6	1.6	1.6	in		
Initial Abstraction, I <sub>a</sub>	0.3	0.3	0.3	in		
Rainfall Depth, P	4.2	4.2	4.2	in		
Runoff, Q	2.7	2.7	2.7	in		
Runoff Vol.	1,136	1,136	1,136	ft <sup>3</sup>		
I <sub>a</sub> /P	0.1	0.1	0.1	-		
Rainfall Distribution	Type III	Type III	Type III	-		
Est. Unit Peak Discharge, q <sub>a</sub>	650	650	650	ft <sup>3</sup> /s/m <sup>2</sup> /m		
Peak Discharge, Q <sub>p</sub>	0.32	0.32	0.32	ft <sup>3</sup> /s		

Soil Loss Analysis: DB 1						Units: U.S.
<b>Phase I</b>						
Type	Description	Application (tons/ac)	Land Slope (%)	Length Limit (ft) <sup>1</sup>	C	
Construction Site Mulching	Straw or hay, tied down by anchoring and tacking equipment	1.5	1-5	300	0.12	
Type	Description	Cover (%)	Plant Type	% surface covered by residue in contact with soil:	C	
Established Plants						
<b>Phase II</b>						
Type	Description	Application (tons/ac)	Land Slope (%)	Length Limit (ft) <sup>1</sup>	C	
Select a C Factor Type						
Type	Description	Cover (%)	Plant Type	% surface covered by residue in contact with soil:	C	
Established Plants	Grass, grasslike plants, or decaying compacted plant litter.	0	Grass	95+	0.003	
<b>Phase III</b>						
Type	Description	Application (tons/ac)	Land Slope (%)	Length Limit (ft) <sup>1</sup>	C	
Select a C Factor Type						
Type	Description	Cover (%)	Plant Type	% surface covered by residue in contact with soil:	C	
Established Plants	Grass, grasslike plants, or decaying compacted plant litter.	0	Grass	95+	0.003	
<b>RUSLE Calculations</b>						
Parameter	Phase I	Phase II	Phase III	Unit		
Total Area	0.11	0.11	0.11	ac		
Rainfall Erosibility, R	350	350	350	in		
Soil Erodibility Factor, K	0.2	0.2	0.2	in/ft <sup>3</sup>		
Soil Bulk Density	83.0	83.0	83.0	lb/ft <sup>3</sup>		
Slope Length	36.0	36.0	36.0	ft		
Slope Gradient	5.0	5.0	5.0	%		
Topographic Factor, LS	0.1	0.1	0.1	-		
Cover and Management Factor, C	0.120	0.003	0.003	-		
Erosion Control Practice Factor, P	1.0	1.0	1.0	-		
Annual Soil Loss, A	0.0723	0.0018	0.0018	tons/yr		
Total Soil Loss (Vol.)	0.0001	0.0000	0.0000	ft <sup>3</sup>		

(a) DA sheet

Design Summary Sheet - Pg. 1										Units: U.S.
<b>Project Information</b>					<b>Rainfall Parameters</b>					
Project:	PI 0001				SCS Distribution Type:	Type III				
State:	AL				2-yr, 24-hr rainfall:	4.20 in.				
County:	Lee				NOAA ATLAS 14					
Designer:	Test									
<b>Design Parameters</b>										
Area ID	Installation Configuration	h	W	L	a	z <sub>1</sub>	z <sub>2</sub>	R	Storage Vol.	
		ft	ft	ft	ft	ft/ft	ft/ft	ft	ft <sup>3</sup>	
1	Linear	2.5	0	140		17			2,975	
2	J Hook	2.5				17	12		1,625	
3	J Hook	2.5				15	7		839	
4	J Hook	2.5				23	4		703	
5	Half C Shape	2.5			35			18	263	
6	Half C Shape	2.5			12			2	10	
7	C Shape	2.5			98			14	1,143	
8	C Shape	2.5			92			7	537	
9	Linear	2.5	0	400		6			3,000	
10	Linear	2.5	0	48		42			2,520	
11	Linear	2.5	15	40		14			2,200	
12	Linear	2.5	8	30		18			1,256	
13	J Hook	2.5				3	16		375	
14	J Hook	2.5				20	4		625	
15	C Shape	2.5			71			21	1,243	
16	Half C Shape	2.5			20			13	106	
17										
18										

Design Summary Sheet - Pg. 2															
<b>Phasing Schedule</b>															
Phase	Description	Start	End	Days	Maint. Cycles										
I	Predeveloped (existing) contours, cleared and grubbed.	1/1/20	2/28/20	58	0.0										
II	Final contours/ building pads, no parking lots, no vegetation	2/29/20	7/1/20	123	0.0										
III	Final grading, permanent features installed, no vegetation.	7/2/20	12/31/20	182	0.0										
<b>Hydrologic Analysis Summary</b>															
Area ID	Phase I					Phase II					Phase III				
	Area	Vol.	Q <sub>p</sub>	Soil Loss	Maint. Cycles	Area	Vol.	Q <sub>p</sub>	Soil Loss	Maint. Cycles	Area	Vol.	Q <sub>p</sub>	Soil Loss	Maint. Cycles
	ac	ft <sup>3</sup>	ft <sup>3</sup> /s	tons	#	ac	ft <sup>3</sup>	ft <sup>3</sup> /s	tons	#	ac	ft <sup>3</sup>	ft <sup>3</sup> /s	tons	#
1	0.11	1,136	0.32	0.01	0.0	0.11	1,136	0.32	0.00	0.0	0.11	1,136	0.32	0.04	0.0
2	0.11	1,114	0.31	0.03	0.0	0.11	1,114	0.31	0.00	0.0	0.11	1,327	0.37	0.08	0.0
3	0.10	983	0.27	0.03	0.0	0.10	983	0.27	0.00	0.0	0.10	1,193	0.33	0.08	0.0
4	0.08	751	0.21	0.02	0.0	0.08	751	0.21	0.00	0.0	0.09	1,035	0.29	0.07	0.0
5	0.25	2,522	0.71	0.07	0.0	0.02	197	0.06	0.00	0.0	0.02	286	0.08	0.02	0.0
6	0.17	1,213	0.34	0.04	0.0	0.00	36	0.01	0.00	0.0	0.00	52	0.01	0.00	0.0
7	0.16	1,625	0.45	0.03	0.0	0.05	518	0.14	0.00	0.0	0.05	629	0.18	0.03	0.0
8	0.08	817	0.23	0.02	0.0	0.06	564	0.16	0.00	0.0	0.06	728	0.20	0.04	0.0
9	0.10	951	0.27	0.01	0.0	0.09	905	0.25	0.00	0.0	0.09	1,315	0.37	0.04	0.0
10	0.07	730	0.20	0.02	0.0	0.07	674	0.19	0.00	0.0	0.07	818	0.23	0.05	0.0
11	0.20	1,995	0.56	0.05	0.0	0.05	475	0.13	0.00	0.0	0.05	577	0.16	0.04	0.0
12	0.15	1,466	0.41	0.04	0.0	0.07	684	0.19	0.00	0.0	0.07	830	0.23	0.06	0.0
13	0.31	3,040	0.85	0.09	0.0	0.33	3,393	0.95	0.00	0.0	0.33	4,414	1.23	0.29	0.0
14	0.44	4,329	1.21	0.12	0.0	0.19	1,865	0.52	0.00	0.0	0.19	2,525	0.71	0.16	0.0
15	0.03	266	0.07	0.01	0.0	0.03	266	0.07	0.00	0.0	0.03	386	0.11	0.02	0.0
16	0.04	416	0.12	0.01	0.0	0.04	416	0.12	0.00	0.0	0.04	605	0.17	0.03	0.0
17															
18															

(b) Summary sheet

Figure 2.4 SILTspread Tool.

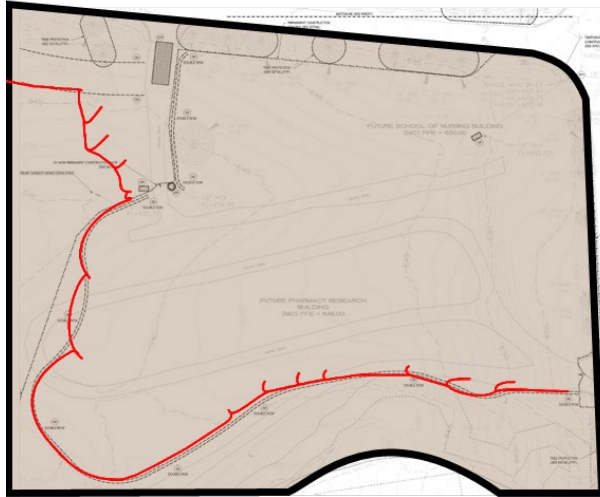
## 2.9. Case Study

To demonstrate the developed design process and design tool, a case study was performed on a 2.5 ha (6.3 ac) construction project located in Auburn, AL consisting of a 1.8 ha (4.4 ac) impervious areas and a 0.76 ha (1.9 ac) vegetated area. The site consists of primary Marvyn loamy sand, (55.8% sand, 26.5% clay, and 17.7% silt). The 2-yr, 24-hr rainfall depth for the project location is 10.7 cm (4.20 in.) (National Oceanic and Atmospheric Administration's National Weather Service 2014). Phases were divided across a 12-month construction schedule with durations of 58, 123, and 182 days, for Phases I, II, and III, respectively.

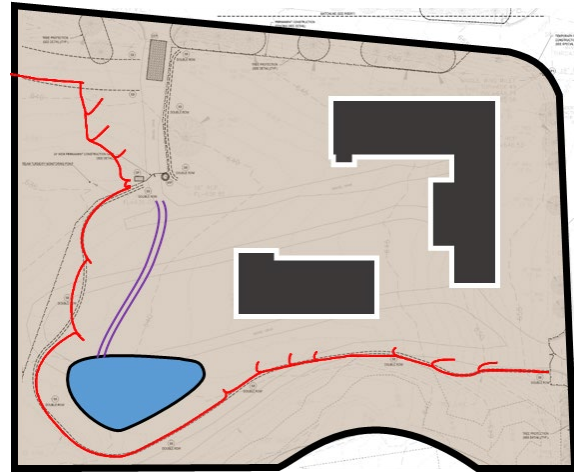
The final construction phase was used to layout 16 silt fence segments, shown in red in Figure 2.5. Drainage areas for each silt fence segments were delineated across the three construction phases, Figure 2.6. Drainage basin delineations were conducted manually for each phase of construction by examining contour lines on construction drawings using the software Bluebeam Revu<sup>®</sup>, however, computer-aided design (CAD), geographic information system (GIS), or manual methods could also be used. Each of these drainage areas were input into individual 'DA' sheets within the SILTspread workbook. Characteristics for area, storm sewer infrastructure, impervious areas, hydrologic soil group, and cover conditions were used for each phase of construction. Initial results indicated the developed silt fence design failed in 11 subareas in the Phase I condition. The Phase I condition was characterized by large drainage areas as it preceded the implementation of stormwater infrastructure. To create a functioning silt fence design, an alternative Phase I, Phase IA, was developed. Phase IA includes the addition of diversion channel and sediment basin. This channel intercepts runoff and directs it to the sediment basin.

After completing the silt fence design, maintenance cycles were evaluated. The first step was to estimate the annual soil loss for each subarea using RUSLE. *R-factor* were referenced from

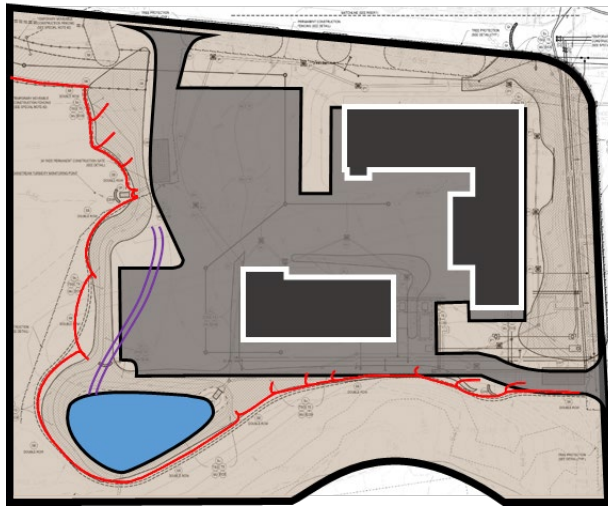
the USEPA according to the latitude and longitude of site location during the project period (USEPA 2019). The *K-factor* was obtained from the USDA Web Soil Survey (USDA 2019). The *LS-factors* were calculated through measurements slope and distance in the construction plan sets. *C-factors* based on the land cover type expected on site were selected based on typical cover management practices used on construction sites (i.e. temporary straw mulching and seeding). *P-factors* of 1.0 were used for the upstream of the silt fence in this case study (i.e., no sediment control practices installed upstream of the slope). The total volume of soil loss was calculated by using dividing the annual soil loss by the bulk soil density  $1.33 \text{ g/cm}^3$  ( $83 \text{ lb/ft}^3$ ). The calculated soil loss volume per year multiplied by the project duration for each phase and then divided by half of the storage volume of the silt fence was used to estimate the maintenance cycle. It was found that there should be no need to remove sediment upstream of the silt fence during the duration of this particular project.



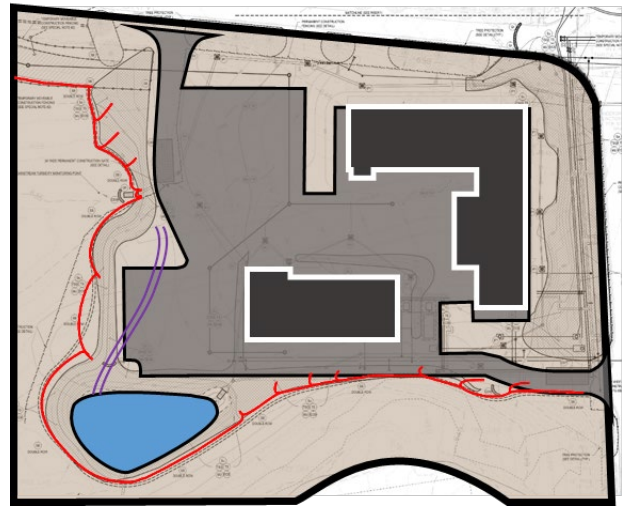
Phase I



Phase IA



Phase II



Phase III

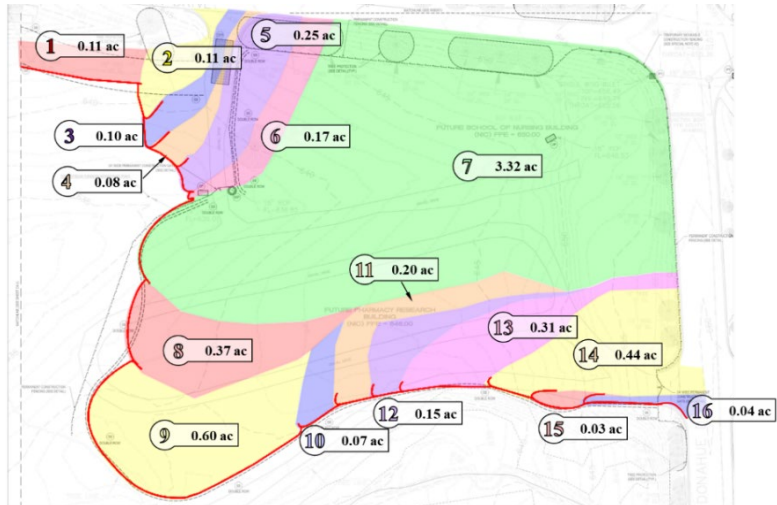
Notes:

[1] drawings not to scale

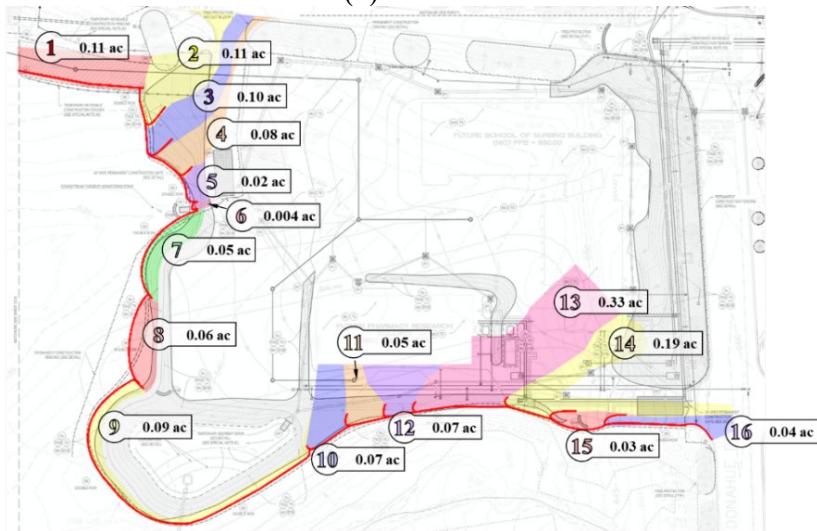
[2] brown fill: exposed soil, red polyline: silt fence layout, purple polyline: channel, blue fill: sediment basin, black fill: building, gray fill: impervious area.

**Figure 2.5 Defined Phases in Case Study.**

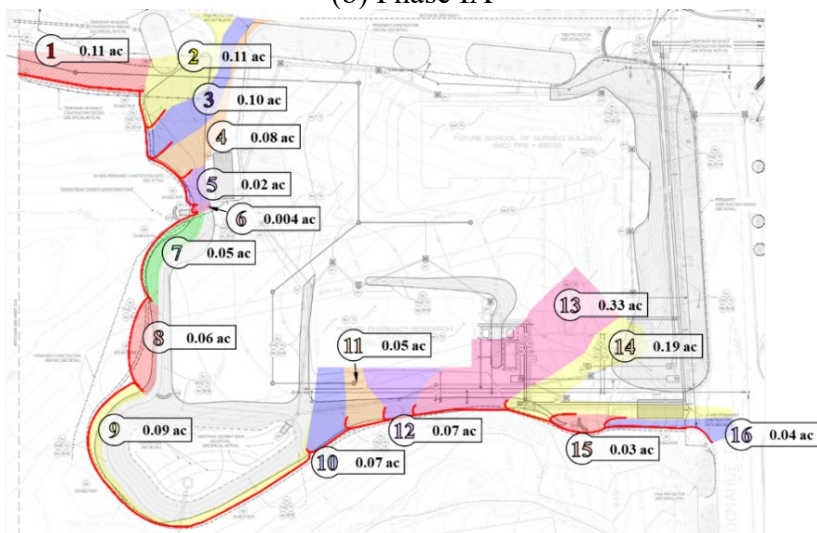




(a) Phase I



(b) Phase IA



(c) Phase II & III

Figure 2.6 Drainage Areas in the Defined Phases (drawings not to scale).

## 2.10. Implementation Pathway

Even through the use of SILTspread, conducting a hydrologic analysis for each silt fence segment across three phases on a construction site may not be practical, especially for large projects. One approach that can be taken by state agencies is to apply the principals of the developed silt fence sediment barrier design methodology to create state-specific silt fence design guidelines. Standardized silt fence dimensions along with spacing guidelines can be used to develop design charts to quickly determine the storage capacity of a silt fence segment. Average 2-yr, 24-hr rainfall depths and typical soil CN's could be used to simplify the hydrologic analysis process. Geographically larger states, or those with diverse climates, could be divided by region or Department of Transportation (DOT) districts to allow for several zones. Simplified VSF and Peak Flow Sizing Factors ( $Q_{PSF}$ ) can be determined using average rainfall conditions, soil type, and cover characteristics. An example of a proposed simplified Alabama silt fence design standard using ALDOT regions and CN of 91, representative of newly graded areas with hydrologic soil group of C, typical of highly compacted soils. The VSF and  $Q_{PSF}$  can be multiplied against the contributing drainage area in acres (ha) to determine the volume and peak flow. Standard weir dimensions and capacities can also be provided in design guidance.

**Table 2.2: Sizing Factors as a Function of Contributing Drainage Area.**

<b>ALDOT Region</b>	<b>Avg. P<sub>2-yr, 24-hr</sub> cm (in.)</b>	<b>SCS Storm Distribution</b>	<b>VSF m<sup>3</sup> (ft<sup>3</sup>)</b>	<b>Q<sub>PSF</sub> m<sup>3</sup>/s (ft<sup>3</sup>/s)</b>
North	10.19 (4.01)	Type II	10,988A	4.73A
East Central	10.41 (4.10)	Type III	11,301A	3.19A
West Central	10.59 (4.17)	Type III	11,545A	3.25A
Southeast	12.28 (4.44)	Type III	12,488A	3.52A
Southwest	12.65 (4.98)	Type III	14,385A	4.06A

*Note: A indicates area in ac (ha)*

## **2.11.Conclusions**

Construction activities disturb large areas of land which leads to an increased risk of downstream water quality degradation. Local, state, and federal regulations require the use of E&SC practices to protect receiving water bodies. Silt fence sediment barriers are common sediment control practices used to protect areas downstream of construction sites from sediment-laden discharge. The widely-accepted design standard of 0.1 ha (0.25 ac) and 0.2 ha (0.5 ac) of contributing drainage area for every 30.5 linear m (100 ft) of unreinforced or reinforced silt fence lacks sound engineering backing and fails to meet the intent of the USEPA CGP to provide site-specific design standards for E&SC practices. This research developed a universally applicable silt fence design standard founded on volumetric-sizing criteria while implementing performance-based research results. A hydrologic design approach and volumetric storage relationships were developed for three standard silt fence installation configurations: linear, J-hook, and C-shape. The design approach provides guidance for dewatering and overtopping through the implementation of the dewatering board and overflow weir. The methodology developed through this research can be applied at a local level using site-specific hydrologic and topographic conditions.

The SILTspread spreadsheet-based tool was developed to simplify the application of the silt fence design approach by incorporating the automation of hydrologic design calculations, silt fence segment volumetric sizing, and estimation of maintenance needs. This developed tool is applicable for various types of projects and locations, due to the ability to manually enter the basic site-specific data. A case study was conducted to highlight the applicability of the SILTspread tool. The case study analysis demonstrated how the tool could be used to determine the placement of additional E&SC practices to minimize the hydrologic load on silt fence sediment barrier

segments. The design approach developed through this research has applicability to most other sediment barrier practices and can be modified to provide sound hydrologic design approaches. Finally, this research presented guidelines for a state agency to adopt and implement the presented design methods using VSF and Q<sub>p</sub>SF estimation approaches.

## CHAPTER 3. BENCH-SCALE LAMELLA SETTLER EXPERIMENTS

### 3.1. Introduction

Stormwater quality has become an increasingly important topic across the agricultural, urban, and construction sectors (Nayebare et al. 2014). Construction sites, in particular, have the potential to create the greatest sources of sediment pollutants that can have profound impacts on the downstream environment (Barrett et al. 1995). Compared to other land uses, construction operations produce a large amount of sediment yield due to earth disturbing activities. In addition to sediment, pollutants carried by soil particles (i.e., nutrients, heavy metals, petrochemicals, etc.) create adverse water quality impacts to downstream receiving water bodies (Reardon 2005). Sediment-laden stormwater runoff can contribute to turbidity plumes, which impact biological structure, ecological functions, and biotic diversity (Donohue and Garcia Molinos 2009; Vasconcelos et al. 2014). To minimize these impacts, stormwater is managed through the use of passive “best management practices” (BMPs). For example, urban stormwater may be managed by detention basins, bioretention cells, and enhanced swales; agricultural stormwater is treated through bioreactors, saturated buffers, and constructed wetlands; and construction sites rely on a suite of erosion and sediment control practices to prevent soil loss and capture eroded soil particles (Forrest and Harding 1994b). While performance-based research has proven the effectiveness of sediment capture for many stormwater BMPs, fine-grained soil particles (i.e., clay and silt with particle sizes  $< 0.05$  mm [0.002 in.]) are challenging to capture with current practices. To capture these fine-grained particles and reduce runoff turbidity, stormwater practices rely primarily on the use of extended detention. Extended detention refers to the process of retaining sediment-laden stormwater to allow fine soil sedimentation to occur prior to offsite discharge. Sediment basins are often used to provide extended detention, which can often require days or weeks to provide

sufficient residence time for microscopic grain particles to settle out of suspension (Leung and Probsteln 1983).

In construction and post-construction applications, chemical-based flocculants are often used with detention-based practices (e.g., sediment basins, sediment traps, detention basins, etc.) to increase sedimentation rates by inducing inter-particle attraction through Brownian motion assisted by turbulent mixing and self-settling (Vasconcelos and Zech 2017). When used in conjunction with extended detention, flocculants can be highly effective in reducing turbidity and TSS (Shih et al. 2001). In construction applications, on-site contractors rely primarily on passive dosing of flocculants through a variety of forms, such as: powders, blocks, and socks. These forms are designed to facilitate flocculant dosing as runoff passes by them, causing dissolution. Regular maintenance is required to keep blocks and socks from over-drying and silting over, which reduce dosing capabilities. Furthermore, the use of powder flocculant requires reapplication following rain events. The effective use of flocculants at field-scale is challenging for several reasons. To begin with, some flocculants are soil-specific and require soil testing (Shih et al. 2001). While soils vary regionally, soil types can also vary greatly across a site. Soil samples used to test for optimum flocculant type and dosage rate may not be a uniform representation of the soil variations across the site, which often results in ineffective use of a flocculant type and/or dosage rate (Teh et al. 2016). For proper contact, dosing of flocculants requires flowing water with a moderate velocity and agitation. In addition, U.S. Environmental Protection Agency (USEPA) regulations require that a sediment control practice, such as a sediment basin, be used downstream to capture flocculated material and prevent resuspension (US Environmental Protection Agency (USEPA) 2017).

The challenges associated with the use of flocculants on construction sites provides an opportunity for innovative passive systems that can be used to provide similar treatment without the use of chemicals. Lamella settlers are one potential technology that can improve sediment capture efficiency by modifying the geometry of a settling chamber. These systems are passive treatment mechanisms traditionally used in wastewater and industrial water treatment applications which consist of a series of inclined parallels that provide increased surface contact area for promoting settling area for suspended solids (Kong, Application, and Data 2011). As shown in Figure 3.1, when lamella settlers are used for stormwater treatment, narrow spacing between parallels decrease vertical sedimentation distance while also reducing flow velocity. The parallel plate system creates laminar flow, by directing flow between the plates where suspended solids settle from water (Weiss 2016). To study the efficiency of lamella settlers, soil turbidity, TSS, and soil grain size distribution were measured and analyzed by researchers (Nguyentranlam and Galvin 2001; Vasconcelos and Zech 2017). Turbidity and total suspended solids (TSS) are general parameters used to assess water quality. Turbidity is a measure of the amount of light that can pass through a water sample, which is an indicator for water clarity. The lower the turbidity, the less particulates are associated with the sample. TSS is the measurement of mass per unit volume (mg/L) of suspended material in a sample and is determined by removing all water through filtration and evaporation.

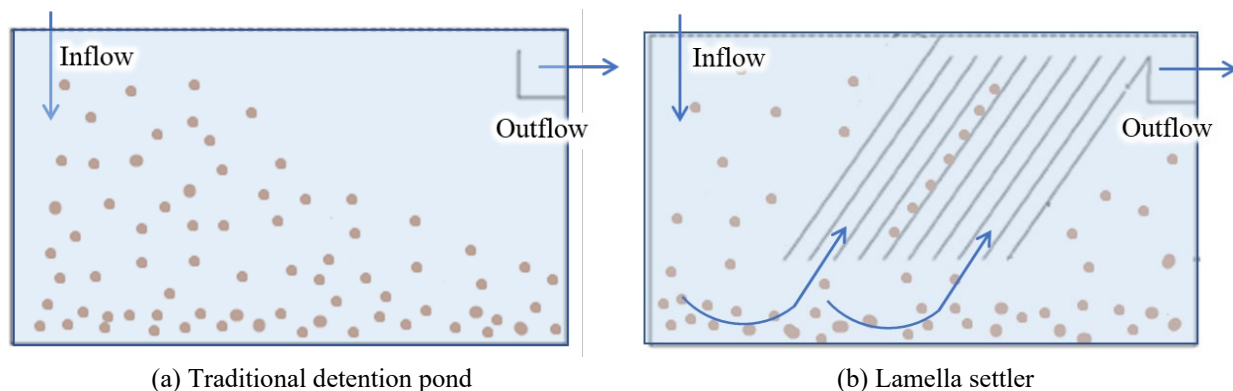


### **Figure 3.1 Lamella Mechanism.**

Recent large-scale testing research of high rate lamella settlers suggested that they could be an effective approach to treat construction site stormwater runoff, improving sediment capture by up to 33% when compared to traditional sediment basin designs (Perez et al. 2019). In addition, research has proved that surface area determines the sedimentation performance in lamella settlers (Weiss 2016). A recent study conducted by Nguyen et al. (2019) suggested that definitive relationships among treatment efficiency design factors have yet to be identified for treatment systems such as these. Thus, additional research is needed to identify design factors influencing sediment capture efficiency.

### **3.2. Research Objectives**

Many design factors (e.g., wetted surface area, settling distance, influent concentration, residence time, flow rate, etc.) can influence the performance of lamella settlers. The purpose of this research effort was to analyze sediment capture capabilities of various lamella system design configurations using bench-scale lamella reactors. This research sought to bridge the gap between theoretical knowledge and practical application of lamella settlers by conducting experiments to determine the settling performance across several design factors. A Full-Factorial Method (FFM) statistical analysis was conducted to estimate influence of different design factors (e.g., sediment concentration, particle settling distance, and residence time) on efficiency of evaluated treatments. The design factors were independent variables used for analysis, and the calculated turbidity reduction rates between influent and effluent water samples were dependent variables. Ultimately, results obtained from this research effort provide design guidance for developing field-scale lamella systems to treat polluted stormwater runoff.



### 3.3. Materials and Methods

#### 3.3.1. Lamella Settler Design

As shown in Figure 3.2, three reactor tanks were designed and constructed for this study: R<sub>A</sub>: control reactor, without lamella plates, R<sub>B</sub>: 9 lamella plates at 2.5 cm (1.0 in.) spacing, and R<sub>C</sub>: 18 lamella plates with 1.3 cm (0.5 in.) spacing. The settling distance, or the vertical distance between plates, were 31.5 cm (12.5 in.), 3.6 cm (1.4 in.), and 1.8 cm (0.7 in.), for R<sub>A</sub>, R<sub>B</sub>, and R<sub>C</sub>, respectively. R<sub>A</sub>, the control reactor, was run to provide a direct comparison of performance. These tempered glass reactor tanks measured 55 cm (21.0 in.) x 32 cm (12.5 in.) x 34 cm (13.5 in.) (length x width x height). Each reactor was outfitted with a rectangular weir with three 0.43 cm (0.17 in.) diameter orifices to discharge water from the surface of the tanks. The control reactor tank had no plates inserted and was treated as a base comparison by simply providing detention in an open reactor. R<sub>B</sub> and R<sub>C</sub> contained acrylic sheets that were 25 cm (9.8 in.) wide by 25.4 cm (10 in.) long and installed at a 55° angle. The plate angle was determined based on optimized industrial water treatment designs for lamella settlers (Vasconcelos et al. 2014). Plates were sealed to the sides of the reactor tank and situated 8.8 cm (3.5 in.) from the base of the reactor.

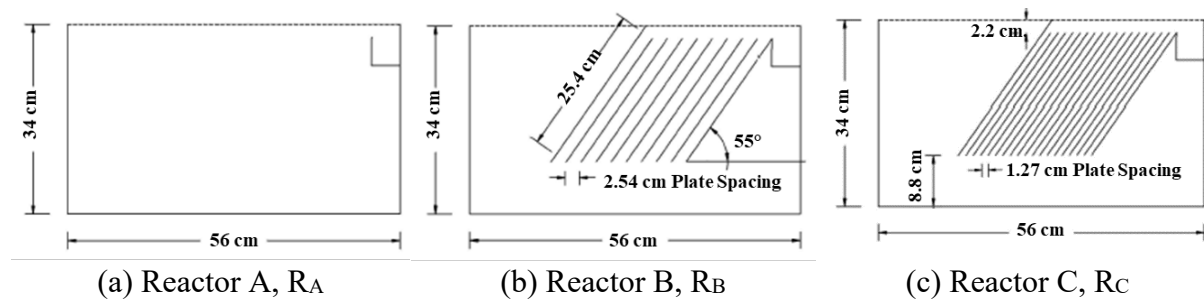


**Figure 3.2 Reactor Tank Design Profiles.**

### ***3.3.2. Sample Preparation and Flow Introduction***

Lamella settlers are intended to improve the settling efficiency of fine-grain particles by decreasing settling distance. Thus, the focus of the evaluations was on fine clay and silt sized particles that are difficult to remove from suspended surface runoff. Five different synthetic soils were selected based on their small grain size diameters, which correlate closely with naturally occurring silt and clay particles. Synthetic soils were selected due to homogeneity and uniformity in material that would minimize inter-batch discrepancies. With exception of Soil E and Soil F, all soil information was obtained through manufacturer's technical data sheets. Soil A was Imsil<sup>®</sup> A25 (25.0% clay, 75.0% silt), a microcrystalline silica filler produced from a natural alpha quartz with a density of 2.65 g/cm<sup>3</sup> (165.4 lb/ft<sup>3</sup>). Soil B, SNOBRITE<sup>®</sup> S75 (19.1% clay, 80.9% silt) and Soil C, SNOBRITE<sup>®</sup> S60 (18.5% clay, 80.3% silt, 1.2% sand), were white extender pigment produced from air floated intermediate kaolin, each with a density of 2.77 g/cm<sup>3</sup> (172.9 lb/ft<sup>3</sup>). Soil D, MINEX<sup>®</sup> M4 (10.1% clay, 89.9% silt), is produced for use as a filler by from nepheline syenite, a natural sodium potassium alumina silicate, an igneous rock (combination of nepheline, microcline, albite, and minor minerals such as mica, hornblende and magnetite). The density of Soil D was 2.60 g/cm<sup>3</sup> (162.3 lb/ft<sup>3</sup>). Soil E and F, Kaolin, primary consists of mineral kaolinite (Al<sub>2</sub>[OH]<sub>4</sub>Si<sub>2</sub>O<sub>5</sub>) with a density of 2.65 g/cm<sup>3</sup> (165.4 lb/ft<sup>3</sup>). The mineral kaolinite (hydrous aluminum silicate) forms from feldspar or other aluminum silicate under chemical weathering. Preliminary pilot tests indicated that Soil E was difficult to uniformly suspend in solution due to its natural tendency to coagulate and flocculate. Solutions prepared through rapid mixing provided inconsistent turbidity measurements. To overcome this limitation with Soil E, a deflocculant agent was added by applying sodium hexametaphosphate prior to suspending in water. Deflocculation is a technique widely applied for soil particle size analysis. Following ASTM D6913/D6913M

standard method, 40 mg/L of sodium hexametaphosphate was prepared with distilled water (ASTM 2009). Soil E was submerged in the prepared solution for 12 hours. The results of deflocculation are shown through the departed spacing of kaolinite particles in the microscopy observations. The treated kaolinite soil is referred to as Soil F. Comparing to other soil samples, Soil A had the smallest fraction of clay, which was expected to result in the lowest turbidity removal compared to other soils under same treatments.

To calculate the particle settling velocities, the median grain sizes and shape factors for the tested samples were used as shown in Table 3.1.

**Table 3.1 Soil Information**

ID	Soil Name	Mineral	Gradation			Median Size, microns, $\mu\text{m}$ (in.)	Specific Gravity	Shape Factor
			Clay, %	Silt, %	Very Fine Sand, %			
Soil A	Imsil <sup>®</sup> A25	Quartz	25.0	75.0	-	5.0 (0.0002)	2.65	0.83
Soil B	Snobrite 75	Kaolin	19.1	80.9	-	0.5 (0.00002)	2.77	0.77
Soil C	Snobrite 60	Kaolin	18.5	80.3	1.2	1.2 (0.00005)	2.77	1.25
Soil D	Minex 4	Nepheline Syenite	10.1	89.9	-	6.8 (0.0003)	2.60	0.67
Soil E & F	Kaolin	Kaolinite	-	-	-	5.0 (0.0002)	2.65	0.81

In addition, SEM was conducted to show shapes of soil particles through the detailed microscopy scanned images at 150% zoom provided in Figure 3.3. SEM is employed in mineral study with a variety of additional signals are generated through electron microscopes. The high-resolution images can help understating geological properties of soil samples. SEM is the instrument consisted of five primary components (electron gun, condenser lens, apertures, objective lens and sample chamber, and detectors). The electron gun emits the electron beam which will be narrowed in the condenser lens. The apertures can control the diameter of the electron beam, the objective lens will focus electron beam and sample chamber is the place to hold the sample preventing interference from unwanted particles. Finally, detectors are used to create magnified images and collect data.

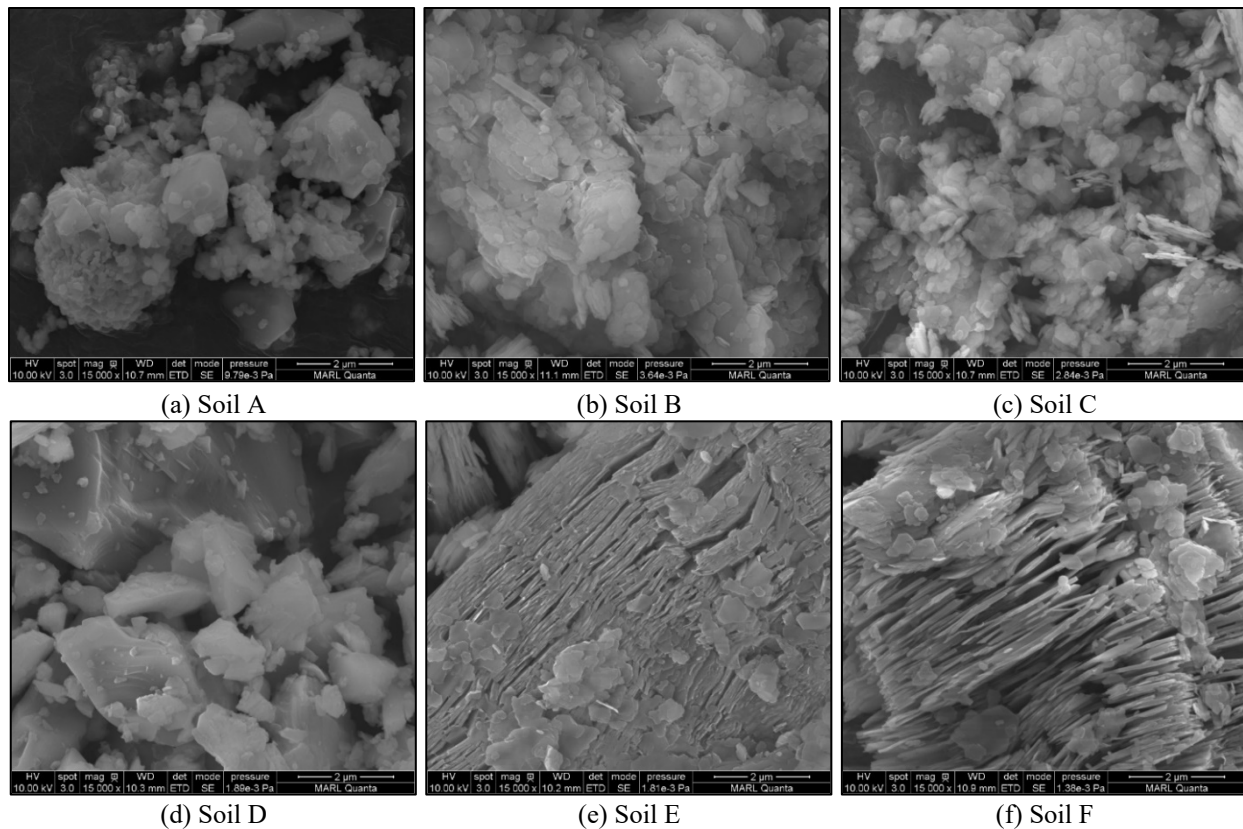


**Figure 3.3 Sample Scanned Electron Microscope Results.**

Performance of the lamella settler reactors was evaluated across three suspended soil concentrations (500 mg/L, 1,000 mg/L and 5,000 mg/L) of simulated runoff. Field monitoring of erosion and sediment control practices has shown that TSS levels in treated construction site stormwater runoff are often around or below 1,000 mg/L (Fang, Zech, and Logan 2015; Markusic 2007). For this study, two concentrations including 500 mg/L and 5,000 mg/L were selected to simulate a low and high range in sediment concentration and can be correlated to construction site stormwater runoff upstream and downstream of a sediment basin.

Experiments were designed to introduce simulated sediment-laden stormwater at the inflow of the reactors. Flow was introduced and controlled to achieve one of three desired residence time: 1.5 hr - 0.42 L/min (0.11 gal/min), 1.0 hr - 0.64 L/min (0.17 gal/min), and 0.5 hr - 1.25 L/min (0.33 gal/min). A ColeParmer® pump drive (model 7591-50) and a MasterFlex®

pump controller were used to transfer solutions from mixing drums to reactor tanks. Sediment-laden stormwater was prepared in two inter-connected 208 L (55 gal.) drums by mixing synthetic soil with 132 L (35 gal.) of room-temperature tap water at a ratio equal to the target concentration (i.e., 500 mg/L, 1,000 mg/L, and 5,000 mg/L) in each drum. To achieve a homogenous concentration, mixing was provided by 7.6 cm (3 in.) right-handed propeller fitted motors (Eastern Instruments, Model 5VB-C) in each drum with power levels maintained at mid-range for a period of 20 minutes prior to introducing the sample solution into the reactors. The mixers remained in use throughout the duration of the experiments to maintain uniform sediment suspension. These mixers were attached to the top of each drum with custom-built mounts. The experimental testing process and setup are shown in Figure 3.4 and 3.5, respectively.

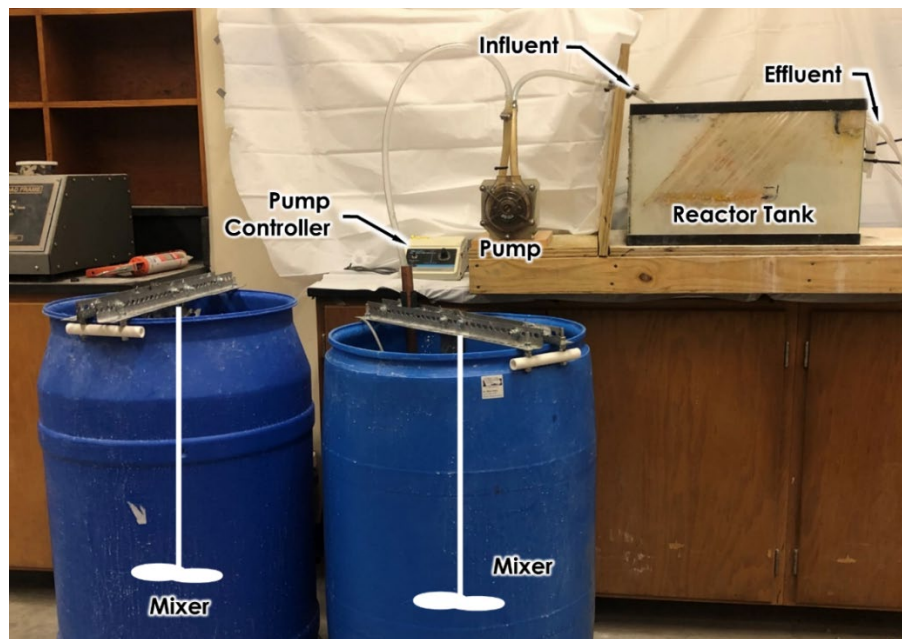


**Figure 3.4 Lamella Reactors Experimental Setup.**

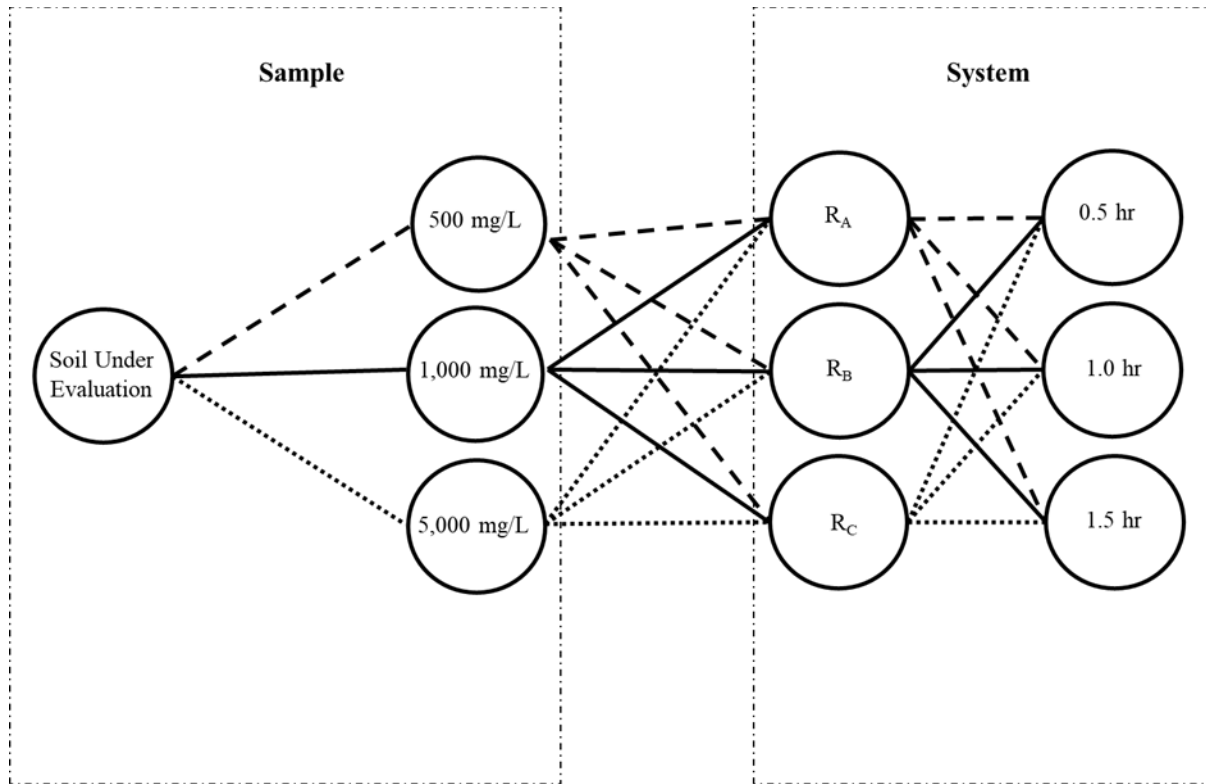


**Figure 3.5 Experimental Procedure.**

### 3.3.3. Turbidity Analysis

Manual grab samples were taken at the surface of the reactor’s inflow and outflow at 5 min. intervals throughout experiments. Turbidity was selected as a measure of performance due to the ease and consistency in the measurement. Inflow and outflow water quality samples were measured using a Hach® 2100Q turbidimeter. Figure 3.6 depicts data from one experiment (Soil A, 1,000 mg/L concentration, 30 min. residence time) to demonstrate data collection and analysis. Collected data were used to determine the average inflow and outflow turbidity rates throughout the experiment. The system’s efficiency was determined by applying Eq.3.1:

$$Turbidity\ Reduction\ \% = \frac{T_i - T_d}{T_i} \times 100\% \quad \text{Eq. 3.1}$$

where  $T_i$  is the inflow turbidity, and  $T_d$  is the discharge turbidity. The greater the turbidity reduction, the more efficient the system. The treatment efficiencies for the example demonstrated in Figure 3.6 are: 7% for  $R_A$ , 16% for  $R_B$ , and 34% for  $R_C$ .

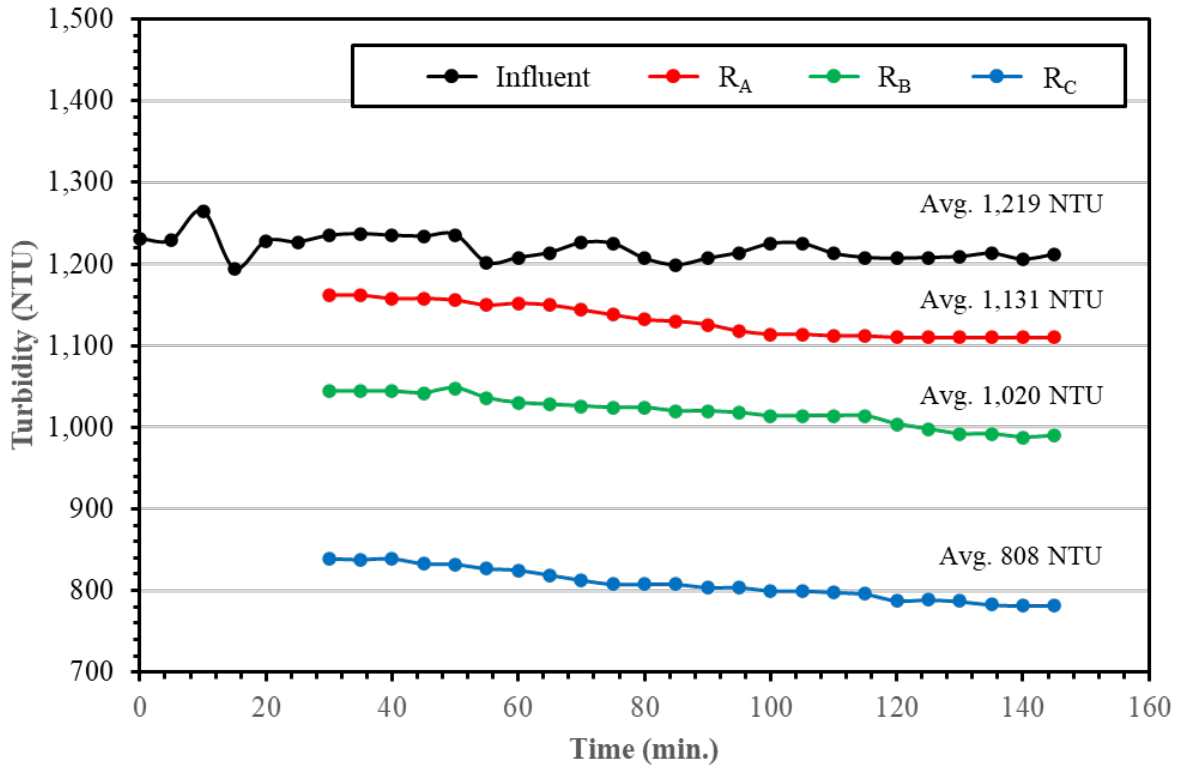


Figure 3.6 Average Turbidity Results for Soil A, 1,000 mg/L, 30 min. Residence Time.

### 3.3.4. Particle Size Distribution (PSD) Analysis

PSD analysis was conducted on samples obtained from 5,000 mg/L samples using a laser spectrometer (Mastersizer® 3000) that is shown in Figure 3.7. The laser spectrometer is capable of measuring PSDs from 10 nm ( $3.94 \times 10^{-7}$  in.) to 3.5 mm (0.14 in.) through laser diffraction technique. This technique uses static light scattering to measure a volume weighted distribution. PSD analysis allowed for the comparison of grain size distribution between inflow and outflow samples. Results from this analysis displayed differences between the  $D_{10}$ ,  $D_{60}$ , and  $D_{90}$ .  $D_x$  is the x% finer diameter found through the size distribution curve. Soil F samples were excluded form

PSD analysis due to the use of deflocculant. A multiple linear regression (MLR) analysis was conducted to evaluate differences across the laser spectrometry.



**Figure 3.7 Mastersizer 3000.**

### ***3.3.5. Settling Velocity Calculation***

The settling time of suspended particles can be modeled through Stokes' law. This method has been widely applied to calculate particle settling velocities in wastewater treatment processes (Azema et al. 2002; Tang and Raper 2002; Vahidifar, Saffarian, and Hajidavalloo 2019). Settling time is a function of a particle's size, specific gravity, and distance to settling surface. Determination of Stoke's settling velocity is shown in Eq.3.2.

$$w_s = \frac{gd^2(\rho_p - \rho_w)}{18\mu} \quad \text{Eq. 3.2}$$



Where,  $w_s$  is settling velocity,  $g$  is gravitational acceleration,  $d$  is particle diameter,  $\rho_p$  is particle density,  $\rho_w$  is water density, and  $\mu$  is dynamic fluid viscosity.

Stokes' law is limited in that it assumes unhindered settling conditions of uniformly sized perfectly spherical particles. Synthetic soils used in this study were mostly angular in shape. To address this inconsistency in particle shape, Eq.3.3 was developed and introduced to calculate the settling velocity more precisely considering gravity acceleration (Vahedi and Gorczyca 2012). In Eq.3.3 the particle density is equal to specific gravity multiplied against water density,  $1 \text{ g/cm}^3$  ( $0.01 \text{ lbs/gal}$ ), which means the values of specific gravity and particle density are equal.

$$(S + C_m) \frac{dw_s}{dt} = (S - 1)g - \frac{F_D}{\rho_p V_s} \quad \text{Eq. 3.3}$$

where  $S$  is specific gravity,  $C_m$  is shape factor,  $w_s$  is settling velocity,  $t$  is settling time,  $F_D$  is frictional force,  $\rho_p$  is particle density,  $V_s$  is volume of sample.

Eq.3.4 can be used to determine settling velocity of different soil samples. Settling velocity was estimated by considering a complete version of force balance without ignoring sample gravity acceleration and inconsistent particle shape. The settling time of a soil particle needed in alternative lamella settler designs can be calculated by integrating the settling velocity equation as shown in Eq.3.5. The results of calculated settling velocities and settling time for different samples can be used to compare with turbidity reductions in the same treatment to determine the model accuracy.

$$w_s = \frac{\rho V_s (S - 1)g}{3\pi\mu d} \left(1 - e^{-\frac{3\pi\mu d}{\rho V_s (S + C_m)} t}\right) \quad \text{Eq. 3.4}$$

$$L = \int_0^t w_s dt = \frac{(S - 1)g\rho V_s}{3\pi\mu d} \left[ \frac{\rho V_s (S + C_m)}{3\pi\mu d} \times e^{\frac{3\pi\mu d}{\rho V_s (S + C_m)} t} + t \right] \Big|_0^t \quad \text{Eq. 3.5}$$

where  $L$  is settling distance. The settling time and velocity calculated with consideration of mass balance were used to estimate settling process throughout the system.

## 3.4.Results

### 3.4.1.Turbidity Reduction

The objective of these experiments was to determine the rate of turbidity reduction as flow passed through the reactors. It was found that turbidity reduction efficiency can be improved when using decreased settling space, increased residence times, or increased inflow sample concentrations as shown in Table 2. The minimum and maximum turbidity reduction rates are shown in bold in Table 2 to highlight the system improvement by modified design parameters. It was found that the averaged turbidity removal rates at the outflow increased from 10.1% in RA to 81.7% in RC with the longest residence time (1.5 hr), where 5,859 NTU to 1,219 NTU (79.2%) for Soil A, 5,610 NTU to 756 NTU (86.5%) for Soil B, 3,748 NTU to 377 NTU (89.9 %) for Soil C, 2,509 NTU to 250 NTU (90.0%) for Soil D, and 4,515 NTU to 1,678 NTU (62.8 %) for Soil F in Reactor C with the longest residence time (1.5 hr). Soil D had the greatest amount of silt (90%) compared to other soils, which can explain why it obtained the greatest turbidity reduction rates compared to other samples. In addition, Soil A, Soil B, and Soil C had similar proportions of clay (<2  $\mu\text{m}$ ), which can explain why they obtained similar turbidity reduction rates. For the treatment of 5,000 mg/L of concentration for 1.5 hour residence time, the turbidity reduction rates of these three soil samples ranged between 50.8 and 56.0% in RA, between 34.7 and 44.4% in RB, and between 20.1 and 41.7% in RC. Based on turbidity reductions calculated from the experiments, the system efficiency was optimized with 1.8 cm (0.7 in.) settling space at 1.5-hour residence time for all tested soils.

**Table 3.2 Turbidity Reduction**

Inflow Concentration	500 mg/L			1,000 mg/L			5,000 mg/L			
	Residence Time	0.5 hr	1.0 hr	1.5 hr	0.5 hr	1.0 hr	1.5 hr	0.5 hr	1.0 hr	1.5 hr
<b>Soil A</b>										
<b>RA</b>	<b>5.3%</b>	10.5%	16.1%	<b>7.6%</b>	11.9%	24.2%	<b>37.2%</b>	44.2%	54.6%	
<b>RB</b>	14.1%	24.1%	39.2%	16.3%	36.3%	52.8%	44.7%	64.1%	73.5%	
<b>RC</b>	30.8%	42.7%	<b>57.3%</b>	32.8%	45.5%	<b>65.5%</b>	55.6%	73.1%	<b>79.2%</b>	
<b>Soil B</b>										
<b>RA</b>	<b>6.6%</b>	18.4%	32.2%	<b>8.0%</b>	22.2%	36.8%	<b>20.1%</b>	34.7%	56.0%	
<b>RB</b>	20.1%	24.3%	46.3%	27.9%	32.5%	52.6%	44.0%	56.5%	71.1%	
<b>RC</b>	28.3%	40.9%	<b>54.3%</b>	34.5%	42.7%	<b>62.9%</b>	57.4%	68.4%	<b>86.5%</b>	
<b>Soil C</b>										
<b>RA</b>	<b>10.1%</b>	23.1%	30.1%	<b>15.1%</b>	27.8%	32.7%	<b>41.7%</b>	44.4%	50.8%	
<b>RB</b>	18.1%	30.7%	41.5%	27.1%	45.9%	50.8%	65.8%	68.9%	77.8%	
<b>RC</b>	32.9%	47.0%	<b>57.0%</b>	36.6%	54.6%	<b>71.6%</b>	73.0%	83.9%	<b>89.9%</b>	
<b>Soil D</b>										
<b>RA</b>	<b>19.2%</b>	32.7%	62.0%	<b>26.5%</b>	44.2%	65.0%	<b>35.1%</b>	63.0%	73.0%	
<b>RB</b>	34.6%	45.0%	74.2%	42.9%	71.2%	81.6%	60.3%	78.1%	81.9%	
<b>RC</b>	42.3%	61.5%	<b>85.9%</b>	64.2%	83.2%	<b>89.8%</b>	74.2%	86.6%	<b>90.0%</b>	
<b>Soil F</b>										
<b>RA</b>	<b>9.5%</b>	23.4%	35.2%	<b>16.2%</b>	26.3%	32.7%	<b>20.6%</b>	25.8%	40.2%	
<b>RB</b>	12.8%	29.0%	42.6%	27.1%	35.7%	46.4%	30.0%	35.2%	53.5%	
<b>RC</b>	26.4%	46.0%	<b>58.5%</b>	39.0%	57.4%	<b>61.7%</b>	39.1%	52.8%	<b>62.8%</b>	
<b>Average of all Soils</b>										
<b>RA</b>	<b>10.1%</b>	21.6%	35.1%	<b>14.7%</b>	26.5%	38.3%	<b>31.0%</b>	42.4%	54.9%	
<b>RB</b>	19.9%	30.6%	48.8%	28.3%	44.3%	56.9%	49.0%	60.6%	71.6%	
<b>RC</b>	32.1%	47.6%	<b>62.6%</b>	41.4%	56.7%	<b>70.3%</b>	59.9%	73.0%	<b>81.7%</b>	

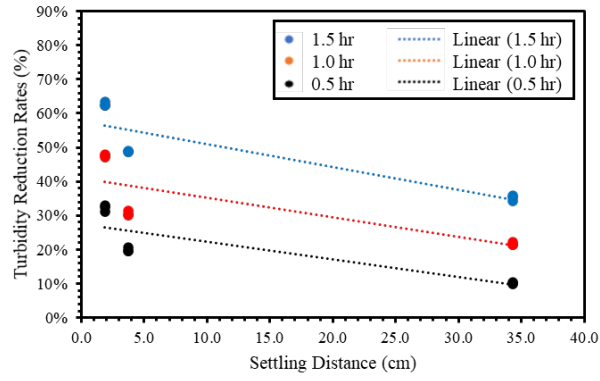
Note: (1) Soil E was not evaluated for turbidity reduction.

(2) reduction percentages in bold indicate minimum and maximum turbidity reduction rates for different inflow.

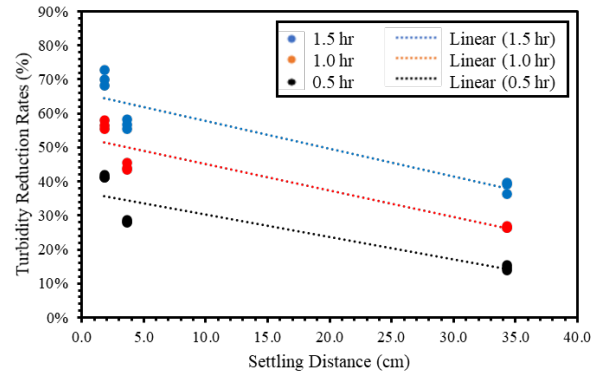
To statistically evaluate the degree of effectiveness of each experimental variable, statistical analysis using the FFM was conducted to identify mathematical relationship (Mahmoudi-Rad and Khanjani 2019). This method was performed by developing scatter plots for evaluated variables. These scatter plots were used to generate the trendlines to explain relationship

in patterns with the turbidity reduction rates. The results of regression analysis were used to produce a lamella settler design recommendation considering varying inflow concentration, particle's settling distance, and residence time. Through the results of the FFM, a proposed factorial model was generated and solved by a multiple regression analysis. In addition, ANOVA tests were performed to evaluate the developed model by identifying if there was significant difference existed among turbidity reduction rates and experimental variables. The null hypotheses of the test was that there was no significant difference among turbidity reduction rates, inflow concentration, particle's settling distance, and residence time. Each considered factor was treated as categorical variable in the analysis. The regression test was conducted for all evaluated soils by using the averaged turbidity measurements, corresponded sample concentration, settling distance, and residence time. When the results of p-values were lower than 0.05, the null hypothesis was rejected which indicated that there is no significant difference between turbidity reduction rates and design parameters.

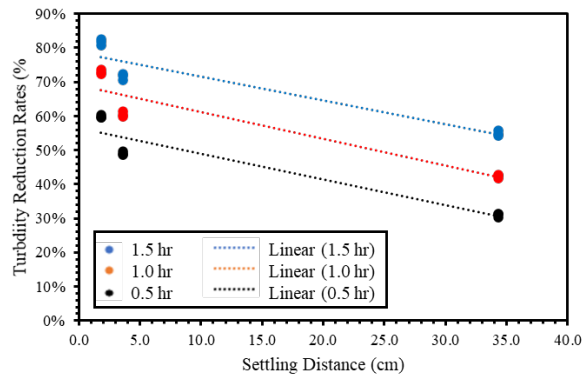
Results of FFM investigated the effects of turbidity reduction rates from different design parameters shown in Figure 3.8 and Figure 3.9. It was found that the turbidity reduction rates increased as concentration increased with decreased settling distance. Through Figure 3.8(a) to Figure 3.8(c), the turbidity reduction rates versus reactor's settling distance for different inflow concentration were demonstrated in linear patterns. The turbidity reduction rates increased with decrease of settling distance. For example, the average turbidity reduction rate at 500 mg/L was 32% at  $R_a$ , which increased to 48% at 3.6 cm (1.4 in.) settling distance and kept increasing to 63% at 1.8 cm (0.7 in.) settling distance. On the other hand, in Figure 3.9(a) through Figure 3.9(c), it was found that the relationship between turbidity reduction rate and concentration was displayed in polynomial patterns.



(a) 500 mg/L



(b) 1,000 mg/L



(c) 5,000 mg/L

**Figure 3.8 Turbidity Reduction Rates versus Plate Spacings.**

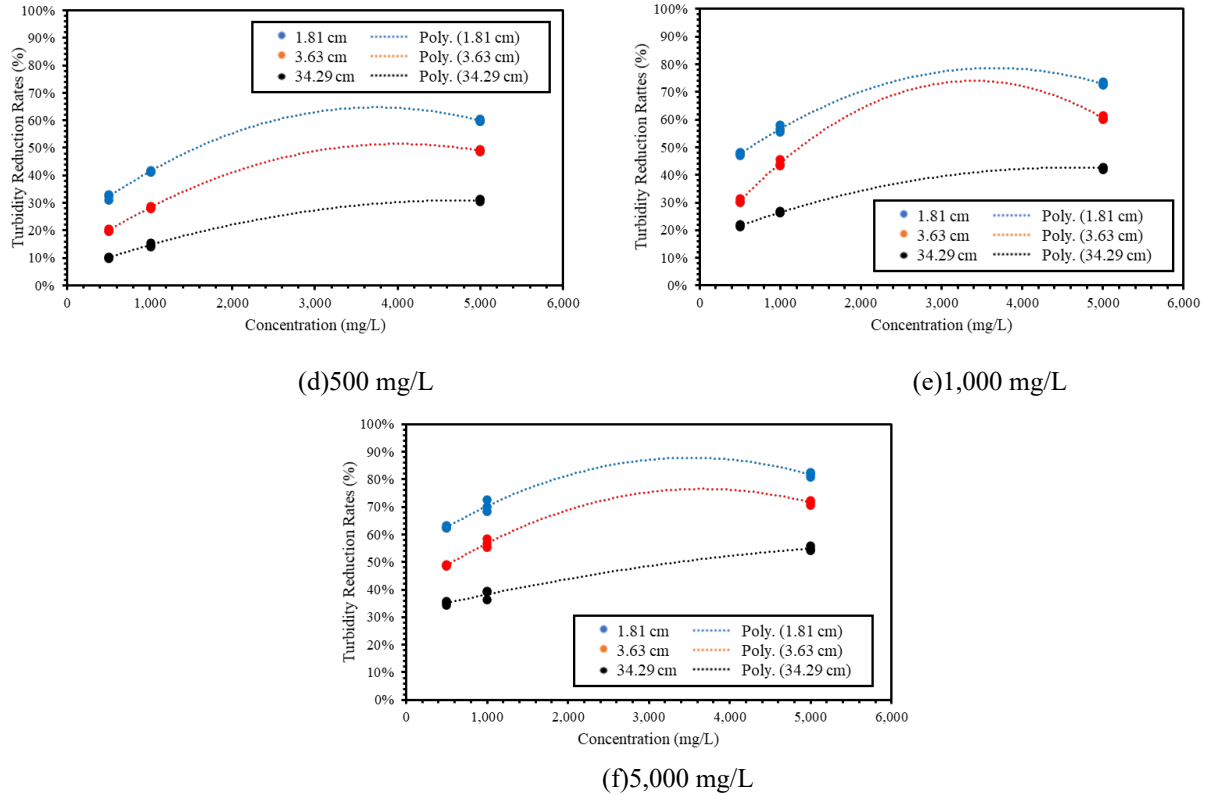


**Figure 3.9 Turbidity Reduction Rates versus Inflow Concentrations**

According to the results of FFM, a factorial model was generated and displayed as a proposed regression equation:

$$\begin{aligned}
 \text{Turbidity Reduction Rates (\%)} &= a_0 + a_1 \times C + a_2 \times S + a_3 \times t + a_4 \times C \times t + a_5 \times S \times t \\
 &+ a_6 \times C \times S + a_7 \times C^2 + a_8 \times S^2 + a_9 \times t^2
 \end{aligned}
 \quad \text{Eq. 3.6}$$

where  $a_0$  to  $a_9$  are the coefficients determined by least square method through regression analysis,  $C$  is inflow concentration,  $S$  is lamella settler's settling distance, and  $t$  is residence time.

The results of regression analysis and ANOVA tests were displayed in Table 3.3 where coefficients represent the degree of influence on turbidity reduction and the p-values identify whether treatments had significant effects on turbidity reductions. It was found that the p-values of two terms ( $t \times C$  and  $t^2$ ) were above 0.05, which indicated the test failed to reject the null hypothesis and there was no significant different among turbidity reduction rates,  $t \times C$  and  $t^2$ . The terms with p-values less than 0.05 were remained as the independent variables and used to re-run

the model as displayed in Table 3.3. The R-square of the final regression analysis was 0.993, which indicated 99.3% of the variation in turbidity reduction rates was explained by the independent variables inflow concentration, residence time, and settling distance through the developed Eq.3.7.

**Table 3.3 Results of ANOVA Test**

	Equation (6)		Equation (7)	
	Coefficients	P-value	Coefficients	P-value
Intercept	0.2150	<0.05 <sup>a</sup>	0.2151	<0.05 <sup>a</sup>
C	0.2108	<0.05 <sup>a</sup>	0.2108	<0.05 <sup>a</sup>
S	-0.7988	<0.05 <sup>a</sup>	-0.7988	<0.05 <sup>a</sup>
t	0.3102	<0.05 <sup>a</sup>	0.3098	<0.05 <sup>a</sup>
t x C	-0.0178	<0.05 <sup>a</sup>	-0.0178	<0.05 <sup>a</sup>
t x S	-0.0193	<0.05 <sup>a</sup>	-0.0193	<0.05 <sup>a</sup>
C x S	-0.0071	<0.05 <sup>a</sup>	-0.0071	<0.05 <sup>a</sup>
t x C x S	0.0049	<0.05 <sup>a</sup>	0.0049	<0.05 <sup>a</sup>
C <sup>2</sup>	-0.0249	<0.05 <sup>a</sup>	-0.0249	<0.05 <sup>a</sup>
S <sup>2</sup>	0.2042	<0.05 <sup>a</sup>	0.2042	<0.05 <sup>a</sup>
t <sup>2</sup>	-0.0002	0.9907 <sup>b</sup>	0	-

Note: <sup>a</sup> statistically significant result; <sup>b</sup> not statistically significant.

$$\begin{aligned}
 & \textit{Turbidity Reduction Rates (\%)} \\
 & = 0.2151 + 0.2108 \times C - 0.7988 \times S + 0.3098 \times t - 0.0178 \times C \times t \\
 & - 0.0193 \times S \times t - 0.0071 \times S \times C + 0.0049 \times t \times C \times S - 0.0249 \times C^2 \\
 & + 0.2042 \times S^2
 \end{aligned}
 \tag{Eq. 3.7}$$

### 3.4.2.PSD

The results of laser diffraction analysis are divided into two parts, the first part includes the PSD curves of different samples in Appendix G. The particle size curves were plotted in two formats based on different treatment setup or residence time. It was found that large size particles were captured through all types of bench-scale treatments. The removal of large particle soils increased with longer residence time or smaller plate spacing of the lamella settler. As residence time increased, the PSD curves of 0.5 in. plate spacing setup and 1.0 in plate spacing setup were overlapping for all tested soil sample except for Soil A. It means that longer residence time can

decrease impact of narrow plate spacing on removing large soil particles. On the other hand, the PSD curves of control reactor at 1.0 hour and 1.5 hour residence times were nearly overlapping. While the PSD curves of lamella settler with 0.5 in. plate spacing vary dramatically, which means the impact of residence time can be increased by decreasing plate spacing.

PSD analysis report  $D_{10}$ ,  $D_{50}$ , and  $D_{90}$  for evaluated soils under 5,000 mg/L concentration experiments as shown in Figure 3.11. It was found that the average  $D_{90}$  of the tested soils decreased considerably with longer residence time or smaller settling space. Among all tested soils,  $D_{90}$  of Soil D had the greatest decrease from 23.04  $\mu\text{m}$  to 3.01  $\mu\text{m}$  with the optimized design parameters obtained from turbidity analysis. While  $D_{90}$  of Soil A dropped from 19.24  $\mu\text{m}$  to 2.36  $\mu\text{m}$  under the same treatment.  $D_{90}$  of Soil B decreased from 28.7  $\mu\text{m}$  to 4.26  $\mu\text{m}$ , and  $D_{90}$  of S60 decreased from 25.22  $\mu\text{m}$  to 4.05  $\mu\text{m}$ . Soil B and Soil C are made from the same material (extender kaolin), where  $D_{90}$  of Soil B is larger than S60, which also has smaller  $D_{10}$ . This shows why Soil B has a smaller median particle size compared to Soil C.  $D_{90}$  of untreated Soil A is smaller than other soils at the same concentration (5000 mg/L) which explains the results of less turbidity reduction rates observed for Soil A. In addition, it was found that  $D_x$  (including  $D_{10}$ ,  $D_{50}$ , and  $D_{90}$ ) dropped off slowly as settling space in treatment system decreased from 31.8 cm (12.5 in.) to 1.8 cm (0.7 in.). Meanwhile,  $D_x$  decreased slowly as residence time increased from 1.0 hour to 1.5 hour in the same treatment system. In other words, both residence time and settling space of lamella settler can improve sediment removal with decreasing of  $D_x$ . The impacts of the optimized design parameters (1.8 cm settling space with 1.5 hour residence time) were not considerably improved from samples treated in the 1.0 in. settling space system after 1.0 hr residence time.

Based on results shown in Table 3.4,  $D_{90}$  was chosen and used to compare results of turbidity analysis due to its dramatical change between different treatment systems. The



performance of system treatment efficiency is presented by comparing with inflow measurements which is listed as the first column of data in each graph. For all tested soil samples, it was found that turbidity, and D<sub>90</sub> decreased as the treatment got improved from Reactor A inserted with shortest residence time (0.5 hr). The decline trends are reasonable as the optimized system with Reactor C at 1.5 hour residence time is expected to capture more large sediment particles.

**Table 3.4 D Values of Size Diffraction**

Soil A										
D <sub>x</sub> , μm	Influent	0.5			1			1.5		
		Reactor C	Reactor B	Reactor A	Reactor C	Reactor B	Reactor A	Reactor C	Reactor B	Reactor A
D <sub>10</sub>	1.02	0.85	0.87	0.97	0.68	0.68	1.05	0.64	0.74	0.85
D <sub>50</sub>	5.73	2.17	2.40	3.61	1.57	1.69	3.66	1.25	1.65	2.36
D <sub>90</sub>	19.24	5.52	7.10	12.10	3.44	3.53	9.82	2.36	3.73	7.15
Soil B										
D <sub>10</sub>	1.58	1.10	0.99	1.27	0.94	1.02	1.05	0.81	0.88	1.19
D <sub>50</sub>	7.11	3.02	2.92	4.80	2.66	3.03	3.48	2.05	2.38	3.61
D <sub>90</sub>	28.70	6.24	7.04	16.00	6.11	6.59	9.40	4.26	5.07	8.27
Soil C										
D <sub>10</sub>	1.15	0.72	0.81	1.03	0.64	0.68	0.80	0.61	0.60	0.78
D <sub>50</sub>	6.14	2.24	2.85	4.39	1.72	1.90	2.88	1.43	1.37	2.80
D <sub>90</sub>	25.22	5.88	6.19	13.80	4.41	5.14	8.25	4.05	5.14	8.46
Soil D										
D <sub>10</sub>	1.79	0.85	0.92	1.51	0.92	0.97	1.39	0.78	0.98	1.23
D <sub>50</sub>	9.25	1.81	2.07	6.07	2.03	2.15	4.32	1.63	2.75	3.68
D <sub>90</sub>	23.04	3.69	4.20	16.50	3.53	4.08	11.40	3.01	7.22	9.56

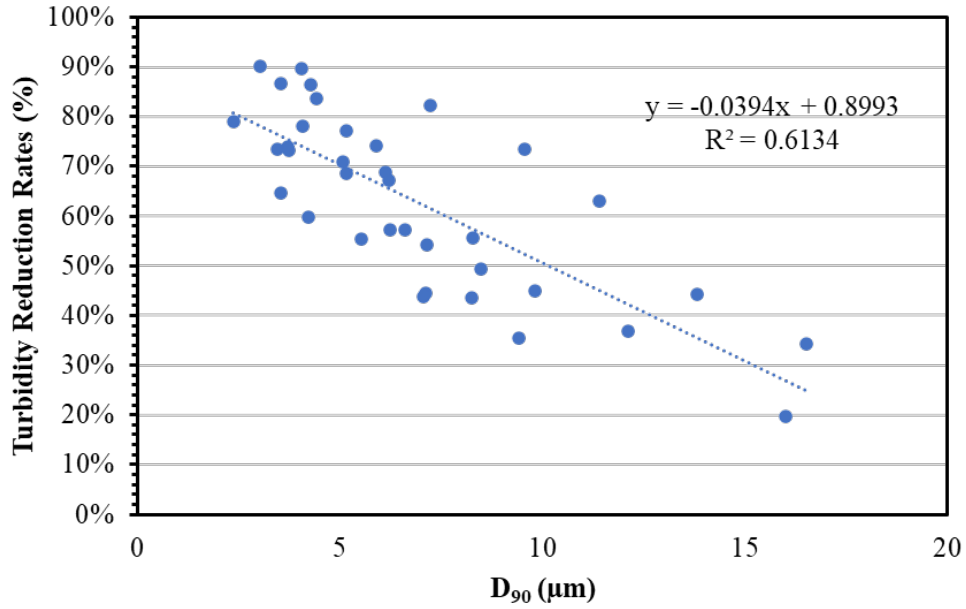


**Figure 3.10 Turbidity Reduction Rates versus D<sub>90</sub>**

In addition, the results of turbidity and PSD measurements were plotted in the following figure. D<sub>90</sub> of untreated Soil A is smaller than other soils which explains the results of less turbidity reduction rates observed for Soil A. In addition, it was found that the average D<sub>x</sub> (including D<sub>10</sub>, D<sub>50</sub>, and D<sub>90</sub>) dropped off slowly as settling distance decreased from 3.6 cm (1.4 in.) to 1.8 cm (0.7 in.) or residence time increased from 1.0 hour to 1.5 hour in the same treatment system.

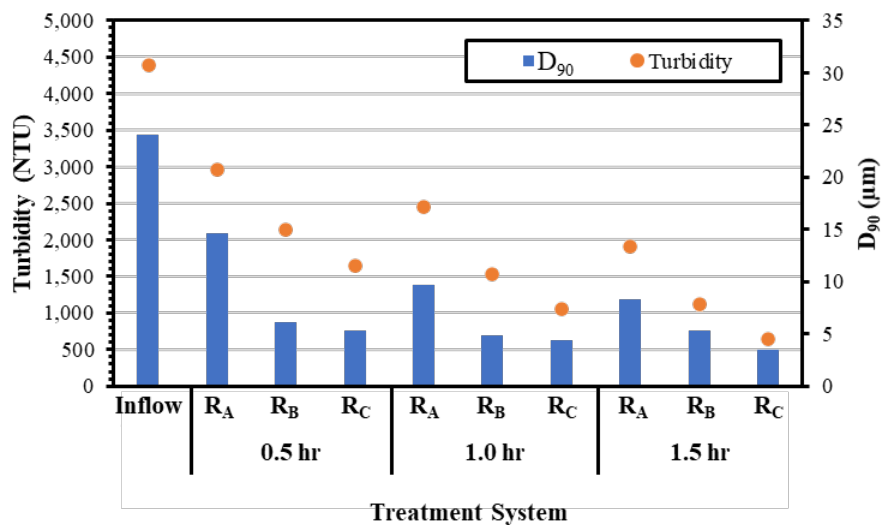


**Figure 3.11 Average Measurements of Turbidity and D<sub>90</sub> for All Tested Soils.**

### 3.4.3. Settling Velocity

Specific gravity and particle diameter are factors which correlate to the particle settling process. Soil D has similar density compared to Soil A with larger median particle size. Soil B and Soil C were the same type of soil with different gradation. Due to limited information about tested soils like average particle size, the median particle sizes of the soils were used to calculate the settling velocity. The average particle size can be more representative for settling velocity calculations compared to median particle size used during the analysis.

Through the results calculated through a Excel spreadsheet shown in Figure 3.12, the developed Eq.3.5 provided the exactly same settling velocities and settling times that were obtained through Stoke's law which shows that Stoke's law is applicable to analyze the settling process in this study. As shown in Table 3.5, the calculated settling velocities ranged from 2 to 348 cm/day (0.8 to 137.0 in./day) for different samples. The settling time of a particle over the vertical spacing between two plates ranged from 0.02 to 3.72 hours in  $R_C$  which was 98.9% faster than the settling process in the control reactor ( $R_A$ ).

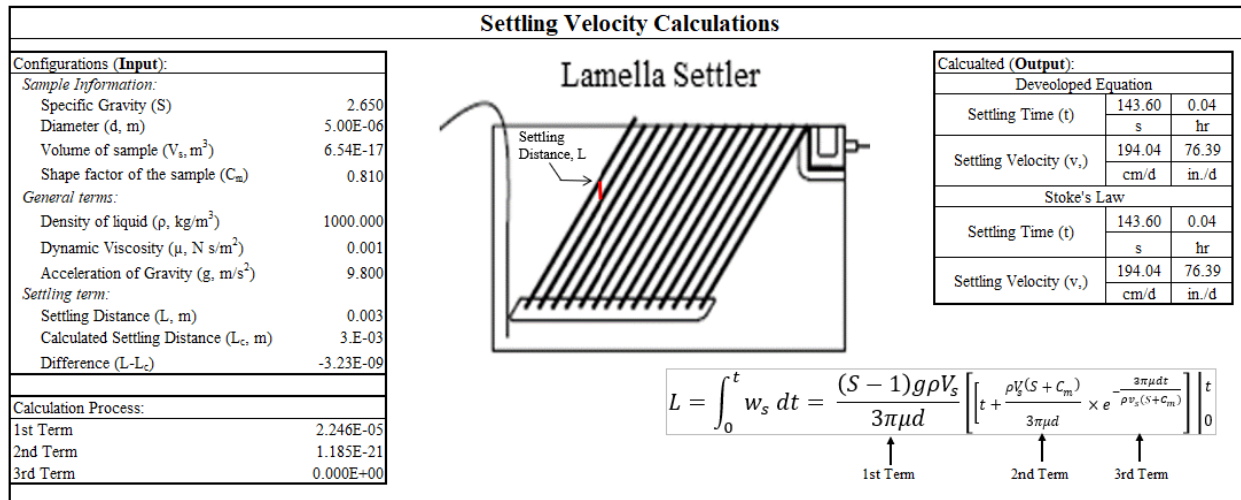


**Figure 3.12 The Calculation of Settling Velocity.**

**Table 3.5 Settling Velocity**

ID	Settling Velocity, cm/day (in./day)	Settling Time (hr)		
		R <sub>A</sub>	R <sub>B</sub>	R <sub>C</sub>
Soil A	194 (76)	3.47	0.02	0.04
Soil B	2 (0.8)	323.86	1.86	3.72
Soil C	12(5)	56.23	0.32	0.65
Soil D	348 (137)	1.94	0.01	0.02
Soil F	194 (76)	3.47	0.02	0.04

Based on calculations, the turbidity reductions for Soil B were expected to be lower compared to other tested minerals in the same application system. Median particle size was assumed as the representative diameters that were used to calculate settling velocity. The difference between experimental results and expectation of sediment removal from settling velocity calculations shows that median particle size may not be ideal for finer particle soils. Therefore, the developed equation [Eq.3.5] for settling velocity estimation are applicable only to larger diameter soils. In addition, the settling velocity and settling time for Soil A and Soil E were similar due to similar specific gravity, particle sizes, and shape factors. Soil E was pretreated by deflocculation which influenced the original sample particle size distribution curve as deflocculation separated particles into smaller sizes. This process influenced the turbidity reduction and caused different results out of prediction. Soil D had the highest settling velocity and achieved the greatest turbidity reduction compared to other samples in the experiments, which displayed consistent results.

### **3.5.Discussion**

The measurements of turbidity and PSD versus the calculated settling velocity were compared for each type of soil. Since Soil F was pre-treated prior the experiments, it was not considered in the discussion. At the 5,000 mg/L inflow concentration, Soil B achieved the lowest turbidity reduction rates, as expected due to the slower settling velocity. In the 500 mg/L and

1,000 mg/L inflow concentrations, the measured turbidity reduction rates of Soil A, Soil B, and Soil C were similar. The order of turbidity reduction rates was: Soil D  $\approx$  Soil C > Soil B > Soil A in the 5,000 mg/L inflow. The order of the calculated settling velocity was: Soil D > Soil A > Soil C > Soil B. These experimental results were acceptable compared to the expectations provided by the calculated settling velocities.

The PSD results of different soils did not vary a lot between each other under the same treatment due to their similar median sizes. Experimental measurements of turbidity and PSD provided consistent results which correlated with the settling velocity calculations. The PSD analysis indicated that  $D_{90}$  of Soil A decreased 16.88  $\mu\text{m}$  (87.7%) after the optimal treatment (5,000 mg/L inflow treated in a 1.8 cm [ 0.7 in.] settling space  $R_c$  with 1.5 hour residence time), and  $D_{90}$  of Soil D decreased 20.03  $\mu\text{m}$  (86.9%). The  $D_{90}$  of Soil A decreased less when compared to Soil D since it contained more clay. For Soil D, the  $D_{90}$  had the greatest decrease with the largest settling velocity and turbidity reduction rates.

The development of the FFM characterized the relationship between turbidity reduction and design parameters mathematically. The average of turbidity reduction rates of five types soils were treated as one group of data during this analysis to create a wide applicable model. The R square of the final developed model was close to one, which displayed high correlation within the model. This developed model can be used in future large-scale lamella experiments to estimate the expected turbidity treatments.

### **3.6. Conclusions**

This study describes different effects from design parameters of lamella settlers and recommends the optimized factors which can determine the entire system's efficiency. In total, 405 experiments measuring turbidity reduction and PSD analysis were conducted to optimize

lamella design factors. The optimal turbidity removal rates for all five soil samples was achieved by using 1.5 hr residence time in  $R_C$  (with 1.8 cm settling distance provided by a 1.27 cm of plate spacing). In addition, higher turbidity removal rates were found when concentrations were higher at the inflow. This optimal combination produced the most efficient turbidity reduction rates at 79.2% for Soil A, 86.5% for Soil B, 89.9% for Soil C, 90.0% for Soil D, and 62.8% for Soil F, respectively. The reduction rates of  $D_{90}$  for each soil type were 87.7% for Soil A, 85.2% for Soil B, 83.9% for Soil C, and 86.9% for Soil D. Since Soil F was pre-treated with sodium hexametaphosphate prior the experiments, it was not analyzed in the size distraction analysis. In addition, a settling velocity equation was developed and used for the tested soils. Calculated settling velocity can be used to predict sedimentation process in the designed reactor systems. The calculated turbidity removal rates for different types of soils were correlated corresponding to the calculated settling velocities. Soil D had largest settling velocity, which created the largest turbidity reduction rate (90.0%) in the same optimized system setup compared to other samples. Soil A was the most suspended samples with the lowest  $D_x$  and turbidity reduction rates (79.2%).

A FFM was conducted to describe the relationship between three quantitative factorial variables (inflow concentration, settling space, and residence time) and the turbidity reduction rates. The final model developed through the regression analysis was acceptable with 0.993 R-square which indicated the adequate fit of the model to the observed data points. In addition, the p-values of the independent variables were below 0.05 which indicated the null hypothesis of there was no significant difference among turbidity reduction rates, inflow concentration, settling distance, and residence time was rejected. This model was developed according to the bench scaled experiments, which can be applied for the large scale in the future. In future large scale experiments, local soil samples will be prepared and treated under the 1.8 cm settling distance

lamella settler at 1.5 hr residence time. Large-scale experiments are expected to achieve higher efficiency of sediment removal due to larger particle sizes contained in the local soils compared to the samples used in the bench scaled experiments. This model can be widely applicable as it focused on the prediction of the turbidity treatment regardless of the sources of stormwater runoff (urban, construction, and agriculture). The model can assist designers by changing the values of design parameters (inflow concentration, settling distance, and residence time) to meet the desired turbidity of outflow at the design stage.

## CHAPTER 4. ELECTROCOAGULATION (EC)

### 4.1.Introduction

EC is the process of electrochemical reaction used in water and wastewater treatment, which corrodes anodes to destabilize and remove contaminants (Holt, Barton, and Mitchell 2005; Sahu, Mazumdar, and Chaudhari 2014). EC process consists of two electrically charged metal elements (e.g., iron, aluminum and stainless steel) as cathode and anode placed in a treatment tank, where the current flows out of cathode (positive charge) and then flows into anode (negative charge). EC's wide applications can be used to remove various unwanted pollutants, including: suspended solids, colloidal material, metals, and dissolved solids-including inorganic contaminants and pathogens (Emamjomeh and Sivakumar 2009; Merzouk et al. 2009; Sahu et al. 2014). To remove the pollutants, EC uses the electrolytic cell in water or electrolyte to transfer ions. Additionally, water is electrolyzed at both cathode and anode, which creates gas bubbles to contact with coagulants and makes them float easily. Furthermore, the cations can also react with hydroxyl ions to form hydroxide which will increase pH and influence the speciation of the aluminum hydroxide complex generated during the EC process. Figure 4.1 summarizes the sequence of reactions, shows chemical equations for each reaction, and explains the EC process (Al et al. 2012; Holt 2002). Recently EC has become a more popular treatment approach as it has been proven to remove particles with higher efficiency, little modification, and without the use or handling of chemicals. (Emamjomeh and Sivakumar 2009).



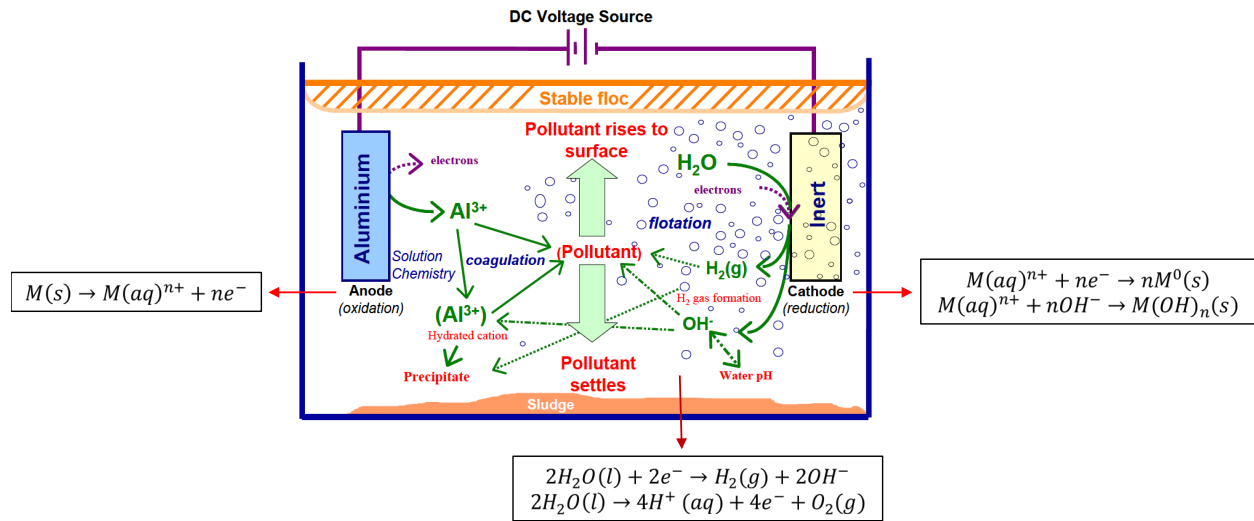


**Figure 4.1 EC Process (Holt 2002).**

## 4.2.Literature Review

### 4.2.1.History

EC's first use was reported in 1889 in England. The basic mechanism is shown in Figure 4.2, where negative (C) and positive (D) electrode rods were placed in the burner (A) filled with solvent mixtures made of Na<sub>2</sub>Al<sub>2</sub>F<sub>8</sub> and isolated by the shell (B). A patent was created for excess aluminum fluoride with dissolution of aluminum oxides from which electrolysis got reactants (Craig 2013). The EC was patented in 1904 by a Minnesota based company, Elmore, which claimed benefits in mineral treatments (Pryor 2012). In 1894, a patent for application of aluminum and iron electrodes was developed using the electrolysis method which is a type of EC applied with DC (Sahu et al. 2014). By 1911, several public wastewater sludge treatment plants in the United States (U.S.) had adopted electrolysis techniques (Holt 2002). However, by the 1930's, the increasing operational costs for the plants' operations and availability of chemical coagulation, the use of electrolysis was abandoned for sludge treatment plants (Holt 2002).

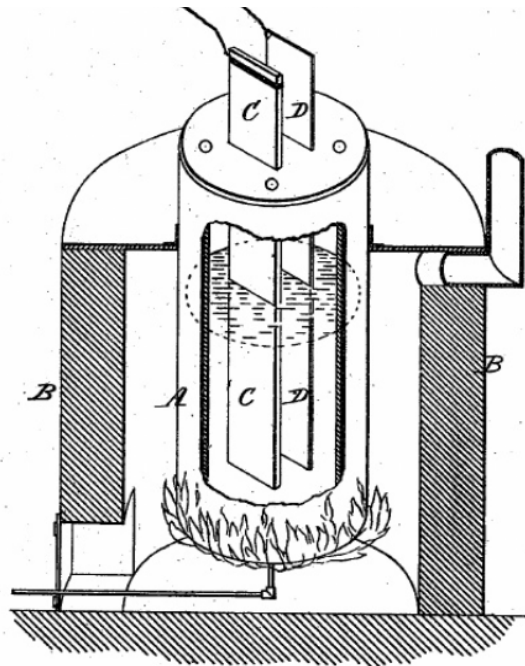


**Figure 4.2 Original Investigation of EC.**

In 1946, Stuart and Bonilla developed the first large-scale EC process for drinking water treatment. However, his system did not attract widespread implementation due to the large electrical supply system (Kobyas, Can, and Bayramoglu 2003; Sahu et al. 2014). Internationally, Russian scientists worked on analyzing EC in water treatment process from 1970's to 1980's, started from metal removal from relative finishing or industries to small-scale natural water treatment with effective EC conductivity with aluminum ions (Emamjomeh 2006). Their studies increased public interests, but considering the commercial benefits, their research did not receive wide-spread attention from industries due to the small-scale based experiments (Holt 2002). During the latter of the twentieth century, U.S. and Russian researchers performed various research investigations about different EC reactors for different pollutants, which added to the knowledge base and helped provide a deeper understanding of electrocoagulation in multiple dimensions (Sahu et al. 2014).

#### ***4.2.2.Mechanism***

EC is a complex process that can be broken into three mechanisms based on the technologies it combines: electrochemistry, coagulation, and floatation, and also includes their advantages, which is explained in Figure 4.3. Among these three mechanisms, electrochemistry and coagulation can be also explained as electrode oxidation and gas bubble generation based on the reactions happened at anode and cathode (Chavalparit and Ongwandee 2009; Holt 2002). EC works in a defined reactor with electrolytic cell which includes one anode and one cathode (Sahu et al. 2014). This is the simplest form of EC and is shown in Figure 4.4 (Mollah et al. 2001). There have been experiments that study the resistance reactor for regulated current measurements. Some of the experiments applied a stirrer to mix and maintain the reaction consistence (Sahu et al. 2014). During the EC process, the metal plates such as iron or aluminum are named as “sacrificial electrodes” (Sahu et al. 2014). They decrease the dissolution potential in anodic reaction, and constrain the passivation in cathodic reaction (Mollah et al. 2001). As these sacrificial electrodes are applied, the anode is corroded to produce ions in water which neutralize the charges of particle and incurs the coagulation (Sahu et al. 2014). During the EC process, the reactions vary based on different types of contaminants. Typically, the unwanted pollutants can be removed by chemical reaction with precipitation or coalesced through the electric filed (Sahu et al. 2014). Colloidal particulates such as oils can be broken down into less soluble forms by altering their chemical and physical properties (Canizares et al. 2007).

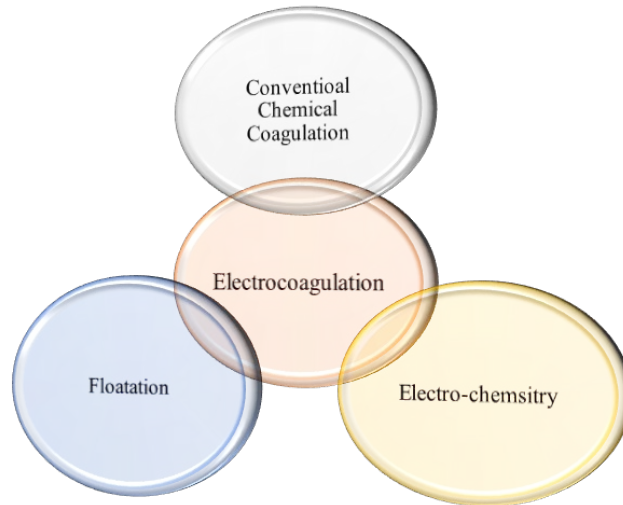
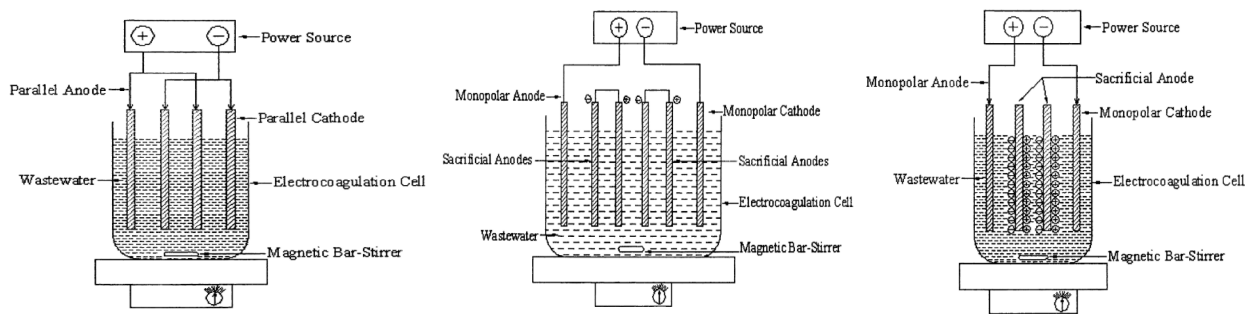


**Figure 4.3 Relationship of the Conventional Technologies (Kuokkanen 2016).**



(a) simplest EC                      (b) series of monopolar electrodes      (c) bipolar electrodes connection

**Figure 4.4 Arrangements of Electrodes Connection.**

From a modeling perspective, the EC process can be explained based on the Butler-Volmer equation (Eq. 4.1), which displays charge transfer into the relationship between current and electrode overpotential (Holt 2002). The overpotential ( $\eta$ ) is the degree of polarization which provides “driving force” of the EC process. This equation mainly describes charge transfer process assuming that diffusion is neglected. (Eq. 4.2) calculates overpotential by making deviation of an electrode’s equilibrium value ( $E_0$ ).

$$i = i_0 \left\{ \exp \left( \frac{\alpha_{An} F \eta}{RT} \right) \right\} \quad (\text{Eq. 4.1})$$

$$\eta = E - E_0 \quad (\text{Eq. 4.2})$$

### 4.2.3. EC Factors

The efficiency of pollutant removal is influenced by the different factors such as arrangement of electrodes connection, materials of electrodes, pH, applied voltage, and reaction time. Other than the simplest form mentioned in Figure 4.4(a), EC can be also made up with series connection of electrodes, from which each pair of “sacrificial electrodes” is internally connected with no interconnection with outer electrodes (Mollah et al. 2001). This arrangement of electrodes is explained in Figure 4.4(b), which is called monopolar electrodes. With increase in electrode pairs in the series, there is an increased need for the same current due to rising resistance occurred in series connection. Two types of electrodes can be identified based on different arrangements, the first one is monopolar electrodes, and the second is bipolar electrodes. Figure 4.4(c) shows an EC reactor with bipolar electrodes for comparison. Bipolar electrodes have no connection, where sacrificial electrodes are placed between two electrically connected electrodes. In this case, two sacrificial electrodes which also called bipolar electrodes are be transformed into opposite charges as the current passes.

Compared to the arrangements of electrode connection, there are few studies related to the types of electrodes materials used. Iron, aluminum, and stainless steel are common materials applied or analyzed in industry and research. For different types of pollutants, the optimized electrodes are different. The previous research displayed that applied aluminum as the electrode performed best on Cr (VI) metal removal (Golder et al. 2007). And the iron performed higher removal efficiency of chemical oxygen demand (COD) (Kobyta et al. 2003). Even for the same

pollutants, some variables needed to be controlled for higher accuracy of the research. For example, pH has a significant influence on the EC reaction.

pH is considered as one of the key parameters during the EC reaction process (Parga et al. 2005). As a very important variable, pH has been well studied and proved their importance for EC analysis. The previous study found that minor change of pH could cause significant change of contaminant removal (Canizares et al. 2009). If pH was same at the end of EC process, the efficiency of the pollutants removal was similar (Cañizares et al. 2009). In chemical perspective, pH changes due to EC reaction, which specified that “pH controlled” means pH was same at the start and end of EC process, pH was not constant through the reaction. Compared to pH, controlled cell voltage is fixed during the whole EC process.

Various metal hydroxide dissolved during the experiments is influenced by pH and vital to sediment pollutant removal with ionic complexation. It has been proven that when various metal hydroxides are dissolved, pH is in the range of 6.0-7.0 (Can and Bayramoglu 2010). The metal hydroxide complexes provide an environment suitable for ion exchange on the surface of pollutants, which allows aggregation and enmeshment of larger flocs (Arroyo et al. 2009). Simply, the presence of metal hydroxide can also influence EC reaction.

The applied cell voltage is another key parameter for the EC reaction. Cell voltage provides current density, which is called EC conductivity. Conductivity is also a term used to describe pollutants removal efficiency. Increased conductivity increases pollutant treatment efficiency. Research has shown that increasing the EC conductivity can occur with increasing current density at constant cell voltage or constant current density with reducing cell voltage (Khandegar and Saroha 2013). If the conductivity is limited due to the capability of the cell voltage, it could be

adjusted by adding adequate salts like sodium chloride or sodium sulphate (Khandegar and Saroha 2013).

The final critical factor is reaction time, which is also a function of EC conductivity. Similarly to the rule behind cell voltage, the increasing reaction time will increase contaminant removal efficiency, where reaction time is the duration of EC process. There is an optimum reaction time for EC conductivity, after the removal efficiency optimizes, it plateaus as reaction time increases. Metal hydroxides produced by anode dissolution increases with longer reaction time at controlled current density and remains stabilized once passed the optimum reaction time (Khandegar and Saroha 2013).

#### ***4.2.4. Power Supply***

As its name states, EC is powered by electricity. The power supply of EC can be divided into two parts: direct current (DC) and alternating current (AC), where DC flows in one direction and AC changes direction periodically. Most research studies DC in the EC process, which conducts oxidation at anode to erode formation, forms an oxidation layer at cathode, blocks current flow, and lowers the contaminant removal efficiency (Khandegar and Saroha 2013). AC can lowers the formation erosion issue in EC process (Vasudevan, Lakshmi, and Sozhan 2011). The following section will explore more detail about power source and function of EC.

Typically, the power supplies of EC are referred to DC or AC. The power source for the electricity provided for cell voltage which produces current. In sustainable perspective, solar cell is arising people's attention as an electric power source, which is also called "the most powerful renewable source" (García-García et al. 2015). The conversion of energy applied with physical principle is not only used to create electricity but also can be used to create heat and synthesized

fuels (García-García et al. 2015). Solar energy application is limited due to cost of conversion and time consumption caused by irregular intervals.

It was reported that using solar sources treats water for reuse, and generates 462 to 1,232 kW extra energy based on amount of wastewater, current densities, and EC contact times (Phalakornkule, Sukkasem, and Mutchimsattha 2010). Recent research has applied solar in wastewater treatment operations. Garcia et al. (2015) used photovoltaic (PV) cells to generate 60 to 200 W directly from photos of sunlight based on its physical properties. In addition to that, this investigation is analyzed internationally. PV EC systems have been proved successful in multiple wastewater treatment plants in India (Nawarkar and Salkar 2019). Applications have shown that solar power source is cost and can reach removal percentages of 90% for chemical oxygen demand (COD), 94.56% for turbidity and 49.78% for total dissolved solids (TDS),(Nawarkar and Salkar 2019).

#### **4.3.Research Objectives**

There is a significant amount of literatures reporting the advantages of using EC for different types of wastewater treatment. While EC is not popular used for stormwater treatment due to its cost concerns. Research studies investigate the performance of EC is necessary to introduce this technology into construction world. The first goal of this research was to evaluate different design parameters including concentrations of sample, EC cells' materials, cells' distance, EC power supply, and reaction time. Through the EC batch experiments, each design factor was adjusted to obtain the optimized sediment removal through the observations of turbidity measurements.



#### 4.4. Bench-Scale Experiments

EC performance using a consistent power supply was tested among different sample concentrations to ensure that experiments of 1,000 mg/L test are replicable for the other concentrations. Results obtained from the experimental observations showed that the concentrations of sample would not influence the efficiency of EC as the power performed consistently at different concentrations. In addition, results of multiple linear regression (MLR) analysis in Table 4.1 displayed that the P values for different concentrations were all above 0.05, which rejected the null hypothesis and proved that there was no significant difference between sample concentration and EC reaction efficiency.

**Table 4.1 Analysis of EC at Different Concentrations**

	Aluminum		Stainless Steel		Low-Carbon Steel	
	Coeff.	P	Coeff.	P	Coeff.	P
<b>Intercept</b>	11.03	1.21x10 <sup>-6</sup>	12.31	2.72x10 <sup>-8</sup>	9.48	1.75x10 <sup>-9</sup>
<b>1,000 mg/L</b>	-0.26	0.90	-0.03	0.99	0.01	1.00
<b>5,000 mg/L</b>	-0.23	0.91	-0.07	0.97	-0.04	0.98

The capability of power supply generation for different metal cells is listed in Table 4.2. It was found that the cell spacing influenced the capacity of power supply, as the increased cell spacing required more power to reach the same desired current density. For example, all three cell materials needed less power to provide 0.9 A at 0.5 cm (0.2 in.) cell spacing but could not perform 0.9 A current with 2.0 cm (0.8 in.) cell spacing. Except for cell spacing, the cell materials can also influence power output capacity due to different resistances. Aluminum needs more power (around three watts) to reach the same current compared to stainless steel and low-carbon steel. The output power became similar as cell spacing increased. For aluminum, it needed more power with 0.5 cm (0.2 in.) but consumed similar power with 2.0 cm (0.8 in.) cell spacing compared to the other metals (stainless steel and low-carbon steel).

**Table 4.2 Power Supply from Different Metal Cells**

Cell Spacing at Different Power	0.5 cm (0.2 in.)			1.0 cm (0.4 in.)			2.0 cm (0.8 in.)		
	Current A	Voltage V	Power W	Current A	Voltage V	Power W	Current A	Voltage V	Power W
Aluminum	0.3	7.6	2.3	0.3	10.0	3.0	0.3	16.1	9.7
	0.6	12.5	7.5	0.6	17.8	10.7	0.6	30.3	27.3
	0.9	16.8	15.1	0.9	25.9	23.3	0.9	-	-
Stainless Steel	0.3	7.6	2.3	0.3	10.4	3.1	0.3	17.9	10.7
	0.6	11.3	6.8	0.6	17.6	10.6	0.6	32.0	28.8
	0.9	15.0	13.5	0.9	24.6	22.1	0.9	-	-
Low-carbon steel	0.3	5.8	1.7	0.3	9.4	2.8	0.3	16.8	10.1
	0.6	10.0	6.0	0.6	15.5	9.3	0.6	30.8	27.7
	0.9	13.9	12.5	0.9	22.5	20.3	0.9	-	-

EC experiments were conducted in fresh prepared sample solutions to ensure accuracy; after a certain reaction time, the solutions were mixed at a high speed (19,000 rpm) for 10 seconds following the experimental method (Zhu, Clifford, and Chellam 2005). Turbidity was measured before and after the reaction to test the system’s efficiency. The observation time after the reaction was determined as residence time (30 min., 60 min, and 90 min.) during the experiments. All experiments were conducted using 1,000 mg/L Soil A to simulate sediment-laden stormwater discharged from a skimmer in the sediment basin. Four blanks were prepared without EC reactions, but followed the same mixing procedure (19,000 rpm for 10 seconds). The turbidity measurements of blanks were recorded as the reference for EC experiments.

Four major factors (current density, reaction time, plates distance, and plate materials) were evaluated during the experiments according to turbidity measurements. The current density under different electric currents was calculated based on the reactive areas of electrodes. In this study, the reactive areas are the surface area of electrodes as the cells were submerged completely under the sample solution during the reaction. As shown in Table 4.3, each factor was evaluated individually as other factors were controlled during the experiments. All controlled experiments were conducted in 2.0 L (0.1 ft<sup>3</sup>) beakers, and each experiment was repeated for three times. A DC

power supply (ELECTRO INDUSTRIES Model DIGI 360) was used to provide power for EC reactions throughout the project. Three types of metal cells (aluminum, stainless steel, and low-carbon steel) were considered to optimize the design parameter. The dimensions of EC cells were designed to allow them to fit into a 2.0 L (0.1 ft<sup>3</sup>) beaker with maximized reaction spacing within this bench-scale reactor. The dimensions of metal cells used in the experiments were 5.08 cm x 15.24 cm x 0.32 cm (2 in. x 6 in. x 1/8 in.) in width x length x thickness.

**Table 4.3 EC Parameters**

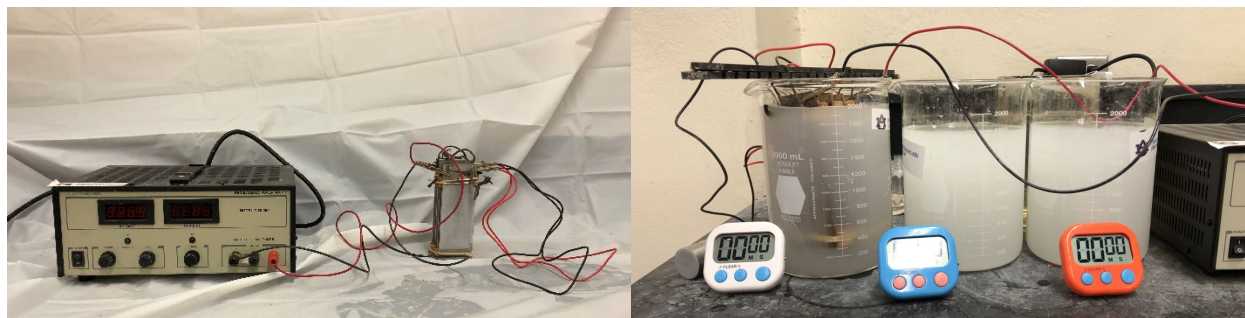
<b>Plate material</b>	<b>Plates spacing, cm (in.)</b>	<b>Current density, A/m<sup>2</sup> (A/ft<sup>2</sup>)</b>	<b>Reaction time, s</b>	<b>Residence time, min</b>
Stainless steel	0.5 (0.2)	39 (3.6)	15	30
Low-carbon steel	1.0 (0.4)	78 (7.2)	75	60
Aluminum	2.0 (0.8)	116 (10.8)	125	90

The experimental setup is shown in Figure 4.5. Four metal sheets were assembled and assigned as one system with rubber bands and lines, which were fixed on the 3D printed plastic bar and suspended at the top of the beaker. Different combinations of design factors were tested, and the turbidity measurements were recorded every 5 minutes in the first hour after the EC reaction and mixing process. For the last 30 minutes, the turbidity was measured every 10 minutes during the observation. The changes in turbidity along residence time with different EC reactions are shown in Appendix J. The turbidity of the original sample was recorded that used as a comparison with the turbidity measurements after the reaction. According to Eq. 3.1, the turbidity reduction rates would be calculated at different residence times (30 min., 60 min., and 90 min.) to display the system's efficiency.

The turbidity reduction rates from the experiments will be used to display the reaction efficiency, which can determine the positive or negative effects from different design factors. In addition, based on the calculated turbidity rates, a multiple linear regression analysis was conducted to quantify the impact from each EC parameter on the turbidity reduction. The

optimized combinations of the EC setup would be used to develop the novel system combined with designed lamella settlers in next project.

With exception of turbidity measurements, the pH along optimal EC reaction was recorded as reference. During the EC reaction, water is electrolyzed at both cathode and anode, which creates bubbles to contact with coagulants and makes them float easily. Furthermore, the cations can also react with hydroxyl ions to form the hydroxide which will increase the pH and influence the electrocoagulation process. In this study, pH was monitored by using a pH meter (Pocket Pro+ pH Tester from Hach) before and after EC reaction to describe system performance in a different approach. To reduce sampler error, the pH probe and sampling cap needs to be cleaned properly with clean tap water between each measurement. In addition, calibration of pH meter is necessary before each set of experiment.



(a) metal plates and EC power supply

(b) EC system setup

**Figure 4.5 EC Bench-Scale Experiments.**

#### **4.5. Electrode's Consumption**

The consumption of the electrodes during the EC reaction is divided into two parts based on economic consideration: electrode's initial cost and consumption. To estimate initial cost for different metal cells, the first step was to compare the costs of the metal bars to estimate the initial cost. All metal cells were ordered through the company McMaster and cut in the lab to fulfill the

designed dimensions. In the website, the original stainless steel is called multipurpose 304 stainless steel bar, aluminum is called multipurpose 304 stainless steel bar, and low-carbon steel is listed as low-carbon steel bar. The prices for different metal sheets were recorded on 4/28/2020 which were used for the comparison of their initial prices.

On the other hand, the consumption of different electrodes was analyzed to identify the optimal cell's material depending on their cost effectiveness. The experiments of electrodes' degradations were conducted under the same optimal EC condition (at 78 A/m<sup>2</sup> [7.2 A/ft<sup>2</sup>], 2.0 cm [0.8 in.] cell spacing) based on the results of turbidity removal efficiency. The consumption tests were made by recording the dry mass of the metal sheets (stainless steel, aluminum, low-carbon steel) before and after the reactions. Before the EC reaction, the oven dry mass (in grams) of each metal sheet was documented as the initial mass. After the reaction, it was necessary to clean and dry all the metal sheets in the oven at 150°C for six hours. Those plates were then put into a desiccant box to cool to room temperature. After waiting for four hours, the mass of the metal sheets was weighed and recorded. The mass loss ratio over accumulated reaction time will be calculated and plotted in the results section in the equation shown below.

$$\text{Mass Loss Ratio} = \frac{M_0 - M_x}{M_0} \times 100\% \quad (\text{Eq. 4.3})$$

where  $M_0$  is initial mass of metal cells (g),  $M_x$  is the mass after accumulated reaction time (g),  $x$  is accumulated reaction time in hour.

Before the first EC experiment, the mass of metal cells was recorded as  $M_0$ . For example, after a one-hour EC reaction, the mass of metal cells was recorded as  $M_1$ , and after another EC experiments for one more hour, the mass of metal cells was recorded as  $M_2$ . The mass loss ratio of the 2-hour EC reaction was calculated by using  $M_0$  minus  $M_2$  and divided by  $M_0$ . The mass

loss rates of different cells would be used to predict the maintenance or replacement needs of electrodes. The mass of loss per year was calculated through three developed equations of mass loss ratio over time. The measurements of mass loss in the bench scale would be used to determine the optimal electrodes' material and estimate its mass loss in large scale.

## **4.6.Results**

### ***4.6.1.Optimal Design Parameters***

The turbidity measurements throughout the experiment were recorded and plotted as shown in Appendix J. For each set of the experiment, three turbidity measurements were used to analyze the reaction efficiency after 30 minutes, 60 minutes, and 90 minutes. The turbidity reductions for different metal cells are shown in Table 4.4, Table 4.5, and Table 4.6, respectively. It was found that the removal of turbidity improved when increasing reaction time, residence time, cell spacing, and current density.

The increase of reaction time had different impact responses of turbidity reduction based on the cell's materials used during the EC reaction. For the EC reactions using aluminum cells, the turbidity removal efficiency could be improved from 31.78% to 97.60% by optimizing the design parameters (1.25-minute reaction time, 116 A/m<sup>2</sup> [10.8 A/ft<sup>2</sup>], and 1.0 cm cell spacing [0.2 in.]). Low-carbon steel has different optimal cell spacing at 2.0 cm (0.8 in.) which could reduce turbidity by 93.91%. Aluminum performed similar turbidity removal rates compared to low-carbon steel. As EC cells degraded during the reactions, low carbon covers dissolved into water, which is considered as the negative impact on the environment. The results of sediment removal efficiency suggest for the aluminum to be the optimal electrode material for EC experiments.

In addition, it was found that aluminum cells with extended 1-minute reaction under lowest current density (39 A/m<sup>2</sup> [3.6 A/ft<sup>2</sup>]) improved turbidity removal rates by around 20%. However,

under higher controlled current densities ( $78 \text{ A/m}^2$  [ $7.2 \text{ A/ft}^2$ ] and  $116 \text{ A/m}^2$  [ $10.8 \text{ A/ft}^2$ ]), the turbidity removal efficiency did not increase dramatically with longer reaction time. For stainless steel cells, the turbidity reduction rates increased by 20% consistently for an extended 1-minute reaction time under different controlled current densities. However, the use of low-carbon steel cells obtained similar turbidity removal rates along with longer reaction time under different controlled current densities.

With exception to cell's materials and EC reaction time, residence time played a vital role in sediment treatment. It was found that residence time at 1.5 hour is the optimal condition for all metal cells. Cell spacing is another design factor that describes the efficiency of EC reaction. Except for low-carbon steel, 2.0 cm (0.8 in.) cell spacing obtained higher turbidity reduction rates under the same controlled conditions. For low-carbon steel, the narrow cell spacing can increase the reaction efficiency on turbidity treatment.

Stainless steel is less active during EC with less turbidity reduction rates compared to the other two materials. It was found that the use of stainless steel electrodes could only reduce turbidity by 83.43% at the same optimal condition of aluminum cells (1.25-minute reaction time,  $78 \text{ A/m}^2$  [ $7.2 \text{ A/ft}^2$ ], and 2.0 cm [0.8 in.] cell spacing). For aluminum cells, the turbidity had a similar reduced level (97.55%) at  $78 \text{ A/m}^2$  ( $7.2 \text{ A/ft}^2$ ) and 2.0 cm (0.8 in.) plate spacing compared to the reaction at  $116 \text{ A/m}^2$  ( $10.8 \text{ A/ft}^2$ ) and 1.0 cm (0.4 in.) plate spacing (97.60%). In other words, the increase of cell spacing reduces the power needed for EC to achieve same sediment removal. According to results of turbidity reductions, the optimal condition for the EC reaction is to use aluminum electrodes for 1.25 minutes at  $78 \text{ A/m}^2$  ( $7.2 \text{ A/ft}^2$ ) current density and 2.0 cm (0.8 in.) cell spacing.

**Table 4.4 Turbidity Reduction Rates with Aluminum Cells**

Reaction Time Residence Time	0.25 min.			0.75 min.			1.25 min.		
	0.5 hr	1.0 hr	1.5 hr	0.5 hr	1.0 hr	1.5 hr	0.5 hr	1.0 hr	1.5 hr
<b>39 A/m<sup>2</sup> (3.6 A/ft<sup>2</sup>)</b>									
<b>0.5 cm (0.2 in.) Spacing</b>	31.8%	49.1%	58.5%	40.6%	59.2%	71.6%	53.3%	76.5%	83.7%
<b>1.0 cm (0.4 in.) Spacing</b>	52.2%	61.9%	68.1%	67.3%	80.2%	86.6%	76.7%	86.1%	91.1%
<b>2.0 cm (0.8 in.) Spacing</b>	57.1%	69.5%	75.0%	75.3%	87.5%	91.1%	82.5%	91.7%	94.8%
<b>78 A/m<sup>2</sup> (7.2 A/ft<sup>2</sup>)</b>									
<b>0.5 cm (0.2 in.) Spacing</b>	53.7%	67.5%	78.4%	68.1%	84.1%	90.6%	77.8%	89.4%	93.4%
<b>1.0 cm (0.4 in.) Spacing</b>	54.0%	72.3%	80.2%	78.9%	89.7%	93.7%	85.9%	93.3%	95.8%
<b>2.0 cm (0.8 in.) Spacing</b>	82.7%	92.0%	95.2%	89.7%	95.2%	96.8%	92.6%	96.3%	97.6%
<b>116 A/m<sup>2</sup> (10.8 A/ft<sup>2</sup>)</b>									
<b>0.5 cm (0.2 in.) Spacing</b>	69.3%	81.9%	88.2%	89.9%	94.9%	96.6%	92.8%	96.1%	97.4%
<b>1.0 cm (0.4 in.) Spacing</b>	84.4%	92.6%	95.6%	89.4%	95.2%	96.5%	94.2%	96.7%	97.6%

**Table 4.5 Reduction Rates with Stainless Steel Cells**

Reaction Time Residence Time	0.25 min.			0.75 min.			1.25 min.		
	0.5 hr	1.0 hr	1.5 hr	0.5 hr	1.0 hr	1.5 hr	0.5 hr	1.0 hr	1.5 hr
<b>39 A/m<sup>2</sup> (3.6 A/ft<sup>2</sup>)</b>									
<b>0.5 cm (0.2 in.) Spacing</b>	24.2%	26.2%	35.8%	27.6%	32.4%	38.3%	25.2%	38.0%	39.2%
<b>1.0 cm (0.4 in.) Spacing</b>	31.2%	36.6%	41.7%	32.2%	41.0%	53.0%	34.1%	42.2%	56.0%
<b>2.0 cm (0.8 in.) Spacing</b>	30.8%	48.2%	51.1%	45.0%	55.4%	66.9%	45.8%	58.1%	70.8%
<b>78 A/m<sup>2</sup> (7.2 A/ft<sup>2</sup>)</b>									
<b>0.5 cm (0.2 in.) Spacing</b>	26.9%	32.9%	38.1%	24.0%	36.3%	37.6%	25.8%	36.9%	39.9%
<b>1.0 cm (0.4 in.) Spacing</b>	27.7%	41.6%	44.1%	32.5%	45.3%	57.2%	36.5%	51.4%	66.1%
<b>2.0 cm (0.8 in.) Spacing</b>	32.3%	52.2%	65.3%	37.1%	66.3%	79.7%	48.4%	68.5%	83.4%
<b>116A/m<sup>2</sup> (10.8 A/ft<sup>2</sup>)</b>									
<b>0.5 cm (0.2 in.) Spacing</b>	27.3%	40.3%	52.3%	32.8%	50.5%	64.9%	35.3%	61.1%	71.2%
<b>1.0 cm (0.4 in.) Spacing</b>	24.3%	29.8%	36.5%	28.1%	35.9%	43.0%	32.2%	45.5%	54.7%

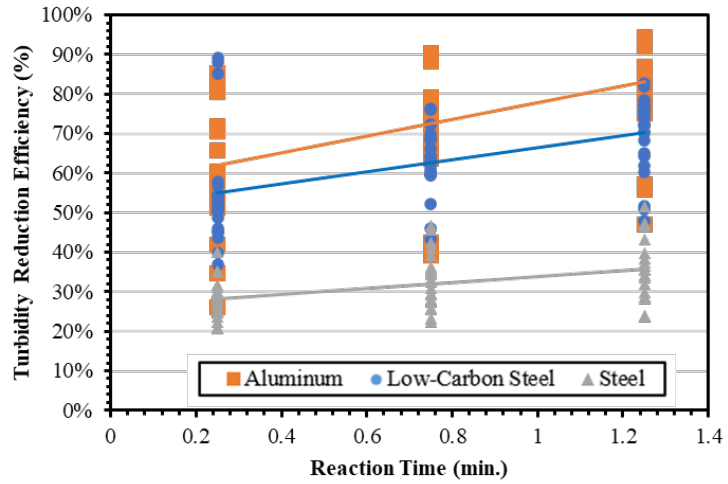
**Table 4.6 Reduction Rates with Low-Carbon Steel Cells**

Reaction Time Residence Time	0.25 min.			0.75 min.			1.25 min.		
	0.5 hr	1.0 hr	1.5 hr	0.5 hr	1.0 hr	1.5 hr	0.5 hr	1.0 hr	1.5 hr
<b>39 A/m<sup>2</sup> (3.6 A/ft<sup>2</sup>)</b>									
<b>0.5 cm (0.2 in.) Spacing</b>	52.2%	73.7%	84.8%	62.1%	82.2%	90.4%	70.9%	85.1%	90.8%
<b>1.0 cm (0.4 in.) Spacing</b>	50.4%	74.0%	86.9%	60.5%	82.3%	90.2%	62.2%	82.4%	89.9%
<b>2.0 cm (0.8 in.) Spacing</b>	40.6%	70.8%	83.8%	47.3%	76.9%	85.6%	50.2%	77.3%	86.7%
<b>78 A/m<sup>2</sup> (7.2 A/ft<sup>2</sup>)</b>									
<b>0.5 cm (0.2 in.) Spacing</b>	56.3%	79.2%	89.5%	72.3%	86.1%	92.5%	76.2%	88.8%	93.0%
<b>1.0 cm (0.4 in.) Spacing</b>	47.3%	76.0%	84.0%	59.8%	83.7%	89.9%	68.6%	86.5%	91.2%
<b>2.0 cm (0.8 in.) Spacing</b>	51.4%	77.5%	86.4%	68.5%	86.7%	92.0%	75.0%	89.4%	93.9%
<b>116A/m<sup>2</sup> (10.8 A/ft<sup>2</sup>)</b>									
<b>0.5 cm (0.2 in.) Spacing</b>	51.4%	81.5%	89.8%	71.1%	87.6%	92.4%	81.0%	90.7%	94.0%
<b>1.0 cm (0.4 in.) Spacing</b>	87.4%	76.7%	87.2%	63.9%	86.4%	91.3%	75.0%	89.4%	93.3%

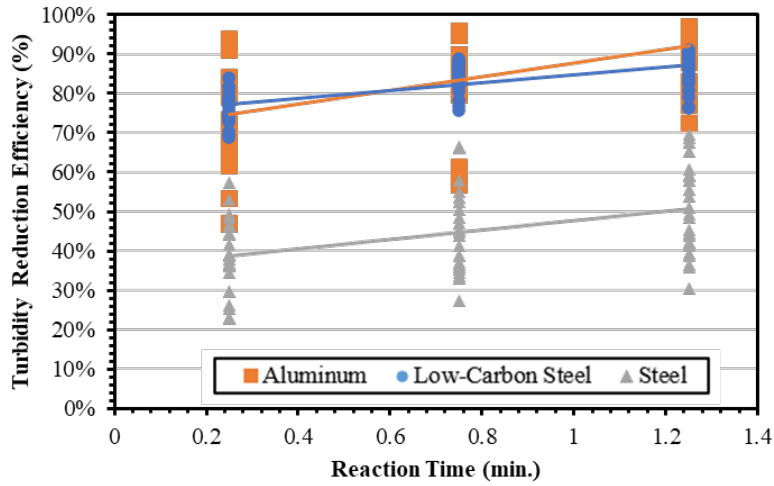


The results of turbidity reduction efficiencies versus different design factors (residence time, reaction time, cell spacing, and current density) are presented from Figure 4.6 to Figure 4.8, respectively. The trendlines generated in the scatter plots display a relationship between turbidity and different design factors separately. In Figure 4.6, it was found that the efficiency of turbidity removal using the metal cells increased with a longer reaction time regardless of cell's materials. Low-carbon steel and aluminum obtained higher efficiency on turbidity reduction compared to stainless steel.

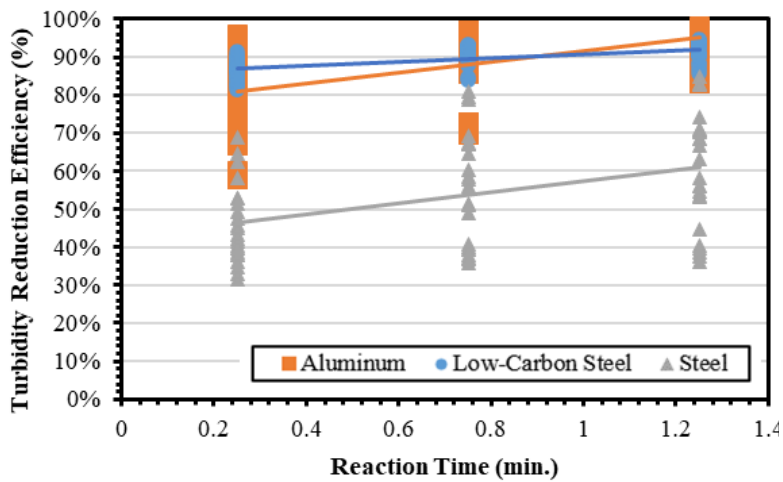
In addition, low-carbon steel performed consistent sediment removal efficiency along with the changes of different design factors compared to the other metal cells, which is proven by the concentrated load points. With exception of low-carbon steel, the turbidity removal can be improved by increasing the reaction time, cell spacing, or current density. For low-carbon steel, the turbidity removal decreased slightly as cell spacing increased. To quantify the amount of effects from each design factor, the MLR analysis was conducted.



(a) 30 minutes residence time

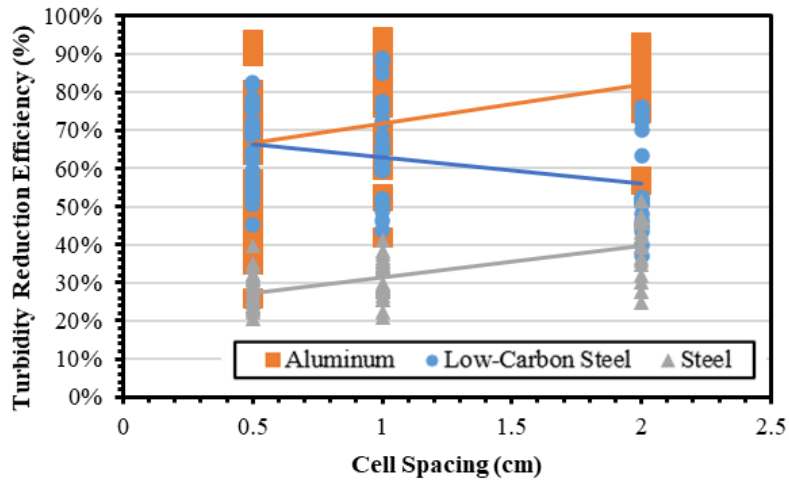


(b) 60 minutes residence time

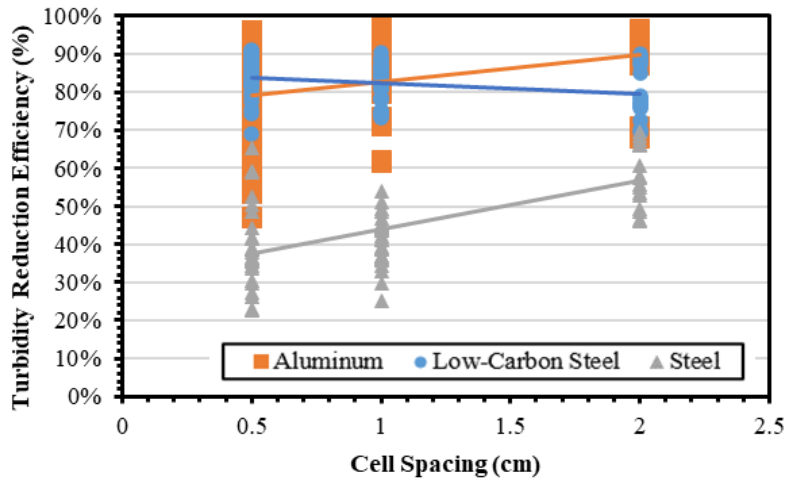


(c) 90 minutes residence time

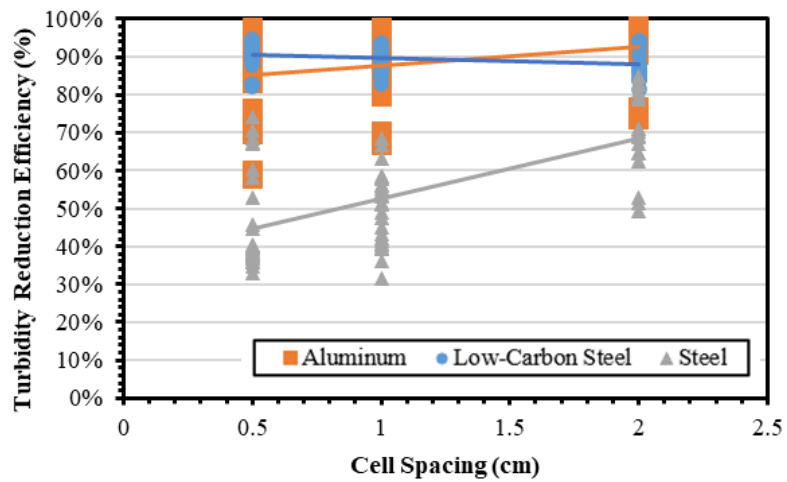
**Figure 4.6 Turbidity Reduction Efficiency versus Reaction Time.**



(a) 30 minutes residence time

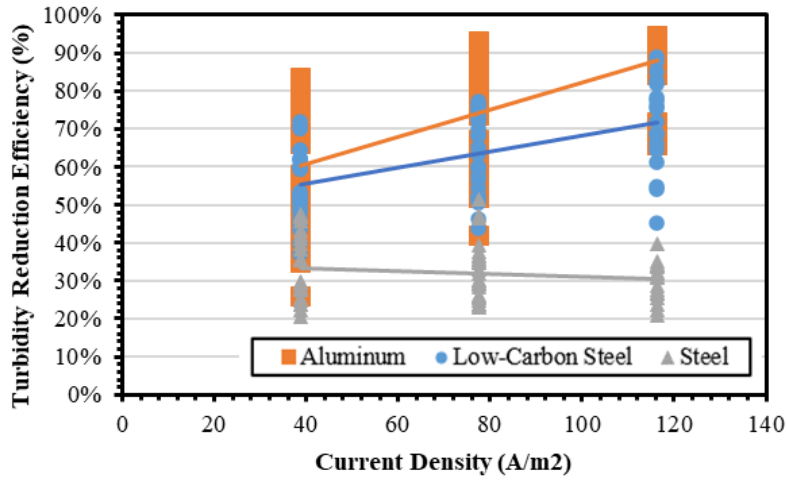


(b) 60 minutes residence time

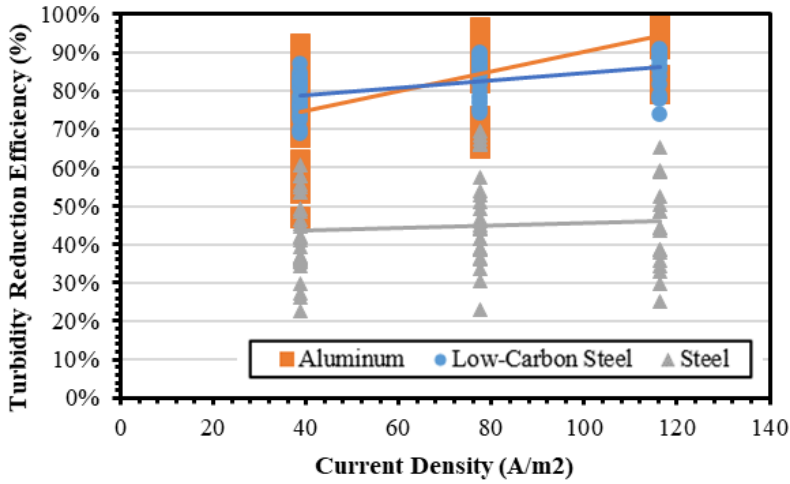


(c) 90 minutes residence time

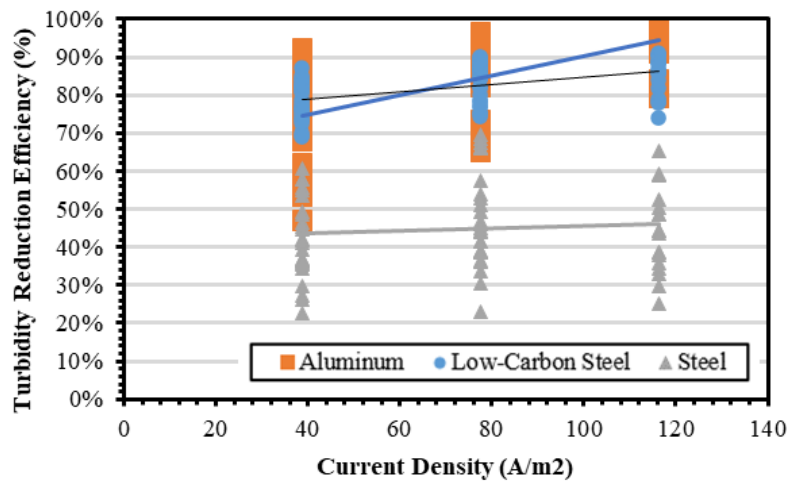
**Figure 4.7 Turbidity Reduction Efficiency versus Cell Spacing.**



(a) 30 minutes residence time



(b) 60 minutes residence time



(c) 90 minutes residence time

**Figure 4.8 Turbidity Reduction Efficiency versus Current Density.**

The MLR analysis was conducted to identify the relationship between turbidity reduction efficiency and each design factor (cell spacing, current density, reaction time, and residence time). The results of the empty control group ( $0 \text{ A/m}^2$  current) were used as the base condition for all analysis. Except for zero current density, the base condition included EC reactors for 0.25 minutes at 0.5 cm (0.2 in.) cell spacing with 30-min. residence time. According to the results of the MLR analysis displayed in Table 4.7, aluminum optimally performed using  $78 \text{ A/m}^2$  ( $7.2 \text{ A/ft}^2$ ) for a 1.25 min. reaction time at 2 cm (0.8 in.) plate spacing. Comparing the difference of coefficients of design factors, using aluminum cells for 0.75 minutes reaction time at  $78 \text{ A/m}^2$  current density and 2.0 cm (0.8 in.) plate spacing after 90 minutes residence time was selected as the optimized combination of design parameters in EC experiments. For stainless steel cells, the optimal condition of turbidity reduction rates is the same as aluminum cells. For low carbon steel, it is recommended to use 0.5 cm (0.2 in.) cell spacing for 0.75 minutes reaction time with  $78 \text{ A/m}^2$  ( $7.2 \text{ A/ft}^2$ ) to achieve optimal sediment treatment efficiency. As  $0 \text{ A/m}^2$  was selected as one of the base conditions, the reaction times under  $0 \text{ A/m}^2$  were not comparable which means it was necessary to conduct further tests and determine the optimal reaction time.

**Table 4.7 Results of MLR Analysis for Different EC cells**

	Coefficients			P-value		
	Aluminum	Stainless Steel	Low-Carbon Steel	Aluminum	Stainless Steel	Low-Carbon Steel
Intercept	0.12	0.11	0.32	<0.05	<0.05	<0.05
0.75 min.	0.11	0.06	0.06	<0.05	<0.05	<0.05
1.25 min.	0.16	0.10	0.09	<0.05	<0.05	<0.05
60 min.	0.11	0.13	0.19	<0.05	<0.05	<0.05
90 min.	0.16	0.22	0.27	<0.05	<0.05	<0.05
39 A/m <sup>2</sup> (3.6 A/ft <sup>2</sup> )	0.32	0.06	0.23	<0.05	<0.05	<0.05
78 A/m <sup>2</sup> (7.2 A/ft <sup>2</sup> )	0.45	0.10	0.29	<0.05	<0.05	<0.05
116 A/m <sup>2</sup> (10.8 A/ft <sup>2</sup> )	0.57	0.13	0.32	<0.05	<0.05	<0.05
1.0 cm (0.4 in.)	0.08	0.03	-0.02	<0.05	<0.05	<0.05
2.0 cm (0.8 in.)	0.18	0.20	-0.04	<0.05	<0.05	<0.05

#### **4.6.2. Electrode's Consumption**

The first factor considered for the electrode's consumption concerned their initial costs. The unit cost for aluminum took \$1.52/lb (\$3.35/kg) which was more expensive compared to other two materials. Low-carbon steel costed \$0.35/lb (\$0.77/kg) and stainless steel costed \$1.16/lb (\$2.56/kg). The densities are 2.7 g/cm<sup>3</sup> (0.10 lb/in<sup>3</sup>) for aluminum, 8.0 g/cm<sup>3</sup> (0.29 lb/in<sup>3</sup>) for stainless steel, and 7.85 g/cm<sup>3</sup> (0.28 lb/in<sup>3</sup>) for low carbon steel. All metal bars were cut into same dimensions (15.2 cm x 5.1 cm x 0.3 cm [6 in. x 2 in. x 1/8 in.]). The mass for each metal cell was calculated by multiplying density and volume. The initial costs of different metal cells in the bench scale experiments were: \$0.89 for aluminum, \$2.00 for stainless steel, and \$0.60 for low carbon steel, respectively. The same calculation process would be used to estimate the initial costs of electrodes in large scale in the future project.

Another factor considered was about the electrode's degradation during the EC reactions. The experiments were conducted under the developed optimal EC conditions (78A/m<sup>2</sup> for a 1.25 minute reaction time at 2 cm plate spacing) to estimate the loss of metal cells over time as shown in Table 4.8. It shows stainless steel degraded least material (0.12%) over 35 hours in the same EC experiments. And the aluminum took 11.5 hours and low-carbon steel took 7 hours to degrade around 1% of initial mass under the same EC reaction. The mass loss ratio of low-carbon steel (4.44%) was highest for 35 hours of the EC reaction compared to stainless steel and aluminum. And aluminum degraded moderate materials (2.91%) during the EC reaction.

**Table 4.8 Mass Loss for Different EC cells**

Reaction Time, hr	Aluminum			Stainless Steel			Low-carbon steel		
	Mass, g	Mass Loss, g	Mass Loss Rates	Mass, g	Mass Loss, g	Mass Loss Rates	Mass, g	Mass Loss, g	Mass Loss Rates
0	129.65	0.00	0.000%	378.56	0.00	0.000%	373.52	0.00	0.000%
1	129.51	0.14	0.109%	378.54	0.02	0.005%	372.89	0.63	0.170%
2	129.37	0.27	0.212%	378.53	0.03	0.009%	372.32	1.20	0.323%
3.5	129.19	0.46	0.354%	378.52	0.05	0.012%	371.49	2.03	0.545%
5	129.02	0.63	0.487%	378.50	0.06	0.017%	370.70	2.82	0.760%
7	128.81	0.84	0.650%	378.46	0.11	0.028%	369.69	3.83	1.037%
9	128.58	1.07	0.833%	378.42	0.14	0.038%	368.63	4.89	1.326%
11.5	128.33	1.32	1.027%	378.39	0.18	0.046%	367.35	6.17	1.680%
14	128.07	1.58	1.230%	378.36	0.21	0.055%	366.02	7.50	2.050%
17	127.83	1.82	1.424%	378.32	0.25	0.065%	364.67	8.85	2.427%
20	127.58	2.07	1.622%	378.29	0.28	0.073%	363.30	10.22	2.814%
23.5	127.22	2.43	1.911%	378.25	0.32	0.084%	361.89	11.63	3.213%
27	126.86	2.79	2.197%	378.21	0.36	0.094%	360.50	13.02	3.611%
31	126.42	3.23	2.552%	378.17	0.40	0.105%	359.07	14.45	4.024%
35	125.99	3.66	2.905%	378.12	0.44	0.117%	357.65	15.87	4.438%

Another approach to display the results of mass loss ratios was generating three scatter plots of mass loss ratios over time as shown in Figure 4.9. The scatter plots show the positive linear relationships between mass loss ratio and total EC reaction time. Three equations of trendlines were developed to estimate material loss over EC reaction for aluminum, low-carbon steel, and stainless steel, respectively. The R-squared values were close to 1 which displays acceptable predictive accuracy of the developed equations. Compared to aluminum and low-carbon steel, the trendline of stainless steel was fairly constant which means it degraded much less materials over the EC reaction. Stainless steel was recommended as optimal cell's material according to the results of mass loss rates during the EC reaction.

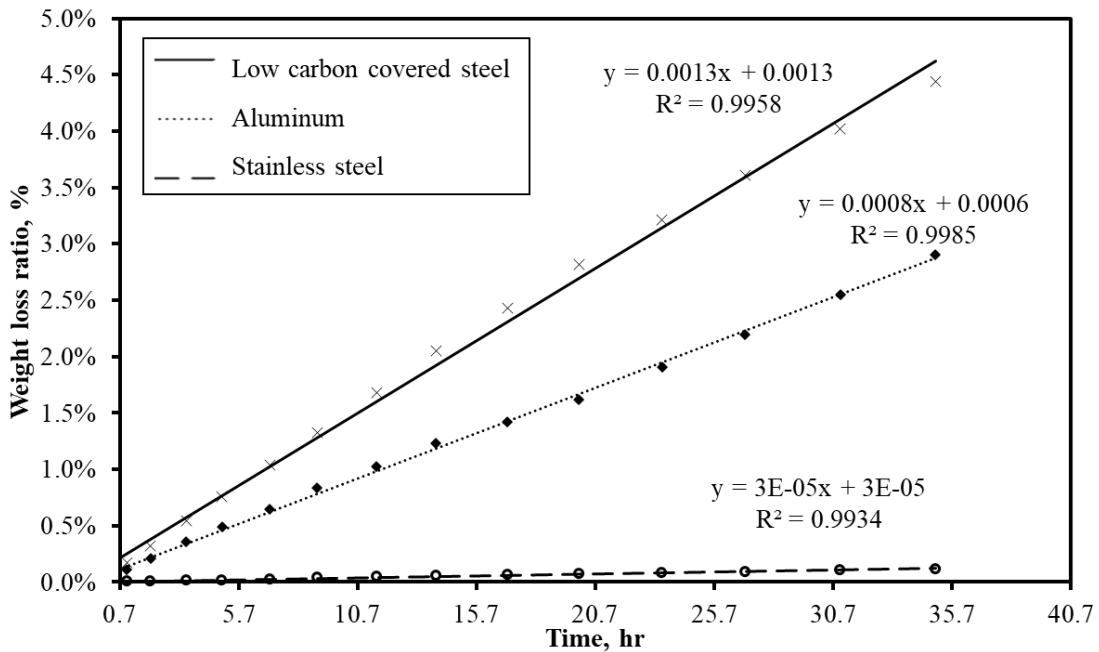


**Figure 4.9 Degradation of Different Metals in EC.**

Another factor considered in the EC consumption was energy saving (cell's material cost, degradation cost, and power cost) which was referred as total costs. The total costs of different metal cells were calculated to estimate which material is more effective. Three major factors were



included in the total costs: the initial cost of metal, the degradation cost of metal, and electric cost. Four metal plates were cut through one metal bar that was ordered through McMaster-Carr company. The mass loss ratios of different metal cells were used to estimate cost of EC degradation. The results of total costs shown that the difference between total cost for aluminum (\$32.38), low-carbon steel (\$31.94), and stainless steel (\$37.13) did not vary dramatically at bench scale. Although the total cost of low carbon steel was the lowest, the environmental concern was considered about degraded carbon in water after treatment. Since the total costs of aluminum was close to low-carbon steel, and aluminum was optimal material with more effective sediment treatment in EC reactions, aluminum was selected as final optimal material of electrodes with higher responses in turbidity removal and energy saving.

#### 4.6.3.pH

The pH under the optimal EC condition (Aluminum cell with 2 cm [0.8 in.] spacing) under different current densities along with the reaction time was recorded as shown in Table 4.9. It was found that pH changed slightly after EC treatment. Similar results were reported, which found that if the pH of reaction solution was neutral (around 6-8), the pH would only had slightly change after EC reaction (Kabdaşlı et al. 2012). In addition, the formation of aluminum hydroxide complex plays a vital role to decrease pH, which explained the slightly decrease of pH in this study.

**Table 4.9 pH Impact at Different Current Densities and Reaction Time**

Reaction Time (hr)	pH	
	39 A/m <sup>2</sup> (3.6 A/ft <sup>2</sup> )	78 A/m <sup>2</sup> (7.2 A/ft <sup>2</sup> )
0	8.38	9.12
1	8.00	8.55
2	8.67	8.86
4	9.07	8.97
5	8.75	8.87

#### 4.7. Conclusions

According to the results of turbidity reduction rates, the optimal condition is using aluminum electrodes for 0.75 minutes at 2 cm (0.8 in.) cell spacing and 39 A/m<sup>2</sup> (3.6 A/ft<sup>2</sup>) current density with 90 minutes residence time after 10 seconds of mixing. Besides the ability of turbidity removal, another factor considered was energy savings for different metal cells. In this study, the total cost considers material, cell degradation and electric power for different metals. According to the results of turbidity removal, aluminum was optimal cell material.

The results about cell degradation during EC reaction can allow designers to estimate maintenance and plate replacement intervals. As one of factors considered into the total energy savings, the results of cell mass loss were used to estimate the cost of cell degradation. Aluminum is more expensive metal compared to stainless steel and low carbon steel. However, the total energy savings of aluminum is close to low-carbon steel which were higher than stainless steel. based on the results of energy savings and turbidity removal, using aluminum electrodes for 0.75 minutes at 2 cm (0.8 in.) cell spacing and 39 A/m<sup>2</sup> (3.6 A/ft<sup>2</sup>) current density and 90 minutes residence time after 10 seconds of mixing is the optimal EC condition. The developed optimized design factors would be considered and used as the developed system design parameters for the application of lamella settler combined with EC displayed in the next Chapter.

## **CHAPTER 5. DEVELOPMENT AND EVALUATION OF LS+EC FOR TREATING SUSPENDED SEDIMENT**

### **5.1.Introduction**

Stormwater quality management has become an increasingly important topic across agricultural, urban, and construction sectors (Nayebare et al. 2014). Compared to other land uses, construction operations produce a large amount of sediment yield due to the earth disturbing nature of land-grading activities. At the federal level, the U.S. Environmental Protection Agency's (USEPA), National Pollutant Discharge Elimination System (NPDES), Construction General Permit (CGP) regulates earth-disturbing construction activities to minimize water quality impacts (USEPA 2009). To obtain NPDES coverage, regulated construction activities require the development, implementation, and maintenance of a Stormwater Pollution Prevention Plan (SWPPP). The SWPPP is a detailed site-specific plan for managing runoff during land development activities.

Sediment has significant impact on water quality and further acts as a media for transporting pollutants. Erosion and Sediment Control (E&SC) practices are commonly used on construction sites to reduce soil erosion and minimize sediment discharge. Erosion controls prevent topsoil from eroding, whereas sediment controls capture eroded sediment from the site. E&SCs installed on construction sites are typically passive "best management practices" (BMPs). There are several types of practices used to prevent soil loss and capture eroded soil particles (Forrest and Harding 1994a). Sediment basins are common practices used to promote the sedimentation process. These practices create extended detention for stormwater runoff to promote sedimentation. Current treatment practices remove large, rapidly settable, soil particles, however fine soil particles tend to remain suspended and contribute to elevated turbidity

conditions. A need exists for an economical and passive treatment mechanism for the removal of fine-sized suspended solids.

LSs are a type of water treatment system that consists of a set of inclined plates installed in a clarifier tank. These systems have traditionally been used wastewater-treatment applications (Kong et al. 2011). LS create a “counter flow” through a clarifier tank whereby suspended solids are directed through a series of parallel plates (Weiss 2013). The narrow spacing between LS plates shortens the vertical travel distance and reduces flow velocity, which creates laminar flow and constrains re-suspension within the system. Recent research using large-scale testing techniques indicate that high-rate lamella settlers could be an innovative approach for treating construction-site stormwater runoff, providing an improvement of up to 33% in the efficiency of an optimized sediment basin (Perez et al. 2019).

EC is another advanced technology that has been widely applied to wastewater treatment (Holt, Barton, and Mitchell 1999; Pouet and Grasmick 1995). EC is powered by electricity. The EC power supply can be divided into two parts: the direct current (DC) and the alternating current (AC), whereby the DC flows in one direction and the AC periodically changes direction. Most research on the EC process has focused on the DC, which causes oxidation at the anode to erode pollutant formations and produces an oxidation layer at the cathode (Khandegar and Saroha 2013). EC functions by generating an electrochemical reaction to corrode anodes, thereby destabilizing and removing contaminants suspended in water (Holt et al. 2005; Sahu et al. 2014). The EC process consists of two electrically charged metal elements, typically iron, aluminum, or stainless steel. An electrical charge is applied to the metal elements, which are placed in a treatment tank. Current flows from the positively charged cathode element into the negatively charged anode element. Additionally, the water surrounding the EC system is electrolyzed. The reaction

generates hydrogen gas bubbles. Furthermore, cations can also react with hydroxyl ions to form hydroxide, which increases the pH and influences the EC process. EC has become a popular treatment approach as it has been found to remove particles with higher efficiency, little modification, and without the need to use or handle chemicals (Emamjomeh and Sivakumar 2009).

The efficiency of pollutant removal is influenced by factors such as arrangement of electrodes, electrode materials, pH, applied voltage, and reaction time. There are few studies regarding the types of electrode materials used in pollutant removal. Iron, aluminum, and stainless steel are commonly applied or analyzed in industrial practices and research (Antropov 1972; Larue et al. 2003). Researchers have also developed optimized electrode configurations for specific target pollutants (Cañizares et al. 2007; Chafi et al. 2011; Mouedhen et al. 2008).

To improve sediment removal efficiency, the combination of EC and LS was considered in this project. With the exception of a patent investigation in 1990 (Figure 5.1), there has been no relevant study of combining these two systems (Maimoni 1990). The system invented in 1990 was developed as a crystallizer that could remove aluminum hydroxide from aluminum-air batteries or power cells. Rather than removing soil particles, the LS crystallizer followed the electrolyte storage tank to remove coarse product and maintain the crystal population. The crystallizer consisted of a set of parallel sheets inclined at 60°. As the slurry enters from the bottom of the settler, the settled solids were collected under each plate where crystallization occurred (Maimoni 1990).

In addition, there are limited relevant references about EC working with a LS for wastewater treatment. In a 1995 study, the performances of EC and of a LS system combined with flocculation were studied and compared to estimate the wastewater pollutant treatment efficiencies of the two systems. Two parameters were measured in that study: turbidity and suspended solids,

which both indicated that the system treatments were efficient. In fact, the authors found the EC and LS systems to achieve the same level of pollutant removal efficiency (around 90% for turbidity and suspended solids), with the only observed difference being the pH (Pouet and Grasmick 1995). The pH in the water treated by EC had increased due to the production of hydroxide ions, whereas the pH had decreased by acidification of the water treated with LS, which was induced by aluminum sulfate. In 2018, another study was conducted to compare the performances of EC and an LS combined with flocculation (Abdel-Fatah et al. 2016). The LS was installed after flocculation treatment (assisted by chemical coagulation) to treat textile wastewater. That is, chemical flocculants were introduced to react with pollutant materials before the samples entered the LS to increase the pollutant removal efficiency. The authors found that the percentage removal of total suspended solids (TSS) increased up to 92.3% when assisted by an optimum dose of the coagulant agent, i.e., 1,000 mg/L magnesium chloride heptahydrate ( $MgCl_2 \cdot 7H_2O$ ) with 1,000 mg/L lime. The results from that study indicated that chemical coagulation could reduce the settling time of pollutants to 30 minutes, but no detailed analysis was provided regarding the improvements obtained by combining flocculants with a LS system.

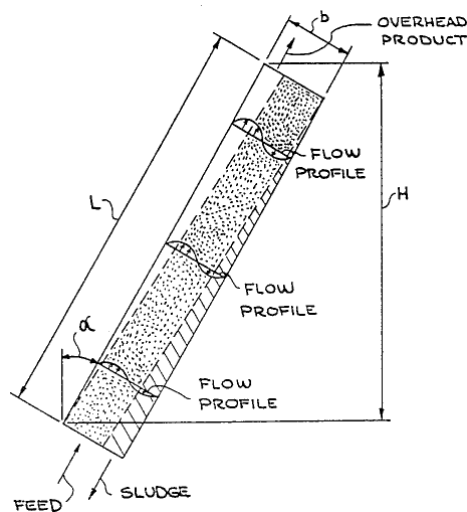


**Figure 5.1 Lamella Settler Crystallizer**

## **5.2. Research Objectives**

In this project, EC and LS technologies were combined to optimize the treatment of suspended sediments. The first goal was to conduct batch tests to determine and evaluate the optimal design parameters for EC reactions. Based on statistical analyses of the turbidity and electrical measurements, design recommendations were obtained. A novel continuous-flow EC system and three LS reactors were developed. Measurements of turbidity, TSS, pH, and the particle sizes of samples were obtained and analyzed to develop final design recommendations for large-scale implementation. In addition, the power consumption of this new system was monitored and recorded for reference purposes in the development of a large-scale system, as no previous research has reported results related to power consumption.

## **5.3. System Development**

In this study, EC was implemented as a pretreatment step, installed upstream of the LS reactors where the LS systems were developed in the previous study (Figure 3.2). Combination of the EC+LS system was considered by using charged metal lamella plates as electrodes, however the laminar flow nature of the LS system and the plate size requirements would provide limitations in agitation and current requirements, respectively. In the developed system, aluminum electrodes with 77.4-cm<sup>2</sup> (12-in<sup>2</sup>) reactive areas were used for the batch experiments. To make the system more effective and efficient, a vertical (downward) water flow was designed to maximize the EC reaction areas. The downward flow system prevented soil settlement and clogging within the EC system, thus simplifying the maintenance process. The EC system was placed in a 10.2 cm (4 in.) polyvinyl chloride (PVC) plastic cylinder in which there were four metal sheets with 2-cm (0.8-in) spacing fixed in a three-dimension (3D) printed component that allowed water flow through at the same time. Removable caps were used to close the two sides of the system to prevent overflow.

A discharge tube was connected at the bottom to introduce flow to the LS reactor. Considering the energy consumption, the desired current density of EC installed before the lamella settler was proposed as  $39 \text{ A/m}^2$  ( $3.6 \text{ A/ft}^2$ ) with 91.1% of turbidity removal rates.

Agitation and mixing improves the EC reaction process (Holt 2002). Two mixing systems were 3D-printed, fixed into a segment of PVC pipe, and installed downstream of the EC reactor to provide agitation and mixing (Aonomus 2014; Shi 2019). These 3D-printed pieces ( $X_1$  and  $X_2$ ) were pilot-tested to obtain the same effects achieved with a hand mixer.  $X_1$  was a helix-shaped static mixer with 1.9 cm (0.7 in.) diameter and 9.3 cm (3.7 in.) height. This mixer was sized to fit into a 1.9-cm (0.75-in) PVC pipe.  $X_2$  was a corrugated plate static mixer with 9.8 cm (3.9 in.) diameter and 10.1 cm (4.0 in.) height.  $X_2$  was sized to fit into a 10.2-cm (4-in) PVC pipe as shown in Figure 5.2. The 3D-printed baffles work by passively churning and mixing the sample solution, and dividing flow into sub streams to promote agitation.



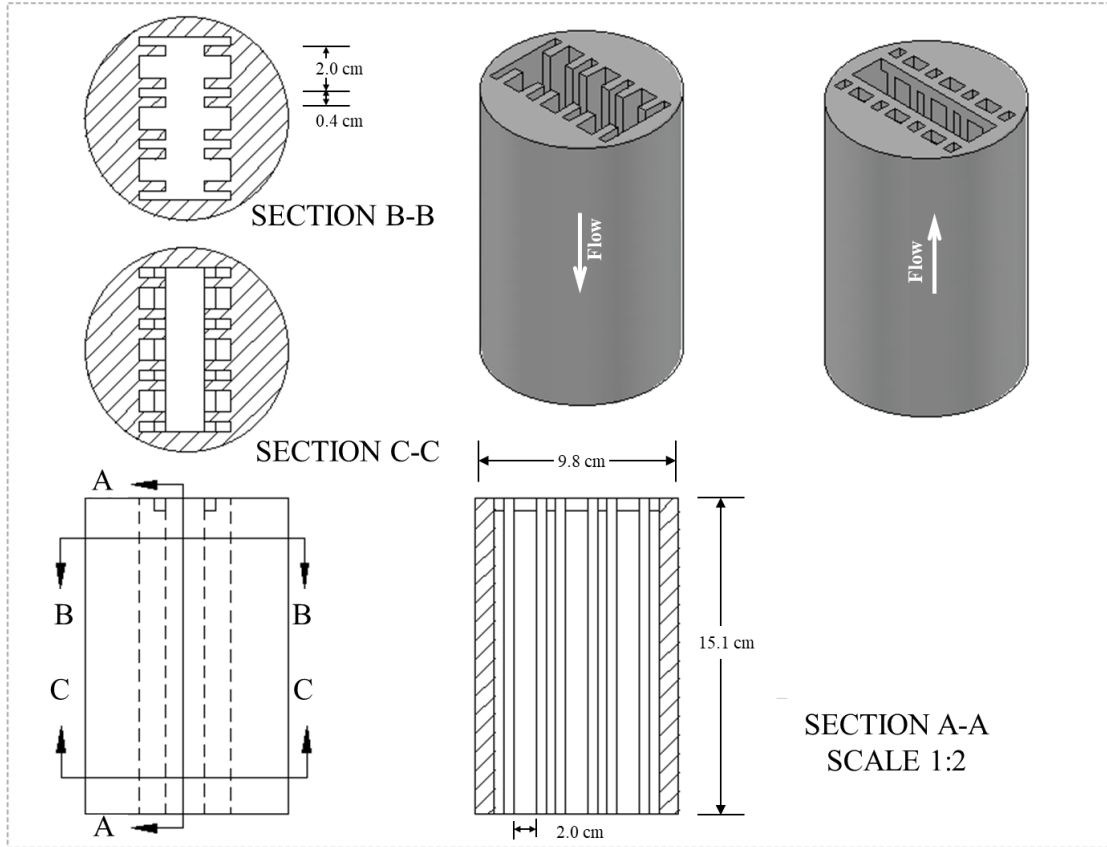


**Figure 5.2 EC Plate Assembly.**

A stand was designed for the EC+LS reactors and all the other components (mixer system, Cole-Parmer pump, and MasterFlex controller). To directly compare their performances, a control reactor was operated in parallel with all the experiments using the same prepared batch water. This parallel arrangement enabled use of the same influent solutions to increase the testing efficiency and ensure accuracy of the comparison of the experiments. As shown in Figure 5.3, the experimental setup included a valve is located between  $X_2$  and the lamella tanks to control the flow rates. To introduce the sample solution into the LS, this valve was opened until the desired 0.3-A current was reached. To prepare sediment-laden stormwater in a 104-L (55 gal) drum, we mixed the A25 synthetic soil, as the target soil sample, with 91 L (24 gal) of room-temperature tap water at a ratio equal to the target concentration (i.e., 500 mg/L, 1,000 mg/L, or 5,000 mg/L). These three

concentrations were selected and prepared to simulate the TSS load in construction runoffs. To achieve a homogenous concentration, mixing was performed by a 7.6-cm (3 in) right-handed propeller-fitted motor (Eastern Instruments, Model 5VB-C) with power levels maintained at mid-range for a period of 20 min. The mixer remained in use for the duration of the experiments to maintain uniform sediment suspension. The mixer was attached by custom-built mounts to the top of each drum.

Experiments were designed to introduce simulated sediment-laden stormwater at the inflow of the EC system. Flow was introduced into each reactor using a Cole-Parmer pump drive (Model 7591-50) and a MasterFlex pump controller at one of three constant rates: low, 0.42 L/min (0.11 gal/min), medium, 0.64 L/min (0.17 gal/min), and high, 1.25 L/min (0.33 gal/min). These flow rates were selected to achieve target-reactor residence times of 0.5 h (low), 1.0 h (medium), and 1.5 h (high). The residence time determines the reaction time of the EC reaction at different flow rates, as shown in Table 5.1. The optimized parameters in the beaker-size EC reaction were 39A/m<sup>2</sup> at 2-cm cell spacing for 0.75 min. With exception of the reaction time, these optimal EC reaction factors were considered and tested using the designed EC+LS system in bench-scale experiments.

**Table 5.1 Reaction Time of EC**

Flow Rates (L/s)	Residence Time (hr)	Reaction Time (min.)
0.021	30	0.128
0.011	60	0.256
0.007	90	0.384



**Figure 5.3 EC+LS Experimental Setup.**

To compare the performance of each designed mixer, same reacted sample solutions were collected after each mixing system. In addition, two more samples were collected directly after the EC system, one would follow with same mixing procedure with hand mixer, another one would be used as a control group without mixing. And each experiment would be repeated three times. Turbidity was monitored and recorded every ten minutes to display different system's performance. The results of turbidity reduction rates of three settling time (30 minutes, 60 minutes, and 90 minutes) were used to compare different mixing systems. As shown in Table 5.2 and Figure 5.4, it was found that the turbidity reduction rates improved 4% with mixing process where  $X_2$  obtained similar turbidity removal efficiency compared to hand mixer.  $X_2$  was chosen as the mixing system combined with M1 to form the complete final system before lamella settlers.

**Table 5.2 Turbidity Reduction with Different Mixing**

Settling Time (min.)	EC only	EC (hand mixer)	EC (X1)	EC (X2)
30	56.7%	65.1%	64.0%	62.4%
60	77.7%	79.7%	76.6%	77.8%
90	84.2%	88.3%	84.5%	86.5%

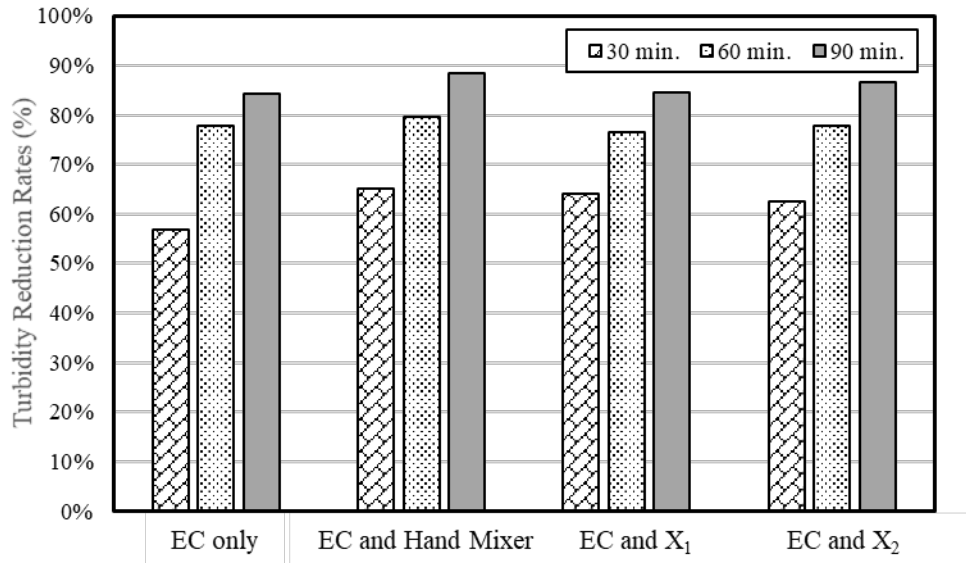


**Figure 5.4 Turbidity Removal Rates for Different Mixers.**

#### 5.4. Turbidity, TSS, Particle Size Analysis, and pH

Following the experiments protocol shown in Figure 5.5, the turbidity and TSS were monitored and analyzed to evaluate the performance of the EC system. The test results for turbidity and TSS removal efficiency after EC treatment were compared with the values obtained after the LS treatment. Results obtained from the LS systems were used to compare its performance with that achieved by the EC treatment using continuous flow at a constant current density for a 0.25-min EC reaction at 2.0 cm (0.8 in.) plate spacing across different residence times. On the other hand, the particle size distribution (PSD) analysis was conducted for the system consists of the recommended parameters which will provide the sediment removal efficiency in

another approach. Results obtained from the LS systems without the pretreatment of EC were used to compare its performance with the results of EC + LS treatment using continuous flow at a constant current density ( $39 \text{ A/m}^2$  [ $3.6 \text{ A/ft}^2$ ]) for a EC reaction at 2.0 cm (0.8 in.) plate spacing across different residence times. The results obtained by adding the EC were expected to provide greater turbidity reduction as the larger flocs formed in the EC reaction are easier to settle in the LS system. In addition, pH was monitored using a pH meter (Pocket Pro+ pH Tester, Hach®) before and after the EC reaction to evaluate system effects. To reduce sampler error, the pH probe and sampling cap were thoroughly cleaned with clean tap water between measurements. In addition, the pH meter was calibrated before each set of experiments.

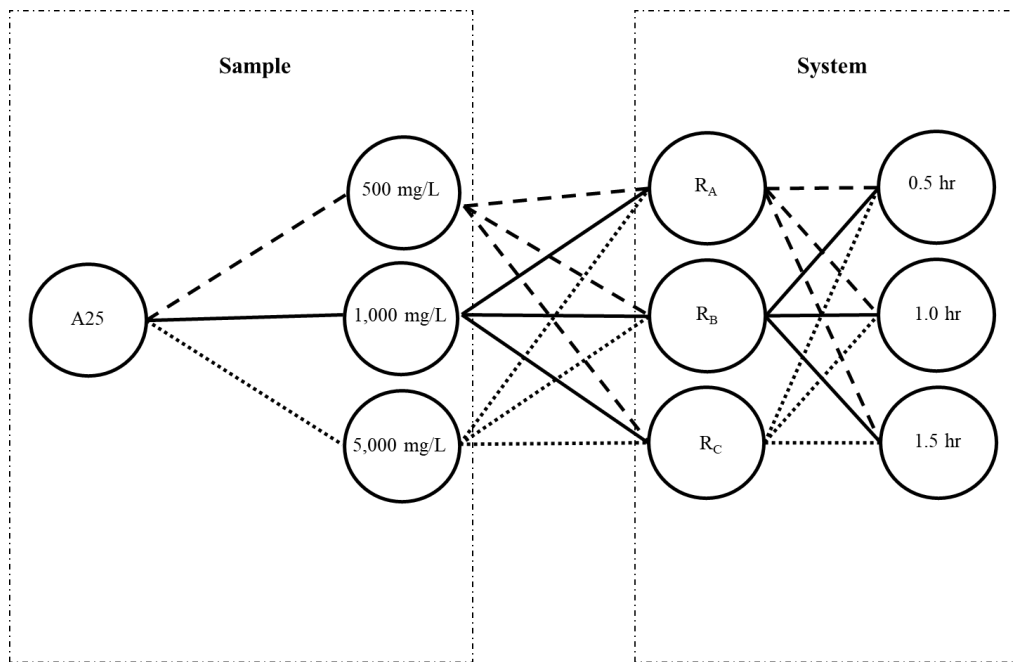


**Figure 5.5 Experimental Protocol.**

To statistically evaluate the degree of effectiveness of each treatment, statistical analysis using the Full-Factorial Method (FFM) was conducted to identify a mathematical relationship. This method was performed by controlling each treatment (i.e., inflow concentration, residence time, and settling distance) to create scatter plots. Trendlines were then plotted on the scatter plots

and used to characterize turbidity reduction rates. The results of regression analysis produced an optimal EC+LS recommendation considering different inflow concentration, particle's settling distance in the tank (i.e., vertical distance between plates), and residence time. Through the results of the FFM, a proposed factorial model was generated and solved by applying multiple regression analysis. In addition, ANOVA tests were performed to evaluate the developed model by identifying if there was significant difference existed among turbidity reduction rates and experimental variables. The null hypothesis of the test was that there was no significant difference among turbidity and TSS reduction rates, inflow concentration, particle's settling distance, and residence time. Each experimental variable was evaluated as a categorical variable in the analysis. ANOVA results with P-values lower than 0.05 indicated that the null hypothesis was rejected.

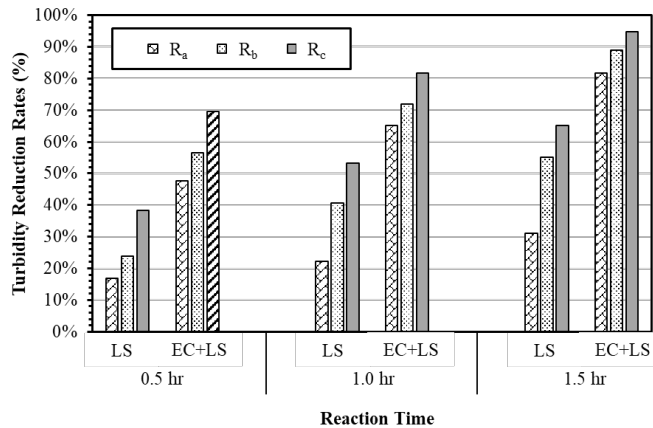
## **5.5.Results**

### ***5.5.1.Turbidity Reduction Rates, PSD, and TSS Analysis***

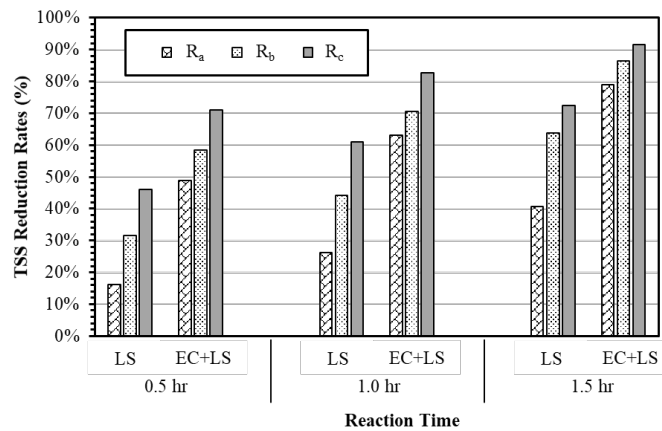
Table 5.2 and Figures 5.6, respectively, show the averaged turbidity and TSS reduction rates of the three concentrations, in which it is evident that the efficiency of sediment treatment increased dramatically with increases in the residence time and narrower plate spacing, with the assistance of EC. The turbidity reduction rate was found to improve from 16.9% to 65.1% with a LS system with 1.3 cm (0.5-in.) plate spacing corresponding to a 1.8 cm (0.7 in.) settling distance. The TSS reduction rates could be improved from 16.1% to 72.4% using the same optimal conditions in the LS system. On the other hand, the turbidity reduction rate of the EC + LS system increased from 47.5% to 94.7%, and the TSS reduction rates improved from 48.7% to 91.6% using the same optimal conditions.

**Table 5.3 Turbidity and TSS removal efficiencies of LS and EC+LS systems**

System		Turbidity Reduction			TSS Reduction		
		0.5 hr	1.0 hr	1.5 hr	0.5 hr	1.0 hr	1.5 hr
LS	$R_a$	16.9%	22.2%	31.1%	16.1%	26.2%	40.6%
EC+LS		47.5%	65.2%	81.7%	48.7%	63.1%	78.9%
LS	$R_b$	24.0%	40.6%	55.1%	31.6%	44.1%	63.8%
EC+LS		56.6%	72.0%	88.8%	58.4%	70.6%	86.5%
LS	$R_c$	38.4%	53.3%	65.1%	46.0%	60.9%	72.4%
EC+LS		69.5%	81.8%	94.7%	71.0%	82.8%	91.6%



(a) Turbidity reduction rates



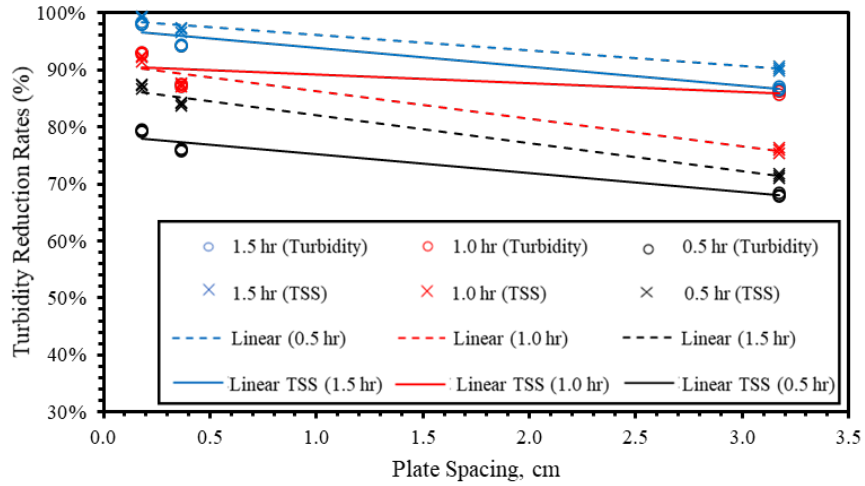
(b) TSS reduction rates

**Figure 5.6 Sediment Removal for A25.**

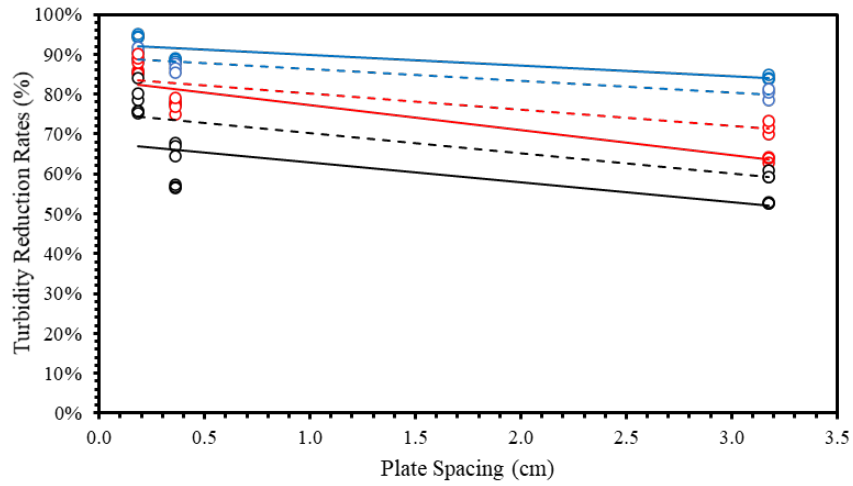
In the EC+LS system, the results of FFM analysis investigated the effects of turbidity reduction rates from experimental variables (i.e., inflow concentration, settling space, and residence time). Turbidity and TSS reduction rates were plotted against the particle settling distance for evaluated inflow concentrations, Figure 5.7. These plots revealed a linear relationship.

Turbidity reduction rates increased with decreased settling distance and increase of inflow concentrations. For example, the turbidity reduction rates at 500 mg/L were 22% at 31.8 cm (12.5 in.) settling distance. Turbidity treatment increased to 37% when the settling distance was reduced to 3.2 cm (1.4 in.), and increased to 54% at 1.8 cm (0.7 in.) settling distance.

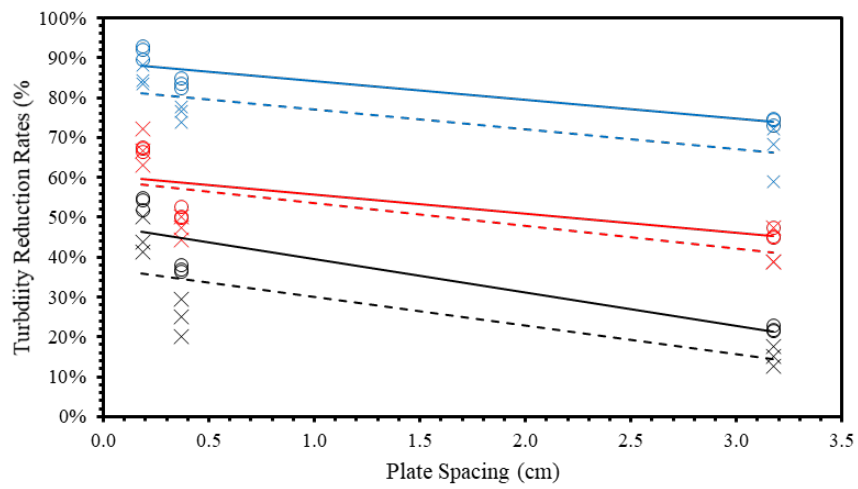




(a) 5,000 mg/L



(b) 1,000 mg/L



(c) 500 mg/L

**Figure 5.7 Turbidity and TSS Reduction Rates vs. Settling Distance at Evaluated Influent Concentrations.**

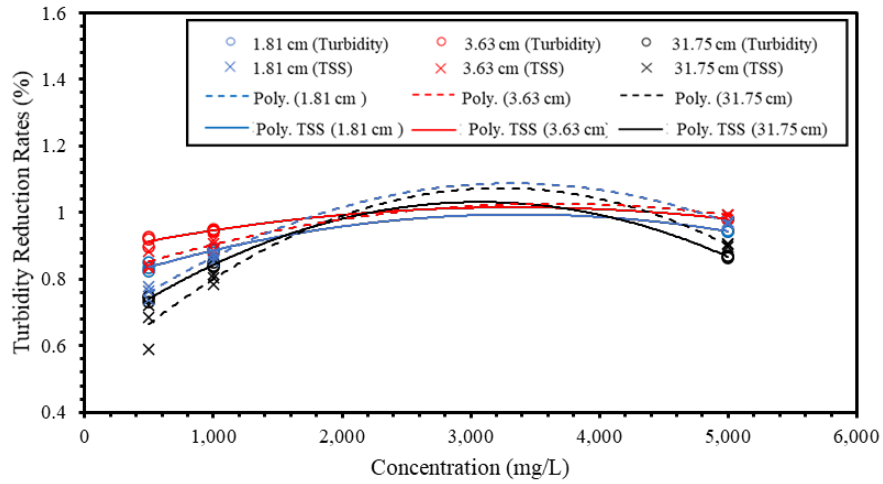
In Figure 5.8, the polynomial relationships between turbidity reduction rates and concentration are displayed. Turbidity reduction rates increased as inflow concentration increased with decreased settling distance. When the settling spacing increased to 31.8 cm (12.5 in.), the turbidity reduction rates decreased as shown in black lines in Figure 5.9. The FFM results were used to develop factorial models for turbidity and TSS reduction rates:

*Turbidity Reduction Rates (%)*

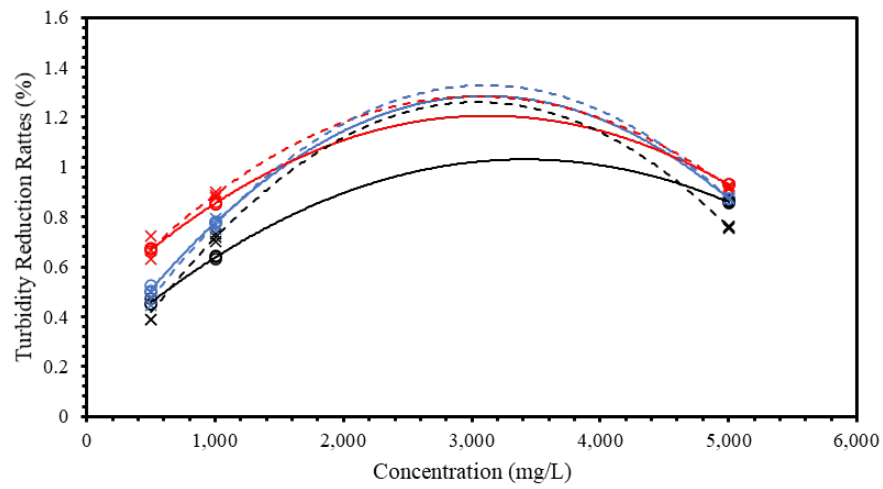
$$= a_0 + a_1 \times C + a_2 \times S + a_3 \times t + a_4 \times C \times t + a_5 \times S \times t + a_6 \times C \times S \quad (\text{Eq. 5.1})$$

$$+ a_7 \times C^2 + a_8 \times S^2 + a_9 \times t^2 + a_{10} \times (+EC)$$

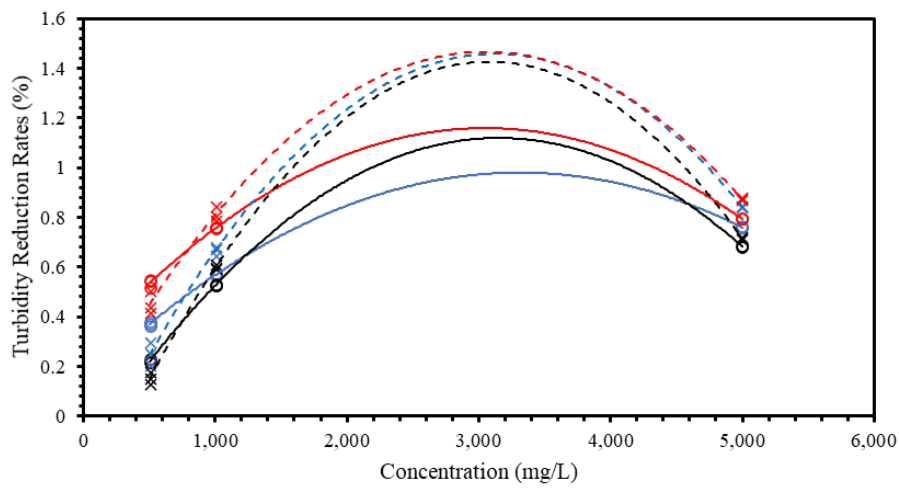
where  $a_0$  to  $a_{10}$  are the coefficients determined by least square method through regression analysis,  $C$  is inflow concentration,  $S$  is particle's settling distance,  $t$  is residence time, and "+EC" was treated as a categorical variable (0 indicates LS system, and 1 indicates the EC+LS system).



(a) 5,000 mg/L



(b) 1,000 mg/L



(c) 500 mg/L

**Figure 5.8 Turbidity and TSS Reduction Rates vs. Inflow Concentration at Evaluated Settling Distance**

Results of regression analysis and ANOVA tests are summarized in Table 5.4 where coefficients represent the degree of influence on turbidity reduction and P-values identify whether treatments had significant effects on turbidity reductions. It was found that the P-values of four terms (i.e.,  $t \times S$ ,  $S \times C$ ,  $t \times S \times C$  and  $t^2$ ) were greater than 0.05, which means the tests failed to reject the null hypotheses and there was no significant difference among turbidity or TSS reduction rates,  $t \times S$ ,  $S \times C$ ,  $t \times S \times C$  and  $t^2$ . The terms with P-values lower than 0.05 are shown in Table 5.4 and were used to re-analyze the model. The final results of the model are shown in Eq. 5.4 and Eq. 5.5. The R-square of turbidity analysis was 0.94, and 0.92 for TSS analysis. These R-square results signify the developed equation performed effectively in fitting the experimental data points.

**Table 5.4 Regression Results of LS and EC Systems**

	Eq. 2		Eq. 3		Eq. 4		Eq. 5	
	Turbidity (NTU)		TSS (mg/L)		Turbidity (NTU)		TSS (mg/L)	
	Coefficient	P-value	Coefficient	P-value	Coefficient	P-value	Coefficient	P-value
Intercept	0.0096	-	-0.0074	-	0.0143	-	-0.0367	-
C	0.3245	<0.05	0.5201	<0.05	0.3317	<0.05	0.5184	<0.05
S	-0.7027	<0.05	-0.7480	<0.05	-0.7052	<0.05	-0.7483	<0.05
t	0.3405	<0.05	0.2701	<0.05	0.3217	<0.05	0.3405	<0.05
$t \times C$	-0.0208	<0.05	-0.0344	<0.05	-0.0225	<0.05	-0.0325	<0.05
$t \times S$	-0.0121	0.3748	-0.0006	0.9709	0	-	0	-
$C \times S$	0.0058	0.2443	-0.0014	0.8021	0	-	0	-
$t \times C \times S$	-0.0014	0.7616	0.0015	0.7679	0	-	0	-
$C^2$	-0.0441	<0.05	-0.0753	<0.05	-0.0441	<0.05	-0.0753	<0.05
$S^2$	0.1872	<0.05	0.1979	<0.05	0.1872	<0.05	0.1979	<0.05
$t^2$	-0.0019	0.9653	0.0355	0.4702	0	-	0	-
+EC	0.3457	<0.05	0.2779	<0.05	0.3457	<0.05	0.2779	<0.05

The coefficients of inflow concentration, residence time, and settling distance provided enhancements in both turbidity and TSS removal rates. The R-square of turbidity analysis was 0.94, and 0.92 for TSS analysis. These R-square results signify the developed equation performed effectively in fitting the experimental data points.

*Turbidity Reduction Rates (%)*

$$\begin{aligned} &= 0.0143 + 0.3317 \times C - 0.7052 \times S + 0.3217 \times t - 0.0225 \times C \times t - 0.0441 \times C^2 \\ &+ 0.1872 \times S^2 + 0.3457 \times (+EC) \end{aligned} \quad \begin{array}{l} \text{(Eq.} \\ 5.2) \end{array}$$

*TSS Reduction Rates (%)*

$$\begin{aligned} &= -0.0367 + 0.5184 \times C - 0.7483 \times S + 0.3405 \times t - 0.0325 \times C \times t - 0.0753 \times C^2 \\ &+ 0.1979 \times S^2 + 0.2779 \times (+EC) \end{aligned} \quad \begin{array}{l} \text{(Eq.} \\ 5.3) \end{array}$$

The PSDs of the systems can also indicate their relative efficiencies. The  $D_{90}$  value of the A25 solution was found to decrease from 19.90  $\mu\text{m}$  to 3.18  $\mu\text{m}$  in the EC+LS system, whereas it dropped from 19.24  $\mu\text{m}$  to 2.36  $\mu\text{m}$  in LS system using the same optimal conditions (1.5 hr treatment in  $R_c$ ). In addition, the  $D_{90}$  value of the A25 solution collected directly after EC treatment increased to 28  $\mu\text{m}$ . pH levels were observed to have decreased slightly at downstream of the EC treatment due to the formation of the aluminum hydroxide complex. Similar results were reported in another study, in which the authors found that if the pH of the reaction solution was neutral (i.e., ranging from 6 - 8), the pH would only slightly change after the EC reaction (Kabdaşlı et al. 2012).

### **5.5.2. Extension of EC+LS**

Additional experiments were run through the optimized EC+LS system using two sets of field-collected stormwater runoff from a local construction site. When using the optimal EC system, the turbidity was determined to have dropped from 386 NTU to 237 NTU and the TSS from 340 mg/L to 213 mg/L in the mixed samples. The turbidity decreased from 4,882 NTU to 2,456 NTU, and the TSS from 3,262 mg/L to 1,013 mg/L in the sample with pure construction runoff using the same optimal experimental conditions. The system's treatment efficiency for the environmental samples reduced 49.7% of turbidity with 66.2% decrease of TSS. A large-scale experiment is planned to examine the system's performance in treating stormwater runoff.

In addition to turbidity and TSS data collection, two sets of 500 mL samples from the field-collected evaluations were characterized for common stormwater contaminants. Results indicated potential reductions in certain tested constituents including: potassium (K) 0.6 ppm, Aluminum (Al) 3.0 ppm, and sodium (Na) 2.5 ppm. Insignificant levels of Nitrogen (N), Phosphorous (P) were present in the samples to determine reduction performance. More replicates would be needed to conduct statistical analysis, however these reductions may indicate a potential in capturing other pollutants along with sediment. Reductions in Al signify that the oxidation of Al in the EC system does not lead to an increased concentration in effluent. Reductions in Na may provide for applications of EC systems in areas where winter weather deicer runoff is an environmental concern.

A subsequent pilot test was conducted in which the EC and flocculant treatments (FL) were compared. The first step was to determine the correct floc log treatment for A25 using different log kits. The FL system was substituted for the EC system by cutting the APS 706b floc log into small pieces and placing them in a 4-in PVC pipe. The same solution of 5,000 mg/L of A25 was prepared and introduced into the system. Before transferring the sample solution into the LSs, the valve was closed to allow 20 min of saturation time for the floc pieces in the FL system. After a treatment of 5,000 mg/L A25 with 1.5-h residence time, the turbidity reduction rate was 98%, which is similar compared to that obtained by EC treatment (98%), and the TSS reduction rate was 90%, which is the lower than that obtained using the EC system (99%). The application of adding the floc logs before the LS improved the removal of sediment compared to the performance of the LS system only but performed similarly performance compared to the EC+LS system. In other words, the EC+LS system can replace the FL system without the involvement of any chemicals.

### 5.5.3. Scaling Guidance

For the practical implementation of an EC+LS system, scaling would be required to provide treatment at flow rates expected in the field. The scaling guidance is split into two sections, the first one is the cell degradation during the EC reaction. The results of mass loss ratios of aluminum at 39 A/m<sup>2</sup> and 78 A/m<sup>2</sup> were plotted separately as shown in Figure 5.9. It was found that aluminum degraded 0.003 g per hour under 39 A/m<sup>2</sup> and 0.0008 g per hour under 78 A/m<sup>2</sup>. This result can be used to estimate material degradation in the future large scale tests.

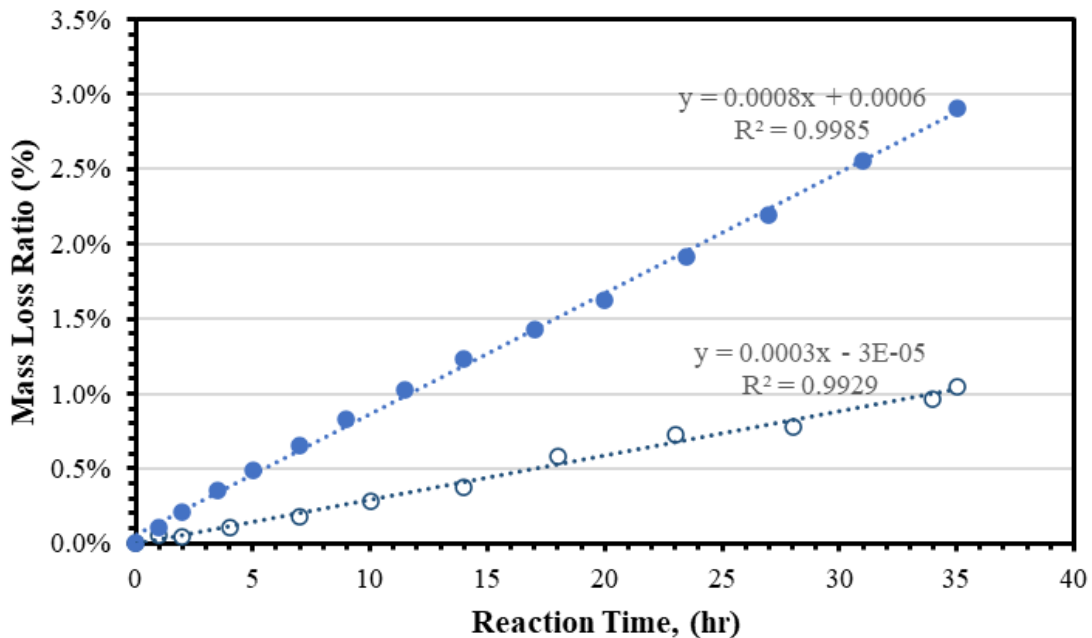


**Figure 5.9 Mass loss ratios of Aluminum under Different Current Densities**

The energy consumption in a field-scale EC system, summarized in Table 5.5, was designed by scaling the evaluated system to meet flow rates from a floating surface skimmer in a construction site sediment basin. A flow rate 0.06 m<sup>3</sup>/min (2.3 ft<sup>3</sup>/min), representative of a 5.1 cm (2.0 in.) diameter. Faircloth Skimmer<sup>®</sup> was used to estimate the treated volume and dimensions of the system (J. W. Faircloth & Son, Inc. 2020). Photovoltaic (PV) panels were considered as a potential DC source of power. PV cells allow for remote installation of the treatment system. 12V batteries could also be included in field implementation to allow for treatment during low sunlight

conditions. Using a production rate of 161.5 w/m<sup>2</sup> (15 w/ft<sup>2</sup>), it was determined that a total of 4.6 m<sup>2</sup> (49.1 ft<sup>2</sup>) would be required. However, current would only be required during periods of discharge and thus a system of 12V batteries could be used to provide energy demands during those times. A smaller PV footprint could be used to recharge batteries. Table 5.5 can be used as a reference to determine the dimensions of the large scale system to achieve same treatment efficiency for different sizes of the skimmers.

**Table 5.5 Field-Scale Design Parameters**

	<b>Bench Scale</b>	<b>Field Scale</b>
Length of EC plates, cm (in.)	31.1 (12.3)	166.6 (65.6)
Cross Sectional Area of EC, cm <sup>2</sup> (in. <sup>2</sup> )	18.9 (2.9)	541.8 (84.0)
Length of Plates, cm (in.)	20.3 (8.0)	108.8 (42.8)
Width of Plates, cm (in.)	3.8 (1.5)	20.4 (8.0)
Original Plate size, cm <sup>2</sup> (in. <sup>2</sup> )	77.4 (12.0)	2219.4 (344.0)
Treated Volume, cm <sup>3</sup> (in. <sup>3</sup> )	588.1 (35.9)	90,264 (5,508)
Power, watts	4.8	737
Power density, w/m <sup>3</sup> (w/ft <sup>3</sup> )	8,162 (231)	8,162 (231)
Unit Solar Power, w/m <sup>2</sup> (w/ft <sup>2</sup> )	-	161.5 (15.0)
Solar Panel Area, m <sup>2</sup> (ft <sup>2</sup> )	-	4.6 (49.1)

Notes: [A] flow rates were determined by using 60-min residence times

#### **5.5.4.pH**

The pH was measured and recorded as shown in Table 5.6. It was found that pH changed slightly after EC treatment. Similar results were reported, which found that if the pH of reaction solution was neutral (around 6-8), the pH would only had slightly change after EC reaction (Kabdaşlı et al. 2012). In addition, the formation of aluminum hydroxide complex plays a vital role to decrease pH, which explained the slight decrease of pH in this study.



**Table 5.6 Observations of pH change along EC reaction**

Inflow Concentration	System	Residence Time		
		0.5 hr	1.0 hr	1.5 hr
500 mg/L	Before EC	8.14	8.16	8.15
	After EC	8.07	7.97	7.84
	R <sub>a</sub>	8.12	8.09	8.00
	R <sub>b</sub>	8.03	8.09	7.87
	R <sub>c</sub>	8.09	8.01	8.04
1,000 mg/L	Before EC	8.18	8.18	8.20
	After EC	7.72	7.41	7.92
	R <sub>a</sub>	7.71	7.42	7.92
	R <sub>b</sub>	7.68	7.77	7.80
	R <sub>c</sub>	7.63	7.69	7.89
5,000 mg/L	Before EC	8.12	8.14	8.24
	After EC	7.49	7.56	8.01
	R <sub>a</sub>	7.51	7.72	8.05
	R <sub>b</sub>	7.63	7.59	8.02
	R <sub>c</sub>	7.50	7.60	8.01

## 5.6. Conclusions

Sediment loading from construction stormwater runoff are difficult to treat using traditional E&SC practices. The treatment of the fine-sized suspended clay and silt particles requires additional treatment considerations. This research presented the potential of using an EC+LS system to provide an enhanced removal rates of suspended sediment. This study developed and investigated the performance of a novel treatment system by using EC as a pretreatment to a LS reactor. A25 soil was used to simulate turbid stormwater conditions at concentrations of 500 mg/L, 1,000 mg/L, and 5,000 mg/L. In total, 489 experiments measuring turbidity and TSS and PSD were conducted to optimize the system's design factors including EC cell material and spacing, current density in the EC batch tests, inflow concentration, residence time and settling distance within the LS reactor.

Based on the results obtained in EC bench-scale experiments, an optimized set of design factors using 39 A/m<sup>2</sup> (3.6 A/ft<sup>2</sup>) current density with 2.0 cm (0.8 in.) aluminum cell spacing within

the EC system and 1.27 cm (0.5 in.) plate spacing with 90 minutes of residence time in a LS. The turbidity and reduction rates reached up to 98% and 99% under this optimal system. In addition, PSD analysis indicated a decrease in the  $D_{90}$  by up to 84%, indicating the optimized reactor was effective in capturing larger diameter soil particles. Based on these experimental results, a regression model was developed to characterize the relationship of turbidity and TSS reductions rates between inflow concentration, residence time, and settling distance in the LS. This model was generated based on bench scale experiments and was developed for future large-scale application. Large scale experiments are expected to achieve higher efficiency of sediment removal due to larger particle sizes contained in local soils compared to the samples used in the bench scaled experiments.

Stormwater samples were collected from a construction site and treated in the developed EC+LS system to examine treatment performance. Turbidity and TSS reduction rates of the field-collected stormwater runoff were 50% and 66%, respectively. In addition, the field collected samples had a Na reduction of 51%, indicating a potential application for treating urban stormwater with high levels of deicing materials. Compared to chemical-based flocculation, the EC+LS system demonstrated similar capability in removing sediment. This research has presented an opportunity for novel considerations in the treatment of stormwater runoff. Opportunities exist for future research to evaluate removal efficiencies of nutrients and other pollutants associated with urban and agricultural stormwater runoff. Large-scale and field-scale experiments are needed to evaluate the applicability of this technology in a scaled apparatus.

## CHAPTER 6. CONCLUSIONS

### 6.1.Introduction

Stormwater quality has become an increasingly important topic across the sectors of agricultural, urban, and construction. Compared to other land uses, construction operations produce a large amount of sediment yield due to the earth disturbing nature of land-grading activities. Environmental protection regulations developed by federal, state, and local agencies require the control of erosion and capture the sediment from construction stormwater to protect the receiving water bodies. This dissertation explored the improvements of design guidance of E&SC and construction stormwater technologies through the development of SILTspread: a silt fence design tool, bench scale tests of different lamella settlers and electrocoagulation technology.

### 6.2.Conclusions

This section summarizes the research outcomes that transfer objectives of this study. The major findings of this dissertation are obtained through the developed ESC design guidance and technology which provide the approach to introduce knowledge, recommendations, and new techniques with industry engineers. The publication of this research transfers the technology and satisfies the objectives of this dissertation.

#### ***6.2.1.SILTspread: Silt Fence Design Tool***

This study describes a silt fence sediment barrier design and installation standard developed through a comprehensive literature review of current state agency guidance and performance-based research. This study proposes a hydrologic design approach using local site conditions while accounting for detention volumes provided by silt fence barrier installations. A streamlined hydrologic design approach and volumetric storage relationships were developed for

three standard silt fence installation configurations (e.g., linear, J-hook, and C-shape). In addition, a user-friendly spreadsheet-based tool was developed to assist designers in calculating hydrologic and volumetric parameters, proper sizing of silt fence segments, and for estimating maintenance needs. A case study and recommendations for state agency implementation is included to demonstrate the application of the developed design approach.

### ***6.2.2. Bench-Scale Lamella Settler Experiments***

The objective of this research was to identify and optimize design configurations for a lamella settler system in treating a variety of synthetic soils. Five types of synthetic soils suspended in simulated stormwater at 500, 1,000, and 5,000 mg/L concentration were treated using system configurations of three lamella settler reactors at 0.5, 1.0, and 1.5-hr residence times. Statistical analyses suggested that each of these variables significantly affected turbidity levels. Through a series of 405 experiments and statistical analyses of results, performance relationships were developed to predict turbidity reduction rates for various lamella settler system designs. Through a full-factorial experimental method analysis, particle settling space was statistically the most influential in increasing treatment efficiency. An optimized lamella settler reactor providing 1.8 cm (0.7 in.) settling space with 1.5-hr residence time reduced turbidity by up to 90% when compared to a control reactor without lamella plates and a 0.5-hr residence time. In addition, particle size distribution analysis indicated a decrease in the  $D_{90}$  by up to 84 %, indicating the optimized reactor was effective in capturing larger diameter soil particles.

### ***6.2.3. Development and Evaluation of Lamella Settlers combined with Electrocoagulation for Treating Suspended Sediment***

In this research, the performance of electrocoagulation combined with lamella settlers was investigated. Electrocoagulation is a water-treatment technology that uses an electrochemical anode corrosion process to destabilize and remove contaminants. Electrocoagulation has been shown to have higher contaminant removal efficiency than conventional coagulation and has widespread applications for treatment of a variety of wastes. Lamella settlers have been shown to enhance soil-particle capture by increasing surface area and reducing settling distance. Combining these two treatment mechanisms has the potential to decrease the required size of the lamella settler while simultaneously maximizing the sedimentation process. Combining a lamella settler with electrocoagulation is a novel approach for treating suspended particles in stormwater. In this project, bench-scale experiments were conducted using electrocoagulation as pretreatment for a lamella settler reactor. Synthetic silica filler at concentrations of 500 mg/L, 1,000 mg/L, and 5,000 mg/L were used to evaluate treatment efficiency at 0.5-h, 1.0-h, and 1.5-h residence times. The collected data, including turbidity, total suspended solids, and particle size distribution were used to statistically characterize the system's sediment removal performance. Through a series of 489 experiments and statistical analyses of the results, an optimized electrocoagulation lamella settler reactor with 1.27-cm (0.5 in) plate spacing and 1.5-h residence time reduced turbidity by up to 98% and total suspended solids by 99% in the effluent when compared to the base condition. In addition, particle size distribution analyses indicated a decrease in the  $D_{90}$  value of up to 84%, indicating that the optimized reactor was effective in capturing larger-diameter soil particles. To validate laboratory results with synthetic sediment-laden influent, stormwater samples were collected from a construction site and treated through the optimized system. After routing through

the optimized treatment system, the turbidity of the construction runoff was found to have been reduced by 50% with a 69% decrease in total suspended solids. This manuscript presents these research results and how they can be used to design a full-scale system for field implementation.

### **6.3.Limitations and Future Study**

This section explores the limitations and future works for each project of the dissertation. Additional studies are suggested based on the summarized literatures and developed results to provide recommended future works.

#### ***6.3.1.SILTspread: Silt Fence Design Tool***

In this study, the SILTspread design tool is only applicable for the silt fence design under a 2-yr, 24-hr storm. Although this tool references geospatial data to support calculations which correlates the soil conditions and hydrologic analysis. The term of unit peak flow rate ( $q_u$ ) is calculated by assuming the storm event is 2-yr, 24-hr. A further development of the tool would be conducted by incorporate the hydrologic analysis for other storm events (ie. 2-yr, 6-hr, 5 yr, 6-hr, 2-yr, 10-yr, 24-hr, etc.)

In addition, the input format of the datasheet would be improved in the future work. Instead of letting the user checking the rainfall depth and soil information, the SILTspread can incorporate geographical data by connecting the hydrologic and soil information with the latitude and longitude. This improvement can ease the design process and reduce risk of errors during the input process. Large-scale experiments are expected to achieve lower efficiency of sediment removal due to larger particle sizes contained in the local soils compared to the samples used in the bench scaled experiments. This model can be widely applicable as it focused on the prediction of the turbidity treatment regardless of the sources of stormwater runoff (urban, construction, and agriculture).

### ***6.3.2. Bench-Scale Lamella Settler Experiments***

The bench scale experiments of this study are limited to the design of new lamella settlers. The current designs of three settlers consist of some 3D pieces and are not changeable, which means the plates spacing and plates angle of each settler were determined and cannot be modified once the settlers are built up. To conduct the experiments for different lamella settlers with a variety of plates' spacings and angles, there is a need to increase the flexibility of modifying the lamella settlers. A new plates' stand would be redesigned to make the rigid bar between the plates move together, which can change the plates spacing and angle at the same time. This proposed method can expand the capability of the bench scale lamella settler tests by building up different lamella settlers with changeable plates' spacing and distance.

In addition, a large-scale experiment would be incorporated with these bench scaled tests to compare the difference of settler's performance between small and large scales. The challenge of the large scale experiments would be inserting and modifying the lamella plates in the basin. It is highly recommended to use the obtained optimal design parameters to design the large scaled lamella settler and examine the settler's performance by testing the same soils used in this project.

### ***6.3.3. Development and Evaluation of Lamella Settlers combined with Electrocoagulation for Treating Suspended Sediment***

The innovative EC+LS system is limited to the ability of removing organic pollutants through EC treatment. It was found that EC does not contribute to removing the lightweight organic compounds or inorganic contaminants that cannot form precipitates (Shammas, Pouet, and Grasmick 2010). It would be helpful to improve and expand EC unit's performance, which can enhance the pollutants removal of EC+LS system. The developed EC+LS system is limited to the piping system developed in bench scale experiments. The highest current density that the

developed EC+LS system achieved was 39 A/m<sup>2</sup> (3.6 A/ft<sup>2</sup>) due to the constraint of high water pressure in the benched scale piping system. This problem will be solved in the large scale experiments with strong supports of the larger piping system.

A large-scale EC+LS would be designed and built by incorporating the optimal conditions obtained through the bench scale experiments. Opportunities exist for future research to evaluate removal efficiencies of nutrients and other pollutants associated with urban and agricultural stormwater runoff. Large-scale and field-scale experiments are needed to evaluate the applicability of this technology in a scaled apparatus.

#### **6.3.4. Summary**

Research outcome from the SILTspread tool can assist the implementation of silt fence using local site conditions. In addition, research results from lamella, and EC projects can be widely applicable as it focused on improving water quality regardless of the sources of stormwater runoff (urban, construction, and agriculture). The models developed from these projects can assist stormwater professionals by providing estimates of turbidity and TSS treatment effectiveness across a variety of design parameters (i.e., inflow concentration, settling distance, and residence time). This research has shown how LS combined with EC can provide significant water quality benefits to turbid water, providing enhancements in many water treatment applications including, construction, post-construction, and agricultural stormwater management. Additional applications in other water treatment processes such as wastewater and drinking water may benefit from the outcomes of this dissertation.



## REFERENCES

1. Abdel-Fatah, Mona A., H. O. Sherif, Fatma Agour, and S. I. Hawash. 2016. "Textile Wastewater Treatment By Chemical Coagulation Technology." *Global Journal of Advance Engineering Technology and Sciences* 3(4):14–31.
2. Alabama Soil and Water Conservation Committee. 2009. "Alabama Handbook for Erosion Control, Sediment Control and Stormwater Management on Construction Sites and Urban Areas."
3. Antropov, Lev Ivanovich. 1972. "Theoretical Electrochemistry." (Imported Pubn).
4. Aonomus. 2014. "39mm (1-1/2" SCH40) Corrugated Plate Static Mixer." *Thingiverse*. Retrieved (<https://www.thingiverse.com/thing:423563>).
5. Arroyo, M. G., V. Pérez-Herranz, M. T. Montanes, J. García-Antón, and J. L. Guinon. 2009. "Effect of PH and Chloride Concentration on the Removal of Hexavalent Chromium in a Batch Electrocoagulation Reactor." *Journal of Hazardous Materials* 169(1–3):1127–33.
6. ASTM. 2009. "Standard Test Methods for Particle-Size Distribution (Gradation) of Soils Using Sieve Analysis." *D6913-04* West Con-shohocken, PA, USA: ASTM International.
7. Azema, N., M. F. Pouet, C. Berho, and O. Thomas. 2002. "Wastewater Suspended Solids Study by Optical Methods." *Colloids and Surfaces A: Physicochemical and Engineering Aspects* 204(1–3):131–40.
8. Barrett, Michael E., John Edmund Kearney, Terry Glen McCoy, and Joseph F. Malina. 1995. "An Evaluation of the Use and Effectiveness of Temporary Sediment Controls." *Center for Research in Water Resources Tech. Rep. 261. Univ. of Texas at Austin, Austin, TX*.
9. Brady, Nyle C., Ray R. Weil, and Nyle C. Brady. 2010. *Elements of the Nature and*

*Properties of Soils*. Pearson educational international Upper Saddle River, NJ.

10. Bugg, R., Wesley Donald, Wesley Zech, and Michael Perez. 2017. "Performance Evaluations of Three Silt Fence Practices Using a Full-Scale Testing Apparatus." *Water* 9(7):502.
11. Can, O. T., and M. Bayramoglu. 2010. "The Effect of Process Conditions on the Treatment of Benzoquinone Solution by Electrocoagulation." *Journal of Hazardous Materials* 173(1–3):731–36.
12. Canizares, Pablo, Carlos Jiménez, Fabiola Martínez, Manuel A. Rodrigo, and Cristina Sáez. 2009. "The PH as a Key Parameter in the Choice between Coagulation and Electrocoagulation for the Treatment of Wastewaters." *Journal of Hazardous Materials* 163(1):158–64.
13. Cañizares, Pablo, Carlos Jiménez, Fabiola Martínez, Manuel A. Rodrigo, and Cristina Sáez. 2009. "The PH as a Key Parameter in the Choice between Coagulation and Electrocoagulation for the Treatment of Wastewaters." *Journal of Hazardous Materials* 163(1):158–64.
14. Cañizares, Pablo, Carlos Jiménez, Fabiola Martínez, Cristina Saez, and Manuel A. Rodrigo. 2007. "Study of the Electrocoagulation Process Using Aluminum and Iron Electrodes." *Industrial & Engineering Chemistry Research* 46(19):6189–95.
15. Canizares, Pablo, Fabiola Martínez, Justo Lobato, and Manuel Andrés Rodrigo. 2007. "Break-up of Oil-in-Water Emulsions by Electrochemical Techniques." *Journal of Hazardous Materials* 145(1–2):233–40.
16. Chafí, M., B. Gourich, A. H. Essadki, C. Vial, and A. Fabregat. 2011. "Comparison of Electrocoagulation Using Iron and Aluminium Electrodes with Chemical Coagulation for

- the Removal of a Highly Soluble Acid Dye.” *Desalination* 281:285–92.
17. Chavalparit, Orathai, and Maneerat Ongwandee. 2009. “Optimizing Electrocoagulation Process for the Treatment of Biodiesel Wastewater Using Response Surface Methodology.” 21:1491–96.
  18. Craig, Norman C. 2013. “United States Patent Office Publication, Including Testi - Mony on the Interference between Charles M. Hall and P. L V. [ Sic ] Hérout, 1887.” 38(1):13–18.
  19. Cronshey, Roger. 1986. *Urban Hydrology for Small Watersheds*. US Dept. of Agriculture, Soil Conservation Service, Engineering Division.
  20. Donald, W. N., W. C. Zech, M. A. Perez, and X. Fang. 2016. “Evaluation and Modification of Wire-Backed Nonwoven Geotextile Silt Fence for Use as a Ditch Check.” *Journal of Irrigation and Drainage Engineering* 142(2):4015050.
  21. Donald, Wesley N., Wesley C. Zech, Xing Fang, and Jeffery J. LaMondia. 2013. “Evaluation of Wheat Straw Wattles for Velocity Reduction in Ditch Check Installations.” *Transportation Research Record* 2358(1):69–78.
  22. Donohue, Ian, and Jorge Garcia Molinos. 2009. “Impacts of Increased Sediment Loads on the Ecology of Lakes.” *Biological Reviews* 84(4):517–31.
  23. Eastman, Tiffany. 2009. “Nonpoint Source, Point Source, and NPDES Permit.” *USEPA*.
  24. Emamjomeh, Mohammad M., and Muttucumaru Sivakumar. 2009. “Review of Pollutants Removed by Electrocoagulation and Electrocoagulation / Flotation Processes.” *Journal of Environmental Management* 90(5):1663–79.
  25. Emamjomeh, Mohammad Mahdi. 2006. “Electrocoagulation Technology as a Process for Defluoridation in Water Treatment.”

26. Fang, Xing, Wesley C. Zech, and Christopher P. Logan. 2015. "Stormwater Field Evaluation and Its Challenges of a Sediment Basin with Skimmer and Baffles at a Highway Construction Site." *Water (Switzerland)* 7(7):3407–30.
27. Faucette, Britt, and Mark Risse. 2001. "University Tests In-Vessel Composting of Food Residuals." *Biocycle* 42(1):68.
28. Faucette, L. Britt, J. Governo, C. F. Jordan, B. G. Lockaby, H. F. Carino, and R. Governo. 2007. "Erosion Control and Storm Water Quality from Straw with PAM, Mulch, and Compost Blankets of Varying Particle Sizes." *Journal of Soil and Water Conservation* 62(6):404–13.
29. Forrest, Carol L., and Michael V Harding. 1994a. "Erosion and Sediment Control: Preventing Additional Disasters after the Southern California Fires." *Journal of Soil and Water Conservation* 49(6):535–41.
30. Forrest, Carol L., and Michael V Harding. 1994b. "Erosion and Sediment Control: Preventing Additional Disasters after the Southern California Fires." *Journal of Soil and Water Conservation* 49(6):535–41.
31. Foster, G. R., R. A. Young, and W. H. Neibling. 1985. "Sediment Composition for Nonpoint Source Pollution Analyses." *Transactions of the ASAE* 28(1):133–39.
32. García-García, Alfredo, Verónica Martínez-Miranda, Iván G. Martínez-Cienfuegos, Perla Tatiana Almazán-Sánchez, Monserrat Castañeda-Juárez, and Ivonne Linares-Hernández. 2015. "Industrial Wastewater Treatment by Electrocoagulation–Electrooxidation Processes Powered by Solar Cells." *Fuel* 149:46–54.
33. Georgia Soil and Water Conservation Commission. 2002. "Erosion and Sediment Control Course Manual."

34. Georgia Soil and Water Conservation Commission. 2016. "Manual for Erosion and Sediment Control in Georgia." Athens, GA.
35. Gogo-Abite, Ikiensinma, and Manoj Chopra. 2013. "Performance Evaluation of Two Silt Fence Geotextiles Using a Tilting Test-Bed with Simulated Rainfall." *Geotextiles and Geomembranes* 39:30–38.
36. Golder, Animes K., Ajoy K. Chanda, Amar N. Samanta, and Subhabrata Ray. 2007. "Removal of Cr (VI) from Aqueous Solution: Electrocoagulation vs Chemical Coagulation." *Separation Science and Technology* 42(10):2177–93.
37. Holt, Peter, Geoffrey Barton, and Cynthia Mitchell. 1999. "Electrocoagulation as a Wastewater Treatment." *The Third Annual Australian Environmental Engineering Research Event* 1000:41–46.
38. Holt, Peter K., Geoffrey W. Barton, and Cynthia A. Mitchell. 2005. "The Future for Electrocoagulation as a Localised Water Treatment Technology." *Chemosphere* 59(3):355–67.
39. Holt, Peter Kevin. 2002. "Electrocoagulation: Unravelling and Synthesising the Mechanisms behind a Water Treatment Process."
40. Issaka, Sakinatu, and Muhammad Aqeel Ashraf. 2017. "Impact of Soil Erosion and Degradation on Water Quality: A Review." *Geology, Ecology, and Landscapes* 1(1):1–11.
41. J. W. Faircloth & Son, Inc. 2020. "Skimmer Sizing." Retrieved (<https://fairclothskimmer.com/skimmer-sizing/>).
42. Kabdaşlı, I., I. Arslan-Alaton, T. Ölmez-Hancı, and O. Tünay. 2012. "Electrocoagulation Applications for Industrial Wastewaters: A Critical Review." *Environmental Technology Reviews* 1(1):2–45.

43. Khandegar, V., and Anil K. Saroha. 2013. "Electrocoagulation for the Treatment of Textile Industry Effluent: A Review." *Journal of Environmental Management* 128:949–63.
44. Kobya, Mehmet, Orhan Taner Can, and Mahmut Bayramoglu. 2003. "Treatment of Textile Wastewaters by Electrocoagulation Using Iron and Aluminum Electrodes." 100:163–78.
45. Kong, Shiao-tong, Foreign Application, and Priority Data. 2011. "Density Current Baffle For a Clarifier Tank." 2(12):12–15.
46. Larue, O., E. Vorobiev, C. Vu, and B. Durand. 2003. "Electrocoagulation and Coagulation by Iron of Latex Particles in Aqueous Suspensions." *Separation and Purification Technology* 31(2):177–92.
47. Leung, Woon Fong, and Ronald F. Probsteln. 1983. "Lamella and Tube Settlers. 1. Model and Operation." *Industrial and Engineering Chemistry Process Design and Development* 22(1):58–67.
48. Mahmoudi-Rad, Mohammad, and Mohammad Javad Khanjani. 2019. "Energy Dissipation of Flow in the Vortex Structure: Experimental Investigation." *Journal of Pipeline Systems Engineering and Practice* 10(4):4019027.
49. Maimoni, Arturo. 1990. "Lamella Settler Crystallizer."
50. Makepeace, David K., Daniel W. Smith, and Stephen J. Stanley. 1995. "Urban Stormwater Quality: Summary of Contaminant Data." *Critical Reviews in Environmental Science and Technology* 25(2):93–139.
51. Mandelker, Daniel R. 1989. "Controlling Nonpoint Source Water Pollution: Can It Be Done." *Chi.-Kent L. Rev.* 65:479.
52. Mannina, Giorgio, and Gaspare Viviani. 2010. "An Urban Drainage Stormwater Quality Model: Model Development and Uncertainty Quantification." *Journal of Hydrology*

- 381(3–4):248–65.
53. Markusic, Melanie Sue. 2007. “Effects of Design Changes on Sediment Retention Basin Efficiency.” *MS Thesis*. 222–231.
54. Mollah, M. Yousu. A., Robert Schennach, Jose R. Parga, and David L. Cocke. 2001. “Electrocoagulation (EC) — Science and Applications.” *Journal of Hazardous Materials* 84(1):29–41.
55. Mouedhen, G., M. Feki, M. De Petris Wery, and H. F. Ayedi. 2008. “Behavior of Aluminum Electrodes in Electrocoagulation Process.” *Journal of Hazardous Materials* 150(1):124–35.
56. National Oceanic and Atmospheric Administration’s National Weather Service. 2014. *NOAA Atlas 14 Precipitation Frequency Estimates in GIS Compatible Format*. Hydrometeorological Design Studies Center, ed. Silver Spring, MD.
57. Nawarkar, C. J., and V. D. Salkar. 2019. “Solar Powered Electrocoagulation System for Municipal Wastewater Treatment.” *Fuel* 237:222–26.
58. Nayebare, Shedrack R., Lloyd R. Wilson, David O. Carpenter, David M. Dziewulski, and Kurunthachalam Kannan. 2014. “A Review of Potable Water Accessibility and Sustainability Issues in Developing Countries - Case Study of Uganda.” *Reviews on Environmental Health* 29(4):363–78.
59. Nguyentranlam, G., and K. P. Galvin. 2001. “Particle Classification in the Reflux Classifier.” *Minerals Engineering* 14(9):1081–91.
60. Norman, David K., Peter J. Wampler, Allen H. Throop, E. Frank Schnitzer, and Jaretta M. Roloff. 1997. “Best Management Practices for Reclaiming Surface Mines in Washington and Oregon.” *Washington State Department of Natural Resources*.

61. Parga, Jose R., David L. Cocke, Jesus L. Valenzuela, Jewel A. Gomes, Mehmet Kesmez, George Irwin, Hector Moreno, and Michael Weir. 2005. "Arsenic Removal via Electrocoagulation from Heavy Metal Contaminated Groundwater in La Comarca Lagunera M ´ Exico." 124:247–54.
62. Perez, M. A., W. C. Zech, W. N. Donald, and X. Fang. 2016. "SEDspread: Sediment-Basin Design Tool for Construction Sites." *Journal of Irrigation and Drainage Engineering* 142(12):4016064.
63. Perez, Michael A., Wesley C. Zech, Wesley N. Donald, and Xing Fang. 2015. "Installation Enhancements to Common Inlet Protection Practices Using Large-Scale Testing Techniques." *Transportation Research Record* 2521(1):151–61.
64. Perez, Michael A., Wesley C. Zech, Jose G. Vasconcelos, and Xing Fang. 2019. "Large-Scale Performance Testing of Temporary Sediment Basin Treatments and High-Rate Lamella Settlers." *Water* 11(2):316.
65. Phalakornkule, Chantaraporn, Pisut Sukkasem, and Chinnarat Mutchimsattha. 2010. "Hydrogen Recovery from the Electrocoagulation Treatment of Dye-Containing Wastewater." *International Journal of Hydrogen Energy* 35(20):10934–43.
66. Pitt, Robert, Shirley E. Clark, and Donald W. Lake. 2007. *Construction Site Erosion and Sediment Controls: Planning, Design and Performance*. DEStech Publications, Inc.
67. Pouet, M. F., and A. Grasmick. 1995. "Urban Wastewater Treatment by Electrocoagulation and Flotation." *Water Science and Technology* 31(3–4):275–83.
68. Pryor, M. R. 2012. *Mineral Processing*. Springer Science & Business Media.
69. Reardon, Roderick. 2005. "Clarification Concepts for Treating Peak Wet-Weather Wastewater Flows." *Florida Water Resources Journal* 11:4431–44.



70. Renard, Kenneth G. 1997. *Predicting Soil Erosion by Water: A Guide to Conservation Planning with the Revised Universal Soil Loss Equation (RUSLE)*. United States Government Printing.
71. Robichaud, P. R., D. K. McCool, C. D. Pannkuk, R. E. Brown, and P. W. Mutch. n.d. "Trap Efficiency of Silt Fences Used in Hillslope Erosion Studies." in *Pp. 541-543 in Soil Erosion Research for the 21st Century, Proc. Int. Symp. (3-5 January 2001, Honolulu, HI, USA)*. Eds. J.C. Ascough II and D.C. Flanagan. St. Joseph, MI: ASAE. St. Joseph, MI: ASABE.
72. Sahu, Omprakash, Bidyut Mazumdar, and P. K. Chaudhari. 2014. "Treatment of Wastewater by Electrocoagulation: A Review." *Environmental Science and Pollution Research*.
73. Shammas, Nazih K., Marie-Florence Pouet, and Alain Grasmick. 2010. "Wastewater Treatment by Electrocoagulation–Flotation." Pp. 199–220 in *Flotation Technology*. Springer.
74. Shi, Katie. 2019. "Helix Static Mixer." *Thingiverse*. Retrieved (<https://www.thingiverse.com/thing:3915237>).
75. Shih, I. ..., Y. ... Van, L. ... Yeh, H. ... Lin, and Y. ... Chang. 2001. "Production of a Biopolymer Flocculant from *Bacillus Licheniformis* and Its Flocculation Properties." *Bioresource Technology* 78(3):267–72.
76. South Carolina Department of Health and Environmental Control (SCDHEC). 2005. "Storm Water Management BMP Handbook." SC.
77. Stevens, E., B. J. Barfield, S. L. Brinson, and J. S. Hayes. 2004. "Filter Fence Design Aid for Sediment Control at Construction Sites." *U.S. Environmental Protection Agency, Office*

*of Research and Development* EPA 600/R-.

78. Tang, P., and Judy A. Raper. 2002. "Modelling the Settling Behaviour of Fractal Aggregates—a Review." *Powder Technology* 123(2–3):114–25.
79. Teh, Chee Yang, Pretty Mori Budiman, Katrina Pui Yee Shak, and Ta Yeong Wu. 2016. "Recent Advancement of Coagulation-Flocculation and Its Application in Wastewater Treatment." *Industrial and Engineering Chemistry Research* 55(16):4363–89.
80. Tennessee Department of Environment and Conservation Activities (TDECA). 2012. "Tennessee Erosion and Sediment Control Handbook."
81. United States Environmental Protection Agency. 1993. "Guidance Specifying Management Measures for Sources of Nonpoint Pollution in Coastal Waters."
82. United States Department of Agriculture; Soil Survey Staff. 2019. "Natural Resources Conservation Service." *Web Soil Survey*. Retrieved (<http://websoilsurvey.sc.egov.usda.gov/>).
83. United States Department of the Interior. 1953. *Water Measurement Manual*. Government Printing Office.
84. United States Environmental Protection Agency. 2000. "Storm Water Phase II Final Rule: Construction Site Runoff Control Minimum Control Measure."
85. United States Environmental Protection Agency. 2009. "Development Document for Final Effluent Guidelines and Standards for the Construction and Development Category." 266.
86. United States Environmental Protection Agency. 2012. "Stormwater Best Management Practice: Silt Fences." (April).
87. United States Environmental Protection Agency. 2019. "Rainfall Erosivity Factor Calculator for Small Construction Sites." Retrieved (<https://lew.epa.gov/>).

88. US Environmental Protection Agency (USEPA). 2017. "National Pollutant Discharge Elimination System General Permit for Discharges from Construction Activities." Washington, DC.
89. Vahedi, Arman, and Beata Gorczyca. 2012. "Predicting the Settling Velocity of Floes Formed in Water Treatment Using Multiple Fractal Dimensions." *Water Research* 46(13):4188–94.
90. Vahidifar, Saeid, Mohammad Reza Saffarian, and Ebrahim Hajidavalloo. 2019. "Numerical Simulation of Particle-Laden Flow in an Industrial Wastewater Sedimentation Tank." *Meccanica* 54(15):2367–83.
91. Vasconcelos, Jose G., Carmen D. Chosie, Holly M. Guest, and Andrew C. Patrick. 2014. "Lamella Settlers: Sediment Removal from Roadway Construction Runoff." (Online).
92. Vasconcelos, Jose G., and Wesley C. Zech. 2017. "Evaluation of High-Rate Settling Technology for Sediment Control in Roadway Construction Sites." *Research Proposal from the Highway Research Center Submitted to the Alabama Department of Transportation*.
93. Vasudevan, Subramanyan, Jothinathan Lakshmi, and Ganapathy Sozhan. 2011. "Effects of Alternating and Direct Current in Electrocoagulation Process on the Removal of Cadmium from Water." *Journal of Hazardous Materials* 192(1):26–34.
94. Weiss, Gebhard. 2013. "Innovative Use of Lamella Clarifiers for Central Storm- Water Treatment in Separate Sewer Systems Utilisation Innovante Des Décanteurs Lamellaires Pour Le Traitement Des Eaux Pluviales Dans Les Réseaux Sépara- Tifs." 1–10.
95. Weiss, Gebhard. 2016. "Lamella Settlers for Treatment of Urban Storm Runoff: Experience with Model and Prototype Tests." *Traitement de La Pollution/Pollution*

*Treatment-Bassins/Detention Basins & Retention Ponds Germany.*

96. Whitman, J B, W. C. Zech, and W. N. Donald. 2019. "Improvements in Small-Scale Standardized Testing of Geotextiles Used in Silt Fence Applications." *Geotextiles and Geomembranes* 47(5):598–609.
97. Whitman, J Blake, Wesley C. Zech, and Wesley N. Donald. 2019. "Full-Scale Performance Evaluations of Innovative and Manufactured Sediment Barrier Practices." *Transportation Research Record* 0361198119827905.
98. Whitman, J. Blake, Wesley C. Zech, Wesley N. Donald, and Jeffrey J. LaMondia. 2018. "Full-Scale Performance Evaluations of Various Wire-Backed Nonwoven Silt Fence Installation Configurations." *Transportation Research Record* 2672(39):68–78.
99. Wischmeier, Walter H., and Dwight David Smith. 1978. *Predicting Rainfall Erosion Losses: A Guide to Conservation Planning*. Department of Agriculture, Science and Education Administration.
100. Zech, Wesley C., Jarid L. Halverson, and T. Prabhakar Clement. 2007. "Development of Silt Fence Tieback Design Methodology for Highway Construction Installations." *Transportation Research Record* 2011(1):21–28.
101. Zech, Wesley Charles, J. S. McDonald, and T. Prabhakar Clement. 2009. "Field Evaluation of Silt Fence Tieback Systems at a Highway Construction Site." *Practice Periodical on Structural Design and Construction* 14(3):105–12.
102. Zhu, Bintuan, Dennis A. Clifford, and Shankararaman Chellam. 2005. "Comparison of Electrocoagulation and Chemical Coagulation Pretreatment for Enhanced Virus Removal Using Microfiltration Membranes." *Water Research* 39(13):3098–3108.

## APPENDICES

## **Appendix A Silt Fence Design**

### Curve Numbers (TR-55)

Land Cover	Detail	A	B	C	D
Open_Space	Poor (grass cover < 50%)	68	79	86	89
Open_Space	Fair (grass cover 50% to 75%)	49	69	79	84
Open_Space	Good (grass cover > 75%)	39	61	74	80
Pasture_Grassland	Poor (continuous forage for grazing )	68	79	86	89
Pasture_Grassland	Fair (continuous forage for grazing )	49	69	79	84
Pasture_Grassland	Good (continuous forage for grazing )	39	61	74	80
Meadow	Continuous grass, prot. from grazing, generally mowed for hay	30	58	71	78
Brush	Poor ( brush-weed-grass mixture w/ brush the major element )	48	67	77	83
Brush	Fair ( brush-weed-grass mixture w/ brush the major element )	35	56	70	77
Brush	Good ( brush-weed-grass mixture w/ brush the major element )	30	48	65	73
Woods_Grass	Poor	57	73	82	86
Woods_Grass	Fair	43	65	76	82
Woods_Grass	Good	32	58	72	79
Woods	Poor	45	66	77	83
Woods	Fair	36	60	73	79
Woods	Good	30	55	70	77
Streets_and_Roads	Paved; curbs and storm sewers (excluding right-of-way)	98	98	98	98
Streets_and_Roads	Paved; open ditches (including right-of-way)	83	89	92	93
Streets_and_Roads	Gravel (including right-of-way)	76	85	89	91
Streets_and_Roads	Dirt (including right-of-way)	72	82	87	89
Western_Desert_Urban_Areas	Natural desert landscaping (pervious areas only)	63	77	85	88
Western_Desert_Urban_Areas	Artificial desert landscaping (impervious weed barrier,desert shrub with 1- to 2-inch sand or gravel mulchand basin borders)	96	96	96	96
Urban_Districts	Commercial and business	89	92	94	95
Urban_Districts	Industrial	81	88	91	93
Residential_Districts_by_Average_Lot_Size1/8 acre or less (town houses)		77	85	90	92
Residential_Districts_by_Average_Lot_Size1/4 acre		61	75	83	87
Residential_Districts_by_Average_Lot_Size1/3 acre		57	72	81	86
Residential_Districts_by_Average_Lot_Size1/2 acre		54	70	80	85
Residential_Districts_by_Average_Lot_Size1 acre		51	68	79	84
Residential_Districts_by_Average_Lot_Size2 acre		46	65	77	82
Newly_Graded_Areas	Pervious areas only no vegetation	77	86	91	94

## C Factors for Established Plants ((Wischmeier and Smith 1978))

Percentage of surface covered by residue in  
contact with the soil:

	Percent cover <sup>1</sup>	Plant type	0%	20	40	60	80	95+
Grass, grasslike plants, or decaying compacted plant litter.	0	Grass	0.45	0.2	0.1	0.042	0.013	0.003
Broadleaf herbaceous plants (including most weeds with little lateral root networks), or undecayed residues.	0	Weeds	0.45	0.24	0.15	0.091	0.043	0.011
Tall weeds or short brush with avg. drop height <sup>2</sup> of $\geq 20$ in.	25	Grass	0.360	0.170	0.090	0.038	0.013	0.003
		Weeds	0.360	0.200	0.130	0.083	0.041	0.011
	50	Grass	0.260	0.130	0.070	0.035	0.012	0.003
		Weeds	0.260	0.160	0.110	0.076	0.039	0.011
	75	Grass	0.170	0.100	0.060	0.032	0.011	0.003
		Weeds	0.170	0.120	0.090	0.068	0.038	0.011
Mechanically prepared sites, w/ no live vegetation, no topsoil, and no litter.	0.00	None	0.94	0.44	0.30	0.20	0.1	N/A

<sup>1</sup> percent cover is the portion of the total area surface that would be hidden from view by canopy if looking straight downward.

<sup>2</sup> drop height is the average fall height of water drops falling from the canopy to the ground.



### Construction Site Mulching C Factors and Length Limits for Different Slopes (Wischmeier and Smith 1978)

Type of Mulch	Mulch Rate (tons/ ac)	Land Slope (%)	Mulching C Factor	Length Limit (ft) <sup>1</sup>
None	0.0	all	1.0	N/A
	1.0	1-5	0.20	200
	1.0	6-10	0.20	100
	1.5	1-5	0.12	300
Straw or hay, tied down by anchoring and tacking equipment	1.5	6-10	0.12	150
	2.0	1-5	0.06	400
	2.0	6-10	0.06	200
	2.0	11-15	0.07	150
	2.0	16-20	0.11	100
	2.0	21-25	0.14	75
	2.0	26-33	0.17	50
	2.0	34-50	0.20	35
	7.0	<16	0.08	75
	7.0	16-20	0.08	50
	12	<16	0.05	150
	12	16-20	0.05	100
Wood chips	12	21-33	0.05	75
	25	<16	0.02	200
	25	16-20	0.02	150
	25	21-33	0.02	100
	25	34-50	0.02	75

<sup>1</sup> Maximum slope lengths for which the specified mulch rate is considered effective. If these limits are exceeded, either a higher application rate or mechanical shortening of the effective slope length is required (such as with terracing).

### **P Factor Values for Construction-Site BMPs (Fifield 2011)**

<b>Treatment</b>	<b>P Factor</b>
Bare soil, packed and smooth	1.00
Bare soil, freshly disked or rough, irregular surface	0.90
Sediment basin	0.10-0.90
Bale or sandbag barriers	0.90
Rock (diameter= 25-50 mm) barriers at sump	0.80
Silt fence barreir	0.60

LS Factors for Freshly Prepared Construction Sites, with Little, or no Cover (Renard 1997)

		Slope Length (ft)																
		<3	6	9	12	15	25	50	75	100	150	200	250	300	400	600	800	1,000
Slope (%)	0.2	0.05	0.05	0.05	0.05	0.05	0.05	0.05	0.05	0.05	0.05	0.06	0.06	0.06	0.06	0.06	0.06	0.06
	0.5	0.07	0.07	0.07	0.07	0.07	0.07	0.08	0.08	0.09	0.09	0.10	0.10	0.10	0.11	0.12	0.12	0.13
	1	0.09	0.09	0.09	0.09	0.09	0.10	0.13	0.14	0.15	0.17	0.18	0.19	0.20	0.22	0.24	0.26	0.27
	2	0.13	0.13	0.13	0.13	0.13	0.16	0.21	0.25	0.28	0.33	0.37	0.40	0.43	0.48	0.56	0.63	0.69
	3	0.17	0.17	0.17	0.17	0.17	0.21	0.30	0.36	0.41	0.50	0.57	0.64	0.69	0.80	0.96	1.10	1.23
	4	0.20	0.20	0.20	0.20	0.20	0.26	0.38	0.47	0.55	0.68	0.79	0.89	0.98	1.14	1.42	1.65	1.86
	5	0.23	0.23	0.23	0.23	0.23	0.31	0.46	0.58	0.68	0.86	1.02	1.16	1.28	1.51	1.91	2.25	2.55
	6	0.26	0.26	0.26	0.26	0.26	0.36	0.54	0.69	0.82	1.05	1.25	1.43	1.60	1.90	2.43	2.89	3.30
	8	0.32	0.32	0.32	0.32	0.32	0.45	0.70	0.91	1.10	1.43	1.72	1.99	2.24	2.70	3.52	4.24	4.91
	10	0.35	0.37	0.38	0.39	0.40	0.57	0.91	1.20	1.46	1.92	2.34	2.72	3.09	3.75	4.95	6.03	7.02
	12	0.36	0.41	0.45	0.47	0.49	0.71	1.15	1.54	1.88	2.51	3.07	3.60	4.09	5.01	6.67	8.17	9.57
	14	0.38	0.45	0.51	0.55	0.58	0.85	1.40	1.87	2.31	3.09	3.81	4.48	5.11	6.30	8.45	10.40	12.23
	16	0.39	0.49	0.56	0.62	0.67	0.98	1.64	2.21	2.73	3.68	4.56	5.37	6.15	7.60	10.26	12.69	14.96
	20	0.41	0.56	0.67	0.76	0.84	1.24	2.10	2.86	3.57	4.85	6.04	7.16	8.23	10.24	13.94	17.35	20.57
	25	0.45	0.64	0.80	0.93	1.04	1.56	2.67	3.67	4.59	6.30	7.88	9.38	10.81	13.53	18.57	23.24	27.66
	30	0.48	0.72	0.91	1.08	1.24	1.86	3.22	4.44	5.58	7.70	9.67	11.55	13.35	16.77	23.14	29.07	34.71
40	0.53	0.85	1.13	1.37	1.59	2.41	4.24	5.89	7.44	10.35	13.07	15.67	18.17	22.95	31.89	40.29	48.29	
50	0.58	0.97	1.31	1.62	1.91	2.91	5.16	7.20	9.13	12.75	16.16	19.42	22.57	28.60	39.95	50.63	60.84	
60	0.63	1.07	1.47	1.84	2.19	3.36	5.97	8.37	10.63	14.89	18.92	22.78	26.51	33.67	47.18	59.93	72.15	

## **Appendix B: Procedure of turbidity and TSS Measurements**

**Step 1: Sample preparation:**

**Every set of experiment should prepare a new sample to make sure the proportion of the finer particles remains same in each experiment.**

① Soil type: Soil A, Soil B, Soil C, and Soil D:

500 mg/L (Repeat 3 times)

Weigh 26.5 g sample

Fill up water in the drum to 22.28 in. high (total 35 gallons)

Pour weighed sample into a 2 L bigger and grab around 500 mL water from drum into the same bigger and mix them first.

Dump the mixed solution into drum and erase three times using water in drum.

1000 mg/L (Repeat 3 times)

Weigh 132.5 g sample

Fill up water in the drum to 22.28 in. high (total 35 gallons)

Pour weighed sample into a 2 L bigger and grab around 500 mL water from drum into the same bigger and mix them first.

Dump the mixed solution into drum and erase three times using water in drum.

5000 mg/L (Repeat 3 times)

Weigh 662.5 g sample

Fill up water in the drum to 22.28 in. high (total 35 gallons)

Pour weighed sample into a 2 L bigger and grab around 500 mL water from drum into the same bigger and mix them first.

Dump the mixed solution into drum and erase three times using water in drum.

## **Step 2: System specification**

The mixing system includes a mixer and a built steel stand.

The tubing system consists of two y-shaped branch pipes to divide the flow.

The controller controls the power of the pump.

All experiments following exactly same parameters:

Mixer: 50/100 of power

Pump: 6.5/10 of power

## **Step 3: Sample collection**

Start the mixer and wait 3-5 minutes to let the solution mixed completely.

After 5 minutes. Start the pump and wait 5 minutes and measure the flow rate (time to fill up 300 mL should be around 46 seconds) to ensure that the system is working properly. This can make sure the detention time (to fill up the settler) should be around 90 minutes.

Collect sample directly from the tube (at inlet) to measure the turbidity at influent.

Collect sample directly from the tube (at outlet) to measure the turbidity at effluent.

Collect data into the data sheet (measure every 5 minutes for effluent).

Measure influent every 15 minutes. Measure Effluent every 5 minutes.

## **Step 4: Turbidity measurements**

Turbidity measurements are recorded through HACH 2100Q turbidimeter. Before measuring turbidity, the turbidimeter needs to be confirmed or recalibrated through standards. Collect 15 mL sample into the sample cell. Dilution is necessary as turbidity in sample is over 1,000 NTU (limit of measurements). Dilute sample by simply pipette 7.5 mL of original sample and add 7.5 mL of tap water. Record turbidity values and counted dilution factor (relative to times of dilution) to calculate the final turbidity of sample. The dilution factor can be calculated as  $F=2^x$ , where x is times of dilution. The turbidity of tap water used for dilution will also be recorded as the reference data to recalibrate the results.

#### **Step 5: TSS measurements**

Before collecting samples, the mass of empty crinkle dish was measured through Mettler balance from which the recorded weight can reach to the nearest 0.0001 g. As the samples used in these experiments were synthetic soils with larger amounts of finer particles, the TSS measurements were conducted by simply collecting 5 mL of sample and dried in oven at 103 °C for 24 hours and wait for mass measurements after it drops to room temperature in the dry box of desiccants for 4 hours. The TSS can be calculated by subtracting initial weight of corresponded crinkle dish.

## **Appendix C: Procedure of Particle Size Distribution Analysis**



## Preparation

1. Open Mastersizer 3000 software
2. Clean system with deionized (DI) water
3. Check cleaning process by running a blank SOP (change another bucket with new DI water, if the obscuration is over 0.5%).
4. To run a SOP that is located in the main page of the software, select SOP and name the samples (SOP include all detailed information about measuring samples, create a new SOP or revise it to test samples).
5. Rename sample is very important between each measurement as the system will not labeling samples automatically.

## Sample Measurement

6. Before adding samples, make sure that it is at homogenous condition. Agitation is recommended before adding samples.



7. Slowly inject samples into the beaker filled with DI water (Note: make sure sufficient volume of DI water in the 600 mL beaker that is about 450ml)
8. Stop adding sample once the obscuration is within 9% to 12%.

9. Press start button to start running samples

10. Preliminary data including  $D_x(90)$ ,  $D_x(50)$ , and  $D_x(10)$  will be shown along with every measurement which means  $x\%$  of the measured volume consisted of particle sizes of  $D_x$  in the sample.

11. Another parameter is Relative Standard Deviation (RSD). RSD that is less than 5% is ideally depending on the sample scope.

12. After the system completes the measurement, it is necessary to clean Mastersizer for six times with six independent beakers with clean DI water.

### **Export Data**

13. Two formats of data (generated figures and tables) can be exported through the “Reports” tab. Either figure or table can be exported by right clicking it.

14. The report can be revised and updated through the tested sample files selected, the order of the selection will influence the order of results shown in the report.

15. Another quick access to export all results of the tested samples is to click “Export” button.

16. The particle size distribution plot can be created in excel with exported raw data

17.  $D_x$  data can be exported as raw data into excel in csv format.

18. OR if you want to export all of the samples from a single record the do not worry about selecting any sample. Click Export all records or Export selected records respectively.

## **Appendix D: Fact Sheets of Soils**

# SOIL A

## TECHNICAL DATA



### FEATURES AND BENEFITS

ELCO, IL

IMSIL® microcrystalline silica fillers are produced from an inert, naturally occurring alpha quartz with a unique grape-like morphology. Easily wetted and dispersed in either solvent or water-based systems, IMSIL is selected for its excellent tint retention, durability over prolonged exposure and resistance to dirt and weathering.

Interior architectural paints formulated with IMSIL® will exhibit strengthened film integrity, increased stain resistance, more uniform sheen control, and excellent “touch-up” characteristics. Low oil absorption, regardless of particle size, enables formulators to increase loading without adversely affecting critical film properties. Exterior coatings containing IMSIL will better resist weathering, chalking and under eave frosting. When used in primers, IMSIL also provides the “tooth” necessary for better intercoat adhesion and greater durability in abrasive or corrosive environments. IMSIL has been proven effective in trade sales paints, OEM finishes, marine and industrial coatings, and potting compounds. Finer, micronized grades are especially useful in formulating higher gloss paints, and systems requiring controlled mineral top size, such as thin coatings and inks.

All IMSIL® grades are processed with rigid adherence to SPC and Unimin QIP<sup>SM</sup> statistical and quality assurance programs. The result is chemical purity and consistently uniform particle size distributions for predictable results and reliable service.

### PARTICLE SIZE ANALYSIS AND PROPERTIES

### ULTRA-FINE GRADES

Mean Values. These Do Not Represent A Specification.

	<u>Microns</u>	<u>A-25</u>	<u>A-15</u>	<u>A-10</u>	<u>A-8</u>	<u>A-7</u>
	75	---	---	---	---	---
	45	100.00	---	---	---	---
Typical Mean %	38	99.99	100.00	---	---	---
Passing on	25	99.85	99.97	100.00	---	---
Individual Sieves	15	99.40	98.50	99.50	100.00	100.00
	10	76.70	90.90	98.50	99.20	99.9
	8	72.60	81.30	97.30	98.50	99.1
	5	51.20	64.50	78.10	87.90	90.0
Median Particle Size (μ)		5.0	3.5	2.4	2.1	1.6
Surface Area (m <sup>2</sup> /g)		5.3	5.6	6.1	6.9	7.3
Brightness (TAPPI)		85.5	85.5	86	87	87
Oil Absorption (g/100g)		28	28	28	28	28
Moisture (%)		0.18	0.20	0.20	0.20	0.20
Weight/Solid Gallon (lbs/gallon)	22.07	ASTM D-153				
Bulking Value	0.0453	ASTM C-29				
Specific Gravity (g/cm <sup>3</sup> )	2.65	ASTM C-128				
pH	6.6	AFS 113-87-S				
Refractive Index	1.54-1.55	ASTM D-801				
Hardness (Mohs)	6.5	Mohs' Scale				

## TECHNICAL DATA



### CHEMICAL ANALYSIS

Mean Values. These Do Not Represent A Specification.

#### Mean Percent by Weight

Silicon Dioxide	(SiO <sub>2</sub> )	98.55
Iron Oxide	(Fe <sub>2</sub> O <sub>3</sub> )	0.08
Aluminum Oxide	(Al <sub>2</sub> O <sub>3</sub> )	0.85
Calcium Oxide	(CaO)	0.03
Titanium Dioxide	(TiO <sub>2</sub> )	0.04
Magnesium Oxide	(MgO)	0.01
Potassium Oxide	(K <sub>2</sub> O)	0.08
Sodium Oxide	(Na <sub>2</sub> O)	0.04
Loss on Ignition	(L.O.I.)	0.42

### ORDERING INFORMATION

Shipping Point: ELCO, IL

Availability: 50 LB BAGS, BULK BAGS, AND BULK TRUCK ONLY



**FOR PRODUCT INFORMATION AND CUSTOMER SERVICE:**  
U.S. and CANADA 800-243-9004 • FAX 800-243-9005  
WORLDWIDE 203-966-1306 • FAX 203-972-1378

Silica Sands • Ground Silica • Feldspar • Ball Clay • Kaolin • Nepheline Syenite • High Purity Quartz • Olivine • Microcrystalline Silica • Hydrated Lime • Dolomite

GRADE NUMBERS INDICATE RELATIVE VALUES OR RESULTS. THEY ARE NOT A SPECIFICATION OR WARRANTY OF PERFORMANCE.

HEALTH HAZARD WARNING: Prolonged inhalation of dust associated with the materials described in this data sheet can cause delayed lung injury including Silicosis, a progressive, disabling and sometimes-fatal lung disease. IARC has determined that crystalline silica, inhaled from occupational sources, can cause cancer in humans. Risk of injury is dependent on the duration and level of exposure. Follow OSHA or other relevant safety and health standards for the form of crystalline silica called Quartz. Current material safety data sheets, containing safety information, are available and should be consulted before usage.

Notice: While information contained herein is correct to the best of our knowledge, Unimin Corporation hereby disclaims any warranties as to the accuracy of the same. Recommendations or suggestions are made without guarantee or representation as to result, since conditions of usage are beyond our control. All materials are sold to Unimin Corporation standard terms and conditions of sale and the condition that buyer shall make his own tests to determine the suitability of such product for buyer's purpose. No statement contained herein shall be construed as a recommendation to infringe any patent.

Silica/Silica Containing  
IMSIL® is a registered trademark of UNIMIN Corporation or its subsidiaries. All rights reserved.

Eico - IMSIL-Ultra-Fine (03/10)

## SOIL B & SOIL C



## TECHNICAL DATA

### FEATURES AND BENEFITS

SNOBRITE® white extender pigments are produced from airfloated intermediate kaolins. With a plate like crystal structure and high aspect ratio SNOBRITE provides good reinforcing properties, increased hardness and stiffness, and improved resistance to abrasion and tear. Its tendency to slowly build viscosity makes SNOBRITE a cost effective formulating tool to enhance performance without adversely affecting production rates. SNOBRITE additions also improve critical working properties, including extrusion, calendaring, mold release and handling.

In molded and extruded rubber, SNOBRITE® can be loaded to relatively high levels and still produce pliable compounds with good durometer values. Unlike finer particle clays, SNOBRITE will not absorb accelerators or adversely affect the cure rate. This is especially important in precision parts where shrinkage and extrusion properties need to be balanced with mechanical strength, hardness and resistance to tear. The high loading and low shrinkage characteristics of SNOBRITE are valued in a wide range of synthetic and natural rubber products, including roofing, footwear, wire and cable jacketing, hose, mill rods, commercial and residential roll matting, soft and novelty rubber goods and polyester gunks.

Selectively mined to maximize whiteness and GEB values, SNOBRITE® is particularly effective in systems where color is critical. Combined with light scattering properties which mimic more expensive opacifiers, SNOBRITE offers functional performance in a wide range of adhesives, sealants, caulking compounds, and mastics. In alkyd and water based coatings, the combination of particle shape and particle size distribution operate to improve film properties, including surface finish, permeability, scrub resistance, and hiding power.

All SNOBRITE® grades are mined, processed and sized under rigid QIPSM statistical quality assurance programs. The result is consistent physical properties and uniform particle size distributions for reliable performance.

### PARTICLE SIZE ANALYSIS AND PROPERTIES

Mean Values. These Do Not Represent A Specification.

	<u>ASTM E-11</u>	<u>MICRONS</u>	<u>75</u>	<u>68</u>	<u>60</u>	<u>75HB</u>
Typical Mean % Retained On Individual Sieves	200 325	75 45	<0.25 <0.50	<0.25 <0.30	<0.30 <0.70	<0.25 <0.50
Subsieve Analysis % Passing		<20 <10 <5 <2 <1 <.5	99 96 91 81 73 58	99 94 86 68 56 40	99 93 80 60 46 34	99 97 92 80 71 56
Median Particle Size (μ)	SEDIGRAPH		0.5	0.9	1.2	0.5
Surface Area (m <sup>2</sup> /g)	ASTM D-1993		24	21	17	24
Oil Absorption (g/100g)	ASTM D-281		42	40	35	42
Brightness Lab Value	GEB SPECTROMETRIC		80 94	80 94	78 94.0	80 94.5
	L a b		0.2 5.0	0.3 5.5	0.2 5.0	0.1 3.9
pH (in solution)	AFS 113-87-S		6.0-8.0	6.0-8.0	6.0-8.0	6.0-8.5
Moisture Content	AFS C-566		<1.0	<1.0	<1.0	<1.0

**CHEMICAL ANALYSIS**

Mean Values. These Do Not Represent A Specification.

Mean Percent By Weight on Oxide Basis

		<u>75*</u>	<u>68**</u>	<u>60***</u>	<u>75HB</u>
Silicon Dioxide	(SiO <sub>2</sub> )	45.50	45.50	45.50	45.40
Aluminum Oxide	(Al <sub>2</sub> O <sub>3</sub> )	38.00	38.25	38.50	38.00
Titanium Dioxide	(TiO <sub>2</sub> )	1.65	1.55	1.50	1.60
Iron Oxide	(Fe <sub>2</sub> O <sub>3</sub> )	0.90	0.70	0.41	0.90
Calcium Oxide	(CaO)	0.25	0.20	0.03	0.20
Magnesium Oxide	(MgO)	0.03	0.05	0.06	0.05
Potassium Oxide	(K <sub>2</sub> O)	0.23	0.23	0.23	0.20
Sodium Oxide	(Na <sub>2</sub> O)	0.04	0.04	0.04	0.05
Loss on Ignition	(L.O.I.)	13.40	13.48	13.73	13.60

\* Prior Grade Designations: SNOBRITE AF, HW; APEX A, K

\*\* Prior Grade Designation: APEX R

\*\*\* Prior Grade Designation: SNOBRITE D6

**ORDERING INFORMATION**

**Shipping Point:** MCINTYRE, GA  
ORIGINATING RAIL CARRIER: NORFOLK SOUTHERN

**Availability:** 50 LB. BAGS, INTERMEDIATE BULK BAGS AND BULK TRUCK AND RAIL

**FOR PRODUCT INFORMATION AND CUSTOMER SERVICE:**

US and Canada 800-243-9004 • Fax 800-243-9005  
Worldwide 203-442-2500 • Fax 203-972-1378



Silica Sands • Ground Silica • Feldspar • Ball Clay • Kaolin • Nepheline Syenite • High Purity Quartz • Olivine • Microcrystalline Silica • Hydrated Lime

GRADE NUMBERS INDICATE RELATIVE VALUES OR RESULTS. THEY ARE NOT A SPECIFICATION OR WARRANTY OF PERFORMANCE.

**HEALTH HAZARD WARNING:** Long term exposure can cause pneumoconiosis. This material contains crystalline silica which can cause pneumoconiosis. Pneumoconiosis is a respiratory disease, which can result in delayed, disabling and sometimes fatal lung injury. IARC and NTP have determined that crystalline silica can cause lung cancer in humans. Risk of injury is dependent on the duration and level of exposure. Avoid creating dust when handling, using or storing. Use only with adequate ventilation to keep exposure below recommended exposure limits. Follow OSHA or other relevant safety and health standards for "Particulates not otherwise classified" (PNOC) and for the form of crystalline silica called Quartz. Current material safety data sheets, containing safety information, are available and should be consulted before opening.

Notice: While information contained herein is correct to the best of our knowledge, Unimin Corporation hereby disclaims any warranties as to the accuracy of the same. Recommendations or suggestions are made without guarantee or representation as to result, since conditions of usage are beyond our control. All materials are sold to Unimin Corporation standard terms and conditions of sale and the condition that buyer shall make his own tests to determine the suitability of such product for buyer's purpose. No statement contained herein shall be construed as a recommendation to infringe any patent.

Kaolin/Silica Containing  
SNOBRITE® is a registered trademark of UNIMIN Corporation or its subsidiaries. All rights reserved.

SNOBRITE (08/14)

## SOIL D



## TECHNICAL DATA

### CHEMICAL ANALYSIS

Mean Values. These Do Not Represent A Specification.

#### Mean Percent by Weight

Silicon Dioxide	(SiO <sub>2</sub> )	60.20
Aluminum Oxide	(Al <sub>2</sub> O <sub>3</sub> )	23.60
Sodium Oxide	(Na <sub>2</sub> O)	10.50
Potassium Oxide	(K <sub>2</sub> O)	4.80
Calcium Oxide	(CaO)	0.35
Iron Oxide	(Fe <sub>2</sub> O <sub>3</sub> )	0.08
Magnesium Oxide	(MgO)	0.02
Loss on Ignition	(L.O.I.)	0.42

These oxides exist in a complex of Albite, Microcline, and Nepheline. There is no free crystalline silica present.

### ORDERING INFORMATION

**Shipping Point:** NEPHTON/BLUE MOUNTAIN, ONTARIO  
ORIGINATING CARRIER: CANADIAN PACIFIC (CP RAIL)

**Availability:** 50 LB. BAGS, 25 KG BAGS, INTERMEDIATE BULK BAGS AND BULK  
TRUCK AND RAIL



### FOR PRODUCT INFORMATION AND CUSTOMER SERVICE:

U.S. and CANADA 800-243-9004 • FAX 800-243-9005  
WORLDWIDE 203-442-2500 • FAX 203-972-1378

Silica Sands • Ground Silica • Feldspar • Ball Clay • Kaolin • Nepheline Syenite • High Purity Quartz • Olivine • Microcrystalline Silica • Hydrated Lime

GRADE NUMBERS INDICATE RELATIVE VALUES OR RESULTS. THEY ARE NOT A SPECIFICATION OR WARRANTY OF PERFORMANCE.

**HEALTH HAZARD WARNING:** Prolonged inhalation of dust associated with the materials described in this data sheet can cause delayed lung injury. Avoid creating dust when handling, using or storing. Follow OSHA Safety and Health Standards for fugitive dust. Current Material Safety Data Sheet containing safety information is available and should be consulted before usage.

Notice: While information contained herein is correct to the best of our knowledge, Unimin Corporation hereby disclaims any warranties as to the accuracy of the same. Recommendations or suggestions are made without guarantee or representation as to result, since conditions of use are beyond our control. All materials are sold to Unimin Corporation standard terms and conditions of sale and on the condition that buyer shall make his own tests to determine the suitability of such product for buyer's purpose. No statement contained herein shall be construed as a recommendation to infringe any patent.

Nepheline Syenite Containing  
MINEX® is a registered trademark of UNIMIN Corporation or its subsidiaries. All rights reserved.

NEPHTON - MINEX FF (03/14)



**FEATURES AND BENEFITS**

MINEX<sup>®</sup> micronized functional fillers and extenders are proven performance enhancers in a broad range of paints, coatings, adhesives, sealants, and inks. Excellent brightness, tint retention, and weatherability can be achieved in exterior paints. Improved color, sheen uniformity, chemical and stain resistance, and durability result when MINEX is used in interior paint formulations. MINEX is easily dispersed in all conventional vehicle systems, and low oil absorption permits high loadings in adhesives, sealants, and aqueous and alkyd based paints. Multiple grades are available to provide optimal performance in a variety of applications. While the preferred MINEX product is application dependent, coarser grades offer cost effective gloss and sheen control and can add texture. The intermediate grade MINEX 4 offers application versatility for a wide range of architectural and industrial uses. Finer MINEX grades are preferred for higher gloss coatings and are also the preferred choice for powder and clear paint systems.

MINEX<sup>®</sup> fillers are produced from nepheline syenite; a naturally occurring, silica deficient, sodium-potassium alumina silicate. Automated scanning electron microscopy confirms that MINEX contains less than one-tenth of one percent crystalline silica. No free crystalline silica is detectable in the mineral complex. All MINEX grades are processed and sized with rigid adherence to UNIMIN's QIP<sup>SM</sup> quality assurance programs. Consistently uniform chemistries, size distributions, and top size controls ensure improved structural and chemical performance with minimal resin demand.

**PARTICLE SIZE ANALYSIS AND PROPERTIES**

Mean Values. These Do Not Represent A Specification.

**MICRONIZED GRADES**

	<u>Microns</u>	<u>2</u>	<u>3</u>	<u>4</u>	<u>7</u>	<u>10</u>
	106	100.0	100.0	---	---	---
	75	99.8	99.2	100.0	---	---
% Finer	45	95.5	98.2	99.8	100.0	100.0
(Sedigraph)	20	69.2	77.7	91.6	99.3	99.5
	16	57.1	67.9	85.2	98.2	99.3
	10	39.2	48.5	62.5	89.1	96.9
	5	21.3	26.0	34.5	55.0	81.0
Median Particle Size	Sedigraph	13.6	11.0	7.6	3.5	2.6
Hegman Value	ASTM D1210-79	N/A	N/A	4.6	5.8	6.4
Specific Surface Area (m <sup>2</sup> /g)	BET	1.0	1.5	2.2	3.6	4.9
Brightness	Tappi	85.5	88.0	88.7	90.0	90.5
Moisture %	ASTM C-566	0.09	0.09	0.10	0.16	0.18
Oil Absorption	ASTM D-281	26.5	27.0	30.0	33.0	35.0
pH	AFS 113-87-S	10.3	10.3	10.4	10.4	10.5
Weight Per Solid Gallon (lbs.)	21.7	ASTM D-153				
Bulking Value	0.0459	ASTM C-29				
Refractive Index	1.51-1.53	ASTM D-801				
Specific Resistance (ohm-cm)	3000	ASTM D-2448				
Hardness	6.0	Moh's Scale				

## **Appendix E: Turbidity Observations for Different Lamella Settlers**

Soil A:

Inflow Concentration (mg/L)	Turbidity at Inflow (NTU)	Turbidity after Rc (NTU)	Turbidity after Rb (NTU)	Turbidity after Ra (NTU)	Turbidity Reduction after Ra (%)	Turbidity Reduction after Rb (%)	Turbidity Reduction after Rc (%)
500	203.37	138.29	177.79	193.71	32%	13%	5%
	194.97	136.58	167.67	182.75	30%	14%	6%
	185.80	129.13	156.63	176.67	31%	16%	5%
	191.50	108.88	143.64	168.00	43%	25%	12%
	180.62	100.12	135.04	163.88	45%	25%	9%
	184.54	110.04	143.72	166.04	40%	22%	10%
	189.14	82.21	112.05	162.21	57%	41%	14%
	187.38	78.26	113.00	154.47	58%	40%	18%
	171.16	73.21	107.53	142.89	57%	37%	17%
1000	1219.33	808.42	1019.50	1131.17	34%	16%	7%
	1171.87	787.25	989.42	1077.00	33%	16%	8%
	1190.63	812.42	989.50	1100.17	32%	17%	8%
	1254.89	678.44	792.12	1109.52	46%	37%	12%
	1258.59	680.72	800.60	1105.92	46%	36%	12%
	1268.89	700.84	816.88	1117.92	45%	36%	12%
	1239.51	431.00	573.89	931.21	65%	54%	25%
	1254.70	440.16	593.79	951.79	65%	53%	24%
	1289.68	435.37	617.32	985.74	66%	52%	24%
5000	6034.93	2731.83	3345.50	3753.00	55%	45%	38%
	5668.80	2500.83	3185.67	3597.67	56%	44%	37%
	5852.13	2564.50	3170.83	3670.50	56%	46%	37%
	5861.08	1617.08	2145.67	3415.67	72%	63%	42%
	5536.97	1388.75	2084.17	3086.00	75%	62%	44%
	5855.68	1640.00	1961.00	3117.67	72%	67%	47%
	5941.19	1196.21	1475.58	2605.26	80%	75%	56%
	5786.05	1192.95	1490.63	2672.84	79%	74%	54%
	5851.24	1269.26	1691.16	2700.21	78%	71%	54%

Soil B:

Inflow Concentration (mg/L)	Turbidity at Inflow (NTU)	Turbidity after Rc (NTU)	Turbidity after Rb (NTU)	Turbidity after Ra (NTU)	Turbidity Reduction after Ra (%)	Turbidity Reduction after Rb (%)	Turbidity Reduction after Rc (%)
500	247.79	175.83	192.25	226.38	29%	22%	9%
	246.72	181.58	201.88	234.96	26%	18%	5%
	248.10	175.08	199.33	232.13	29%	20%	6%
	229.11	133.96	174.72	183.16	42%	24%	20%
	214.14	128.76	169.12	173.80	40%	21%	19%
	249.42	146.76	179.56	209.00	41%	28%	16%
	240.31	107.16	126.53	166.37	55%	47%	31%
	240.89	109.00	132.84	162.74	55%	45%	32%
	256.19	120.79	136.42	170.84	53%	47%	33%
1000	1044.55	689.54	754.04	966.38	34%	28%	7%
	1213.14	793.46	870.04	1099.33	35%	28%	9%
	1112.76	724.42	804.04	1032.50	35%	28%	7%
	1041.03	611.56	699.48	828.36	41%	33%	20%
	1257.58	700.76	838.88	983.88	44%	33%	22%
	1376.17	788.44	943.92	1041.36	43%	31%	24%
	985.78	379.37	482.89	607.84	62%	51%	38%
	1224.97	410.16	574.79	796.53	67%	53%	35%
5000	5467.86	2319.83	3052.17	4352.33	58%	44%	20%
	5742.07	2386.17	3139.67	4479.67	58%	45%	22%
	5576.41	2444.00	3207.33	4573.33	56%	42%	18%
	5463.78	1728.32	2302.88	3617.28	68%	58%	34%
	5522.00	1780.80	2422.72	3564.80	68%	56%	35%
	5476.67	1686.72	2431.52	3573.44	69%	56%	35%
	5479.67	647.74	1636.32	2359.58	88%	70%	57%
	5760.00	800.74	1699.58	2640.21	86%	70%	54%
	5591.00	821.00	1535.58	2405.26	85%	73%	57%

Soil C:

Inflow Concentration (mg/L)	Turbidity at Inflow (NTU)	Turbidity after Rc (NTU)	Turbidity after Rb (NTU)	Turbidity after Ra (NTU)	Turbidity Reduction after Ra (%)	Turbidity Reduction after Rb (%)	Turbidity Reduction after Rc (%)
500	153.17	101.17	125.67	138.04	34%	18%	10%
	149.79	101.25	123.92	132.17	32%	17%	12%
	145.66	98.50	118.08	133.25	32%	19%	9%
	138.94	73.28	92.80	109.36	47%	33%	21%
	154.65	83.40	106.56	120.44	46%	31%	22%
	148.42	77.52	107.08	109.92	48%	28%	26%
	158.44	68.72	91.94	110.61	57%	42%	30%
	140.17	62.44	84.28	100.61	55%	40%	28%
1000	147.36	60.44	84.33	100.50	59%	43%	32%
	1067.38	668.46	766.21	896.21	37%	28%	16%
	968.93	612.21	714.21	814.58	37%	26%	16%
	994.02	638.92	727.17	861.83	36%	27%	13%
	945.13	424.68	501.92	640.64	55%	47%	32%
	1074.75	479.36	587.92	792.92	55%	45%	26%
	995.21	465.76	543.12	747.68	53%	45%	25%
	1163.06	332.74	554.11	737.74	71%	52%	37%
5000	993.19	263.32	486.58	679.95	73%	51%	32%
	884.67	264.79	450.79	618.32	70%	49%	30%
	3464.69	943.17	1186.67	2026.33	73%	66%	42%
	3466.55	909.00	1178.25	2005.00	74%	66%	42%
	3532.97	969.08	1214.67	2067.00	73%	66%	41%
	3952.67	690.68	1284.56	2200.80	83%	68%	44%
	3402.00	526.32	1119.52	1945.92	85%	67%	43%
	3744.44	579.80	1041.84	2016.48	85%	72%	46%
	3939.89	384.21	837.74	1934.32	90%	79%	51%
3549.33	374.68	827.00	1718.32	89%	77%	52%	
3754.00	371.58	824.42	1879.79	90%	78%	50%	

Soil D:

Inflow Concentration (mg/L)	Turbidity at Inflow (NTU)	Turbidity after Rc (NTU)	Turbidity after Rb (NTU)	Turbidity after Ra (NTU)	Turbidity Reduction after Ra (%)	Turbidity Reduction after Rb (%)	Turbidity Reduction after Rc (%)
500	113.24	65.83	77.79	91.79	42%	31%	19%
	129.14	76.00	85.13	106.71	41%	34%	17%
	134.69	75.67	82.92	105.88	44%	38%	21%
	142.17	53.24	77.52	95.08	63%	45%	33%
	123.25	49.52	69.24	83.36	60%	44%	32%
	133.69	50.52	72.68	89.92	62%	46%	33%
	135.53	21.21	36.95	51.79	84%	73%	62%
	136.83	15.79	31.63	51.21	88%	77%	63%
1000	135.36	20.26	36.42	52.00	85%	73%	62%
	727.45	266.79	396.67	535.29	63%	45%	26%
	696.86	251.42	417.88	506.71	64%	40%	27%
	660.71	229.13	374.71	489.63	65%	43%	26%
	662.67	102.56	172.60	365.88	85%	74%	45%
	628.82	103.00	185.72	345.96	84%	70%	45%
	561.25	103.24	172.88	320.96	82%	69%	43%
	660.65	71.47	118.74	218.21	89%	82%	67%
5000	772.74	64.21	143.00	278.47	92%	81%	64%
	737.72	85.74	137.21	266.16	88%	81%	64%
	2691.59	737.13	1117.58	1730.58	73%	58%	36%
	2564.48	675.08	987.92	1690.42	74%	61%	34%
	2468.21	583.96	964.00	1588.67	76%	61%	36%
	2551.50	353.44	570.68	927.24	86%	78%	64%
	2585.17	317.12	563.80	950.04	88%	78%	63%
	2485.28	346.28	535.68	938.72	86%	78%	62%
	2508.06	269.63	453.42	703.26	89%	82%	72%
2610.56	239.95	454.53	704.05	91%	83%	73%	
2407.72	239.74	450.53	625.21	90%	81%	74%	

Soil F:

Inflow Concentration (mg/L)	Turbidity at Inflow (NTU)	Turbidity after Rc (NTU)	Turbidity after Rb (NTU)	Turbidity after Ra (NTU)	Turbidity Reduction after Ra (%)	Turbidity Reduction after Rb (%)	Turbidity Reduction after Rc (%)
500	240.59	173.83	207.54	216.75	28%	14%	10%
	244.69	181.42	208.67	218.54	26%	15%	11%
	239.14	178.13	215.42	220.42	26%	10%	8%
	220.72	120.00	155.04	168.40	46%	30%	24%
	224.44	122.72	158.08	170.32	45%	30%	24%
	228.92	121.40	165.80	177.64	47%	28%	22%
	231.47	96.53	136.37	152.42	58%	41%	34%
	230.47	93.53	129.79	148.68	59%	44%	35%
1000	226.97	95.89	129.16	145.05	58%	43%	36%
	879.24	551.17	650.08	736.71	37%	26%	16%
	879.53	547.00	613.79	731.21	38%	30%	17%
	944.29	549.88	709.29	797.25	42%	25%	16%
	743.75	326.16	466.76	557.96	56%	37%	25%
	987.71	385.84	648.40	724.92	61%	34%	27%
	882.13	397.00	568.36	640.48	55%	36%	27%
	851.82	322.84	467.89	587.05	62%	45%	31%
5000	1005.00	333.58	467.68	595.21	67%	53%	41%
	794.18	348.68	470.68	585.53	56%	41%	26%
	4575.17	2749.33	3158.67	3636.83	40%	31%	21%
	4585.10	2748.00	3159.17	3579.67	40%	31%	22%
	4378.90	2745.50	3159.17	3528.00	37%	28%	19%
	4485.33	2116.80	2883.84	3326.24	53%	36%	26%
	4573.00	2125.12	2930.08	3326.56	54%	36%	27%
	4378.78	2101.12	2887.68	3315.84	52%	34%	24%
	4586.44	1627.05	2038.11	2617.68	65%	56%	43%
4582.00	1672.42	2077.05	2686.53	64%	55%	41%	
4375.89	1735.58	2169.89	2789.68	60%	50%	36%	

## **Appendix F: Regression Analysis for Turbidity Measurements**



500 mg/L (all soils):

NTU%-all	C, g/L	S, dm	T	T x C	T x S	C x S	T x C x S	C <sup>2</sup>	S <sup>2</sup>	T <sup>2</sup>
10.4%	0.5	3.175	0.5	0.25	1.5875	1.5875	0.79375	0.25	10.08063	0.25
10.2%	0.5	3.175	0.5	0.25	1.5875	1.5875	0.79375	0.25	10.08063	0.25
9.8%	0.5	3.175	0.5	0.25	1.5875	1.5875	0.79375	0.25	10.08063	0.25
19.6%	0.5	0.36	0.5	0.25	0.18	0.18	0.09	0.25	0.1296	0.25
19.7%	0.5	0.36	0.5	0.25	0.18	0.18	0.09	0.25	0.1296	0.25
20.5%	0.5	0.36	0.5	0.25	0.18	0.18	0.09	0.25	0.1296	0.25
32.9%	0.5	0.18	0.5	0.25	0.09	0.09	0.045	0.25	0.0324	0.25
31.2%	0.5	0.18	0.5	0.25	0.09	0.09	0.045	0.25	0.0324	0.25
32.3%	0.5	0.18	0.5	0.25	0.09	0.09	0.045	0.25	0.0324	0.25
22.1%	0.5	3.175	1	0.5	3.175	1.5875	1.5875	0.25	10.08063	1
21.3%	0.5	3.175	1	0.5	3.175	1.5875	1.5875	0.25	10.08063	1
21.5%	0.5	3.175	1	0.5	3.175	1.5875	1.5875	0.25	10.08063	1
31.4%	0.5	0.36	1	0.5	0.36	0.18	0.18	0.25	0.1296	1
30.1%	0.5	0.36	1	0.5	0.36	0.18	0.18	0.25	0.1296	1
30.2%	0.5	0.36	1	0.5	0.36	0.18	0.18	0.25	0.1296	1
48.0%	0.5	0.18	1	0.5	0.18	0.09	0.09	0.25	0.0324	1
47.1%	0.5	0.18	1	0.5	0.18	0.09	0.09	0.25	0.0324	1
47.7%	0.5	0.18	1	0.5	0.18	0.09	0.09	0.25	0.0324	1
34.2%	0.5	3.175	1.5	0.75	4.7625	1.5875	2.38125	0.25	10.08063	2.25
35.3%	0.5	3.175	1.5	0.75	4.7625	1.5875	2.38125	0.25	10.08063	2.25
35.9%	0.5	3.175	1.5	0.75	4.7625	1.5875	2.38125	0.25	10.08063	2.25
48.8%	0.5	0.36	1.5	0.75	0.54	0.18	0.27	0.25	0.1296	2.25
49.0%	0.5	0.36	1.5	0.75	0.54	0.18	0.27	0.25	0.1296	2.25
48.6%	0.5	0.36	1.5	0.75	0.54	0.18	0.27	0.25	0.1296	2.25
62.2%	0.5	0.18	1.5	0.75	0.27	0.09	0.135	0.25	0.0324	2.25
63.3%	0.5	0.18	1.5	0.75	0.27	0.09	0.135	0.25	0.0324	2.25
62.3%	0.5	0.18	1.5	0.75	0.27	0.09	0.135	0.25	0.0324	2.25

Note: C is inflow concentration, S is settling distance between plates in the lamella settler, and T is residence time.

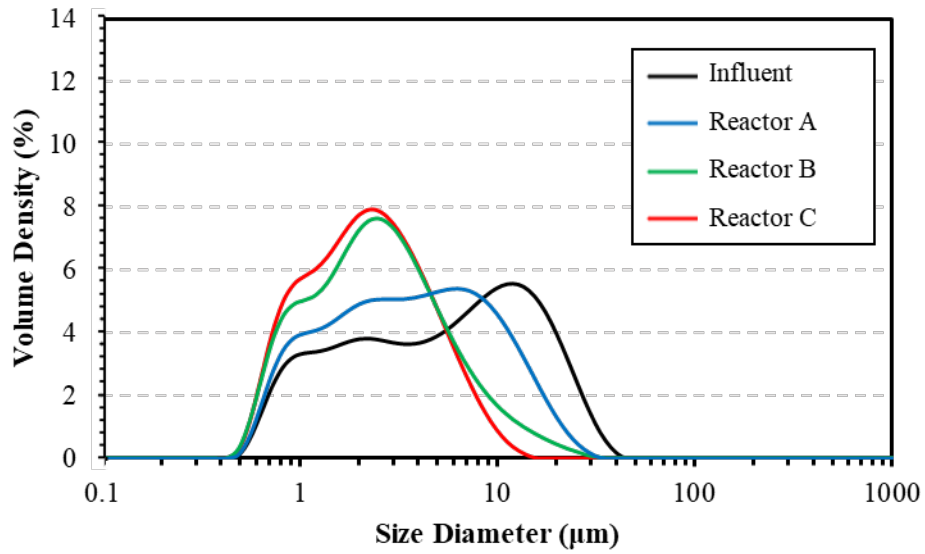
1,000mg/L

NTU%-all	C, g/L	S, dm	T	T x C	T x S	C x S	T x C x S	C <sup>2</sup>	S <sup>2</sup>	T <sup>2</sup>
14.7%	1	3.175	0.5	0.5	1.5875	3.175	1.5875	1	10.08063	0.25
15.5%	1	3.175	0.5	0.5	1.5875	3.175	1.5875	1	10.08063	0.25
13.9%	1	3.175	0.5	0.5	1.5875	3.175	1.5875	1	10.08063	0.25
28.8%	1	0.36	0.5	0.5	0.18	0.36	0.18	1	0.1296	0.25
28.1%	1	0.36	0.5	0.5	0.18	0.36	0.18	1	0.1296	0.25
27.9%	1	0.36	0.5	0.5	0.18	0.36	0.18	1	0.1296	0.25
41.1%	1	0.18	0.5	0.5	0.09	0.18	0.09	1	0.0324	0.25
41.2%	1	0.18	0.5	0.5	0.09	0.18	0.09	1	0.0324	0.25
41.9%	1	0.18	0.5	0.5	0.09	0.18	0.09	1	0.0324	0.25
26.8%	1	3.175	1	1	3.175	3.175	3.175	1	10.08063	1
26.3%	1	3.175	1	1	3.175	3.175	3.175	1	10.08063	1
26.3%	1	3.175	1	1	3.175	3.175	3.175	1	10.08063	1
45.6%	1	0.36	1	1	0.36	0.36	0.36	1	0.1296	1
44.0%	1	0.36	1	1	0.36	0.36	0.36	1	0.1296	1
43.4%	1	0.36	1	1	0.36	0.36	0.36	1	0.1296	1
56.6%	1	0.18	1	1	0.18	0.18	0.18	1	0.0324	1
58.0%	1	0.18	1	1	0.18	0.18	0.18	1	0.0324	1
55.5%	1	0.18	1	1	0.18	0.18	0.18	1	0.0324	1
39.6%	1	3.175	1.5	1.5	4.7625	3.175	4.7625	1	10.08063	2.25
39.1%	1	3.175	1.5	1.5	4.7625	3.175	4.7625	1	10.08063	2.25
36.2%	1	3.175	1.5	1.5	4.7625	3.175	4.7625	1	10.08063	2.25
56.8%	1	0.36	1.5	1.5	0.54	0.36	0.54	1	0.1296	2.25
58.3%	1	0.36	1.5	1.5	0.54	0.36	0.54	1	0.1296	2.25
55.4%	1	0.36	1.5	1.5	0.54	0.36	0.54	1	0.1296	2.25
69.9%	1	0.18	1.5	1.5	0.27	0.18	0.27	1	0.0324	2.25
72.7%	1	0.18	1.5	1.5	0.27	0.18	0.27	1	0.0324	2.25
68.3%	1	0.18	1.5	1.5	0.27	0.18	0.27	1	0.0324	2.25

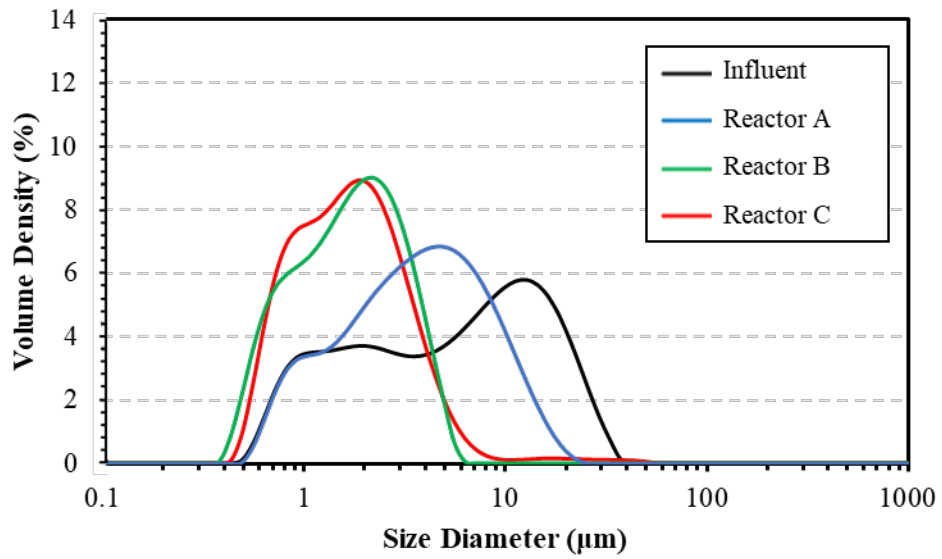
5,000 mg/L

NTU%-all	C, g/L	S, dm	T	T x C	T x S	C x S	T x C x S	C <sup>2</sup>	S <sup>2</sup>	T <sup>2</sup>
31.2%	5	3.175	0.5	2.5	1.5875	15.875	7.9375	25	10.08063	0.25
31.3%	5	3.175	0.5	2.5	1.5875	15.875	7.9375	25	10.08063	0.25
30.4%	5	3.175	0.5	2.5	1.5875	15.875	7.9375	25	10.08063	0.25
48.8%	5	0.36	0.5	2.5	0.18	1.8	0.9	25	0.1296	0.25
49.5%	5	0.36	0.5	2.5	0.18	1.8	0.9	25	0.1296	0.25
48.5%	5	0.36	0.5	2.5	0.18	1.8	0.9	25	0.1296	0.25
59.5%	5	0.18	0.5	2.5	0.09	0.9	0.45	25	0.0324	0.25
60.4%	5	0.18	0.5	2.5	0.09	0.9	0.45	25	0.0324	0.25
59.7%	5	0.18	0.5	2.5	0.09	0.9	0.45	25	0.0324	0.25
41.9%	5	3.175	1	5	3.175	15.875	15.875	25	10.08063	1
42.6%	5	3.175	1	5	3.175	15.875	15.875	25	10.08063	1
42.8%	5	3.175	1	5	3.175	15.875	15.875	25	10.08063	1
60.4%	5	0.36	1	5	0.36	1.8	1.8	25	0.1296	1
59.9%	5	0.36	1	5	0.36	1.8	1.8	25	0.1296	1
61.4%	5	0.36	1	5	0.36	1.8	1.8	25	0.1296	1
72.5%	5	0.18	1	5	0.18	0.9	0.9	25	0.0324	1
73.7%	5	0.18	1	5	0.18	0.9	0.9	25	0.0324	1
72.8%	5	0.18	1	5	0.18	0.9	0.9	25	0.0324	1
55.8%	5	3.175	1.5	7.5	4.7625	15.875	23.8125	25	10.08063	2.25
54.8%	5	3.175	1.5	7.5	4.7625	15.875	23.8125	25	10.08063	2.25
54.2%	5	3.175	1.5	7.5	4.7625	15.875	23.8125	25	10.08063	2.25
72.3%	5	0.36	1.5	7.5	0.54	1.8	2.7	25	0.1296	2.25
71.7%	5	0.36	1.5	7.5	0.54	1.8	2.7	25	0.1296	2.25
70.7%	5	0.36	1.5	7.5	0.54	1.8	2.7	25	0.1296	2.25
82.4%	5	0.18	1.5	7.5	0.27	0.9	1.35	25	0.0324	2.25
81.8%	5	0.18	1.5	7.5	0.27	0.9	1.35	25	0.0324	2.25
80.8%	5	0.18	1.5	7.5	0.27	0.9	1.35	25	0.0324	2.25

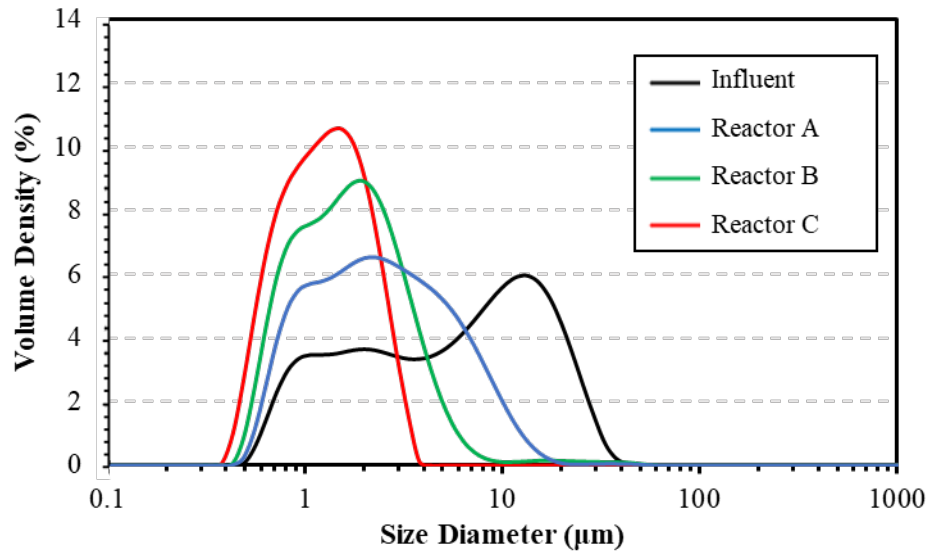
## **Appendix G: PSD Analysis for All Types of Soils**



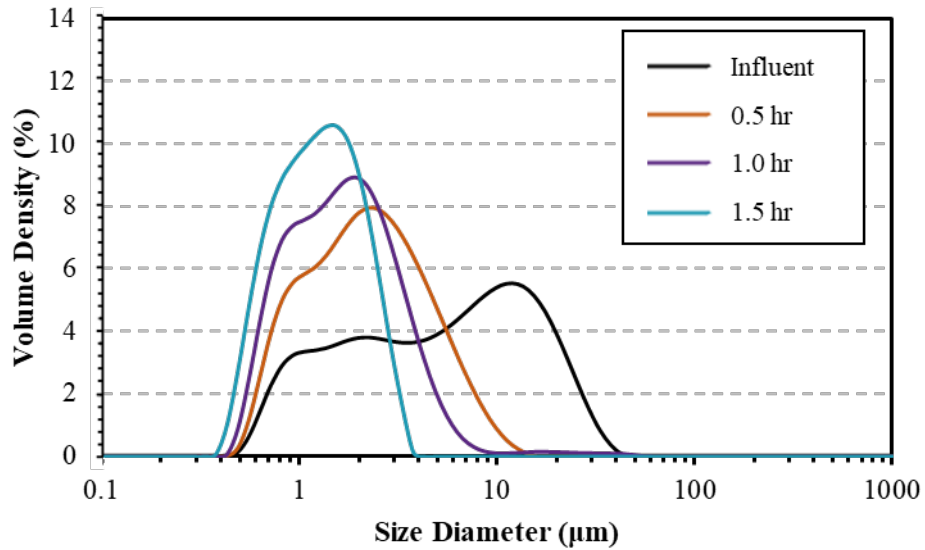
**Size Distribution Analysis for Soil A @ 0.5 hr.**



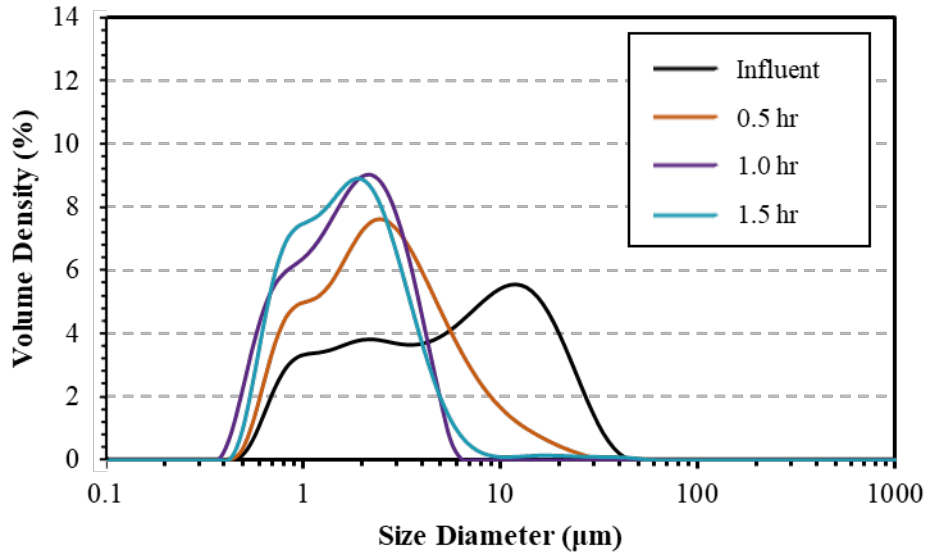
**Size Distribution Analysis for Soil A @ 1.0 hr.**



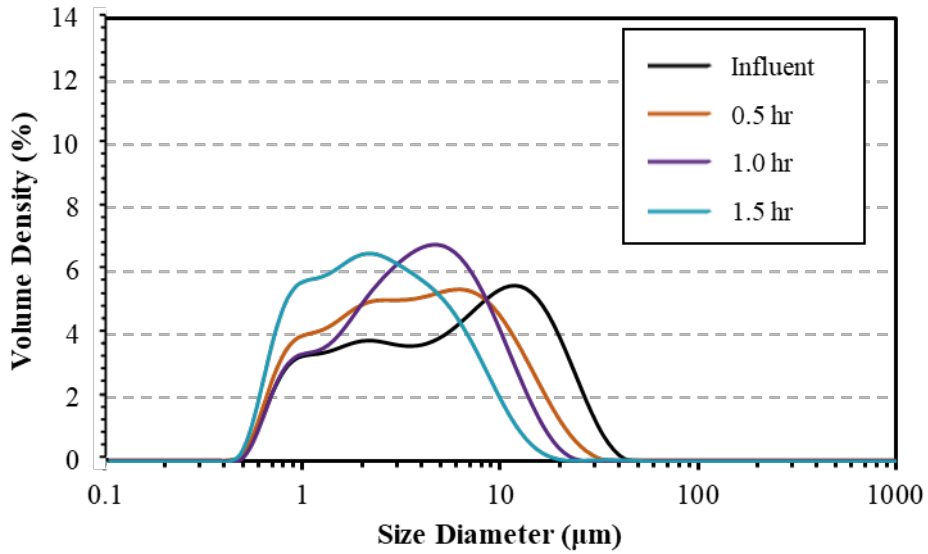
**Size Distribution Analysis for Soil A @ 1.5 hr.**



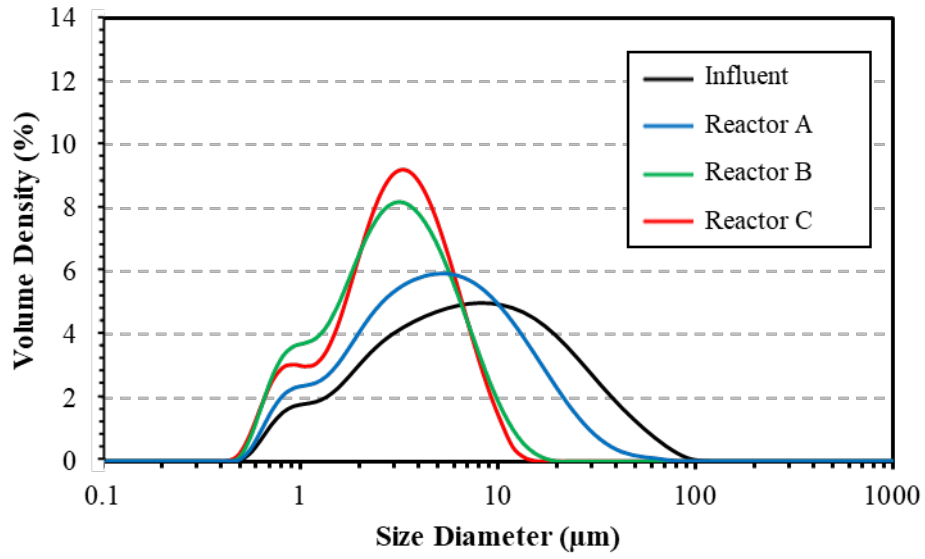
**Size Distribution Analysis for Soil A in Reactor C.**



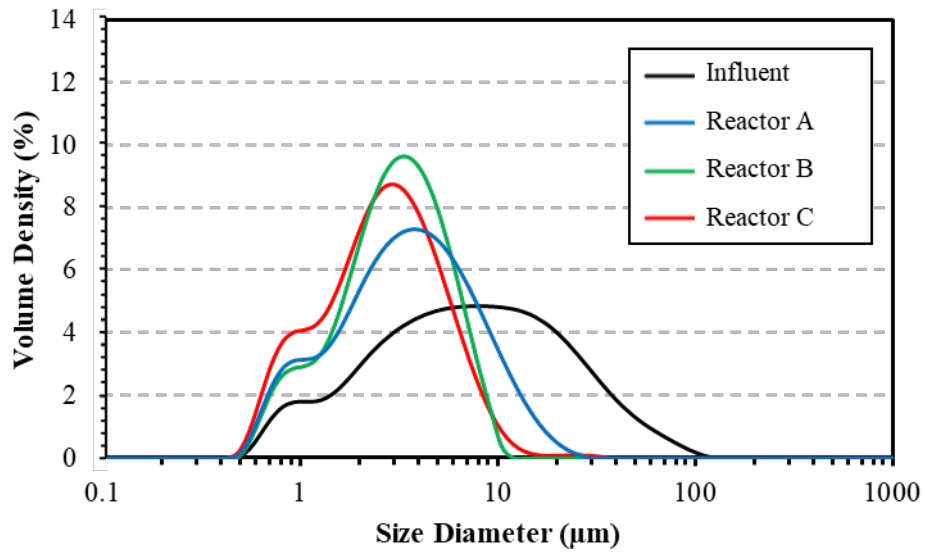
**Size Distribution Analysis for Soil A in Reactor B.**



**Size Distribution Analysis for Soil A in Reactor A.**

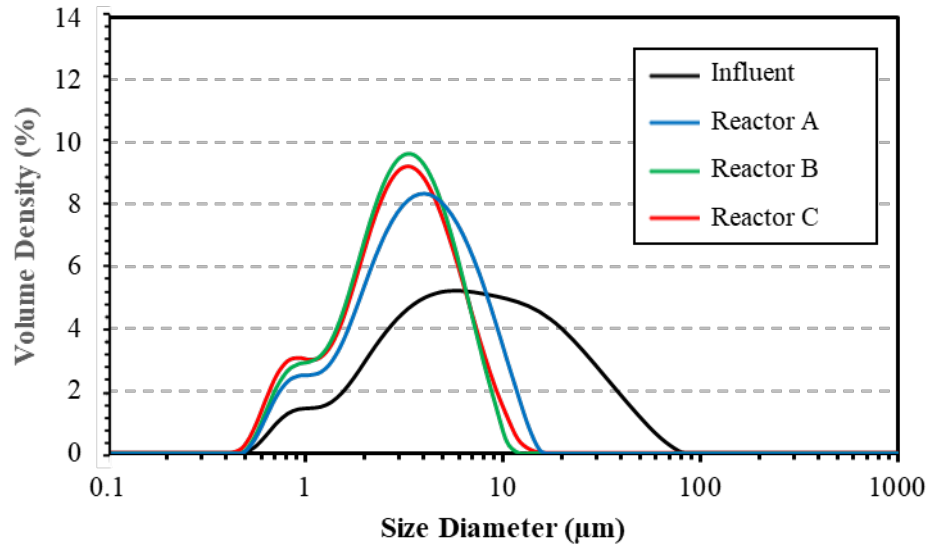


**Size Distribution Analysis for Soil B @ 0.5 hr.**

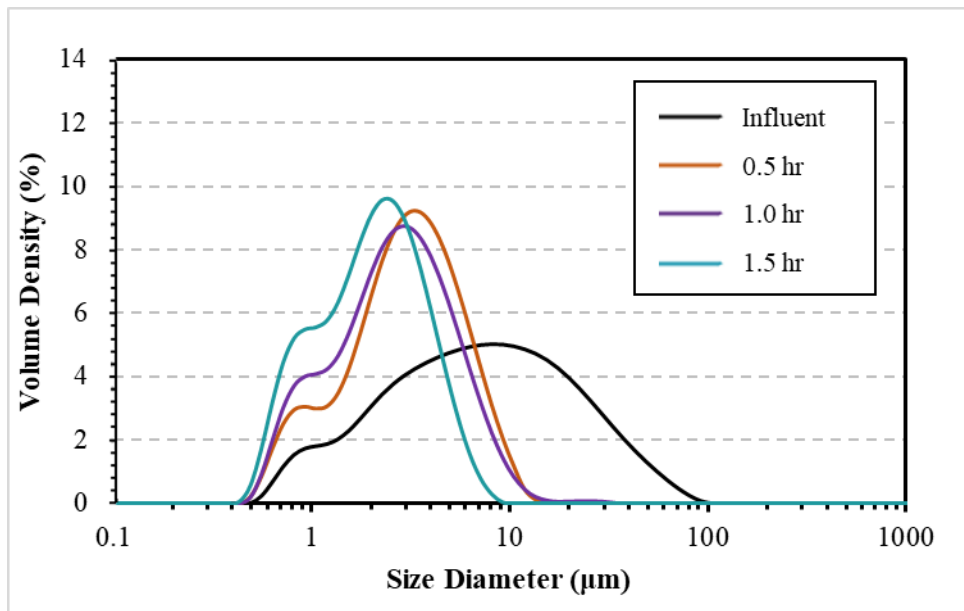


**Size Distribution Analysis for Soil B @ 1.0 hr.**

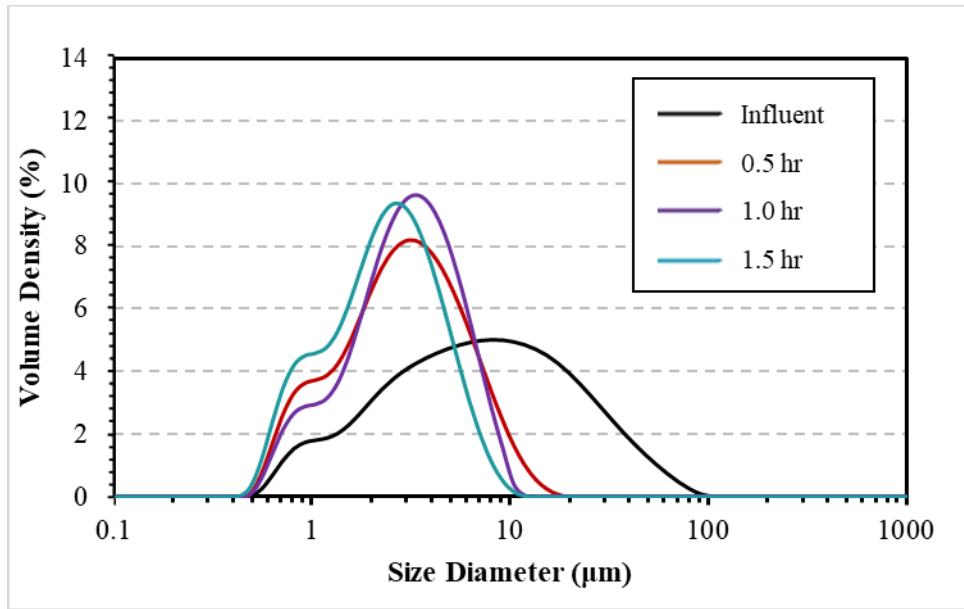




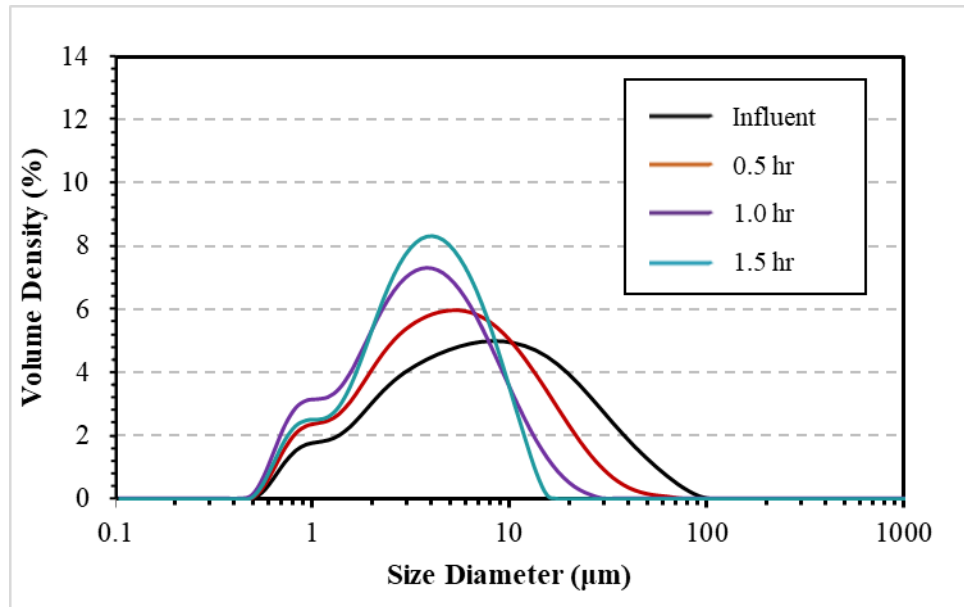
**Size Distribution Analysis for Soil B @ 1.5 hr.**



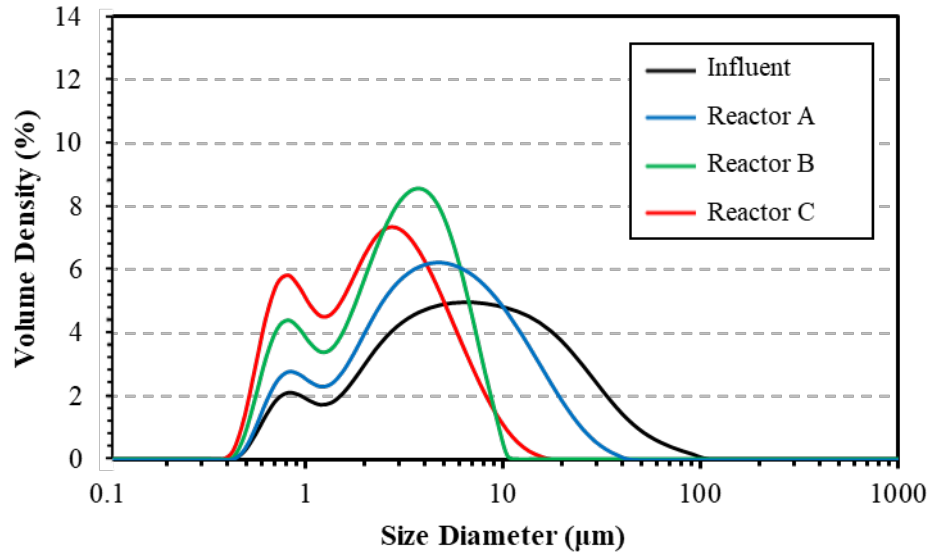
**Size Distribution Analysis for Soil B in Reactor C.**



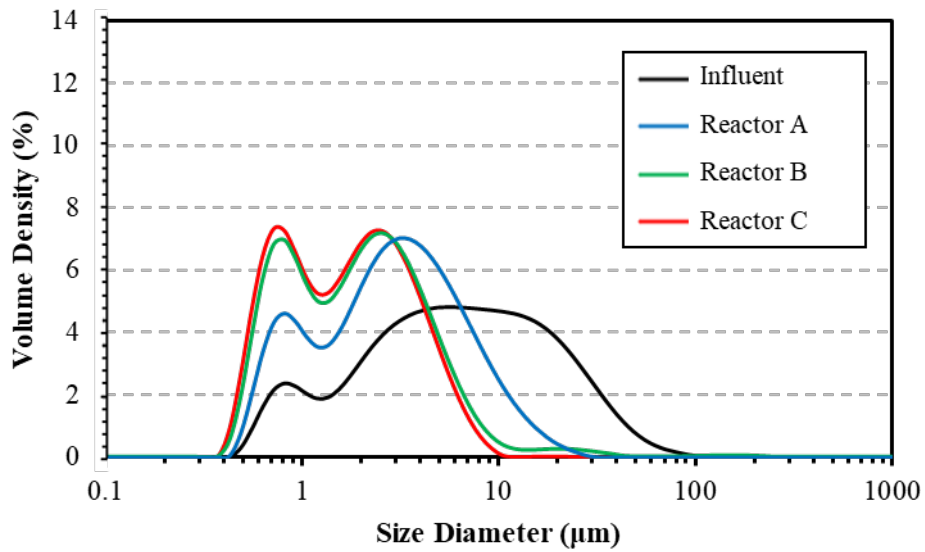
**Size Distribution Analysis for Soil B in Reactor B.**



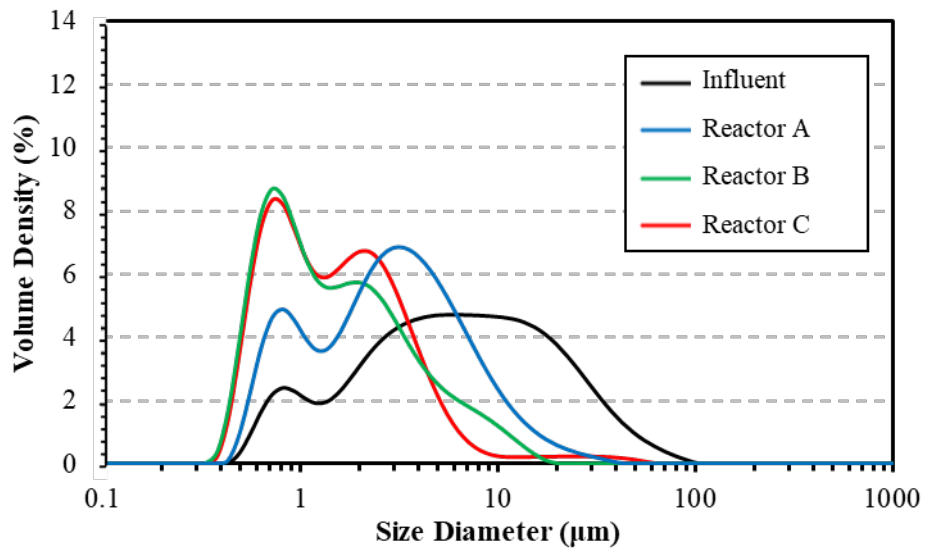
**Size Distribution Analysis for Soil B in Reactor A.**



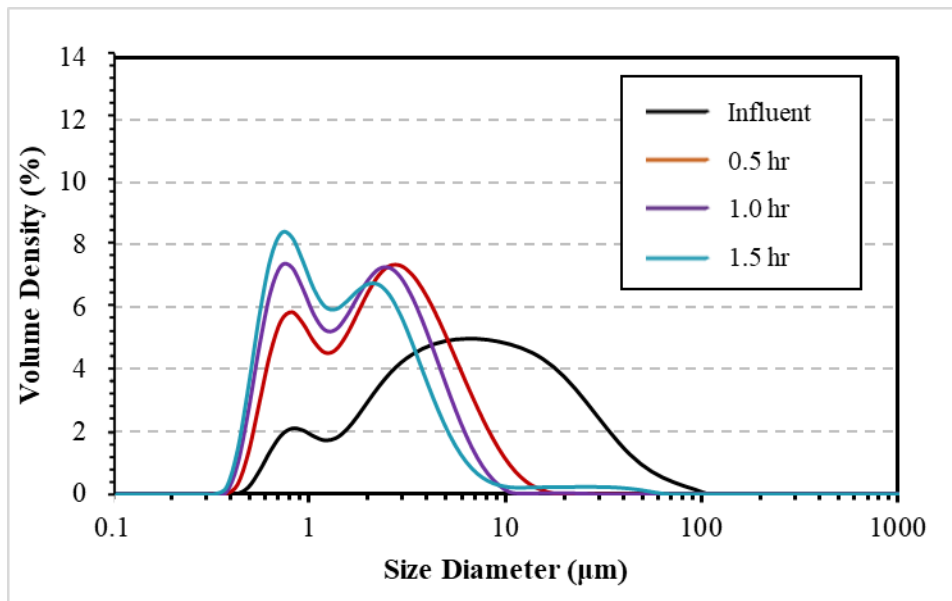
**Size Distribution Analysis for Soil C @ 0.5 hr.**



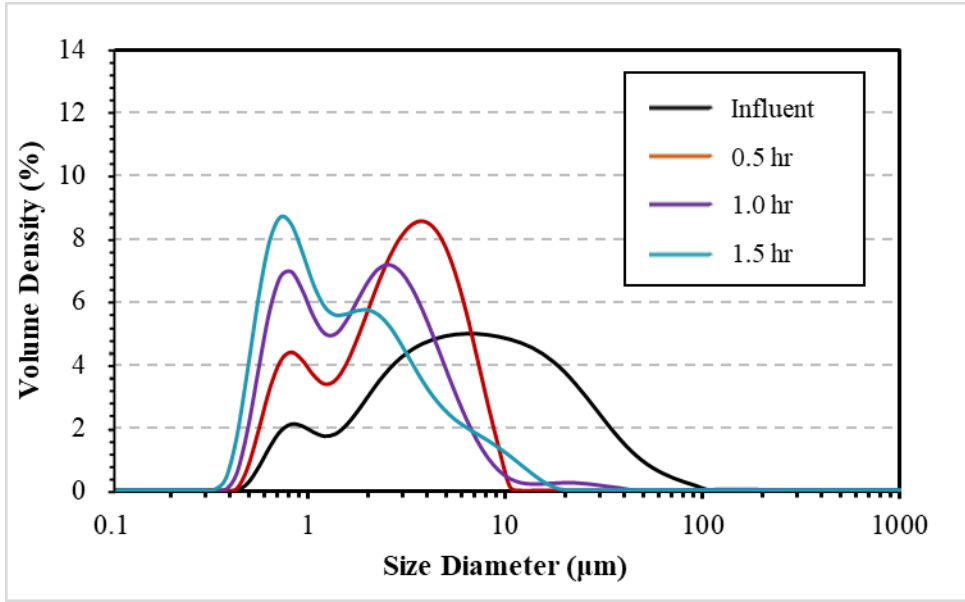
**Size Distribution Analysis for Soil C @ 1.0 hr.**



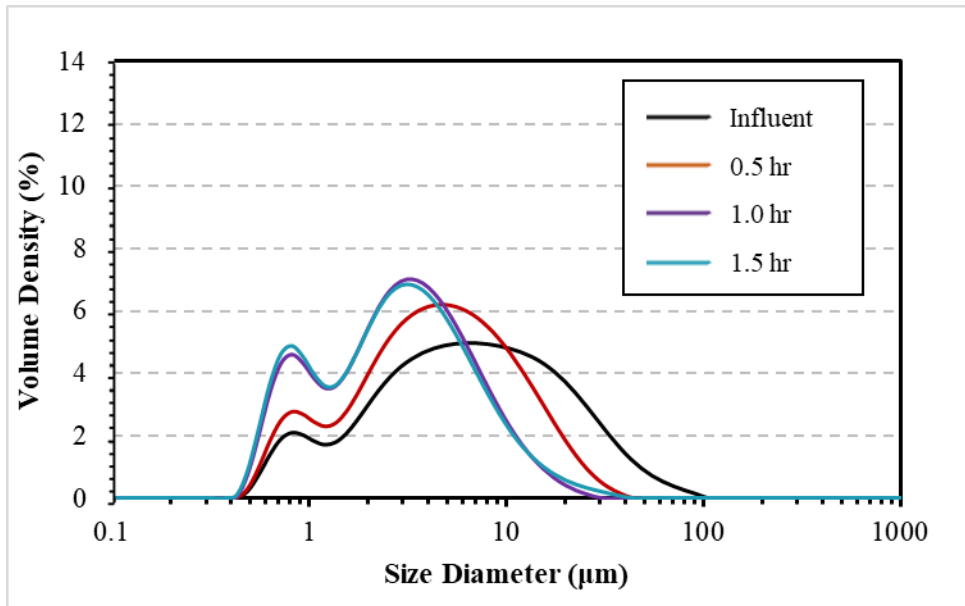
**Size Distribution Analysis for Soil C @ 1.5 hr.**



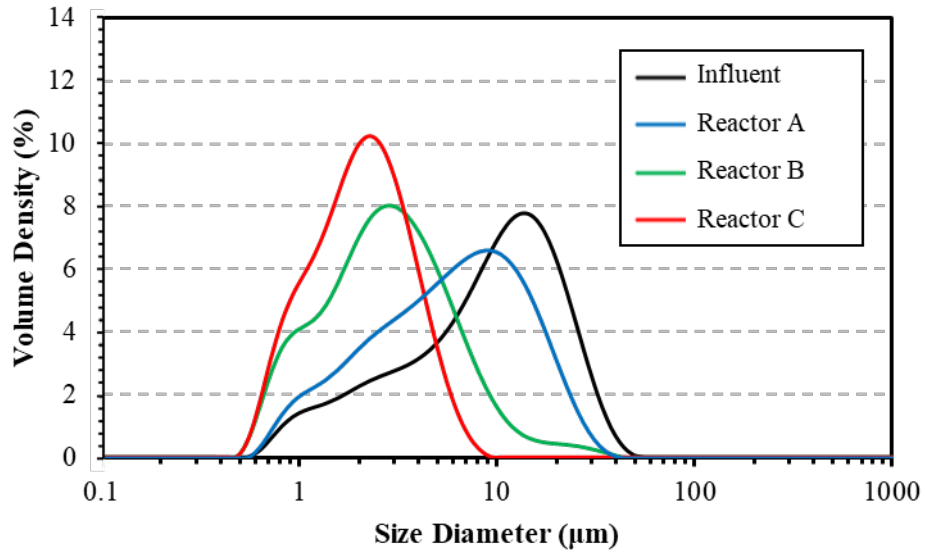
**Size Distribution Analysis for Soil C in Reactor C.**



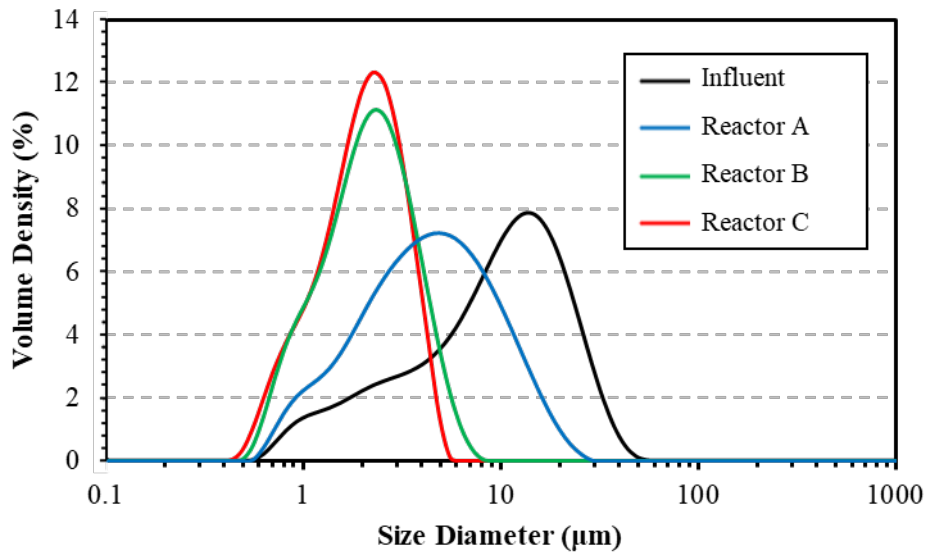
**Size Distribution Analysis for Soil C in Reactor B.**



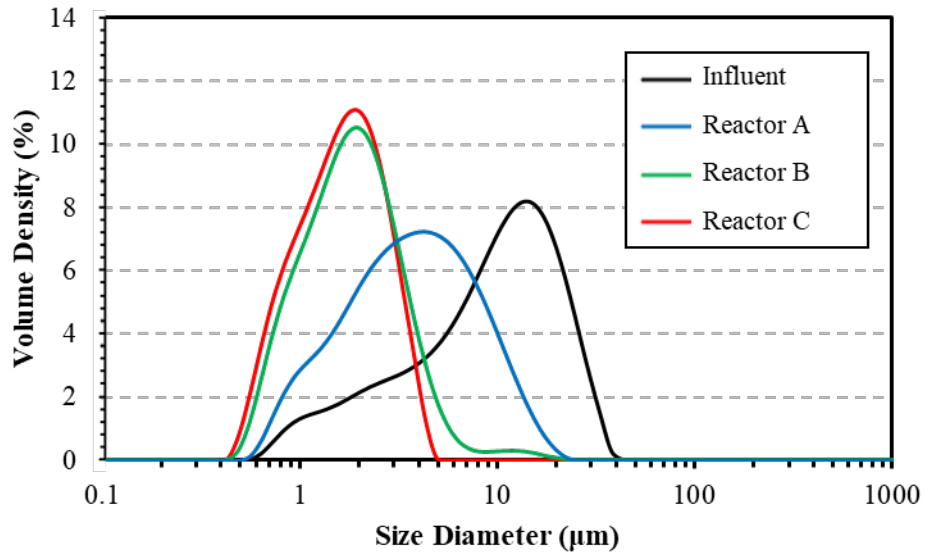
**Size Distribution Analysis for Soil C in Reactor A.**



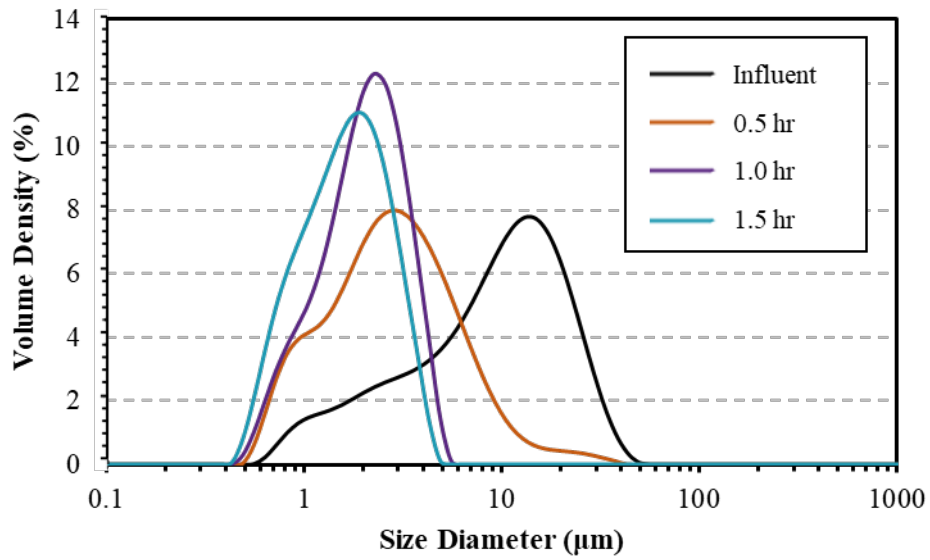
**Size Distribution Analysis for Soil D @ 0.5 hr.**



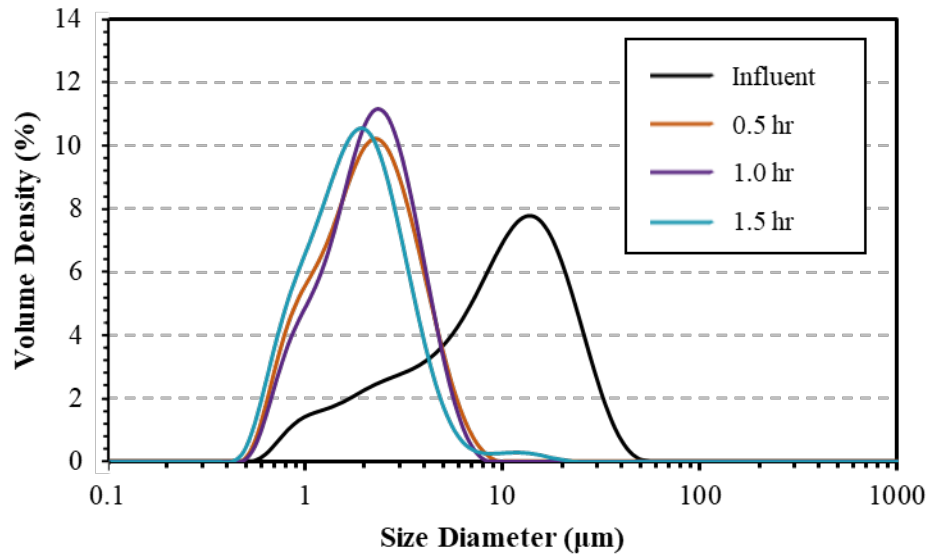
**Size Distribution Analysis for Soil D @ 1.0 hr.**



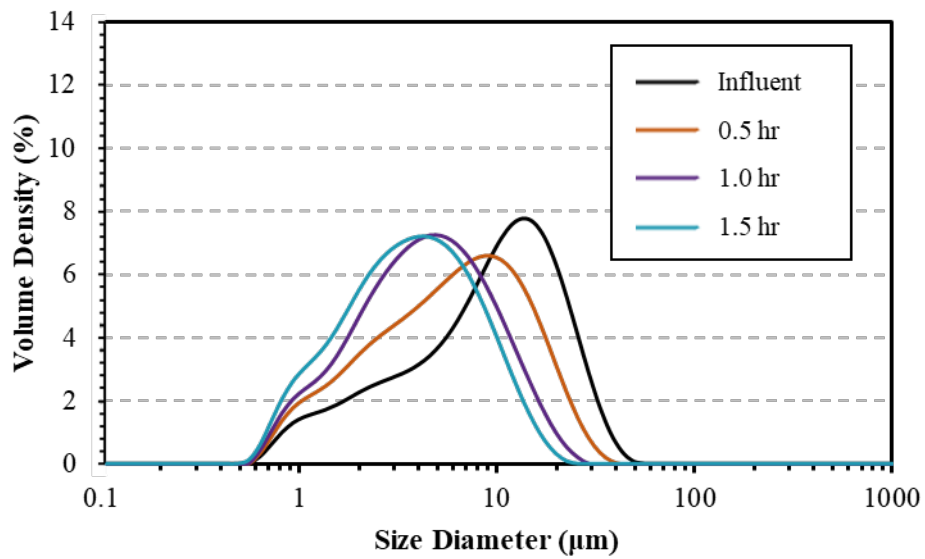
**Size Distribution Analysis for Soil D @ 1.5 hr.**



**Size Distribution Analysis for Soil D in Reactor C.**



**Size Distribution Analysis for Soil D in Reactor B.**



**Size Distribution Analysis for Soil D in Reactor A.**



## **Appendix H: PSD Measurements**

Soil	Turbidity Reduction	Averaged Turbidity Reduction	Dx (10)	Dx (50)	Dx (90)	Settling Box			Residence Time		
						Reactor A	Reactor B	Reactor C	0.5 hr	1.0 hr	1.5 hr
Soil A	37.82%	37%	0.97	3.61	12.10	1	0	0	1	0	0
Soil A	36.54%					1	0	0	1	0	0
Soil A	37.28%					1	0	0	1	0	0
Soil A	44.56%	45%	0.87	2.40	7.10	0	1	0	1	0	0
Soil A	43.80%					0	1	0	1	0	0
Soil A	45.82%					0	1	0	1	0	0
Soil A	54.74%	56%	0.85	2.17	5.52	0	0	1	1	0	0
Soil A	55.88%					0	0	1	1	0	0
Soil A	56.18%					0	0	1	1	0	0
Soil A	41.72%	43%	1.05	3.66	9.82	1	0	0	0	1	0
Soil A	44.26%					1	0	0	0	1	0
Soil A	43.69%					1	0	0	0	1	0
Soil A	63.39%	63%	0.68	1.69	3.53	0	1	0	0	1	0
Soil A	62.36%					0	1	0	0	1	0
Soil A	64.58%					0	1	0	0	1	0
Soil A	72.41%	73%	0.68	1.57	3.44	0	0	1	0	1	0
Soil A	74.92%					0	0	1	0	1	0
Soil A	71.99%					0	0	1	0	1	0
Soil A	56.16%	55%	0.85	2.36	7.15	1	0	0	0	0	1
Soil A	53.81%					1	0	0	0	0	1
Soil A	53.86%					1	0	0	0	0	1
Soil A	75.17%	74%	0.74	1.65	3.73	0	1	0	0	0	1
Soil A	74.25%					0	1	0	0	0	1
Soil A	71.11%					0	1	0	0	0	1
Soil A	79.88%	79%	0.64	1.25	2.36	0	0	1	0	0	1
Soil A	79.39%					0	0	1	0	0	1
Soil A	78.32%					0	0	1	0	0	1

Soil B	20.40%	20%	1.27	4.80	16.00	1	0	0	1	0	0
Soil B	21.98%					1	0	0	1	0	0
Soil B	17.99%					1	0	0	1	0	0
Soil B	44.18%	44%	0.99	2.92	7.04	0	1	0	1	0	0
Soil B	45.32%					0	1	0	1	0	0
Soil B	42.48%					0	1	0	1	0	0
Soil B	57.57%	57%	1.10	3.02	6.24	0	0	1	1	0	0
Soil B	58.44%					0	0	1	1	0	0
Soil B	56.19%					0	0	1	1	0	0
Soil B	33.79%	35%	1.05	3.48	9.40	1	0	0	0	1	0
Soil B	35.45%					1	0	0	0	1	0
Soil B	34.75%					1	0	0	0	1	0
Soil B	57.85%	51%	1.02	3.03	6.59	0	1	0	0	1	0
Soil B	56.13%					0	1	0	0	1	0
Soil B	55.60%					0	1	0	0	1	0
Soil B	68.37%	59%	0.94	2.66	6.11	0	0	1	0	1	0
Soil B	67.75%					0	0	1	0	1	0
Soil B	69.20%					0	0	1	0	1	0
Soil B	56.94%	56%	1.19	3.61	8.27	1	0	0	0	0	1
Soil B	54.16%					1	0	0	0	0	1
Soil B	56.98%					1	0	0	0	0	1
Soil B	70.14%	71%	0.88	2.38	5.07	0	1	0	0	0	1
Soil B	70.49%					0	1	0	0	0	1
Soil B	72.54%					0	1	0	0	0	1
Soil B	86.10%	86%	0.81	2.05	4.26	0	0	1	0	0	1
Soil B	88.06%					0	0	1	0	0	1
Soil B	85.32%					0	0	1	0	0	1

Soil C	41.51%	41%	1.03	4.39	13.80	1	0	0	1	0	0
Soil C	42.13%					1	0	0	1	0	0
Soil C	40.34%					1	0	0	1	0	0
Soil C	65.75%	66%	0.81	2.85	6.19	0	1	0	1	0	0
Soil C	65.99%					0	1	0	1	0	0
Soil C	64.94%					0	1	0	1	0	0
Soil C	72.78%	73%	0.72	2.24	5.88	0	0	1	1	0	0
Soil C	73.76%					0	0	1	1	0	0
Soil C	72.03%					0	0	1	1	0	0
Soil C	44.31%	44%	0.80	2.88	8.25	1	0	0	0	1	0
Soil C	42.80%					1	0	0	0	1	0
Soil C	45.11%					1	0	0	0	1	0
Soil C	67.50%	68%	0.68	1.90	5.14	0	1	0	0	1	0
Soil C	68.85%					0	1	0	0	1	0
Soil C	68.02%					0	1	0	0	1	0
Soil C	82.52%	84%	0.64	1.72	4.41	0	0	1	0	1	0
Soil C	85.26%					0	0	1	0	1	0
Soil C	84.04%					0	0	1	0	1	0
Soil C	50.91%	51%	0.78	2.80	8.46	1	0	0	0	0	1
Soil C	51.58%					1	0	0	0	0	1
Soil C	49.93%					1	0	0	0	0	1
Soil C	78.74%	78%	0.60	1.37	5.14	0	1	0	0	0	1
Soil C	76.70%					0	1	0	0	0	1
Soil C	78.04%					0	1	0	0	0	1
Soil C	90.25%	90%	0.61	1.43	4.05	0	0	1	0	0	1
Soil C	89.44%					0	0	1	0	0	1
Soil C	90.10%					0	0	1	0	0	1

Soil D	35.70%	35%	1.51	6.07	16.50	1	0	0	1	0	0
Soil D	34.08%					1	0	0	1	0	0
Soil D	35.64%					1	0	0	1	0	0
Soil D	58.49%	60%	0.92	2.07	4.20	0	1	0	1	0	0
Soil D	61.48%					0	1	0	1	0	0
Soil D	60.94%					0	1	0	1	0	0
Soil D	72.61%	74%	0.85	1.81	3.69	0	0	1	1	0	0
Soil D	73.68%					0	0	1	1	0	0
Soil D	76.34%					0	0	1	1	0	0
Soil D	63.66%	63%	1.23	3.68	9.56	1	0	0	0	1	0
Soil D	63.25%					1	0	0	0	1	0
Soil D	61.97%					1	0	0	0	1	0
Soil D	77.64%	78%	0.97	2.15	4.08	0	1	0	0	1	0
Soil D	78.19%					0	1	0	0	1	0
Soil D	78.30%					0	1	0	0	1	0
Soil D	86.14%	87%	0.92	2.03	3.53	0	0	1	0	1	0
Soil D	87.73%					0	0	1	0	1	0
Soil D	85.97%					0	0	1	0	1	0
Soil D	71.96%	73%	1.39	4.32	11.40	1	0	0	0	0	1
Soil D	73.03%					1	0	0	0	0	1
Soil D	74.03%					1	0	0	0	0	1
Soil D	81.92%	82%	0.98	2.75	7.22	0	1	0	0	0	1
Soil D	82.59%					0	1	0	0	0	1
Soil D	81.29%					0	1	0	0	0	1
Soil D	89.25%	90%	0.78	1.63	3.01	0	0	1	0	0	1
Soil D	90.81%					0	0	1	0	0	1
Soil D	90.05%					0	0	1	0	0	1

## **Appendix I: Settling Velocity Estimation**

**Process of equation derivation:**

$$F_D = 6\pi\mu aU_0 = 3\pi\mu dU_0$$

Where  $F_D$  is viscos drag force  $F$ ,  $A$  is radius of a sphere,  $d$  is diameter of sphere,  $U_0$  is velocity through a viscous fluid, and  $\mu$  is fluid viscosity.

Equation 1 only applies to creeping flow (Reynolds number  $Re = \rho aU_0/\mu$  less than 1), which means equation 1 only applies to spheres with small diameter surrounded by either gas or liquid.

Analyze equation 1 through dimensional analysis

$$D \longrightarrow L$$

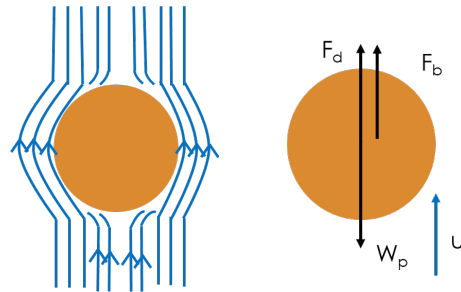
$$U_0 \longrightarrow L/T$$

$$\mu \longrightarrow M/L/T$$

$$F_D \longrightarrow ML/T^2$$

$$F_D = Cd\mu U_0 \text{ (C is constant)}$$

When this sphere particle reaches terminal velocity  $\rightarrow$



no acceleration ( $U_0=v_t$ )

$$\frac{dU}{dt} = 0$$

Where  $U$  is relative velocity between sphere and fluid

$$\text{Gravity: sphere weight: } W_s = v_s \rho_s g = \frac{\pi}{6} d^3 \rho_s g$$

Where  $\rho_s$  is density of sphere,  $\rho_f$  is density of fluid

Force balance:

$$m_s g + m_s \frac{dU}{dt} = m_f g + F_D$$

Sphere weight; Force due to acceleration; Force due to up thrust; Drag force against sphere weight

$$\frac{\pi}{6} d^3 \rho_s g + 0 = \frac{\pi}{6} d^3 \rho_f g + 3\pi\mu d v_t$$

$$\frac{\pi}{6} d^3 g (\rho_s - \rho_f) = 3\pi\mu d v_t$$

$$v_t = \frac{d^2 g (\rho_s - \rho_f)}{18\mu} \quad (\text{vt = ws in this proposal treated as settling velocity})$$

$$\rho v_s (S + C_m) \frac{dw_s}{dt} = \rho v_s (S - a) g - F_D$$

Acceleration addition weight and drag force and buoyance

$$(S + C_m) \frac{dw_s}{dt} = (S - 1)g - \frac{F_D}{\rho v_s}$$

$$F_D = 3\pi\mu d w_s$$

$$\frac{dw_s}{dt} = \frac{1}{(S + C_m)} \left[ (S - 1)g - \frac{3\pi\mu d}{\rho v_s} w_s \right]$$

$$a = -\frac{3\pi\mu d}{\rho v_s} \frac{1}{S + C_m}$$

$$b = (S - 1)g \frac{1}{S + C_m} \longrightarrow \text{constant}$$

$$\frac{dw_s}{dt} = b + a w_s$$

$$\int \frac{1}{a} \frac{d(aw_s + b)}{aw_s + b} = \int dt$$

$$\ln(aw_s + b) = a(t + C_1)$$

$$t = 0, w_s = 0$$

$$C_1 = \frac{1}{a} \ln b$$

$$e^{\ln(aw_s + b)} = e^{a(t + C_1)}$$

$$aw_s + b = e^{atb}$$

$$w_s = \frac{b(e^{at} - 1)}{a}$$

$$w_s = \frac{-\rho v_s (S - 1)g}{3\pi\mu d} \left( e^{-\frac{3\pi\mu d}{\rho v_s (S + C_m)} t} - 1 \right)$$

$$w_s = \frac{\rho v_s (S - 1)g}{3\pi\mu d} \left( 1 - e^{-\frac{3\pi\mu d}{\rho v_s (S + C_m)} t} \right)$$

$C_m$  is the shape factor to calibrate “added” mass for irregular particles

It should equal to 1 for sphere (not 0)

According to the  $w_s$  equation shown above,

$$L = \int_0^t w_s dt$$

$$= \frac{\rho v_s (S - 1)g}{3\pi\mu d} \left[ t + \frac{\rho v_s (S + 1)}{3\pi\mu d} e^{-\frac{3\pi\mu d}{\rho v_s (S + 1)} t} \right] \Big|_0^t$$



### Calculations about shape factor:

In this research,  $C_m$  is the Corey shape factor which was used to calculate the settling velocity.

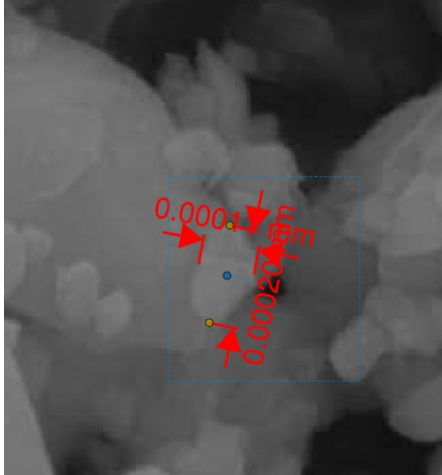
According to the microscopy image, the smallest and longest principal lengths were measured through the bluebeam software, and the medium size was used as the intermediate length from the following equation (Corey Shape Function), the Corey shape factor was calculated:

$$C_m = \frac{d_{min.}}{(d_{med.} \times d_{max.})^{1/2}}$$

where  $d_{med}$  is the intermediate length (median size),  $d_{min.}$  is the smallest length,  $d_{max}$  is the longest length, and  $C_m$  is the size factor.

The measurements of particle dimensions were shown in the following figures and the results of size factors were shown below:

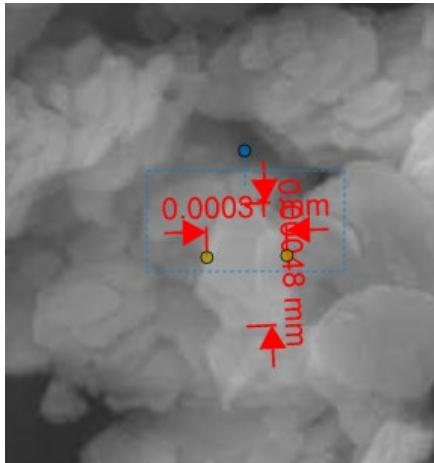
	<b>Median Size (<math>\mu\text{m}</math>)</b>	<b>Smallest principal length (<math>\mu\text{m}</math>)</b>	<b>Longest principal length (<math>\mu\text{m}</math>)</b>	<b>Shape Factor</b>
<b>Soil A</b>	5	0.11	0.2	0.11
<b>Soil B</b>	0.5	0.22	0.43	0.47
<b>Soil C</b>	1.2	0.3	0.48	0.40
<b>Soil D</b>	6.8	0.44	0.72	0.20
<b>Soil F</b>	5	0.18	0.57	0.11



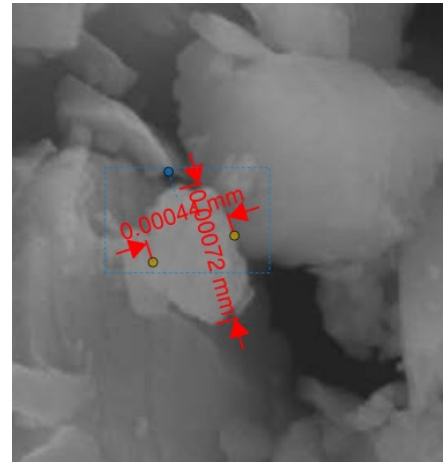
(a) Soil A



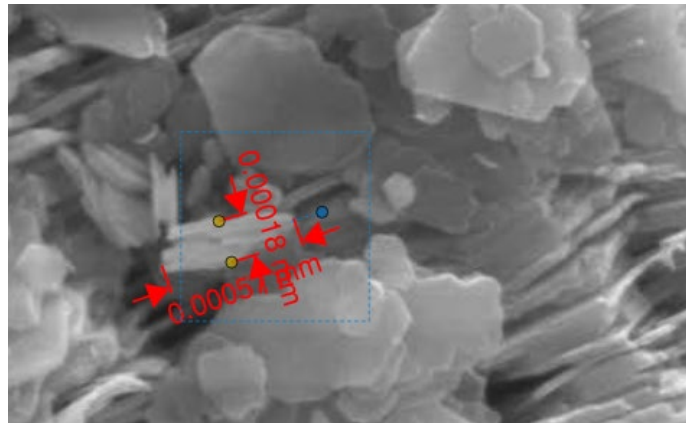
(b) Soil B



(c) Soil C



(d) Soil D

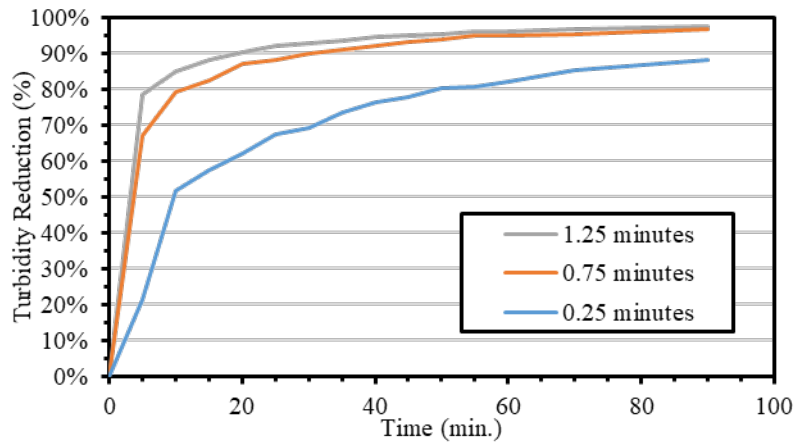


(e) Soil F

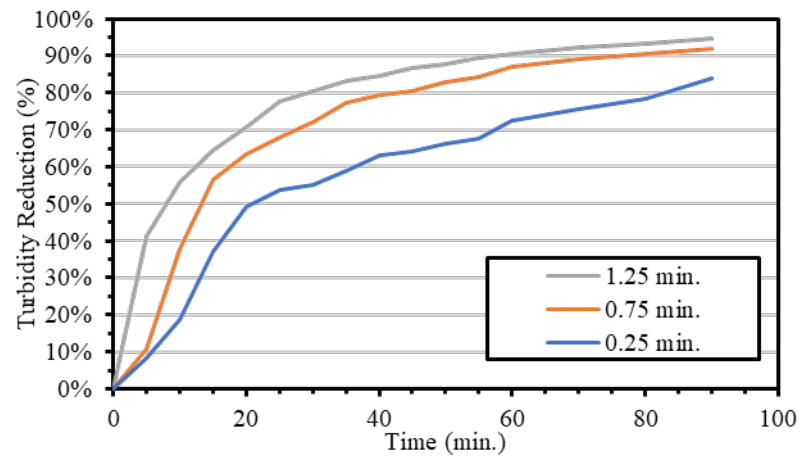
Through the review, an equation was corrected in the original excel spreadsheet, from which the updated settling velocity (also incorporated with corrections made in problem) is going to be recalculated and updated in the proposal and oral exam.

As mentioned before, the Corey shape factor could be larger than 1. And usually the shape factor used in the research analysis is usually normalized which is ranging from zero to one. According to literature reference, the Corey shape factor ranges from zero to ten. With this applied Cory shape function, the shape factor shouldn't be over ten, which means they should not range between 260 and 2.77 with this applied method.

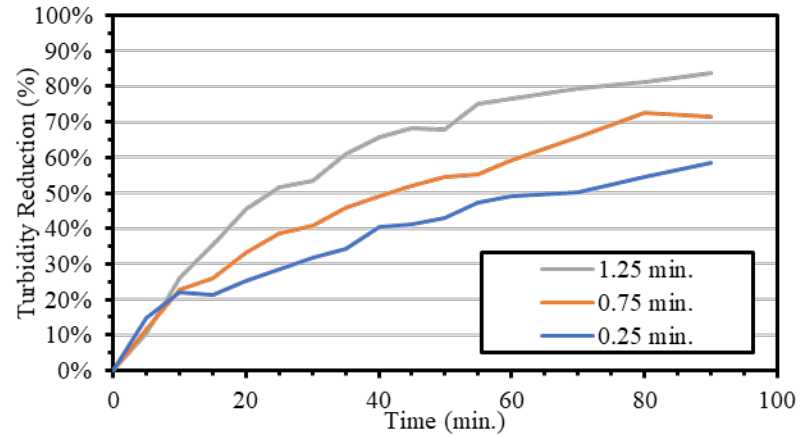
## **Appendix J: Turbidity Observations Along Time in EC**



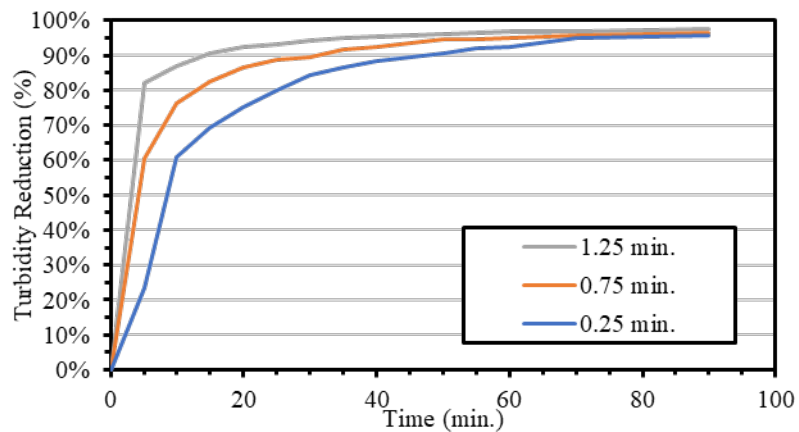
EC at 0.9 A and 0.5 cm Aluminum Cell Spacing



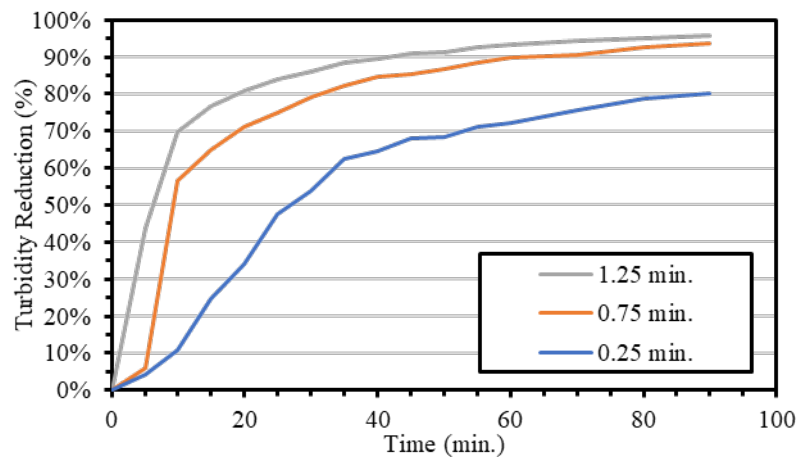
EC at 0.6 A and 0.5 cm Aluminum Cell Spacing



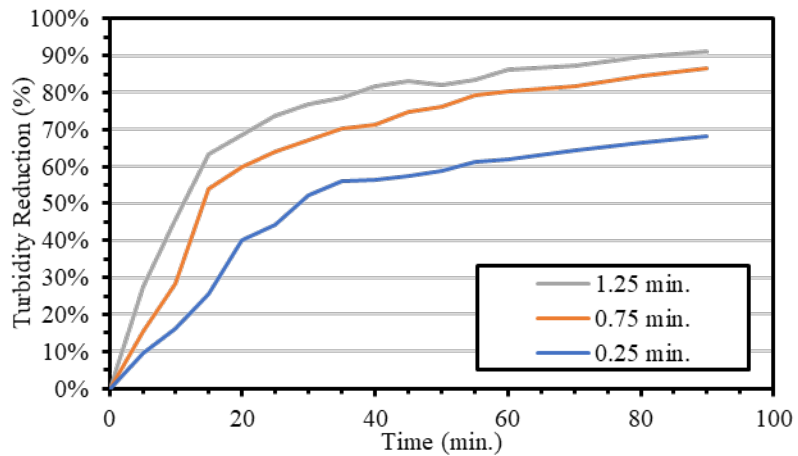
EC at 0.3 A and 0.5 cm Aluminum Cell Spacing



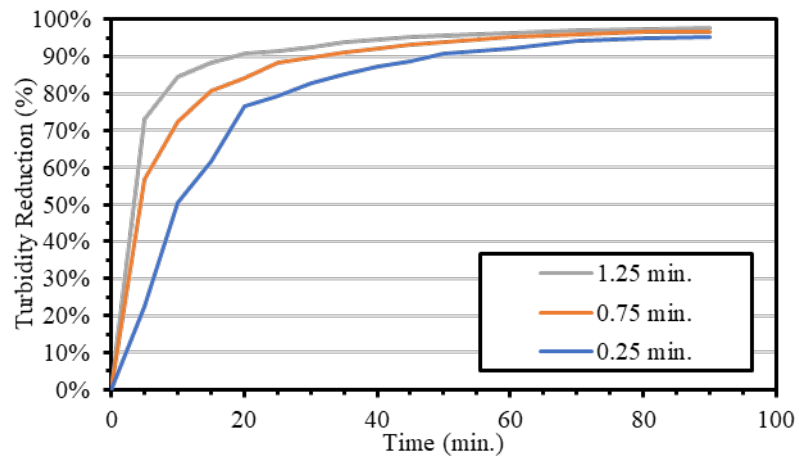
EC at 0.9 A and 1.0 cm Aluminum Cell Spacing



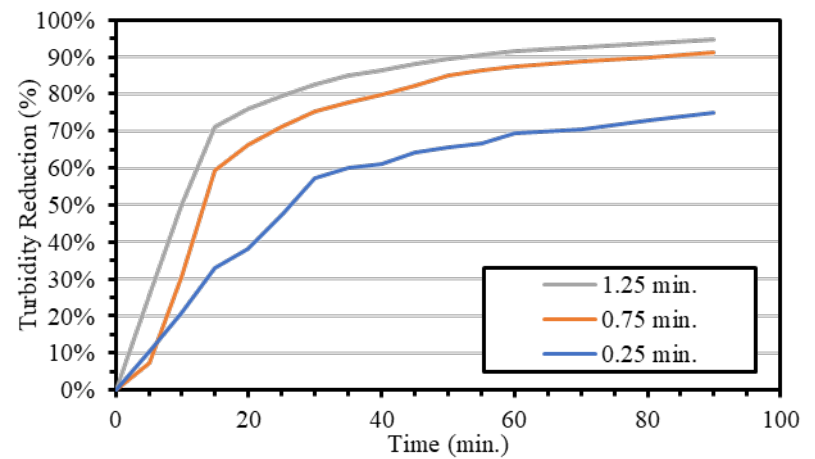
EC at 0.6 A and 1.0 cm Aluminum Cell Spacing



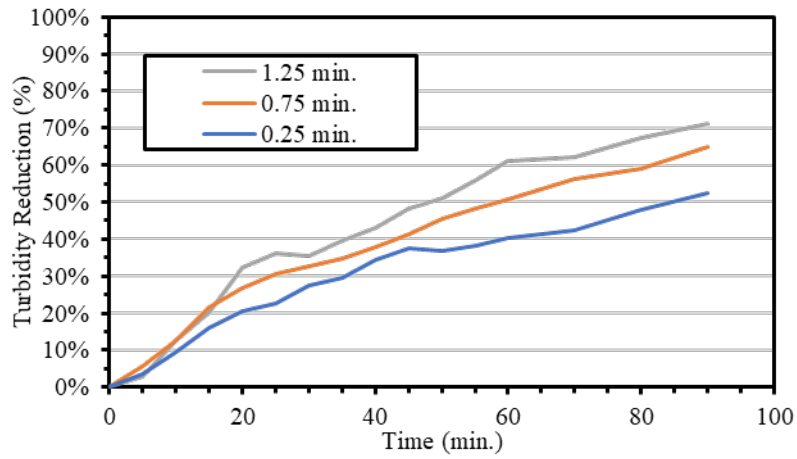
EC at 0.3 A and 1.0 cm Aluminum Cell Spacing



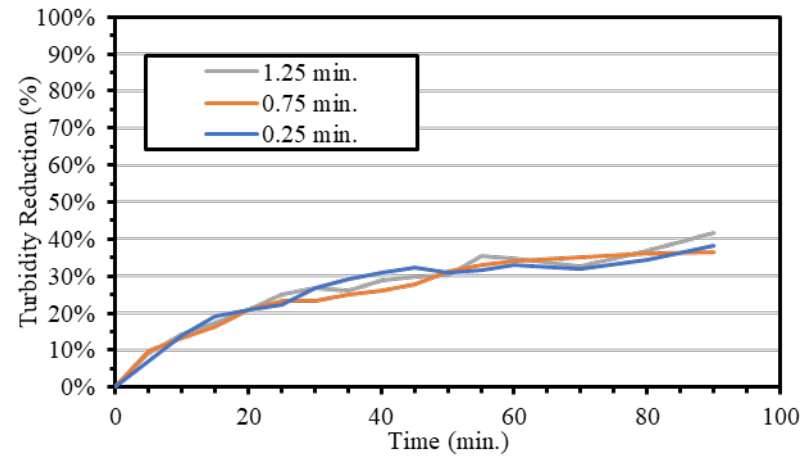
EC at 0.6 A and 2.0 cm Aluminum Cell Spacing



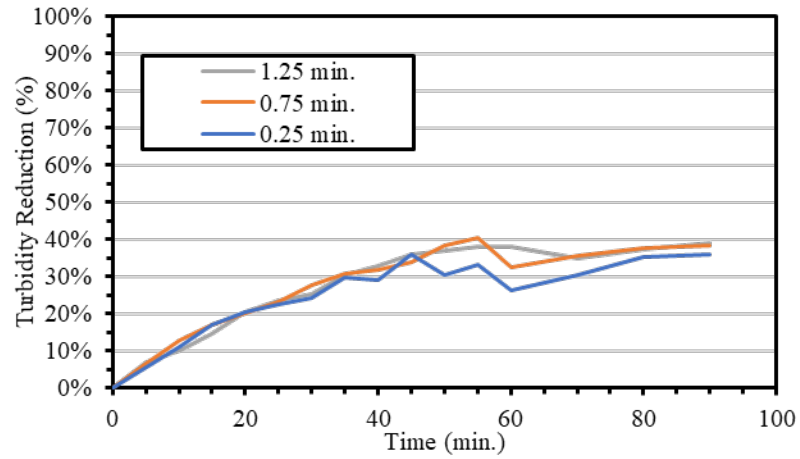
EC at 0.3 A and 2.0 cm Aluminum Cell Spacing



EC at 0.9 A and 0.5 cm Stainless Steel Cell Spacing

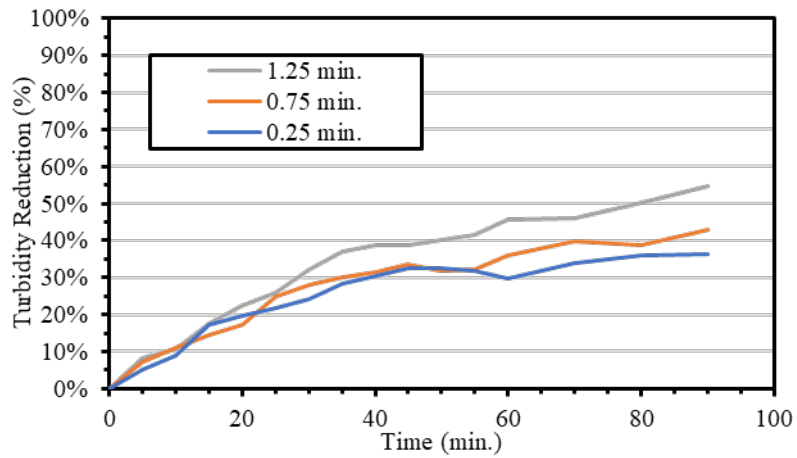


EC at 0.6 A and 0.5 cm Stainless Steel Cell Spacing

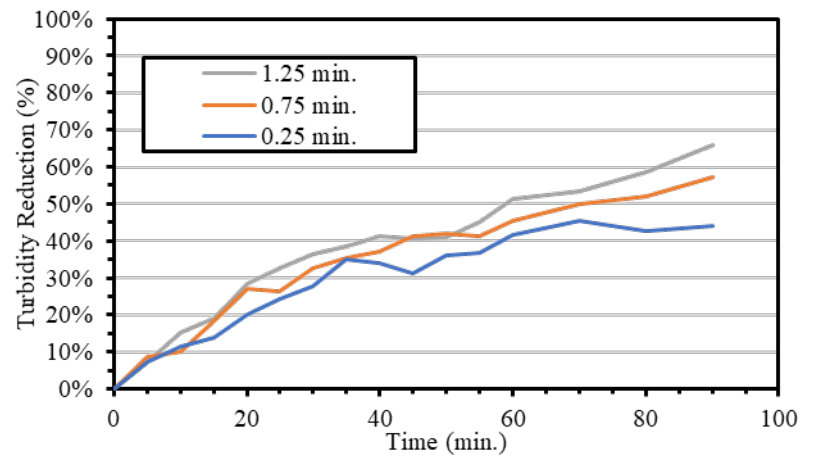


EC at 0.3 A and 0.5 cm Stainless Steel Cell Spacing

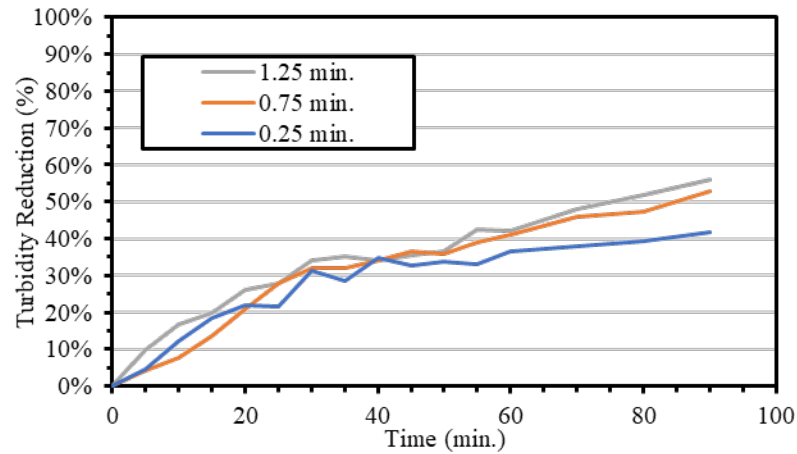




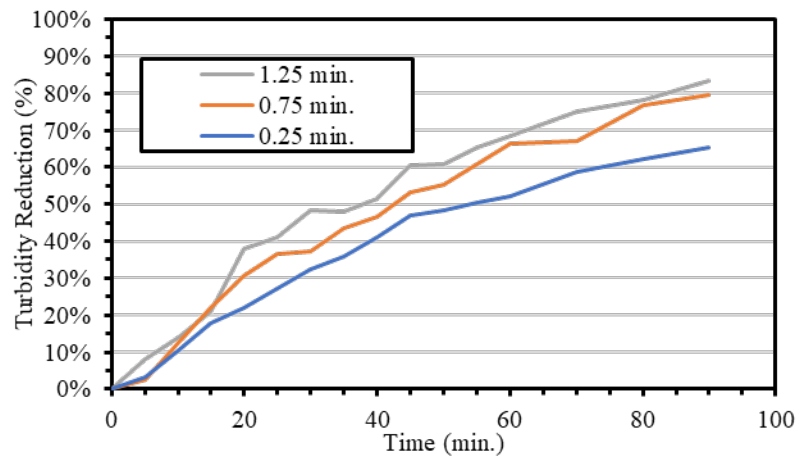
EC at 0.9 A and 1.0 cm Stainless Steel Cell Spacing



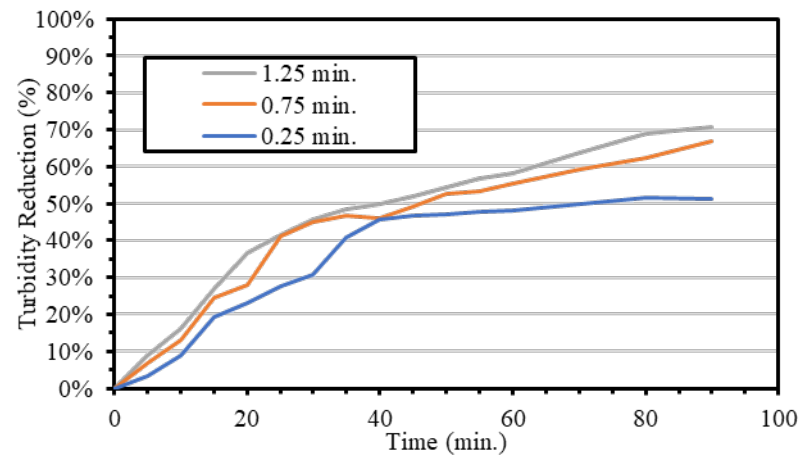
EC at 0.6 A and 1.0 cm Stainless Steel Cell Spacing



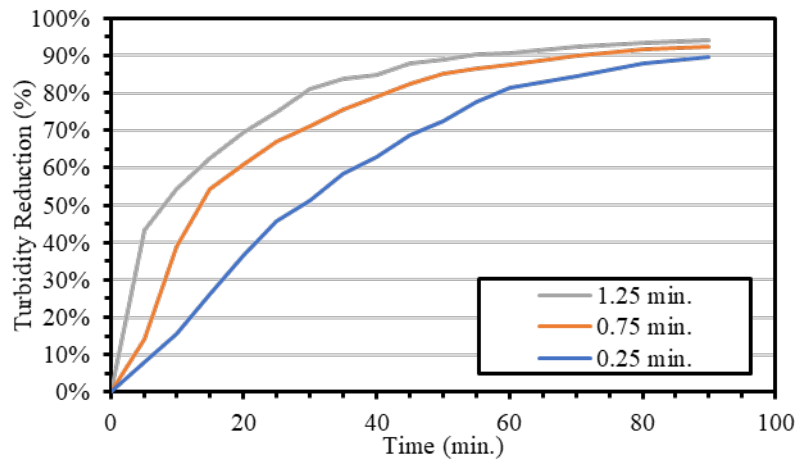
EC at 0.3 A and 1.0 cm Stainless Steel Cell Spacing



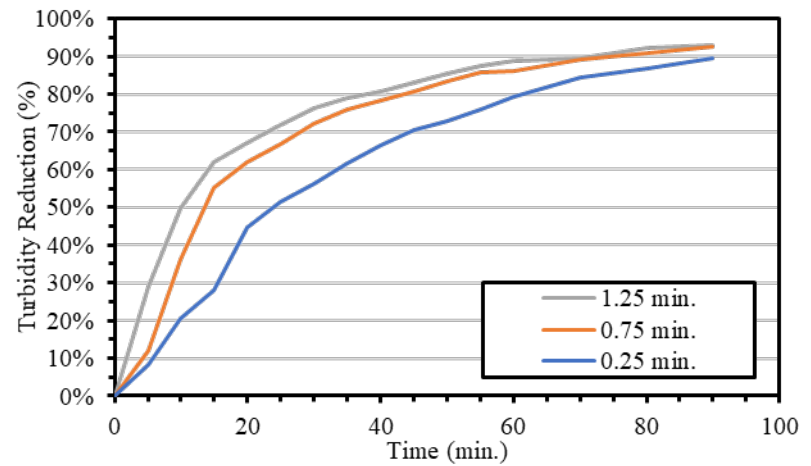
EC at 0.6 A and 2.0 cm Stainless Steel Cell Spacing



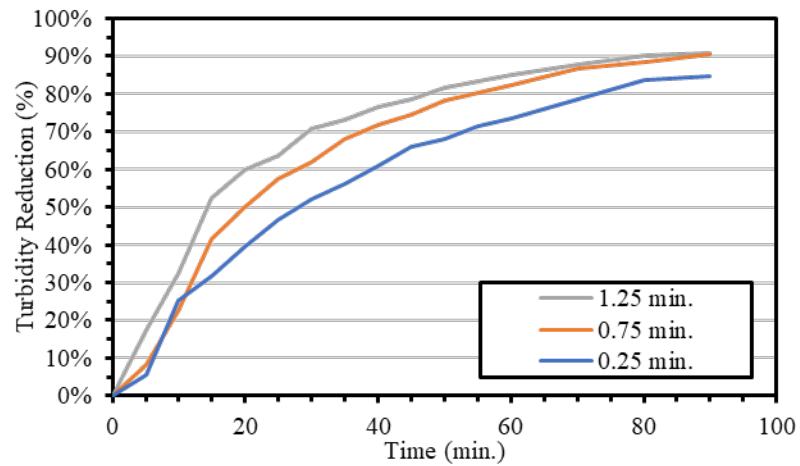
EC at 0.3 A and 2.0 cm Stainless Steel Cell Spacing



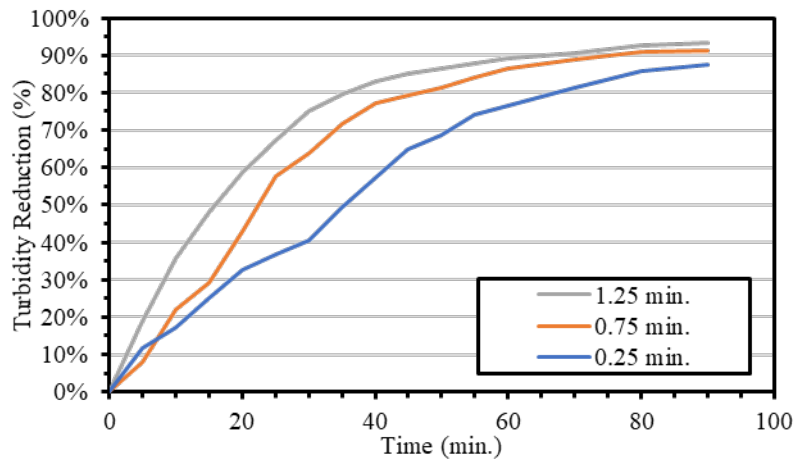
EC at 0.9 A and 0.5 cm Low-Carbon Steel Cell Spacing



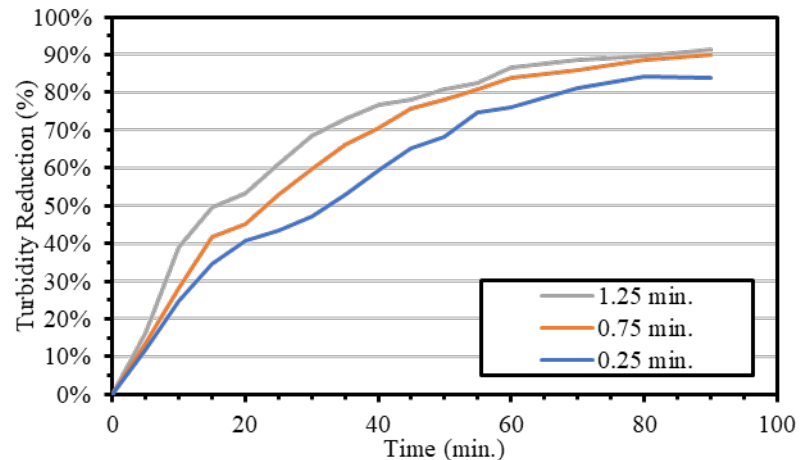
EC at 0.6 A and 0.5 cm Low-Carbon Steel Cell Spacing



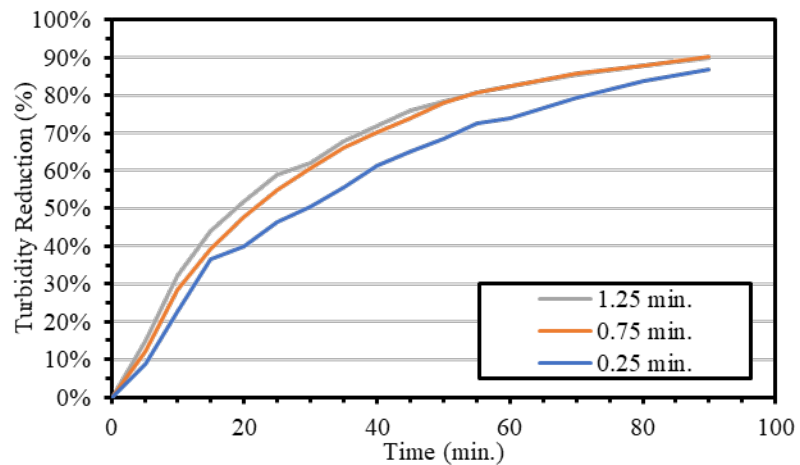
EC at 0.3 A and 0.5 cm Low-Carbon Steel Cell Spacing



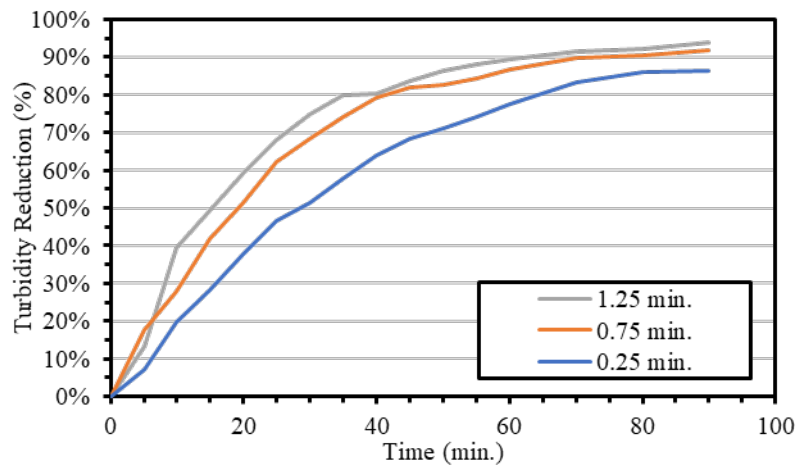
EC at 0.9 A and 1.0 cm Low-Carbon Steel Cell Spacing



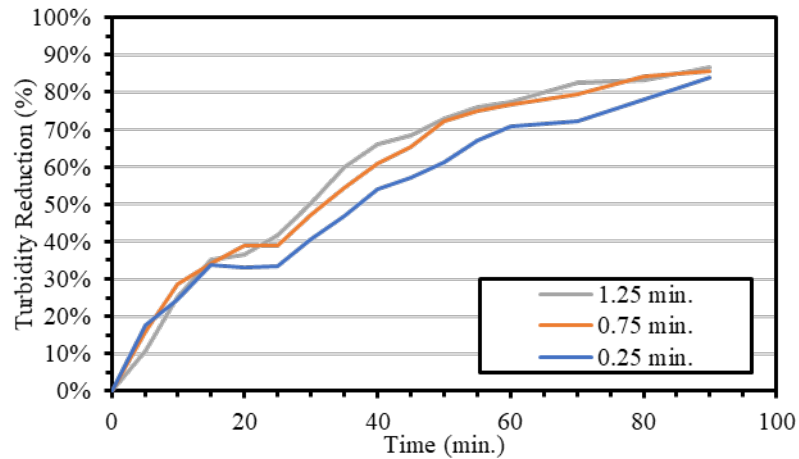
EC at 0.6 A and 1.0 cm Low-Carbon Steel Cell Spacing



EC at 0.3 A and 1.0 cm Low-Carbon Steel Cell Spacing



EC at 0.6 A and 2.0 cm Low-Carbon Steel Cell Spacing



EC at 0.3 A and 2.0 cm Low-Carbon Steel Cell Spacing

**Appendix K: Turbidity and TSS Observations in EC +LS System**

Turbidity measurements of EC+LS:

Inflow Concentration (mg/L)	Inflow (NTU)	After EC (NTU)	R <sub>C</sub> (NTU)	R <sub>B</sub> (NTU)	R <sub>A</sub> (NTU)	R <sub>C</sub> (%)	R <sub>B</sub> (%)	R <sub>A</sub> (%)
500	254.43	249.00	123.00	162.25	199.50	51.7%	36.2%	21.6%
	246.00	240.86	112.50	152.50	190.00	54.3%	38.0%	22.8%
	236.86	229.86	107.25	149.50	186.25	54.7%	36.9%	21.4%
	234.50	219.30	76.25	111.50	123.75	67.5%	52.5%	47.2%
	241.90	228.60	81.50	121.25	133.00	66.3%	49.9%	45.0%
	215.70	208.40	71.00	107.50	118.75	67.1%	50.2%	44.9%
	198.46	195.31	14.50	35.00	50.75	92.7%	82.4%	74.4%
	223.46	200.23	18.00	33.75	56.50	91.9%	84.9%	74.7%
	238.92	211.31	25.00	39.50	64.25	89.5%	83.5%	73.1%
1000	1266.29	1225.71	314.50	541.50	601.50	75.2%	57.2%	52.5%
	1245.43	1207.71	302.00	539.75	590.50	75.8%	56.7%	52.6%
	1224.57	1212.57	295.25	533.00	577.25	75.9%	56.5%	52.9%
	1262.40	1232.60	185.25	275.00	454.00	85.3%	78.2%	64.0%
	1240.60	1235.20	175.50	280.00	459.50	85.9%	77.4%	63.0%
	1290.60	1252.60	190.25	288.00	462.00	85.3%	77.7%	64.2%
	1260.31	1230.31	72.75	149.50	203.75	94.2%	88.1%	83.8%
	1252.62	1238.15	67.50	142.50	199.00	94.6%	88.6%	84.1%
	1234.46	1200.31	60.25	135.00	185.75	95.1%	89.1%	85.0%
5000	5684.57	5558.86	1178.00	1377.00	1833.00	79.3%	75.8%	67.8%
	5779.43	5641.14	1187.00	1383.50	1843.00	79.5%	76.1%	68.1%
	5899.43	5800.00	1232.50	1419.00	1868.00	79.1%	75.9%	68.3%
	5620.00	5500.80	397.75	725.00	803.50	92.9%	87.1%	85.7%
	6005.60	5788.00	417.00	754.00	829.25	93.1%	87.4%	86.2%
	5907.20	5645.60	407.25	739.50	811.50	93.1%	87.5%	86.3%
	6052.31	5777.23	127.00	333.00	785.75	97.9%	94.5%	87.0%
	5801.85	5607.38	99.75	330.25	787.00	98.3%	94.3%	86.4%
	5971.08	5693.54	116.00	343.25	799.50	98.1%	94.3%	86.6%

TSS of EC+LS:

Inflow Concentration (mg/L)	Inflow (mg/L)	After EC (mg/L)	R <sub>C</sub> (mg/L)	R <sub>B</sub> (mg/L)	R <sub>A</sub> (mg/L)	R <sub>C</sub> (%)	R <sub>B</sub> (%)	R <sub>A</sub> (%)
500	266.67	226.67	133.33	213.33	226.67	50.0%	20.0%	15.0%
	226.67	226.67	133.33	160.00	186.67	41.2%	29.4%	17.6%
	213.33	213.33	120.00	160.00	186.67	43.8%	25.0%	12.5%
	240.00	240.00	80.00	120.00	146.67	66.7%	50.0%	38.9%
	253.33	226.67	93.33	133.33	133.33	63.2%	47.4%	47.4%
	240.00	213.33	66.67	133.33	146.67	72.2%	44.4%	38.9%
	226.67	240.00	26.67	53.33	93.33	88.2%	76.5%	58.8%
	240.00	226.67	40.00	53.33	66.67	83.3%	77.8%	72.2%
	253.33	213.33	40.00	66.67	80.00	84.2%	73.7%	68.4%
1000	1080.00	1040.00	173.33	346.67	440.00	84.0%	67.9%	59.3%
	1053.33	973.33	226.67	346.67	413.33	78.5%	67.1%	60.8%
	1013.33	1000.00	200.00	360.00	413.33	80.3%	64.5%	59.2%
	1333.33	1293.33	160.00	333.33	400.00	88.0%	75.0%	70.0%
	1320.00	1333.33	146.67	306.67	373.33	88.9%	76.8%	71.7%
	1346.67	1280.00	133.33	280.00	360.00	90.1%	79.2%	73.3%
	1306.67	1280.00	146.67	160.00	280.00	88.8%	87.8%	78.6%
	1293.33	1240.00	120.00	173.33	253.33	90.7%	86.6%	80.4%
	1280.00	1226.67	106.67	186.67	240.00	91.7%	85.4%	81.2%
5000	4906.67	4826.67	653.33	773.33	1400.00	86.7%	84.2%	71.5%
	4920.00	4840.00	613.33	786.67	1386.67	87.5%	84.0%	71.8%
	4933.33	4813.33	626.67	800.00	1426.67	87.3%	83.8%	71.1%
	5280.00	5106.67	413.33	666.67	1253.33	92.2%	87.4%	76.3%
	5320.00	5133.33	453.33	653.33	1280.00	91.5%	87.7%	75.9%
	5293.33	5080.00	400.00	680.00	1306.67	92.4%	87.2%	75.3%
	6026.67	5920.00	40.00	200.00	613.33	99.3%	96.7%	89.8%
	5973.33	5853.33	53.33	160.00	560.00	99.1%	97.3%	90.6%
6000.00	5893.33	40.00	173.33	586.67	99.3%	97.1%	90.2%	



Turbidity measurements of LS:

Inflow Concentration (mg/L)	Inflow (NTU)	R <sub>C</sub> (NTU)	R <sub>B</sub> (NTU)	R <sub>A</sub> (NTU)	R <sub>C</sub> (%)	R <sub>B</sub> (%)	R <sub>A</sub> (%)
500	224.50	165.50	199.50	212.50	26.3%	11.1%	5.3%
	216.75	154.00	195.00	207.00	29.0%	10.0%	4.5%
	223.75	161.50	199.50	209.50	27.8%	10.8%	6.4%
	192.20	116.00	146.50	171.50	39.6%	23.8%	10.8%
	193.80	115.50	145.50	174.50	40.4%	24.9%	10.0%
	202.20	116.00	150.50	182.50	42.6%	25.6%	9.7%
	186.43	89.50	116.50	157.50	52.0%	37.5%	15.5%
	187.00	98.50	119.00	159.00	47.3%	36.4%	15.0%
	198.14	82.50	115.00	165.00	58.4%	42.0%	16.7%
1000	1241.00	819.50	1041.00	1107.00	34.0%	16.1%	10.8%
	1237.00	831.00	1026.00	1135.00	32.8%	17.1%	8.2%
	1234.50	824.00	1025.00	1129.00	33.3%	17.0%	8.5%
	1273.20	711.50	834.00	1113.00	44.1%	34.5%	12.6%
	1271.20	711.00	832.50	1125.00	44.1%	34.5%	11.5%
	1282.00	719.50	841.00	1138.00	43.9%	34.4%	11.2%
	1274.57	459.50	605.00	953.50	63.9%	52.5%	25.2%
	1276.86	459.50	603.50	965.50	64.0%	52.7%	24.4%
	1294.00	481.00	620.50	960.00	62.8%	52.0%	25.8%
5000	5738.00	2620.00	3198.00	3634.00	54.3%	44.3%	36.7%
	5738.67	2634.00	3158.00	3672.00	54.1%	45.0%	36.0%
	5786.67	2668.00	3222.00	3714.00	53.9%	44.3%	35.8%
	5540.80	1400.00	2070.00	3088.00	74.7%	62.6%	44.3%
	5697.60	1415.00	2120.00	3114.00	75.2%	62.8%	45.3%
	5537.60	1403.00	2082.00	3082.00	74.7%	62.4%	44.3%
	5848.00	1216.00	1493.00	2714.00	79.2%	74.5%	53.6%
	5795.43	1202.00	1493.00	2874.00	79.3%	74.2%	50.4%
	5787.43	1203.00	1493.00	2682.00	79.2%	74.2%	53.7%

TSS measurements of LS:

Inflow Concentration (mg/L)	Inflow (mg/L)	R <sub>C</sub> (mg/L)	R <sub>B</sub> (mg/L)	R <sub>A</sub> (mg/L)	R <sub>C</sub> (%)	R <sub>B</sub> (%)	R <sub>A</sub> (%)
500	226.67	146.67	200.00	213.33	35.3%	11.8%	5.9%
	213.33	160.00	186.67	200.00	25.0%	12.5%	6.3%
	226.67	146.67	186.67	213.33	35.3%	17.6%	5.9%
	160.00	66.67	120.00	146.67	58.3%	25.0%	8.3%
	173.33	80.00	133.33	146.67	53.8%	23.1%	15.4%
	186.67	93.33	133.33	173.33	50.0%	28.6%	7.1%
	226.67	93.33	120.00	200.00	58.8%	47.1%	11.8%
	226.67	80.00	106.67	146.67	64.7%	52.9%	35.3%
	240.00	93.33	133.33	160.00	61.1%	44.4%	33.3%
1000	1040.00	560.00	786.67	893.33	46.2%	24.4%	14.1%
	1013.33	533.33	733.33	880.00	47.4%	27.6%	13.2%
	1000.00	586.67	720.00	906.67	41.3%	28.0%	9.3%
	1080.00	506.67	666.67	840.00	53.1%	38.3%	22.2%
	1066.67	533.33	613.33	866.67	50.0%	42.5%	18.7%
	1093.33	480.00	653.33	813.33	56.1%	40.2%	25.6%
	1053.33	293.33	346.67	586.67	72.2%	67.1%	44.3%
	1053.33	320.00	360.00	600.00	69.6%	65.8%	43.0%
	1080.00	306.67	373.33	586.67	71.6%	65.4%	45.7%
5000	4693.33	1813.33	2160.00	3253.33	61.4%	54.0%	30.7%
	4693.33	1826.67	2173.33	3280.00	61.1%	53.7%	30.1%
	4706.67	1840.00	2146.67	3306.67	60.9%	54.4%	29.7%
	4546.67	1133.33	1546.67	2480.00	75.1%	66.0%	45.5%
	4573.33	1120.00	1533.33	2466.67	75.5%	66.5%	46.1%
	4560.00	1093.33	1520.00	2440.00	76.0%	66.7%	46.5%
	4746.67	720.00	1066.67	2320.00	84.8%	77.5%	51.1%
	4733.33	733.33	1080.00	2346.67	84.5%	77.2%	50.4%
	4720.00	746.67	1093.33	2333.33	84.2%	76.8%	50.6%

## **Appendix L: Regression Analysis for EC + LS System**

500 mg/L:

NTU%-all	TSS%-all	C, g/L	S, dm	T	T x C	T x S	C x S	T x C x S	C <sup>2</sup>	S <sup>2</sup>	T <sup>2</sup>	+EC
21.6%	15.0%	0.5	3.18	0.50	0.25	1.59	1.59	0.79	0.25	10.08	0.25	1
22.8%	17.6%	0.5	3.18	0.50	0.25	1.59	1.59	0.79	0.25	10.08	0.25	1
21.4%	12.5%	0.5	3.18	0.50	0.25	1.59	1.59	0.79	0.25	10.08	0.25	1
36.2%	20.0%	0.5	0.36	0.50	0.25	0.18	0.18	0.09	0.25	0.13	0.25	1
38.0%	29.4%	0.5	0.36	0.50	0.25	0.18	0.18	0.09	0.25	0.13	0.25	1
36.9%	25.0%	0.5	0.36	0.50	0.25	0.18	0.18	0.09	0.25	0.13	0.25	1
51.7%	50.0%	0.5	0.18	0.50	0.25	0.09	0.09	0.05	0.25	0.03	0.25	1
54.3%	41.2%	0.5	0.18	0.50	0.25	0.09	0.09	0.05	0.25	0.03	0.25	1
54.7%	43.8%	0.5	0.18	0.50	0.25	0.09	0.09	0.05	0.25	0.03	0.25	1
47.2%	38.9%	0.5	3.18	1.00	0.50	3.18	1.59	1.59	0.25	10.08	1.00	1
45.0%	47.4%	0.5	3.18	1.00	0.50	3.18	1.59	1.59	0.25	10.08	1.00	1
44.9%	38.9%	0.5	3.18	1.00	0.50	3.18	1.59	1.59	0.25	10.08	1.00	1
52.5%	50.0%	0.5	0.36	1.00	0.50	0.36	0.18	0.18	0.25	0.13	1.00	1
49.9%	47.4%	0.5	0.36	1.00	0.50	0.36	0.18	0.18	0.25	0.13	1.00	1
50.2%	44.4%	0.5	0.36	1.00	0.50	0.36	0.18	0.18	0.25	0.13	1.00	1
67.5%	66.7%	0.5	0.18	1.00	0.50	0.18	0.09	0.09	0.25	0.03	1.00	1
66.3%	63.2%	0.5	0.18	1.00	0.50	0.18	0.09	0.09	0.25	0.03	1.00	1
67.1%	72.2%	0.5	0.18	1.00	0.50	0.18	0.09	0.09	0.25	0.03	1.00	1
74.4%	58.8%	0.5	3.18	1.50	0.75	4.76	1.59	2.38	0.25	10.08	2.25	1
74.7%	72.2%	0.5	3.18	1.50	0.75	4.76	1.59	2.38	0.25	10.08	2.25	1
73.1%	68.4%	0.5	3.18	1.50	0.75	4.76	1.59	2.38	0.25	10.08	2.25	1
82.4%	76.5%	0.5	0.36	1.50	0.75	0.54	0.18	0.27	0.25	0.13	2.25	1
84.9%	77.8%	0.5	0.36	1.50	0.75	0.54	0.18	0.27	0.25	0.13	2.25	1
83.5%	73.7%	0.5	0.36	1.50	0.75	0.54	0.18	0.27	0.25	0.13	2.25	1
92.7%	88.2%	0.5	0.18	1.50	0.75	0.27	0.09	0.14	0.25	0.03	2.25	1
91.9%	83.3%	0.5	0.18	1.50	0.75	0.27	0.09	0.14	0.25	0.03	2.25	1
89.5%	84.2%	0.5	0.18	1.50	0.75	0.27	0.09	0.14	0.25	0.03	2.25	1

1,000 mg/L:

NTU%-all	TSS%-all	C, g/L	S, dm	T	T x C	T x S	C x S	T x C x S	C <sup>2</sup>	S <sup>2</sup>	T <sup>2</sup>	+EC
52.5%	59.3%	1.0	3.18	0.50	0.50	1.59	3.18	1.59	1.00	10.08	0.25	1
52.6%	60.8%	1.0	3.18	0.50	0.50	1.59	3.18	1.59	1.00	10.08	0.25	1
52.9%	59.2%	1.0	3.18	0.50	0.50	1.59	3.18	1.59	1.00	10.08	0.25	1
57.2%	67.9%	1.0	0.36	0.50	0.50	0.18	0.36	0.18	1.00	0.13	0.25	1
56.7%	67.1%	1.0	0.36	0.50	0.50	0.18	0.36	0.18	1.00	0.13	0.25	1
56.5%	64.5%	1.0	0.36	0.50	0.50	0.18	0.36	0.18	1.00	0.13	0.25	1
75.2%	84.0%	1.0	0.18	0.50	0.50	0.09	0.18	0.09	1.00	0.03	0.25	1
75.8%	78.5%	1.0	0.18	0.50	0.50	0.09	0.18	0.09	1.00	0.03	0.25	1
75.9%	80.3%	1.0	0.18	0.50	0.50	0.09	0.18	0.09	1.00	0.03	0.25	1
64.0%	70.0%	1.0	3.18	1.00	1.00	3.18	3.18	3.18	1.00	10.08	1.00	1
63.0%	71.7%	1.0	3.18	1.00	1.00	3.18	3.18	3.18	1.00	10.08	1.00	1
64.2%	73.3%	1.0	3.18	1.00	1.00	3.18	3.18	3.18	1.00	10.08	1.00	1
78.2%	75.0%	1.0	0.36	1.00	1.00	0.36	0.36	0.36	1.00	0.13	1.00	1
77.4%	76.8%	1.0	0.36	1.00	1.00	0.36	0.36	0.36	1.00	0.13	1.00	1
77.7%	79.2%	1.0	0.36	1.00	1.00	0.36	0.36	0.36	1.00	0.13	1.00	1
85.3%	88.0%	1.0	0.18	1.00	1.00	0.18	0.18	0.18	1.00	0.03	1.00	1
85.9%	88.9%	1.0	0.18	1.00	1.00	0.18	0.18	0.18	1.00	0.03	1.00	1
85.3%	90.1%	1.0	0.18	1.00	1.00	0.18	0.18	0.18	1.00	0.03	1.00	1
83.8%	78.6%	1.0	3.18	1.50	1.50	4.76	3.18	4.76	1.00	10.08	2.25	1
84.1%	80.4%	1.0	3.18	1.50	1.50	4.76	3.18	4.76	1.00	10.08	2.25	1
85.0%	81.2%	1.0	3.18	1.50	1.50	4.76	3.18	4.76	1.00	10.08	2.25	1
88.1%	87.8%	1.0	0.36	1.50	1.50	0.54	0.36	0.54	1.00	0.13	2.25	1
88.6%	86.6%	1.0	0.36	1.50	1.50	0.54	0.36	0.54	1.00	0.13	2.25	1
89.1%	85.4%	1.0	0.36	1.50	1.50	0.54	0.36	0.54	1.00	0.13	2.25	1
94.2%	88.8%	1.0	0.18	1.50	1.50	0.27	0.18	0.27	1.00	0.03	2.25	1
94.6%	90.7%	1.0	0.18	1.50	1.50	0.27	0.18	0.27	1.00	0.03	2.25	1
95.1%	91.7%	1.0	0.18	1.50	1.50	0.27	0.18	0.27	1.00	0.03	2.25	1

5,000 mg/L

NTU%-all	TSS%-all	C, g/L	S, dm	T	T x C	T x S	C x S	T x C x S	C <sup>2</sup>	S <sup>2</sup>	T <sup>2</sup>	+EC
67.8%	71.5%	5.0	3.18	0.50	2.50	1.59	15.88	7.94	25.00	10.08	0.25	1
68.1%	71.8%	5.0	3.18	0.50	2.50	1.59	15.88	7.94	25.00	10.08	0.25	1
68.3%	71.1%	5.0	3.18	0.50	2.50	1.59	15.88	7.94	25.00	10.08	0.25	1
75.8%	84.2%	5.0	0.36	0.50	2.50	0.18	1.81	0.91	25.00	0.13	0.25	1
76.1%	84.0%	5.0	0.36	0.50	2.50	0.18	1.81	0.91	25.00	0.13	0.25	1
75.9%	83.8%	5.0	0.36	0.50	2.50	0.18	1.81	0.91	25.00	0.13	0.25	1
79.3%	86.7%	5.0	0.18	0.50	2.50	0.09	0.91	0.45	25.00	0.03	0.25	1
79.5%	87.5%	5.0	0.18	0.50	2.50	0.09	0.91	0.45	25.00	0.03	0.25	1
79.1%	87.3%	5.0	0.18	0.50	2.50	0.09	0.91	0.45	25.00	0.03	0.25	1
85.7%	76.3%	5.0	3.18	1.00	5.00	3.18	15.88	15.88	25.00	10.08	1.00	1
86.2%	75.9%	5.0	3.18	1.00	5.00	3.18	15.88	15.88	25.00	10.08	1.00	1
86.3%	75.3%	5.0	3.18	1.00	5.00	3.18	15.88	15.88	25.00	10.08	1.00	1
87.1%	87.4%	5.0	0.36	1.00	5.00	0.36	1.81	1.81	25.00	0.13	1.00	1
87.4%	87.7%	5.0	0.36	1.00	5.00	0.36	1.81	1.81	25.00	0.13	1.00	1
87.5%	87.2%	5.0	0.36	1.00	5.00	0.36	1.81	1.81	25.00	0.13	1.00	1
92.9%	92.2%	5.0	0.18	1.00	5.00	0.18	0.91	0.91	25.00	0.03	1.00	1
93.1%	91.5%	5.0	0.18	1.00	5.00	0.18	0.91	0.91	25.00	0.03	1.00	1
93.1%	92.4%	5.0	0.18	1.00	5.00	0.18	0.91	0.91	25.00	0.03	1.00	1
87.0%	89.8%	5.0	3.18	1.50	7.50	4.76	15.88	23.81	25.00	10.08	2.25	1
86.4%	90.6%	5.0	3.18	1.50	7.50	4.76	15.88	23.81	25.00	10.08	2.25	1
86.6%	90.2%	5.0	3.18	1.50	7.50	4.76	15.88	23.81	25.00	10.08	2.25	1
94.5%	96.7%	5.0	0.36	1.50	7.50	0.54	1.81	2.72	25.00	0.13	2.25	1
94.3%	97.3%	5.0	0.36	1.50	7.50	0.54	1.81	2.72	25.00	0.13	2.25	1
94.3%	97.1%	5.0	0.36	1.50	7.50	0.54	1.81	2.72	25.00	0.13	2.25	1
97.9%	99.3%	5.0	0.18	1.50	7.50	0.27	0.91	1.36	25.00	0.03	2.25	1
98.3%	99.1%	5.0	0.18	1.50	7.50	0.27	0.91	1.36	25.00	0.03	2.25	1
98.1%	99.3%	5.0	0.18	1.50	7.50	0.27	0.91	1.36	25.00	0.03	2.25	1